DOCTOR OF PHILOSOPHY

Behaviour of massive reinforced concrete sections in seawater

Thistlethwaite, Christopher

Award date:
2014

Awarding institution:
University of Dundee

BEHAVIOUR OF MASSIVE REINFORCED CONCRETE SECTIONS IN SEAWATER

CHRISTOPHER JAMES THISTLETHWAITE

BEHAVIOUR OF MASSIVE REINFORCED CONCRETE SECTIONS IN SEAWATER

VOLUME I

Christopher James Thistlethwaite

July 2013

A Thesis Presented in Application for the Degree of Doctor of Philosophy

University of Dundee

United Kingdom

DECLARATION

I hereby declare that I am the author of this Thesis, that the work of which it is a record has been carried out by me, and it has not been previously presented for a higher degree.

Christopher James Thistlethwaite

CERTIFICATE

This is to certify that **Christopher James Thistlethwaite** has completed this research under our supervision, and that he has fulfilled the conditions of Ordinance 14 of the University of Dundee, so that he is qualified to submit this Thesis in application for the Degree of Doctor of Philosophy.

Professor M. R. Jones
School of Engineering, Physics and Maths
University of Dundee
United Kingdom

Dr. M. D. Z. Newlands
School of Engineering, Physics and Maths
University of Dundee
United Kingdom

ACKNOWLEDGEMENTS

I would like to express my most sincere gratitude to my project supervisors, Professor Martyn R. Jones and Dr Moray Newlands, for their assistance throughout my research. Their unwavering support throughout, specifically through hours and hours of endless meetings with Prof Jones where his provision of straightforward guidance throughout early phases, expert knowledge throughout experimental phases, and no nonsense checking of written work assisted me along my journey to this submission of my PhD thesis.

Many thanks must be given to industrial support for technical support throughout the project. Terry Kimber, Fairfield Energy; Joe Pitken, Chris Buchanan, Trevor Hodgson, and Alan Marson, Atkins, among others, have all contributed to the success of this research and provided the foundations allowing this research to be possible. I am further grateful for the financial support from Fairfield Energy, TAQA and CNR International, along with the EPSRC.

Also, I would like to thank Dr Li Zheng, Dr Laszlo Cestenyi, Dr Michael McCarthy, Dr Judith Halliday, and Dr Tom Dyer for any assistance they have provided throughout my studies.

My gratitude is extended to friends and research colleagues in the CTU, in particular Dr Z. F. Abu Hassan, Dr G. M. S. Islam, and Mr Z. Song for guidance and assistance on experimental works. Mr T. Hope, Mr T Horne, Mr B. Yun, Miss N. Khosravi, Miss K McKinley, Mr E Mackenzie and Mr L. Loh are all thanked for their hard work on experiments, with special thanks reserved for Mr. M. Robinson for his continued assistance over the past two years, of which some of the work would not have been possible.

Research technicians throughout the Civil Engineering laboratories, Mr C Walker, Mr D Ritchie, Mr M McKernie, Mr W Henderson and Mr G Callon among others, are recognised for their continued support and technical assistance with experiments.

I would like to extend my gratitude to Mr Alan Brant (Deputy Chief Engineer Andoc – now retired) for early assistance in hunting down information on offshore concrete specific to this project, of which all concrete mix designs were subsequently based.

Finally, I extend my sincere appreciation to my girlfriend Sophie for putting up with me through the stresses of my final year, and to my family for their continued support, financially and morally, throughout year after year of studying leading up to this point. Hopefully my achievement of a doctorate will not 'devalue' my father's doctorate.

PUBLICATIONS

Jones, M.R., Newlands, M. and Thistlethwaite, C., 2010. *Determination of the probable failure mechanisms and service life of offshore concrete gravity structures in the OSPAR Maritime Area – research proposal.* In: Advances in modelling concrete service life, proceedings of the 4th Intenational RILEM PhD Workshop, Madrid, Spain, 19th Nov 2010, pp.107-118.

Jones, M.R., Forth, J.P., Thistlethwaite, C. and Higgins, L., 2012. *Reducing the variability of predicting the longevity of reinforced concrete marine structures subjected to physical and chemical degradation.* In: Concrete in the low carbon era, proceedings of the International Conference, Dundee, Scotland, 9-11th July 2012, pp.1554-1562.

ABSTRACT

This study combined research available through literature with extensive experimental studies and substantial physical modelling to estimate the remaining ultimate life of large offshore reinforced concrete structures. Although much research has focussed on concrete degradation due to chloride ingress, corrosion of permanently submerged concrete is regarded as negligible due to the long-assumed apparent worst case of tidal or splash zone exposure. Around 350 specimens were tested with a further 200 exposed for further testing by future research groups. Specimens ranged in size from standard cubes to various beam lengths up to 1.5 metres, allowing for material and structural properties to be assessed.

My original contribution to knowledge in the sector enhances the fundamental understanding of corrosion in subsea concrete, challenging the generally held belief of negligible corrosion. Results and modelling provides an improved ability to ultimately estimate the longevity of fully submerged offshore reinforced concrete. Throughout this thesis, the results from experimental works, carried out as a direct result of the lack of data or information in literature, are reported, assessed and then utilised to provide updated ultimate life estimations. With the current offshore concrete structures currently coming to the end of their service life, and the likelihood of further offshore development using concrete for the renewables sector, understanding the long-term degradation is vital in determining the most effective decommissioning and derogation options. The research carried out directly provides detailed information of the likely time-to-failure, allowing for an informed decision to be made on operational and decommissioning plans.

Experimental work was carried out over four main phases; corrosion initiation due to bulk diffusion of chlorides (Phase I), corrosion propagation in low oxygen environments (Phase II), corrosion in statically and dynamically cracked sections (Phase III) and structural response of heavily corroded individual and lapped bar sections (Phase IV).

Phase I work shows a marked difference between submerged exposures to seawater as opposed to NaCl solution, the unsuitability for accelerated testing with seawater and the likelihood of rapid initiation in offshore structures. Further experimental works through Phases II and III found that although exposed to low oxygen concentrations, reinforcement corrosion continued at significant rates. A variation between anode sizes on the reinforcement is noted, but critically the cross sectional area of the steel was still reduced, albeit in fewer locations. Corrosive products were visibly different, with fewer expansive products, if any,

present. Additionally, this study further highlights the importance of cracking on corrosion, currently ignored by recent model codes, such as the fib Model Code 2010, up to 0.2mm crack width. A linear relationship was found between crack width and corrosion rates, with cracking above 0.1mm considered significant.

The loss of cross sectional area due to propagation was determined for the given environment, and consequently further studies were initiated in an attempt to determine the relationship between this corrosion propagation and the reduced serviceability or ultimate life of concrete beams. Serviceability, defined by beam stiffness, was reduced due to bond loss along reinforcement. Most importantly, however, results prove that the loss of cross sectional area to be the critical influence on loss of ultimate life.

Initial estimates on the remaining ultimate life of the large offshore structures support early rough work that the structures would last centuries. This thesis, however, has shown this is due to the ability of concrete structures with such large volumes of steel to continue to ultimately withstand loading at high corrosion percentages and not due to negligible corrosion, or long initiation periods, commonly suggested in submerged, low oxygen environments.

TABLE OF CONTENTS

LIST OF TABLES

LIST OF FIGURES

GLOSSARY & ABBREVIATIONS

ANDOC	Anglo Dutch Offshore Concrete
BSI	British Standards Institution
CEN	European committee for Standardisation (Comité Européen de Normalisation)
C_{crit}	Critical chloride threshold, % wt. concrete or % wt. binder
C_i	Initial chloride concentration, % wt. concrete/% wt. cement
CONDEEP	Concrete deep water structure
C_s	Surface chloride concentration, % wt. concrete/% wt. cement
CSA	Cross sectional area, mm^2
CSH	Calcium silica hydrates
D_{app}	Apparent diffusion coefficient, m^2/s
DCS	Dutch continental shelf
DO/DO_2	Dissolved oxygen
Ettringite	Calcium aluminate sulphate [$(CaO)_6(Al_2O_3)(SO_3)_3 \cdot 32H_2O$]
FA/fa	Fly ash
fib	The International Federation for Structural Concrete (fédération international du béton)
GBS	Gravity based structures
GGBS/ggbs	Ground granulated blast-furnace slag
Gypsum	Calcium sulphate [$CaSO_4 \cdot 2H_2O$]
HC	Half-cell
i_{corr}	Corrosion current, mA or µA or $\mu A/cm^2$ (as stated)
ITZ	Interfacial transition zone between aggregates and cement matrix

lab.	Laboratory
LAT	Lowest astronomical tide
LPR	Linear polarization resistance, Ω
MR	Multi-Regime
MSH	Magnesium silica hydrates
NaCl	Sodium chloride
Navaid	Navigational aid
NCS	Norwegian continental shelf
NT	Nordtest
OCP	Open circuit potential, mV
OSPAR	Oslo/Paris Convention
PD	Potentiodynamic
PG	Project Group (1 or 2)
ppm	Parts per million
RC	Reinforced concrete
RH	Relative humidity
SF	Silica fume
SRB	Sulphate reducing bacteria
Stdev	Standard deviation
SW	Seawater
t_{decom}	Time of decommissioned period, years
t_i	Time to initiation, years
t_{op}	Time of operational period, years

t_{prop}	Time of propagation, years
UKCS	UK continental shelf
w/b, wb	Water/binder ratio
w/c, wc	Water/cement ratio
wt.	Weight, g
XRD	X-ray diffraction
XRF	X-ray fluorescence
XS	Exposure classes for concrete exposed to chlorides from seawater

CHAPTER ONE

1 INTRODUCTION

When concrete is employed in sub-sea conditions, it is generally assumed that corrosion of the material's steel reinforcement will occur extremely slowly (Böhni, 2005), only becoming a cause for concern on structures after a long period of time. This is due to the assumption that the relatively low dissolved oxygen concentrations in seawater reduce the rate of corrosion sufficiently. Corrosion, however, will continue and offshore concrete structures will degrade at an unknown rate. When considering the ultimate capacity of such structures, knowledge of the corrosion rate is vital to our estimates because the remaining structural capacity is directly related to the cross-sectional area of steel.

As there are few cases where reinforced concrete (RC) structures remain entirely below the lowest astronomical tide (LAT), the longevity of sub-sea concrete is generally ignored due to the perception that more rapid corrosion is found in splash or tidal zones. However, the majority of offshore structures have large volumes of concrete that remain fully submerged (International Association of Oil & Gas Suppliers, 2003; 2012), which will have a significant influence on their overall remaining life.

With decommissioning a current and increasingly pressing issue within the North Sea and worldwide, further understanding of the degradation processes and failure mechanisms of offshore concrete infrastructure will impact on the future decommissioning options and further investment planning of the industry.

Throughout this thesis, the widespread assumption of little, or negligible, degradation to corrosion of sub-sea RC structures will be challenged. Including the effects of static and dynamic loading conditions experienced by concrete structures will allow for an improved understanding of large concrete infrastructure for use in the offshore oil, gas and renewable energy sectors.

Furthermore, existing offshore concrete structures in the North Sea have been exposed for less than fifty years. Experience of the degradation of such structures is consequently limited, forcing operating companies and governing bodies to rely on long term predictions with large variability. The research undertaken between the University of Dundee and the University of Leeds aims to reduce the variability of these long term models allowing for operations to

continue and long term derogation to be effective. The findings are also likely to have implications on the lifetime modelling of other large structures where the majority of the concrete remains submerged.

1.1 RESEARCH BACKGROUND

Production of oil and gas in the North Sea has been active since the early 1970s with around 600 platforms in this area consisting of four types:

- small steel platforms (under 4000 tonnes)
- large steel platforms
- concrete gravity-based structures (GBS)
- floating platforms (Concrete offshore in the Nineties, 1990; VSL, 1992).

Twenty-seven of these platforms are concrete GBS, of which 12 lie on the UK Continental Shelf (UKCS). Figure 1.1 shows a variety of North Sea GBS constructed at Hinna, Norway and floated to site. As shown, the depths and design of the structures vary depending on the depth and size of platform required.

Due to the depletion of natural resources in the UK sector, owners of GBS are planning for derogation of their assets. Prior to this decommissioning, the four options available to the owners and operators are assessed and evaluated (OSPAR, 1998). These options are:

- total removal for onshore disposal and recycling
- float and disband in deep water
- cut and remove structure at -55m LAT
- leave in situ with a navigation aid (navaid) (Figure 1.2)

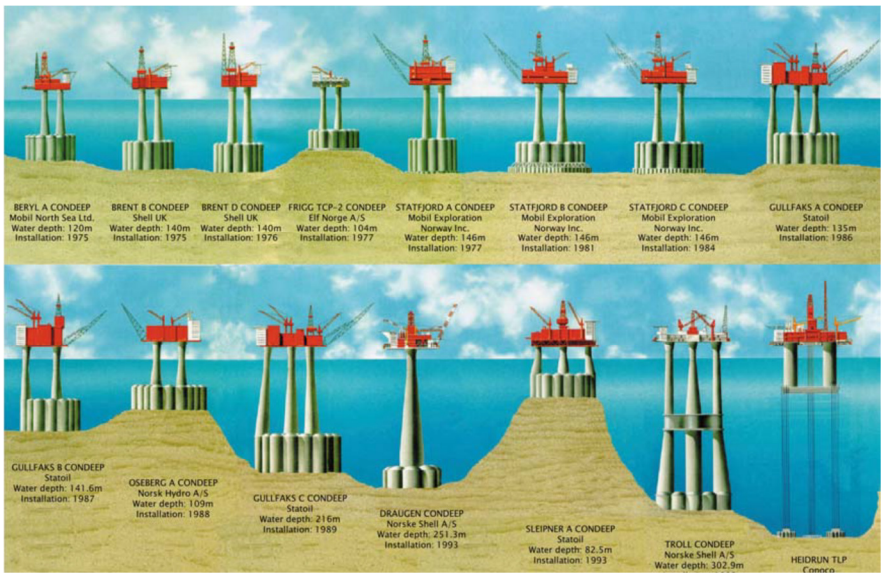

FIGURE 1.1 CONCRETE GBS CONSTRUCTED AT HINNA, NORWAY (SANDVIK ET AL., 2004)

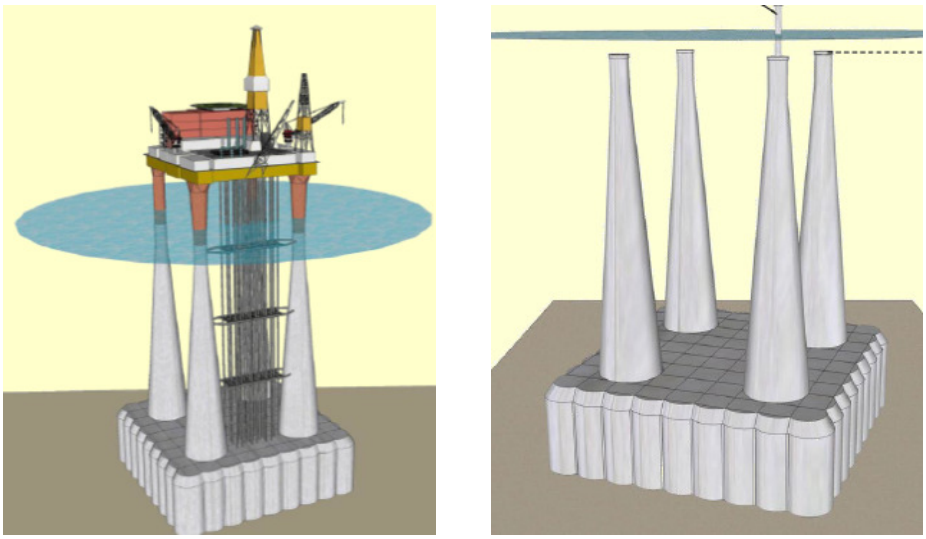

FIGURE 1.2 EXAMPLE PLATFORM PRIOR TO DECOMMISSIONING AND LEFT IN SITU (FAIRFIELD ENERGY, 2012)

Any alternative to full removal and disposal must be agreed upon between all OSPAR (Oslo/Paris convention) members. Additionally, works on the UKCS must also comply with the OSPAR regulations (OSPAR, 1998) and government guidelines (Scottish Enterprise, 2009). The OSPAR Maritime Area covers the Norwegian Continental Shelf (NCS) and the Dutch Continental Shelf (DCS) along with the UKCS. This decommissioning phase of work is likely to occur during the next twenty to thirty years (International Association of Oil & Gas Suppliers, 2003).

As structures constructed in the 1970s and 80s exceed their original design service lives (Gjørv, 2009) and investment in concrete for further offshore applications continues, understanding

the degradation of RC sub-sea structures is becoming more important. The processes of chemical and mechanical degradation are complex, with multiple variables having significant effects on the longevity of these structures such as concrete mix, temperature, salinity, etc.

At present, there is little experience on the long-term durability of offshore RC structures in the North Sea. The first concrete platform was only constructed in 1973 at the Ekofisk field and therefore only around 40 years of deterioration have been monitored and minimally recorded. Additionally, information on the quality of construction and material properties is difficult to obtain due to the loss or misplacement of documents over the years. The combination of missing construction information, insufficient monitoring and recording of degradation, the complex nature of concrete deterioration in a marine environment, and the relatively short exposure make modelling and predicting the longevity of sub-sea RC structures extremely challenging.

Due to the relatively young exposure duration of existing structures, the durability and failure mechanisms are unknown, and previous works to determine the most probable ultimate life and failure mechanisms have been limited. This was the starting point for this research to further the understanding of how and, as importantly, when such structures will fail. This thesis focuses on sub-sea concrete of a similar material design and construction as the majority of the offshore concrete used on the UKCS. Environmental exposures attempt to replicate the environment of the North Sea with the focus on seawater-driven deterioration of RC.

1.2 AIM AND OBJECTIVES

The overall aim of this research project is to enhance the quality of time-to-failure estimates for sub-sea offshore reinforced concrete exposed to the North Sea environment. To accomplish this, a combination of desktop studies, experimental programmes and modelling attempts is required. It is hoped that the findings will reduce the variability in the estimation of probable failure mechanisms, providing stakeholders of offshore assets reliable estimations on the remaining life of their structures.

The specific objectives of this thesis are:

- A comprehensive review of current methods of service life estimation for concrete structures in sub-sea environments

- Investigation of chloride ingress into submerged concrete from seawater and sodium chloride solutions
- Determination of corrosion rates of steel in un-cracked, statically loaded and dynamically loaded RC in replicated sub-sea environments
- Production of a structural evaluation of RC concrete with corrosion of varying severity occurring in multiple areas
- Generation of estimates of time-to-failure of sub-sea RC offshore GBS

In order to achieve these objectives, experimental programmes will be carried out with assistance from undergraduate engineering students over the course of a three year period. Numerical modelling will then be used in an attempt to quantify the remaining ultimate life with multiple failure scenarios considered.

1.3 SCOPE

The research will primarily be focussed on material properties from an individual concrete gravity structure in the North Sea in water around 150 metres in depth. Due to the minimal information available on the platform's concrete mix design, experimental work will cover a range of grades and admixtures. The CEM I concrete mix assumed to be used for construction of this particular platform will be used extensively throughout (Tegelaar, 1975). Similar mixes for alternative platforms can be estimated using reported concrete properties of other platforms of a similar age and construction. With such a wide range of variables to be tested, the research will be valid for a range of different structures, provided the prevailing conditions are sufficiently similar to the experiment's recreation of the North Sea composition and climate. Where possible a range of concrete mix designs of offshore platforms will be tested and compared. The principles of the model and the probabilistic method will be transferable to a number of structures and conditions.

Works will be completed on chloride diffusion, corrosion under low-oxygen environments in unloaded, statically loaded and dynamically loaded states and experimental replication of offshore concrete. Further works carried out within the research group will be used to inform the probabilistic modelling of the sub-sea structures in Chapter 8.

Research completed for the main platform will be applicable to other installations in the North Sea and, it is hoped, provide a basis for future concrete structures that are likely to be used in offshore renewable energy installations.

1.4 OUTLINE OF THESIS

The thesis is a chronological progression of literature research, experimental design and execution, material modelling and evaluation of the likely time-to-failure.

Chapter 2 reviews information available on the degradation of concrete structures in a marine environment. Theoretical assumptions are challenged whilst reviewing and comparing current modelling techniques with experimental and 'real world' data across a range of topics. Chloride diffusion and chloride-induced corrosion are explored, including a wide ranging set of variables with a focus on sub-sea concrete. Current experimental protocols and design codes are reviewed, allowing for the development of a detailed set of experiments. An understanding of the response of structures to corrosion is gained and various methods of ultimate life estimation are assessed. Where information is available, comparisons are made between 'real world' structures and laboratory works.

Chapter 3 sets out the experimental programmes performed with two project groups under supervision and assisted throughout by the author. Experimental variables and procedures are explained in detail, describing all variables and expected results. Experimental work includes chloride diffusion and migration through a range of concretes in multiple exposures, corrosion in un-cracked, statically and dynamically cracked concrete in sub-sea exposure simulations, and structural analysis of beams with lapped and individual corroded reinforcement.

Chapters 4-7 report on results obtained through experimental programmes, highlighting key observations and exploring a theoretical basis to explain observed results. Investigations are carried out into the diffusion of chlorides and the subsequent initiation of corrosion, the propagation of corrosion within cracked sections in low-oxygen environments, and the structural effects of corrosion on remaining capacity of beams. Conclusions are drawn on rates of corrosion and methods for investigating the remaining ultimate life of RC structures.

Chapter 8 evaluates the potential for offshore concrete platforms to have a lengthy remaining life through deterministic and probabilistic modelling. Current chloride-induced corrosion models are utilised to provide a background for existing structures, before adapting the modelling process to incorporate findings discussed throughout this thesis.

Finally, Chapter 9 draws conclusions from the presented works, highlighting a number of contradictory findings and setting out a number of recommendations for further studies and experimental programmes. Continuation of a number of the experiments undertaken for this study will be described and set out for future undergraduate or postgraduate research to further the long term knowledge of concrete behaviour.

CHAPTER TWO

2 REVIEW OF LITERATURE

2.1 INTRODUCTION

Due to the widespread use of concrete, vast numbers of research projects and studies have been completed on the durability of varying concrete mixes in an extensive array of environments (e.g. Neville, 2011). As there are large numbers of research papers on the general topic, this review will predominantly consist of relevant research carried out by large research groups and well-known, respected researchers within the industry. Where the author perceives a lack of reported data, experiments carried out by others of a similar nature are evaluated and reported.

To achieve the overall aim of this research project, a comprehensive understanding of the degradation of concrete in a North Sea, or similar, environment is required. Focus will, for the main part, be restricted to a sub-sea environment, however, where information is sparse, similar concrete design, environments, or loading schemes are reviewed.

The severity of the exposure of concrete structures is taken into account during design through exposure classes in the European standards, Table 2.1 (British Standards Institution, 2000c).

Exposure class XS2, fully submerged sub-sea concrete, will be the focus of this thesis, although reference will be made to XS3 where necessary. Exposure classes of structural areas are shown in Figure 2.1.

It is uncommon for an entire structure to be located in the submerged zone, as the majority of offshore platforms and other marine structures protrude through the surface of the water. Although the splash zones are considered to be worst affected by corrosion damage (Bertolini et al., 2013), the largest bending moments and stresses on the structure are often located well below the surface of the water.

TABLE 2.1 EXPOSURE CLASSES FOR CORROSION INDUCED BY CHLORIDES FROM SEAWATER (EXTRACT FROM TABLE 1, BRITISH STANDARDS INSTITUTION, 2000C)

Class designation	Description of the environment	Informative examples where exposure classes may occur
4. Corrosion induced by chlorides from seawater		
XS1	Exposed to airborne salt but not in direct contact with sea water	Structures near to or on the coast
XS2	Permanently submerged	Parts of marine structures
XS3	Tidal, splash and spray zones	Parts of marine structures

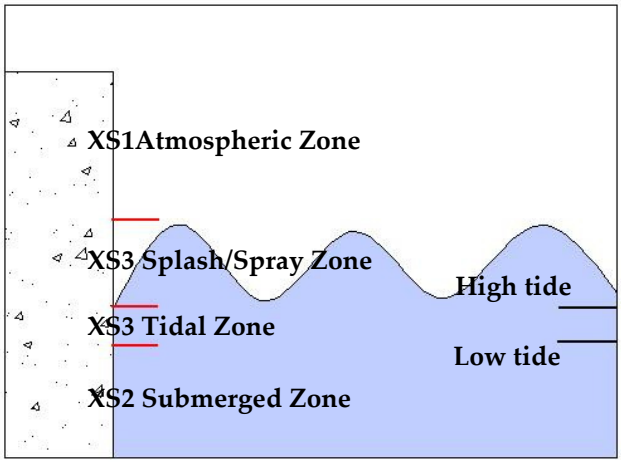

FIGURE 2.1 DIAGRAM OF EXPOSURE ZONES

2.2 NORTH SEA CONCRETE GBS CONSTRUCTION

The first concrete gravity based platform, in the Ekofisk field, was constructed in 1973. Since then, 26 more platforms have been constructed in the North Sea. The majority of these are of a CONDEEP (concrete deep water structure) construction, with other types of construction including Sea Tank, Doris, a proposed type by C G DORIS (Compagnie General pour les Developments Operationelles des Richesses Sous-Marines), and ANDOC (Anglo Dutch Offshore Concrete) (Figure 2.2). Each construction is individualised for the location and nature of the work. A full list of North Sea concrete GBS are in Table 2.2.

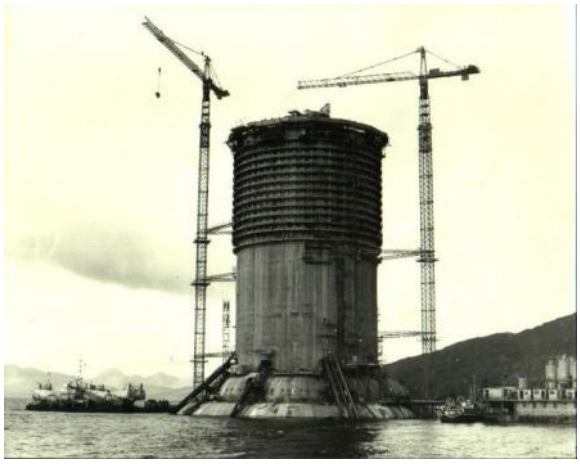

a) Doris (Ninian Central)

(Lee Robinson, 1978)

b) SeaTank (Cormorant Alpha)

(Beckman, n.d.)

c) Condeep (Oseberg A)

(Statoil, n.d.)

d) Andoc (Dunlin Alpha)

(Fairfield Energy, n.d.)

FIGURE 2.2 EXAMPLE CONCRETE GBS CONSTRUCTION TYPES

TABLE 2.2 NORTH SEA CONCRETE GBS (INTERNATIONAL ASSOCIATION OF OIL AND GAS PRODUCERS, 2003)

Field	Construction type	Water depth, m	Installation date
Ekofisk Tank	Doris	70	1973
Frigg TCP2	Condeep	103	1977
Statfjord A	Condeep	145	1977
Gulifaks A	Condeep	134	1986
Gulifaks B	Condeep	142	1987
Gulifaks C	Condeep	217	1989
Draugen	Condeep	250	1993
Oseberg A	Condeep	109	1988
Statfjord B	Condeep	145	1981
Statfjord C	Condeep	145	1984
Sleipner A	Condeep	83	1992
Troll Gas	Condeep	330	1995
Frigg CDP1	Doris	98	1975
Frigg TP1	SeaTank	103	1976
Dunlin A	Andoc	151	1977
Ninian Central	Doris	135	1978
Cormorant A	SeaTank	150	1978
Brent B	Condeep	139	1975
Brent C	SeaTank	141	1978
Brent D	Condeep	142	1976
North Ravensburn	Arup	43	1989
Harding (34m base caisson)	Technip	110	1995
Beryl A	Condeep	117	1975
MCP01	Doris	94	1976
South Arne	Blocks 5604/29 + 5604/30 Denmark	61	1999
F/3	Block F/3 Netherlands	42	1992
Halfweg	Block Q/1 Netherlands	30	1995

2.3 OSPAR RULES FOR DECOMMISSIONING AND ABANDONING STRUCTURES

OSPAR Decision 98/3 (OSPAR, 1998) on the disposal of disused offshore installations states in Paragraph 2;

> "The dumping, and the leaving wholly or partly in place, of disused offshore installations within the maritime area is prohibited."

This subscribes to the notion that the concrete GBS must be removed completely from the sea bed and preferably reused or recycled onshore. This decision could, however, be negated because removing large-scale concrete structures has the potential for hazardous structural damage. Paragraph 3 states;

> "any other disused offshore installation to be dumped or left wholly or partly in place, when exceptional and unforeseen circumstances resulting from structural damage or deterioration, or from some other cause presenting equivalent difficulties, can be demonstrated."

Although the preferred option for OSPAR is the removal of the structures, proposals to leave other concrete GBS in situ are being put forward (International Association of Oil and Gas Producers, 2003).

2.4 HISTORY OF SUB-SEA OIL/GAS REINFORCED CONCRETE REMOVAL

A total of four concrete GBS structures have so far been decommissioned and left in situ with a navaid installed atop the remaining structure. In each case, the derogation consultation showed that for a reduced cost and minimal danger to the workforce, the optimum solution is to leave the entire structure in situ. Removal to shore and cutting the legs to -55m LAT are both deemed unpractical and unpredictable at present.

MCP01, Frigg CDP1, TCP2, and TP1 have all been decommissioned and left in situ (Figure 2.3 and Figure 2.4).

2.4.1 MCP01

MCP01 was initially used as a compression platform to transport gas from the offshore Frigg fields to Aberdeen. Operated by Total, decommissioning was started in 2006 after the pipelines leading into the substructure were rerouted (Total E&P UK Limited, 2007).

Figure 2.3 shows the final configuration of the decommissioned concrete structure. To maintain integrity, the central column where the navigational aid is located must remain vertical. Spalling of cover concrete from the external beams due to corrosion in the splash zones is likely to occur first, while on-going corrosion in the concrete substructure will decrease the structure's load-bearing capacity. At some time in the future, during extreme weather conditions, wave loading will then cause structural failure when loading becomes greater than the capacity.

2.4.2 FRIGG FIELD

Further into the North Sea, the Frigg field consists of three concrete GBS that have all been decommissioned with topsides removed and navigational aids located on each substructure (Total E&P Norge AS, 2003). Again, these structures all protrude the water surface with concrete in the splash zone assumed to degrade more rapidly than the submerged concrete.

Estimating the remaining service life of these structures is difficult, with a complex interaction between corroding reinforcement and the cement paste. Additionally, dynamic loading could cause fatigue, relaxation of pre-stressed tendons could reduce structural capacity, and large, infrequent storms could generate forces that exceed capacity.

2.4.3 EKOFISK TANK

Operated by ConocoPhillips, the Ekofisk tank in Norway is being decommissioned with the final configuration shown in Figure 2.5. All steel topsides will be removed and the concrete tank also left in situ with the navigational aid on top.

Due to vast volume of concrete in the large GBS and the consequential infeasibility in removing them for recycling (e.g. TEP UK, N.D.), future platforms are likely to be left in situ with only very rough estimations on ultimate life.

FIGURE 2.3 DECOMISSIONED MCP01 PLATFORM (TEP UK, N.D.)

FIGURE 2.4 FRIGG CDP1, TCP2 AND TP1 AFTER DECOMMISSIONING (TOTAL E&P NORGE AS, 2011)

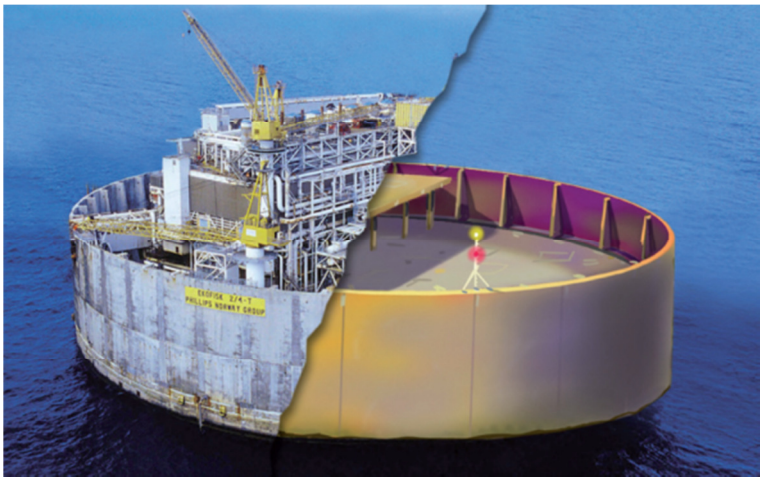

FIGURE 2.5 EKOFISK TANK BEFORE/AFTER TOPSIDE REMOVAL (NORWEGIAN PETROLEUM DIRECTORATE, N.D.)

2.5 INITIATION OF SUB-SEA REINFORCEMENT CORROSION

2.5.1 SCOPE

Corrosion of reinforcing steel is widely regarded as the most significant cause of concrete degradation. For this reason, the mechanisms for its initiation must be reviewed and modelled to inform predictions for the time-to-initiation and future service life of an offshore structure.

As this research deals with concrete in a sub-sea environment, this review focusses on chloride-induced corrosion caused by exposure to chloride-laden environments. Attention is paid to the effects of additional ions found in seawater, the length of exposure and the concrete mixes used in sub-sea concrete structures.

Due to the structural properties of concrete, and the large moments exerted on offshore structures, cracks of up to 0.3mm are expected under design loads. Although the effects of cracking on initiation of corrosion have been researched, they are commonly ignored in models where the structure has cracks of up to 0.2mm (fib, International Federation for Structural Concrete, 2010a; 2010b).

Diffusion is the predominant transport mechanism in sub-sea concrete. The effects of concrete properties have been extensively studied (e.g. Neville, 2011) and are reviewed providing a broader background for generating a model. Additionally, critical chloride contents that define the start of propagation, temperature and construction quality are taken into consideration when proposing the variables that should be used in a model.

As there are a large number of factors contributing to the rate of chloride ingress, results and relationships developed for some variables will be collated and integrated into any modelling used or developed in this study.

The adequacy of currently available initiation models is critically analysed to determine suitability for use in predicting the service life of marine and offshore structures. Careful attention is paid to submerged concrete in seawater, with comparisons drawn between these 'real' exposures and those of laboratory exposure. Owing to the significant variability in the predicted initiation from different experimental methods, the most suitable of the available methods will be utilised.

2.5.2 KINETICS OF CHLORIDE INGRESS

Chloride can penetrate into concrete by absorption, permeation, diffusion, migration and/or convection. The likelihood of each type of penetration is heavily dependent on the exposure conditions. Exposure in the submerged zone will initially be diffusion driven, followed by a combination of ionic migration, due to the electrochemistry of corrosion when an anode has been established, and diffusion. In tidal, splash and atmospheric zones however, transport of chlorides is likely to be a combination of all these mechanisms. Submerged concrete commonly produces higher chloride concentrations at all depths of concrete (e.g. McCarter et al., 2008) and can be considered the worst case for chloride ingress.

Although the potential mechanisms vary significantly, chloride transport is commonly modelled using Crank's solution to Fick's Second Law in all conditions, shown in Equation 2.1 and Equation 2.2 (Crank, 1956; Poulsen, 2006).

$$\frac{\partial C}{\partial t} = D\frac{\partial^2 C}{\partial x^2} \qquad \textbf{EQUATION 2.1}$$

Where;

C chloride concentration, % wt. concrete

t time, s

x depth of penetration, mm

D diffusion coefficient, mm^2/s

$$C(x,t) = C_s - (C_s - C_i)\cdot erf\left(\frac{x}{2\sqrt{D_a t}}\right) \qquad \textbf{EQUATION 2.2}$$

Or rearranging to form an equation for time to initiation;

$$t_i = \frac{1}{D_a}\left(\frac{x}{2\cdot erf^{-1}\left[\frac{C_s - C_t}{(C_s - C_i)}\right]}\right)^2 \qquad \textbf{EQUATION 2.3}$$

Where;

C(x,t) chloride concentration at depth, x, and time, t, % wt. concrete

x depth from the exposed surface, m

C_s surface chloride concentration, % wt. concrete

C_i initial chloride concentration, % wt. concrete

D_a apparent chloride diffusion coefficient, m^2/s

t duration of exposure, s

t_i time to initiation, s

C_t chloride threshold, % wt. concrete

Inaccuracies when measuring the transport of chlorides in tidal or splash zones, where other mechanisms exert an influence, can result in the overestimation of life estimated because a combination of mechanisms is likely to increase the flux of chlorides into the concrete.

The rate of transport of chlorides is affected by the pore structure which is heavily dependent on the water/cement ratio, cementitious additives, and the binding capacity (Dhir et al., 2004; Dhir et al., 2006; Spiesz, Ballari and Brouwer, 2012; Thomas et al., 2012). Chloride transport can also be affected by the exposure period, chloride surface concentration, exposure conditions, aggregate type and cracking. These additional factors will be discussed throughout this section.

2.5.2.1 Effect of exposure period

It is acknowledged that the coefficient of chloride diffusion is variable and commonly decreases over time (Bamforth, 2004; Andrade, Castellote and d'Andrea, 2011). The rate of decrease is due to further hydration, binding of chlorides and ion exchange with the external environment. These processes can physically constrict the pores as well as preventing the chloride from progressing due to the binding.

To take into account an ageing factor, the coefficient of diffusion is modelled to vary exponentially with respect to time as shown in Equation 2.4. This methodology has limitations due to the nature of the equation where the diffusion coefficient should be constant. Although this equation is then commonly substituted into Equation 2.2, this has been shown to be incorrect without integrating with respect to time. Integrating with respect to time, Equation 2.2 is converted to Equation 2.5, as proved by Tang and Gulikers (2007).

$$D_a = D_{ref}\left(\frac{t}{t_{ref}}\right)^{-n} \qquad \textbf{EQUATION 2.4}$$

$$\frac{C(x,t)}{C_S} = 1 - erf\left(\frac{x}{2\sqrt{\frac{D_{ref}}{1-n}}\cdot\left(\frac{t_{ref}}{t}\right)^{n}\cdot t}\right) \qquad \textbf{EQUATION 2.5}$$

Where;

D_a apparent chloride diffusion coefficient, m^2/s

D_{ref} coefficient of diffusion for a given exposure duration t_{ref}, m^2/s

t duration of exposure, s

n factor of ageing dependent

C(x,t) chloride concentration at depth, x, and time, t, % wt. concrete

x depth from the exposed surface, m

C_s surface chloride concentration, % wt. concrete

erf Gaussian error function

The authors then state that this method:

"may be used for long-term prediction without significant mathematical errors if the age factor n is small (<0.3), however it may underestimate the service life if high values for n are used".

Using this method may reduce the common errors that occur in service life predictions and avoid overestimation of the remaining time to initiation.

The fib model code 2010 (fib International Federation for Structural Concrete, 2010a; 2010b) accords with the approach of using an ageing factor, applying variables for the environment and test method to the chloride migration coefficient to determine an average apparent diffusion coefficient. This is widely used in Crank's solution to Fick's Second Law to determine the expected chloride concentration profiles within concrete at a given depth and time.

Although used frequently, an extremely wide range of ageing factors have been reported for a number of concrete mix designs with varying water/cement ratios and admixtures as shown

in Table 2.3. For the purposes of modelling initiation periods, averages and standard deviations of grouped reported factors could be used. However, for a mildly conservative approach in cases where CEM I concretes are used, as in a number of offshore platforms, no ageing factor should be applied. Concrete mixes including blastfurnace slag or fly ash show much larger reduction in diffusion coefficient due to the ageing factor in Equation 2.24.

Additionally, there are instances reported in literature where the diffusion coefficient appears to increase over time for CEM I concrete, although this observation is less frequent (Vallinin and Aldred, 2003; Andrade Castellote and d'Andrea, 2011).

TABLE 2.3 SELECTION OF REPORTED AGEING FACTORS

Concrete Type	PC	GGBS	FA	SF	w/b	Ageing Factor	StDev	Reference
CEM I	✓				0.66 0.50	0.1 0.14		Thomas and Bamforth (1999)
GGBS		✓			0.48	1.2		
FA			✓		0.54 0.50	0.7 0.6		
CEM I	✓					0.32		Stanish and Thomas (2003)
FA			✓			0.6-0.8		
CEM I	✓				0.4	0.69		Vallini and Aldred (2003)
GGBS		✓			0.4	0.7-0.8		
CEM I	✓				0.4-0.6			Thomas and Matthews (2004)
15% FA			✓		0.4-0.6	~0.75		
30%-50% FA			✓		0.4-0.6	0.8-1.2		
Shore Approach				✓	0.36/0.34	0.61	~0.04#	Maage and Helland (2008)
				✓		0.54	~0.06#	
				✓		0.13	~0.5#	
	✓					0.1		
CEM I	✓					0.264		Helland (2008)
CEM I (Old)	✓					0.54		
PFA			✓			0.699		
GGBS		✓				0.621		
SF				✓	0.4	0.56		
PC	✓				0.4-0.6	0.3	0.012	
PFA			✓		0.4-0.62	0.6	0.15	
GGBS		✓			0.4-0.6	0.45	0.2	
Norwegian bridges	✓				0.45-0.6	0.57		

TABLE 2.3 CONT'D…

Concrete Type	PC	GGBS	FA	SF	w/b	Ageing Factor	Stdev	Reference
Heidrun Platform				✓	0.39	0.82		Helland et al. (2010)
CEM I	✓				0.45	-0.24 -0.03		Andrade et al. (2011)
FA			✓		0.28	0.07 1.00		
SF				✓	0.41	0.07 0.30		
FA/SF			✓	✓	0.31	-0.20 0.46		
FA (mortar)			✓		0.37	0.49 0.79		
FA (mortar)			✓		0.49	0.24 1.30		
CEM I	✓					0.4	0.08	Gjørv (2011)
GGBS		✓				0.5	0.1	
FA			✓			0.6	0.12	

[#] Estimated standard deviation from reported data

2.5.2.2 EFFECT OF CHLORIDE SURFACE CONCENTRATION

As with the coefficient of diffusion, the surface chloride concentration, C_s, is commonly variable with time due to condensing of chlorides in the surface layer, wetting and drying cycles for tidal and splash zones and leaching of ions from concrete (Song, Lee and Ann, 2008). C_s can commonly be modelled as a constant value, a linear build-up (Equation 2.6) square root build-up (Equation 2.7) or in alternative ways using empirical data (Equation 2.8 to Equation 2.10).

$$C_S(t) = k_1 t \quad \text{EQUATION 2.6}$$

$$C_S(t) = k_2 \sqrt{t} \quad \text{EQUATION 2.7}$$

$$C_S(t) = C_0 + \alpha ln(t) \quad \text{EQUATION 2.8}$$

Where;

$C_S(t)$ time dependent surface chloride concentration, % wt. concrete

C_0 surface chloride concentration at a standard time, t_{ref}, % wt. concrete

k_1, k_2 constants

α constant derived from empirical data

t exposure duration, s

C_s depends heavily on the type of exposure. Chlorides can be applied to structures through the spreading of salts for use as a de-icer, airborne chlorides carried by wind, or direct contact with seawater. De-icing is standard practice in countries where the temperature regularly drops below freezing throughout the winter months. As the application of chlorides depends on the seasonal temperature and salt spreading regimes, quantifying the exposure conditions for such structures is difficult. C_s values for structures exposed to a sub-sea environment are likely to be more predictable, although there are a number of alternative factors to be taken into account.

A selection of compiled C_s values presented by Song, Lee and Ann (2008) is recorded in Table 2.4. As the pore size decreases, due to a reduction in water/cement ratio or through the addition of GGBS of PFA, the apparent C_s increases. This is not necessarily observed directly through measured concentrations but through the method of fitting a profile through measured chloride concentrations. Spiesz, Ballari and Brouwers (2012) discuss the use of modelling binding properties of concrete, which would more reasonably determine the chloride surface concentration due to the shape of the fitted curve.

Measuring the chloride surface concentration is commonly achieved by plotting an error function curve to measured diffusion profiles (British Standards Institution, 2010). Using the method of extrapolating back to determine a value of C_s could lead to overestimation, which

in turn could result in underestimation of the diffusion coefficient and, ultimately, an increase in the predicted life to overly optimistic timescales.

As the chlorides penetrate further into the concrete, the area of constant concentration, 2mm depth in Figure 2.6, propagates further into the concrete. Although fitting a curve in a similar manner to such a profile will provide a similar or lower D_{app} measurement, the modelled C_s will be increased. In practice, however, the chloride concentration at the surface is likely to reach a peak much lower than the reported, measured value. The value of C_s will predominantly be constant for submerged concrete structures, whereby the modelling technique must be adapted to take this into account.

Ann et al. (2009) suggest that using a square-root or linear build-up of chlorides at the surface of the concrete provides a more realistic estimation of chloride penetration than using an initial, conservative value derived from chloride profiling. It is also suggested that seawater concentration, humidity, temperature have rarely been taken into account when modelling surface chloride concentrations.

Andrade et al (2013) acknowledge that of all the input variables for models predicting chloride penetration into concrete, variation in C_s is the most crucial factor, causing large deviations from actual chloride ingress.

Although there is general agreement on the method of using fitted C_s values for predicting initiation, the author believes the method to be flawed as the outer layers of the concrete can measure artificially lower, due to washing out of chlorides in a tidal zone, or higher with the precipitation of salts in the surface layers. Agreement on a diffusion-based surface chloride concentration based on the measured environment concentration is, therefore, deemed important for future initiation predictions.

TABLE 2.4 SELECTED SURFACE CONCENTRATIONS FOR MARINE CONCRETE (SON, LEE AND ANN, 2008)

Binder	w/c ratio	Exposure	Time, years	C_s, %wb¤
CEM I	0.4		2	4.08
CEM I	0.5	Submerged (lab.)	2	2.55
CEM I	0.6		2	1.33
CEM I	unknown	Tidal/splash	16	3.74 - 5.54
CEM I	0.5	Tidal/splash	24	1.5 - 3.10
CEM I	0.4	Submerged	1, 4	2.93, 4.72
FA				2.10, 4.80
CEM I	0.66	Tidal/splash	3, 8	0.48, 3.05
CEM I				3.53
GGBS	0.45	Submerged	15	4.12
FA				5.80
CEM I	0.44-0.6	Tidal/splash	33	10.51
			38	10.51
			60	9.26
			64	11.96

¤ %wt. of binder

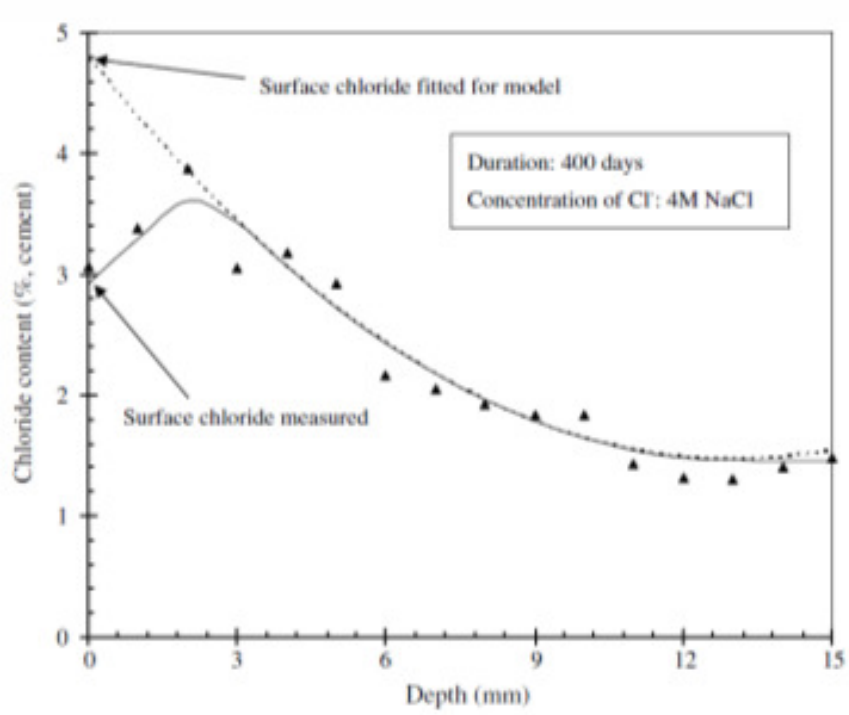

FIGURE 2.6 EXAMPLE OF CHLORIDE PROFILE WITH FITTED CURVES (SONG, LEE AND ANN, 2008)

2.5.2.3 EFFECTS OF SEAWATER COMPOSITION

Application of chlorides to concrete in laboratory chloride resistance tests is commonly achieved using sodium chloride solutions. Chloride ions from this solution penetrate to concrete samples relatively quickly and, since the effect of co-occurring ions on transport is not considered, this method may inaccurately determine the time to onset of corrosion.

Although this scenario may be suitable to simulate de-icing salts, it is not appropriate for marine environments, where concrete is exposed to a number of additional ions; the most prevalent are shown in Table 2.5.

Chloride cations and sulphates are the two most significant ions in seawater influencing chloride transport. Salts are commonly in the form of sodium chloride, NaCl, although in seawater, sodium sulphate, $NaSO_4$, magnesium chloride, MgCl, and magnesium sulphates, $MgSO_4$, are also present.

TABLE 2.5 AVERAGE COMPOSITION OF SEAWATER (TABLE 2.1 IN MEHTA, 1991)

Ion	Concentration, g/litre
Na^+	11.00
K^+	0.40
Mg^{2+}	1.33
Ca^{2+}	0.43
Cl^-	19.80
SO_4^{2-}	2.76

Sulphate ion attack on concrete commonly causes the formation of tricalcium sulfoaluminate hydrate (ettringite), $3CaO{\cdot}Al_2O_3{\cdot}3CaSO_4{\cdot}32H_2O$, and gypsum, $CaSO_4{\cdot}H_2O$. Ettringite is naturally expansive and is commonly attributed to stresses and micro cracking in the concrete structure (Zhang et al., 2013). Expansive cracking can cause an increase in chloride ingress due to a larger, more connected pore structure. This is evident from experimental research wherein chloride diffusion coefficients are larger in a composite, sulphate and chloride, solution than in a chloride solution (Zuquan et al., 2007). In continuously submerged speciments, however, the diffusion coefficients are lower for the composite solution and this suggests that alternative ions and mechanisms have a significant effect on chloride ingress.

Results indicate that seawater improves the microstructure of concrete's outer region through additional deposition of Friedel's salt, $3CaO{\cdot}Al_2O_3{\cdot}CaCl_2{\cdot}10H_2O$, and ettringite (Mohammed, Yamaji and Hamada, 2002b). This result is similar to the findings of Kurdowski (2004), where Friedel's salts are the likely chloride-blocking deposits.

Alternatively, magnesium ions, in the form of $MgSO_4$ and $MgCl_2$, also have a notable effect on the surface 'skin' of concrete and have been associated with a reduction in chloride ingress in marine environments. These effects, however, are less well understood, with differing opinions on whether reactions with the cement matrix have a beneficial or detrimental effect on the durability of the concrete.

Brown and Doerr (2000) noted that the base-exchange reaction readily occurs in the surface region of the concrete (Equation 2.9). The brucite, $Mg(OH)_2$, can also replace the calcium hydroxide, $Ca(OH)_2$, over a large section of the cement-aggregate interface (Equation 2.10 - Equation 2.12).

$$Mg^{2+} + Ca(OH)_2(s) \Rightarrow Mg(OH)_2(s) + Ca^{2+} \quad \textbf{EQUATION 2.9}$$

$$MgCl_2 + Ca(OH)_2 \rightarrow Mg(OH)_2 + CaCl_2 \quad \textbf{EQUATION 2.10}$$

$$MgSO_4 + Ca(OH)_2 \rightarrow Mg(OH)_2 + CaSO_4 \cdot 2H_2O \quad \textbf{EQUATION 2.11}$$

$$MgSO_4 + [Ca(OH)_2 + 2CaO \cdot 2SiO_2 \cdot 3H_2O] \rightarrow 4MgO \cdot SiO_2 \cdot 8H_2O + CaSO_4 \cdot 2H_2O \quad \textbf{EQUATION 2.12}$$

This brucite deposition in the surface layer is said to physically block the concrete pores, thus restricting the transport of water and chlorides into the concrete (Buenfeld and Newman 1984; Buenfeld, Newman and Page, 1986; Santhanam, Cohen and Aloek, 2006). Mohammed, Yamaji and Hamada (2002a) found brucite was only present in CEM I and PFA mixes and was not evident for blast furnace slag mixes, suggesting that the pore structure of the concrete is still a more influential factor in restricting chloride ingress than a surface skin layer.

Kurdowski (2004) supports the formation of a brucite skin but disputes any long term benefits on the grounds that the stability of the layer is insufficient to offer lasting protective action. Evidence of a brucite layer exists on 8 year old foundations to concrete steps, as well as on old mass concrete structures in Wales. The brucite, along with calcite and carbonate, was found in microcracks in the surface layer, suggesting a self-healing process (Sibbick, Fenn and Crammond, 2003).

Furthermore, as brucite continues to form, the hydroxyl ions are gradually used up, causing a reduction in pH. As the pH decreases, calcium compounds become susceptible to magnesium ion attack where the breakdown of calcium silica hydrates (CSH) into magnesium silica hydrates (MSH) can occur.

Differing thicknesses have been reported for the brucite layer, with values ranging from 25μm to 100μm (Buenfeld and Newman, 1986; Santhanam, Cohen and Aloek, 2006). Buenfeld and Newman suggest that after 130 days, a 25μm layer of brucite is formed with an outer layer of

aragonite, $CaCO_3$, reducing the permeability of the concrete. However, it is suggested that no difference will be recorded in the chloride profiles due to the ingress of chlorides prior to the formation of the brucite. The protective nature of the brucite layer may be commonly overstated, as the layer formed was not observed to be continuous (Polder and Larbi, 1995).

In contrast, Sosa et al. believe the gypsum and brucite to be dangerous compounds for concrete. Evidence from experimental results shows immersed concrete to be at greater risk, with more negative half-cell readings and increased corrosion rates.

Although focus is on these reactions and the potential reduction in the transport rate of chlorides, migration testing completed by Tong and Gjørv (2001) appears to suggest D_{app} of concrete is higher when exposed to seawater than when exposed to NaCl solution. In comparison though, natural diffusion experimental work shows initiation is at least threefold slower in synthetic seawater exposure in comparison with NaCl solution, suggesting that blocking mechanisms protect concrete from chloride ingress (Erdogd, Bremner and Kondratova, 2001).

Although evidence of brucite and other mineral deposits in the surface layers is unquestionable, the author believes the reported beneficial properties of seawater, in comparison to sodium chloride solutions, are overstated. The author believes the evidence does support that a reduced chloride diffusion rate is experienced when concrete is in contact with seawater, but modelling of initiation periods should be careful not to overestimate the benefits. Evidence shows that the ageing factors applied, and methodology behind coefficient determination, incorporate effects of alternative ions without acknowledging that it is a combination of ageing and surface layer effects. Therefore, the author believes estimations of time-to-initiation are commonly overestimated.

2.5.2.4 Effects of loading cracks

British standards currently allow for cracks of up to 0.3mm under the serviceability limit state for exposure class XS2 (Table 2.6).

TABLE 2.6 RECOMMENDED VALUES FOR W_{MAX} (TABLE7.1, BRITISH STANDARDS INSTITUTION, 2004)

Exposure Class	Reinforced members and prestressed members with unbounded tendons	Prestressed members with bonded tendons
	Quasi-permanent load combination	Frequent load combination
X0, XC1	0.4mm	0.2mm
XC2, XC3, XC4	0.3mm	0.2mm
XD1, XD2, XS1, XS2, XS3		Decompression

Although the European standards allow for a 0.3mm recommended maximum crack width, the fib model (fib International Federation for Structural Concrete, 2006) extrapolates the diffusion coefficient at steady state as a constant for cracking with a width of up to 0.2mm, assuming that no changes occur in the concrete to alter this. When cracks are between 0.2mm and 0.4mm wide, however, the code allows for a free transfer of chlorides to the reinforcement with no impedance, theoretically assuming chloride induced corrosion to instantaneously initiate.

Studies have disputed this showing that with an increasing crack width, the transport of chlorides increases accordingly (Coppola et al., 1996; Sahmaran 2007). Cracking does not occur uniformly between the surface of the concrete and the reinforcement, and, as a result, using such a method whereby chlorides either penetrate the depth of the crack or not is conservative for cracks above 0.2mm and for cracks with widths smaller than 0.2mm, time-to-initiation may be underestimated. The depth of the crack will also have an effect on the chloride penetration and will increase the rate of chloride transport, although this will not necessarily occur instantaneously as suggested in the fib code.

However, Win, Watanabe and Machida (2004) show that after the initial 10mm cover, the chloride concentrations are relatively constant throughout the depth of cracks (0.2mm width), with reported concentrations of between 0.1 and 0.2%Cl^-/wt. concrete for a water to cement

ratio of 0.45-0.65. This supports the theory that chloride ions penetrate the cracks extremely quickly, with significant maximum concentrations at the steel reinforcement in the majority of cracked sections. This suggests modelling cracks above 0.2mm as having a free transfer of chlorides is reasonable, albeit conservative when predicting time-to-initiation or propagation rates. Further studies conducted by Yamamoto, Yamaji and Mizuma (2008) showed a similar characteristic through cracks of 0.7mm width, showing a free transport of chlorides through the cover with a consistent concentration at every depth.

Sahmaran (2007) reports an apparent critical crack width, 0.135mm, whereby the rate of increase of D_{app} through the cracked area is accelerated.

Concrete has a reported self-healing ability, which can reduce the detrimental long-term effects that cracking can cause. Two major hypotheses have been proposed regarding self-healing mechanisms: further hydration of anhydrous cement in the matrix and the precipitation of calcium carbonate (Neville, 2002 cited by Termkhajornkit, 2009). There is still considerable debate between the effects of any self-healing on the chloride ingress; particularly the critical crack width whereby healing is no longer beneficial, the decrease in chloride ingress observed and any effects on the acceleration of the corrosion rate. Sahmaran (2007) loosely supports earlier work by Reinhardt and Joos (2003) where the self-healing of cracks with widths below 0.1mm is reported. It is suggested that, solely as a result of calcite ($CaCO_3$) formation, crack widths of less than 0.05mm show a much reduced D_{app}. The results obtained provide limited support for this hypothesis, as testing was only carried out over 30 days and the slow measured rates of diffusion may have resulted solely from the small initial crack widths. The work was, however, supported by previous research carried out by Edvardsen (1999) in which full autogenous healing solely due to $CaCO_3$ was reported. Furthermore, active and dormant cracks are reported to heal.

Fagerlund and Hassanzadeh (2010) are also in agreement with previous researchers regarding the extent to which healing, due to continued hydration and deposition of $CaCO_3$, occurs throughout the cracks. It is noted however, that cracked specimens still have much higher chloride diffusion rates than un-cracked specimens due to a visibly incomplete sealing of the crack.

The evidence considered provides compelling support for the hypothesis that cracking causes a much more rapid initiation of corrosion in concrete and the author believes the reported self-healing of cracks has little effect on mitigating corrosion. Modelling of initiation must,

therefore, take into account cracking and tensile areas of cover concrete, which permit corrosion to propagate at concentrated anodes where cracks reach the reinforcing steel.

Design codes for crack widths are deemed too relaxed, with researchers pointing to crack widths closer to 0.1mm whereby the rate of chloride transport begins to increase. For the majority of modelling purposes, the initiation time of concrete should be assumed to be negligible where cracks are greater than 0.2mm, as suggested by the fib model. Table 2.7 provides a summary of recent research into the effects of crack widths on initiation.

TABLE 2.7 EFFECTS OF CRACK WIDTH ON INITIATION OF CORROSION

Concrete mix details	Crack width, mm	Effect on transport of chlorides	Reference
Unknown	0.3#	Tensile zone has accelerated diffusion of chlorides due to damage to the ITZ above crack width to cover ratio of 0.1	Gowripalan, Sirivivatnanon and Lim, 2000
CEM I 0.25-0.65 w/c ratio	0.2	Rapid transport of chlorides to the steel, reduced transport with reduced water/cement ratio	Win, Watanabe and Machida, 2004
	0.5	Free transfer of chlorides to the steel	
CEM I 0.5 w/c ratio	< 0.4	Flexural cracks do not influence the corrosion of tension reinforcement	Vidal, Castel and François, 2007
CEM I mortar	0.03 – 0.39	Increase in D_{app} in two linear stages up to a factor of 14 larger than un-cracked	Sahmaran, 2007
CEM I 0.6 w/c ratio	0.7 - 1.5	Free transfer of chlorides to the steel	Yamamoto, Yamaji and Mizuma, 2008

crack width determined by the author from the reported cover and crack width to cover ratio

2.5.3 CRITICAL CHLORIDE CONTENT

Initiation of corrosion occurs when chlorides reach the steel/concrete interface and break down the passive layer. The initiation threshold, the concentration of chlorides required to initiate the corrosion process, is known as the critical chloride threshold, C_{crit}. It is commonly reported as a percentage of chloride ions per weight of concrete (% wt. concrete) or as a

percentage of chloride ions per weight of cement (% wt. cement). Compiled chloride threshold values range from 0.1% wt. cement to around 1.2% wt. cement (Table 2.8) (Alonso et al., 2000).

It is suggested that no single critical chloride content is measureable due to the multiple variables affecting corrosion initiation: steel roughness, concrete properties and the 'aggressiveness' of the environment (Izquierdo et al., 2004; Alonso, Castellote and Andrade, 2004). Investigating the potential of the steel as a factor, it is shown as the polarized potential of the steel becomes more negative, C_{crit} increases. This observation applies to the initial polarized potential of the steel, as the introduction of chlorides will reduce the polarized potential and corrosion will propagate.

Angst et al. (2009) provide a detailed review of chloride threshold values presented in various forms of literature. Of these, only eight references relate to values derived from real structures under capillary and diffusion chloride transport mechanisms. All reported values are in the range 0.2-1.5 % wt. binder for NaCl and 0.4-1.5 % wt. binder for seawater-induced chlorides. Angst et al. agree with previous comments on the need for further research to understand chloride induced corrosion processes and recommends that future works should use ribbed steel in concrete specimens.

Jiang et al. (2013) carried out a set of experiments to determine the effects of additional salt cations on C_{crit}. Since seawater contains the additional ions, comparisons between the effects of MgCl, KCl, NaCl and $CaCl_2$ were carried out, with evaluation of C_{crit} performed in terms of Cl^-/OH^- ratio and total and free chlorides. The results suggest that exposure to MgCl and $CaCl_2$, in contrast to NaCl and KCl, reduces both the pH and the chloride threshold as a proportion of free chlorides. Measured as a Cl^-/OH^- ratio or as total chloride content, C_{crit} is higher for those concrete specimens exposed to MgCl and $CaCl_2$. Although additional ions have been shown to reduce the chloride threshold as a proportion of free chlorides, values for all concretes are still greater than 0.3 % wt. binder. The author suggests the use of previous results is not suitable for long term prediction of initiation due to the effects of the additional ions. However, as the results are relatively similar, no alteration of estimation techniques is required for an appropriate estimation of time-to-initiation for corrosion.

Conservative estimations of service life should, therefore, continue to use 0.2% wt. binder as a threshold, unless information can be gained from electrochemical measurements of the concrete samples.

TABLE 2.8 REPORTED CRICITICAL CHLORIDE THRESHOLDS (ALONSO ET AL. 2000, JIANG ET AL. 2013)

Critical chloride levels required to initiate the corrosion of the reinforcing steel. Literature data				
Conditions	**Environ./ Concrete type**	**Values**		**De-passivation detection method**
		Free Cl^-	**Total Cl^-**	
		% wb	**% wb**	
Mortar suspensions	CEM I		2.42	anodic polarization
	GGBS		1.21	
Cements with high or low alkali content	80% RH		0.6-1.8	corrosion rate
	100% RH		0.5-1.7	
Three OPC mortar (external chloride)	50% RH		0.6-1.4	increase in current density, potentiostatic test
Concrete exposed to external chloride contamination	CEM I		3.04	anodic polarization
	GGBS		1.01	
	CEM I		0.6	anodic polarization
Cl^- added as admixture, medium (MS) and high strength (HS) concretes with supplements	MS	1.15		assuming a threshold of Cl/OH value of 0.6, calculation of free chlorides
	HS	0.85		
	SF	0.8		
	SF/PFA	0.45		

TABLE 2.8 CONT'D

Conditions	Environ./ Concrete type	Values		De-passivation detection method
		Free Cl % wb	Total Cl % wb	
			0.5-1	assuming a threshold Cl/OH value of 0.3
			1-1.5	
			1-1.5	
			0.5	visual observation + mass loss
Reinforced concrete prisms with fly ash as marine exposure	CEM I		0.7	mass loss
	PFA 15%		0.65	
	PFA 30%		0.5	
	PFA 50%		0.2	
Concrete slabs with added Cl with various exposure conditions	CEM I		0.097-0.19	corrosion rate, AC impedance, visual inspection and mass loss
Concrete cubes exposed to MgCl, NaCl, KCl, and $CaCl_2$ solutions through an immersion and drying cycle	CEM I	0.4-0.7	0.8-1.4	corrosion rate, half-cell potentials
	PFA	0.3-0.7	0.8-1.5	
	GGBS	0.3-0.7	0.8-1.5	

% wb is the % chlorides per weight of binder

2.5.4 EXPERIMENTAL METHODOLOGIES

Due to the perceived importance of bulk transport to the process of chloride ingress, there are a number of frequently used experimental procedures to determine the non-steady and steady state chloride migration coefficients through concrete. Twenty-seven laboratories participated in round-robin testing on chloride penetration test methods, with the results being published by Castellote and Andrade (2006). This undertaking acknowledged the complexity of the

chloride penetration process and the need for a comparison of the test methods due to the variations in their recorded measurements.

Owing to the existence of a large number of different test methodologies, review will be restricted to only the most regularly used experimental methods. These methods have also been used frequently within the department and therefore numerous results are readily available. The results from the round-robin set of testing show large variations in results from the majority of test methods.

2.5.4.1 NATURAL DIFFUSION

Natural diffusion testing is common, with sampling methods applied to existing structures as well as laboratory specimens. The tests are often accelerated by applying a higher molar concentration of chlorides than experienced in common environments. However, they are still relatively time-consuming methods of determining apparent diffusion coefficients.

Each of the diffusion test methods discussed uses concrete samples with cut surfaces to determine the bulk transport properties of the mixes. To model the lifespan of a structure as accurately as possible, the concrete properties, including the skin effects, should be taken into account. This method can, therefore, be adapted by using a cast surface as the exposed face of the concrete to provide data on this chloride diffusion rate.

Sampling the concrete after exposure can influence the results obtained. Three methods are recommended for sampling concrete: dry cutting and crushing, profile grinding, or drilling (Vennesland, Climent and Andrade, 2013).

<u>NT Build 443</u>

The *Nordtest* method, NT Build 443 (1994), exposes vacuum-saturated, 28 day concrete specimens to a NaCl solution. This method then uses profile grinding and titration to determine the chloride concentration at predetermined depths within the specimen. Expected coefficients of variation for the measured and calculated values are: C_s = 20% and D_e = 15%. These values are calculated using a linear regression analysis on the recorded chloride concentrations. Tang and Sørensen (2001) report the repeatability COV to be between 8 and 14%, with the reproducibility COV between 16 and 23%. However, due to the difficulties with profile grinding and titration measurements, variations of results from this test procedure would be expected to be higher. The results from *Table 5* in Castellote and Andrade (2006), ignoring values outside 95% (the mean plus 1.96 standard deviations empirically), still show that the data can commonly be spread up to 180% higher than the mean value.

A comparison between results from this testing method and exposed beams in natural conditions was performed by Vallini and Aldred (2003). The results showed the exposed beams to have diffusion coefficients that were between 5 and 178 times lower than those for the Nordtest methods.

CEN/TS 12390 Part 11

This recently documented methodology from the CEN/TC 51 research group (British Standards Institution, 2010) provides clear instructions on a natural diffusion test. Specimens with a cut surface are exposed to 1M sodium chloride solution for 90 days through either immersion, inversion or ponding (Figure 2.7). After 90 days, a minimum of 8 layers of concrete are ground and then titrated to determine the chloride content of each sample.

From the resulting chloride profile, Crank's solution to Fick's second law is fitted to the curve to determine an apparent chloride diffusion coefficient, D_{app}. Understanding the appropriate value for C_s is vital, as the measured D_{app}, could be significantly affected by the use of an incorrect measurement.

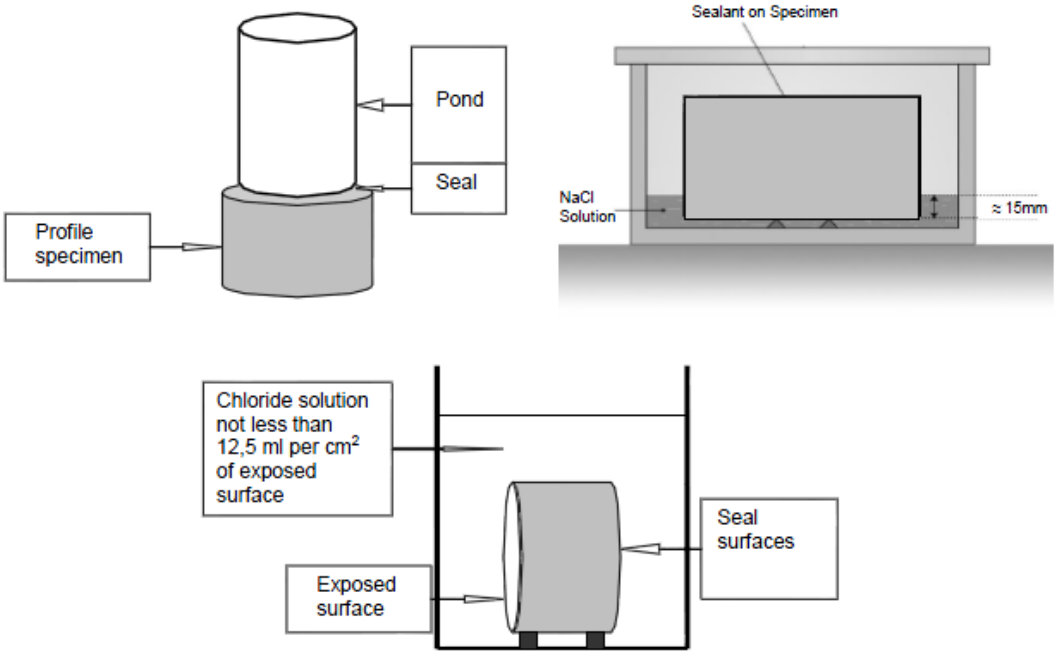

FIGURE 2.7 (CLOCKWISE FROM TOP LEFT) PONDING, INVERSION AND IMMERSION SETUPS (BRITISH STANDARDS INSTITUTE, 2010)

2.5.4.2 CHLORIDE MIGRATION

Chloride migration testing uses an applied potential to force chlorides through the concrete, either for a set duration or until a steady state is reached. Migration methods allow for a

much more rapid determination of transport properties, although the applied currents can cause a distortion in the results when compared to 'real world' structures.

ASTM C1202

The ASTM C1202 method measures the charge passed through a 50 mm thick and 100mm diameter concrete core and relates this to chloride ion permeability. Current is plotted against time in at least 30 minute intervals and then integrated to determine the charge passed. This is related to ion permeability through Table 2.9. Results obtained through this method are relatively vague, with no accurate method of predicting the time to initiation directly from results.

It is reported that two tests by the same operator on the same concrete batch can produce results that differ by up to 42%, or 51% with round-robin testing (Grace Construction Products, 2006).

TABLE 2.9 RELATIONSHIP BETWEEN CHARGE PASSED AND CHLORIDE ION PERMEABILITY

Charge passed, C	Chloride ion permeability
> 4,000	High
2,000 – 4,000	Moderate
1,000 – 2,000	Low
100 – 1,000	Very low
< 100	Negligible

Multi-Regime (MR)

The MR methodology uses an externally applied potential difference, 12V, to force chlorides through a cut sample (Castellote, Andrade and Alonso, 2001; Castellote and Andrade, 2006). A 1M sodium chloride solution is applied to one side and distilled water to the other. A negatively charged steel rod is placed into the sodium chloride solution, and a positively charged rod is inserted into the distilled water. The negatively charged chloride ions are then drawn to the positive steel rod. An overview of the setup is shown in Figure 2.8.

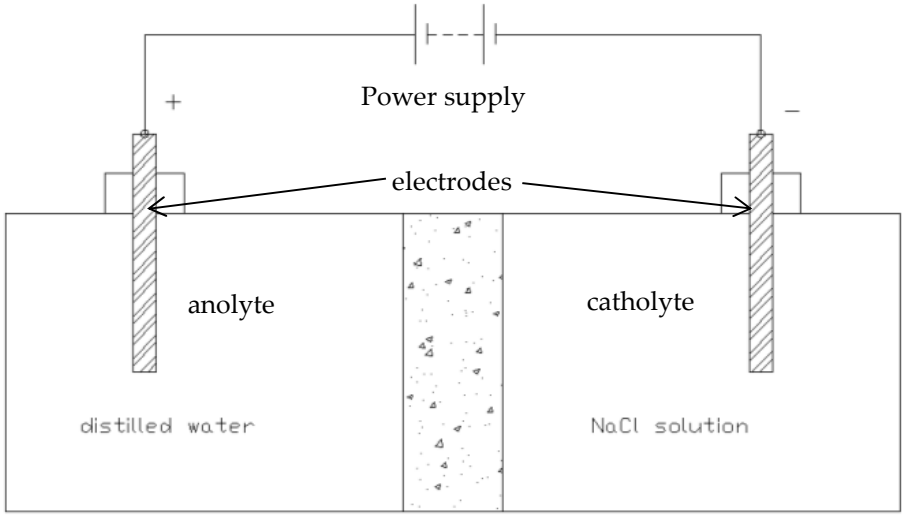

FIGURE 2.8 MULTI-REGIME METHOD

Results are obtained by measuring the conductivity of the 'downstream' solution at the positive electrode and recording the drop in potential across the specimen. The temperature at the time of measurement is also recorded, as this will have an effect on the conductivity of the solution. Using the measured increase in conductivity over time, the steady and non-steady state coefficients of diffusion can be calculated.

This method does not, however, allow for the use of artificial seawater because the negatively charged sulphate ions would also be drawn through the concrete and would dissolve into the anodic solution. The conductivity of the 'downstream' solution would increase due to addition of chlorides and sulphates, providing a reading that is not proportional to the concentration of chlorides alone. Consequently, using this method for artificial seawater would produce a diffusion coefficient greater than that which occurs naturally.

NT Build 492

The Nordtest method, NT Build 492 (1999), uses a visual measurement of chloride penetration using a silver nitrate spray that precipitates easily visible silver chlorides when chloride ions reach a sufficient concentration. This method is reported to have a repeatability of 9% and reproducibility of 13%, making it slightly more reproducible than NT Build 443. However, comparison of the accuracies of experimental results will provide an approximation of variations for use in probabilistic estimations of service life.

Additionally, there is debate concerning the concentration of chlorides at the colour change boundary when using this methodology (Yuan et al., 2008). Reported concentrations at the colour change boundary vary from 0.01% to 1.41% wt. cement. Further information on the concentration of hydroxyl ions, measured through the pH of the pore solution, could provide an indication of actual chloride concentrations at the penetration front.

2.5.4.3 SUMMARY OF EXPERIMENTAL METHODS

Although many methods use similar techniques, results vary between each experimental design. The author believes, however, that the summarised methods (Table 2.10) are suitable for distinguishing between the resistances to chloride transport of various concrete designs, using short-term chloride penetration data for long-term modelling.

TABLE 2.10 SUMMARY OF COMMONLY USED EXERIMENTAL METHODS TO DETERMINE CHLORIDE DIFFUSION OR MIGRATION COEFFICIENTS

Method	Type	Comments	Reference
NT Build 443	Natural diffusion	Immersion for at least 35 days	NT Build 443, 1994
CEN/TS 12390:Part 11	Natural Diffusion	28 days curing followed by 90 days of exposure	British Standards Institution, 2010
ASTM C1202	Migration	6 hour rapid test, reported repeatability variation in results up to 51%	Grace Construction Products, 2006
Multi regime (MR)	Migration	Up to a month long test, potential to gain steady and non-steady state coefficients	Castellote, Andrade and Alonso, 2001; Castellote and Andrade, 2006
NT Build 492	Migration	24 hour rapid test	NT Build 492, 1999

2.5.5 CURRENT MODELLING METHODOLOGIES

The majority of initiation models use a variation of Crank's solution to Fick's second law as reported in Section 2.5.2. Modelling is commonly deterministic, with the equation being used explicitly with a fixed value for each parameter. Due to the number of available modelling techniques, a selection of common methods is reviewed.

DuraCrete

The Brite-EURam project 'DuraCrete' (Lindvall, 1998; Siemes, 1999) was undertaken in an attempt at "providing a code-like guide for durability design and assessment of concrete structures" (BE-1347/TG7/ Report R17, 2000). A design equation, g, is used to determine the time-to-initiation of corrosion (Equation 2.13).

$$g = c_{cr}^{d} - c^{d}(x,t) = c_{cr}^{d} - c_{s,cl}^{d}\left[1 - erf\left(\frac{x^{d}}{2\sqrt{\frac{t}{R_{cl}^{d}(t)}}}\right)\right] \qquad \textbf{EQUATION 2.13}$$

Where;

$c_{s,cl}^{d}$ design value of critical chloride concentration, % wt. concrete

c_{cr}^{d} design value of the chloride surface concentration, % wt. concrete

R_{cl}^{d} design value of the cover thickness, mm

x^{d} design value of the chloride resistance, mm

t time, s

A complex set of parameters are defined depending on exposure conditions and material properties amongst others. Evaluation of the existing structures of interest, based on this method, will be covered in Chapter 8.

Concrete Society Technical Report 61

As with DuraCrete, this method is based on diffusion-driven chloride transport mechanisms, where a deterministic approach is used (Bamforth, 2004). Input parameters have been defined by experience and experimental results over a range of studies (Table 2.11).

TABLE 2.11 INPUT PARAMETERS FOR REPORT NO. 61

Concrete type	Parameter	Value
PC	C_s, % wt. concrete	0.36 0.75˜
	ageing factor (n)	-0.264
	D_{app} ($x10^{-12}$), m^2/s	log D_{ca} = -12.926+1.999(w/c)
	C_{crit}, % wt. concrete	0.4
pfa/ggbs	C_s, % wt. concrete	0.51 0.90˜
	ageing factor (n)	-0.699 (ggbs) -0.621 (pfa)
	D_{app} ($x10^{-12}$), m^2/s	log D_{ca} = -13.325+1.409(w/c)
	C_{crit}, % wt. concrete	0.4(1-0.005(%ggbs-20)) (ggbs) 0.4(1-0.01(%pfa-10)) (pfa)
sf	C_s, % wt. concrete	0.51 0.90˜
	ageing factor (n)	-1+1.10(w/c)
	D_{app} ($x10^{-12}$), m^2/s	log D_{ca} = -13.800+3.100(w/c)
	C_{crit}, % wt. concrete	0.05(1-0.025(%sf))

˜ values at 95% confidence level due to high variability

Life365

As with the majority of corrosion initiation models, the transport of chlorides is again modelled through the application of Fick's second law (Life-365 Consortium II, 2012). Input parameters are similar to alternative models; albeit with variations in ageing factors, C_s, D_{app} and C_{crit} depending on the source of the data. Input parameters for Life365 modelling are presented in Table 2.12.

TABLE 2.12 INPUT PARAMETERS FOR LIFE365

Concrete type	Parameter	Value
PC	C_s, % wt. concrete	0.8
	ageing factor, n	0.20
	D_{app} ($x10^{-12}$), m^2/s	$\log D_{ca} = -12.06+2.40(w/c)$
	C_{crit}, % wt. concrete	0.05
pfa/ggbs	C_s, % wt. concrete	0.8
	ageing factor, n	0.2 + 0.4(%FA/50 + %ggbs/70)
	D_{app} ($x10^{-12}$), m^2/s	D_{PC}
	C_{crit}, % wt. concrete	0.05
sf ˜	C_s, % wt. concrete	0.8
	ageing factor, n	0.2
	D_{app} ($x10^{-12}$), m^2/s	$D_{PC} \cdot e^{-0.165\ SF}$
	C_{crit}, % wt. concrete	0.05

˜ up to 15% silica fume

Effects of temperature are taken into account using Equation 2.14.

$$D(T) = D_{ref} \cdot e^{\left[\frac{U}{R}\left(\frac{1}{T_{ref}}-\frac{1}{T}\right)\right]} \qquad \textbf{EQUATION 2.14}$$

Where;

D(T) diffusion coefficient at temperature T, m^2/s

D_{ref} diffusion coefficient at temperature T_{ref}, m^2/s

U activation energy of the diffusion process, 35000 J/mol

R gas constant, 8.8314 J/mol K

T absolute temperature, K

Fib Model Code 2010

The fib model codes continue the theme of employing Crank's solution to Fick's Second Law. There is some consideration for the effects of cracking, crack widths under 0.2mm are ignored. The input parameters are similar to those used in the Technical Report 61 method (fib International Federation for Structural Concrete, 2006; 2010a; 2010b).

TABLE 2.13 EQUIVALENT PARAMETERS USED IN FIB MODEL CODE FOR SERVICE LIFE

Parameter	Distribution	Mean (m)	StDev (σ)
C_0, %wb	Constant	Laboratory analysis	-
$C_{s,Dx}$, mm	Lognormal	To be determined	-
$D_{RCM,0}$, m^2/s	Normal	Laboratory test	0.2m
C_{crit}, %wb	Beta	0.6	0.15
Ageing factor, n	Beta	CEM I: 0.3 FA: 0.6 GGBS: 0.45	CEM I: 0.12 FA: 0.15 GGBS: 0.2

Additional modelling

Numerous other models have been proposed for initiation of chloride-induced corrosion. The suitability of the application of Fick's second law to estimate chloride ingress should be questioned. Marchand and Samson (2009) suggest that "any material database incorporating apparent diffusion coefficients for service-life predictions cannot be expected to provide reliable results given all the limitations outlined". It is suggested that a model incorporating multispecies ionic interactions should be used to provide more realistic estimation.

Wang, Li and Page (2005) had considered ionic interaction between species previously, defining the transport of ions as:

$$\tau^2 \frac{\delta}{\delta t}(C_i + S_i) = z_i \frac{F}{RT} \nabla(D_i C_i \nabla\varphi) + \nabla(D_i \nabla C_i) \qquad \text{EQUATION 2.15}$$

Where;

τ tortuosity of the pore structure

C_i concentration of species i in solution, % wt.

S_i concentration of bound ions in solution, % wt.

z_i charge number of species, i

F Faraday's constant, 9.6485×10^4 C/mol

R gas constant, 8.314 J/mol·K

T temperature, K

Although this has been shown to provide a more realistic estimation of the ionic distribution in concrete, a detailed set of variables and initial input parameters is required, which is unlikely to be determinable for an existing structure. The simplified methodology will provide a conservative estimate of the chloride concentration and, consequently, is suitable for engineering applications.

Additionally, taking chloride binding into account will provide a more realistic estimation of the expected chloride profile after exposure. As free chlorides are consumed in reactions with the cement paste, the transport of chloride ions through the cement matrix will be reduced. Val and Trapper (2008) account for convection and chloride binding but only consider a single ion diffusion mechanism.

2.5.6 SUMMARY

The transport of chlorides into concrete is complex and the accurate estimation of corrosion initiation requires measured data. Current modelling techniques are disputed and a consistent approach to estimate the initiation of chloride-induced corrosion is required.

Using a more accurate multi-ionic approach will provide a more 'realistic' estimate of the chloride transport and time-to-initiation but, due to the complexity of the input parameters, which can vary greatly, a simplified model is generally sufficient for long-term life prediction where the propagation period is likely to be much longer than the initiation.

The use of artificial seawater is suitable for natural diffusion tests to provide a reasonable estimate of the bulk transport of chlorides through concrete in a more realistic multi-ionic environment. Although migration results are faster, the variability between results is large, and therefore suggesting the reliability of results from migration is questionable.

In practice, 'real world' reinforced concrete structures will contain cracks from the surface to the neutral axis beyond the steel. If more realistic estimates of the time-to-initiation are to be produced, this requires integration of the effects of cracking on diffusion-driven chloride entry. Due to the rapid ingress of chlorides reported through cracked concrete, it can be assumed that corrosion has initiated on a large number of concrete structures, some of which may show no visible signs of the process.

This propagation period can continue without a significant effect on the serviceability and ultimate capacity and for structures achieving the design service life, it is likely that propagation will have already begun to occur. Propagation of the corrosion and the effective structural response must therefore be considered.

2.6 PROPAGATION OF SUB-SEA REINFORCEMENT CORROSION

2.6.1 SCOPE

Reinforcement corrosion can be complex and, for sub-sea structures, it is not yet completely understood. The conditions facilitating corrosion are explored, along with the mechanisms of action and the formation of corrosion products.

It is widely accepted that, over time, chlorides from seawater will reach the steel-concrete interface and break down the passive layer on the steel. The flux of chloride ions to the steel has a large effect on the metal's polarised potential and, as a result, the rate of propagation of corrosion.

It is commonly assumed that sub-sea areas of marine or offshore structures experience protection from corrosion due to the low oxygen concentrations in the water. Recently there have been two contradictory reports (Hussain, 2011; Toro, 2011) on corrosion in low oxygen environments, with one suggesting that corrosion is negligible, and the other that corrosion rates are still significantly high. Further work is required on the effects of oxygen concentrations on corrosion in order to determine the rate of corrosion on unloaded and loaded sub-sea concrete needed for expected life modelling.

As with initiation, cracks caused by static or dynamic loading can increase the rate of corrosion. The effects of crack widths, depths, and loading patterns are reviewed and experimental works on areas with insufficient data are carried out. Modelling of propagation is then reviewed and its suitability for sub-sea concrete structures assessed.

2.6.2 MECHANISMS OF CORROSION

Corrosion of the steel can occur by a variety of mechanisms, most commonly due to attack from chlorides, sulphates or a drop in pH caused by carbonation of the concrete pore solution. As service life is commonly modelled on the time taken for the mass of chlorides at the surface of the steel reinforcement to reach a critical chloride threshold level, C_{crit}, corrosion propagation rates are often ignored. In this situation, the propagation time, t_p, is often assumed to be constant (Life365 Consortium II, 2012).

During this propagation phase, anodic and cathodic reactions will commonly occur at the steel surface (Figure 2.9). At the anodic area of reinforcement, corrosive products form on the surface of the steel as the metallic ions, most commonly Fe^{2+}, are each released along with two electrons (Equation 2.16) (Isgor and Razaqpur, 2006; Warkus, Raupach and Gulikers, 2006). The cathodic reaction is typically the breakdown of oxygen and water into hydroxyl ions, consuming the electrons released by the anodic reactions. The resulting hydroxyl ions then react with the metallic ions producing corrosive products (Böhni, 2005).

As corrosion is occurring, both the anodic and the cathodic reactions should be balanced. If the dominant cathodic reaction is the breakdown of oxygen, the supply of oxygen to the area of reinforcement acting as a cathode will have a critical effect on the rate of corrosion. This supply of oxygen will also have an effect on both the size of the anode and cathode and the corrosion mechanism taking place (Warkus, Raupach and Gulikers, 2006).

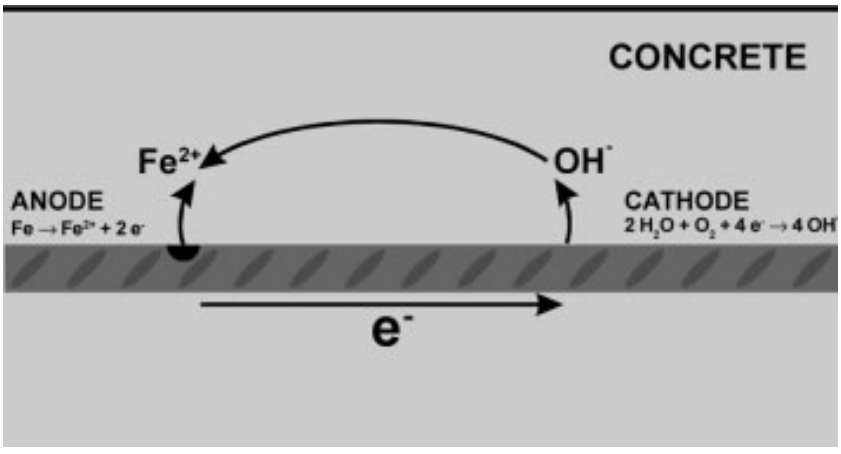

FIGURE 2.9 MACROCELL CORROSION ALONG AN INDIVIDUAL BAR (WARKU, RAUPACH AND GULIKERS, 2006)

In this subsea environment, anodic reactions occur when the chlorides have broken down the passive layer of steel reinforcement. Iron ions are released from the steel (Equation 2.16)

(Raupach, 2006), and often react with hydroxyl ions to form ferrous hydroxides, $Fe(OH)_2$, or ferrous oxides, FeO (Equation 2.17 and Equation 2.18).

$$Fe \rightarrow Fe^{2+} + 2e^{-} \quad \text{EQUATION 2.16}$$

$$Fe^{2+} + 2(OH)^{-} \rightarrow Fe(OH)_2 \quad \text{EQUATION 2.17}$$

$$Fe^{2+} + 2(OH)^{-} \rightarrow FeO + H_2O \quad \text{EQUATION 2.18}$$

The chlorides act as a catalyst in these reactions and, if there is a lack of available hydroxyl ions near the anode, complex transient iron chlorides can be formed which can transport the iron ions away from the steel surface. These could then react with hydroxyl ions available in the concrete pore solution, causing corrosive products to be formed throughout the concrete structure (Equation 2.19) (Rosenberg et al., 1977). This allows for further corrosion to occur at the steel surface, and will be observed as a loss of cross sectional area without a build-up of ferrous hydroxides on the steel surface.

$$Fe^{2+} + Cl^{-} \rightarrow [FeCl\ complex]^{-} \quad \text{EQUATION 2.19}$$

Cathodic reactions that commonly occur to produce hydroxyl ions are the breakdown of oxygen and water (Equation 2.20) or the breakdown of water where oxygen is not available (Equation 2.21).

$$O_2 + 2H_2O + 4e^{-} \rightarrow 4(OH)^{-} \quad \text{EQUATION 2.20}$$

$$2H_2O + 2e^{-} \rightarrow H_2 + 2(OH)^{-} \quad \text{EQUATION 2.21}$$

It is acknowledged that corrosion requires a cathodic reaction to occur (Böhni, 2005), as the electrons released from the oxidation of iron at the anode must be consumed elsewhere. Oxygen, in contrast, is not necessarily required for the corrosion of the steel to occur, as demonstrated by Equation 2.19 and Equation 2.21. It should be noted, however, that hydrogen evolution from water, is extremely unlikely in natural environments within a concrete structure.

Jiang and Yuan (2012) suggest that with atmospheric or saturated concrete with high dissolved oxygen concentrations, the corrosion rate is not controlled by the cathodic reaction. Once corrosion has initiated, it is believed that some corrosion products with high-valence iron ions replace oxygen as a new depolarization agent in the cathode process (Equation 2.22 - Equation 2.25).

$$8FeOOH + Fe^{2+} + 2e^{-} \rightarrow 3Fe_3O_4 + 4H_2O \qquad \textbf{EQUATION 2.22}$$

$$Fe^{3+} + e^{-} \rightarrow Fe^{2+} \qquad \textbf{EQUATION 2.23}$$

$$Fe_3O_4 + H_2O + 2e^{-} \rightarrow 3FeO + 2OH^{-} \qquad \textbf{EQUATION 2.24}$$

$$Fe(OH)_3 + e^{-} \rightarrow Fe(OH)_2 + OH^{-} \qquad \textbf{EQUATION 2.25}$$

Furthermore, it is possible that, owing to the lack of oxygen and the availability of nutrients within the seawater, sulphate reducing bacteria (SRB) could be the predominant propagation mechanism in an anaerobic environment after a period of diffusion-based corrosion (Melchers and Wells, 2006). Energy sources known to be important for the metabolism of SRB are carbon, hydrocarbons and hydrogen, all of which are available in immersed steel environments. It is generally accepted that anaerobic conditions bring about corrosion of the steel due to action of metabolites, predominantly hydrogen sulphides, resulting from SRB activity. The resultant reduction in the alkalinity of the surrounding area further increases the corrosion rate of the steel (Figure 2.10).

Although this mechanism merits consideration, corrosion propagation will continue without the presence of oxygen due to the variation in electrochemical properties along the reinforcement, with or without the presence of SRBs. It is therefore to be assumed for modelling purposes that alternative mechanisms will be dominant.

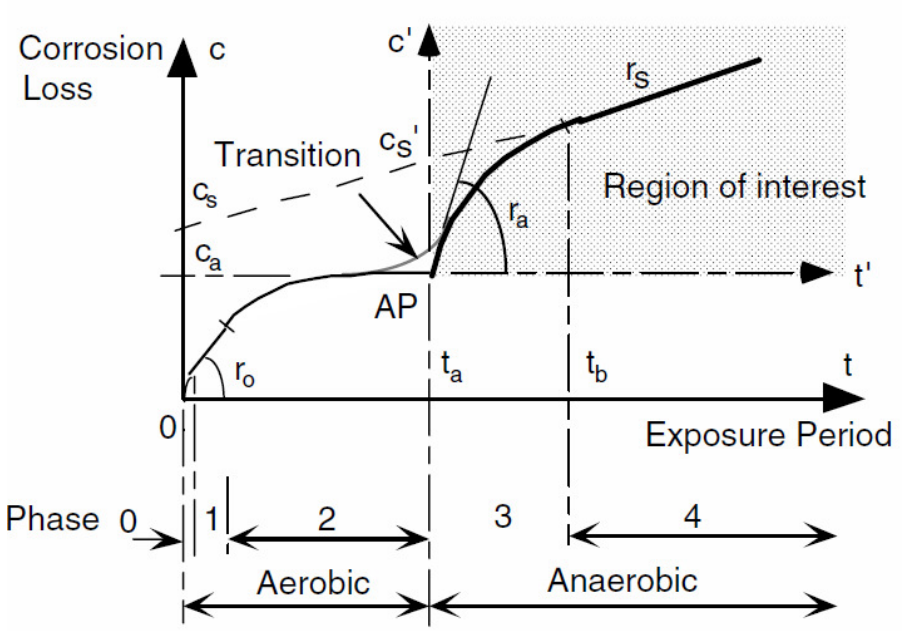

FIGURE 2.10 POSSIBLE 4 PHASE MECHANISM OF CORROSION OF STEEL IN A MARINE ENVIRONMENT (MELCHERS AND WELLS 2006)

Corrosion mechanisms are often reported to be one of two forms: microcell or macrocell. Microcell corrosion is defined as a situation when corrosion occurs on adjacent areas of the same metal, whilst macrocell is often described as corrosion occurs between two coupled sections of metal. A combination of macrocell and microcell currents can be superimposed to determine the total corrosion current (Hansson, Poursaee and Laurent, 2006).

Although macrocell corrosion is commonly associated with multiple steel reinforcing bars, a macrocell type effect can occur along an individual bar, depending on localised changes in environment at the surface. Examples of such surface variations include chloride attack through cracking (Warkus and Raupach, 2008) and changes in oxygen concentrations (Warkus, Raupach and Gulikers, 2006).

In addition, large-scale macrocell corrosion can occur where a structure may have different exposure surfaces. In a situation where one face of the concrete is exposed to the atmosphere and the other submerged, such as a tunnel or hollow leg, a large corrosion current is possible, as shown in Figure 2.11 (Polder and Larbi, 1995).

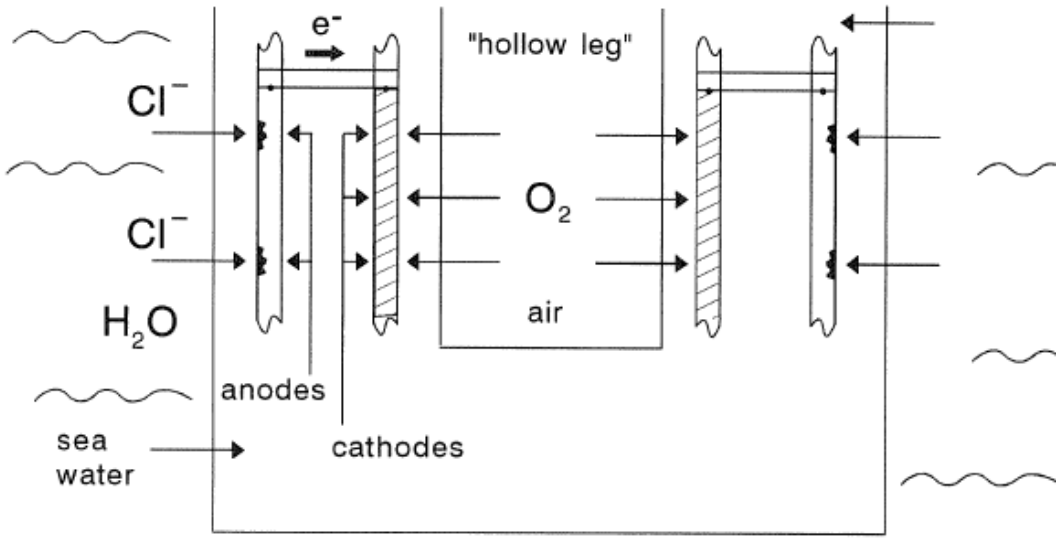

FIGURE 2.11 SCHEMATIC REPRESENTATION OF MACROCELL CORROSIO IN A HOLLOW LEG (POLDER AND LARBI, 1995)

2.6.2.1 CORROSION PRODUCTS

Corrosive products that form on reinforcing bars are commonly divided into two categories: 'red rust' and 'black rust'. 'Red rust' is typically a form of ferrous hydroxides ($Fe(OH)_2$), ferrous oxides (FeO) or ferric oxides (Fe_2O_3).

'Black rust' is likely to be formed on the surface of steel due to anaerobic conditions by submersion or burying. This variety of rust is most commonly magnetite (Fe_3O_4), which can be formed by the Schikorr reaction (Equation 2.26).

$$3Fe(OH)_2 \rightarrow Fe_3O_4 + 2H_2O + H_2 \qquad \textbf{EQUATION 2.26}$$

Other, more complex methods of determining the propagation make use of resistor networks, finite element models and boundary element models. These models increase in accuracy with increasing complexity but more input data are required to accurately determine the corrosion conditions in 'real world' structures.

For the structures that are to be assessed in this research project, there is very limited data on corrosion that may or may not be occurring at present. Due to this lack of information, a simplistic probabilistic model is required to determine the rate of propagation. Experimental work aimed at improving the understanding of corrosion under low-oxygen subsea conditions and static and dynamic loading is proposed in Chapter 3.

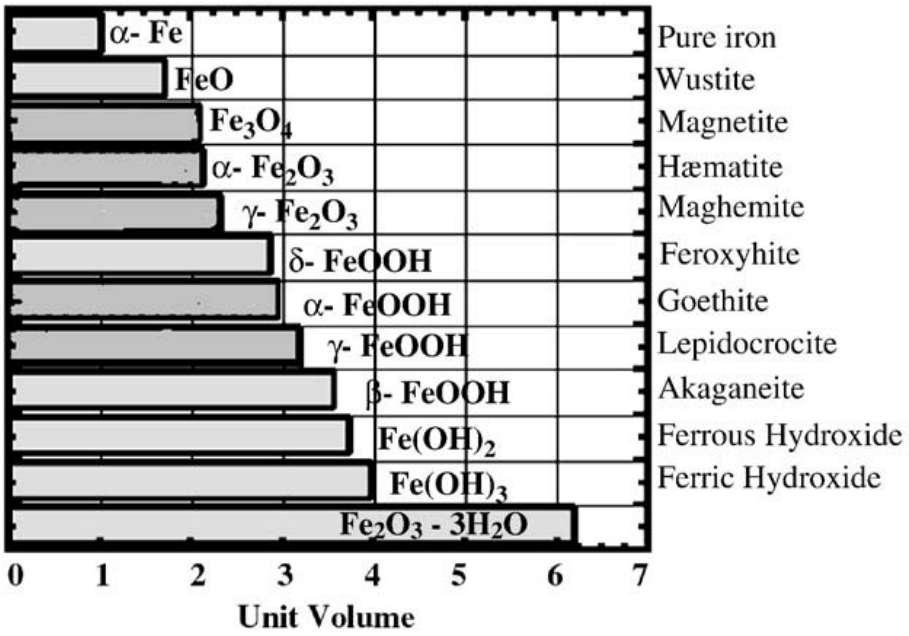

FIGURE 2.12 UNIT VOLUME OF IRON OXIDE PRODUCTS (JAFFER AND HANSSON, 2009)

2.6.2.2 EFFECTS OF SEAWATER OXYGEN CONCENTRATION

> "Only for the constantly submerged parts of high quality concrete structures, the availability of oxygen is generally so low that an electrochemical corrosion of embedded steel does not represent any practical problem" Det Norske Veritas (2006)

Throughout industry, it is commonly assumed submerged concrete will not corrode due to extremely low oxygen concentrations in the subsea environment. Although rates of corrosion are expected to be reduced, the notion of ignoring the corrosion of submerged concrete should be challenged. Dissolved oxygen concentrations at the seabed can be as high as 380 μmol/L, equivalent to around 6 ppm. The seabed typically has between 2 to 6 ppm dissolved oxygen, with oxygen concentrations increasing towards the surface of the water (Schlüter and Jerosch, n.d.).

Gjørv, Vennesland and El-Busaidy (1986) believe the corrosion current is directly limited by the oxygen concentration at the surface of the steel in a chloride-laden environment. The results of oxygen diffusion experiments, presented in Table 2.14, are reported as diffusion coefficients and oxygen flux given by:

$$J = \frac{D}{\delta} \cdot \Delta c \qquad \textbf{EQUATION 2.27}$$

Where;

J oxygen flux, mol / (s·cm^2)

D diffusion coefficient, cm^2 / s

δ thickness of concrete, cm

Δc oxygen concentration gradient, mol / cm^3

Page and Lambert (1987) suggest that under extremely low oxygen exposure, the supply of oxygen to a cathodic reaction required to maintain an anodic 'leakage' current does not exist. The continuous passive film on the steel surface would then break down. In this case, a slow general dissolution of the steel could occur, limited by the availability of oxygen. The researchers differentiate between passivity, low oxygen corrosion, active oxygenated corrosion and the potential for galvanic corrosion due to interactions between exposed metals and reinforcement, although the likelihood of a combination of these mechanisms is high making corrosion difficult to model.

Work carried out by Raupach (1996) on the influence of oxygen on corrosion of steel indicates that the diffusion of oxygen is a limiting factor on the corrosion of concrete structures in a fully-saturated state. It is thought that once all remaining oxygen within the concrete is consumed, the corrosion rate will be only influenced by the oxygen concentration of the surroundings and the diffusion coefficient.

TABLE 2.14 MEASURED OXYGEN DIFFUSION AND FLUX THROUGH CONCRETE AND MORTAR (GJØRV, VENNESLAND AND EL-BUSAIDY, 1986)

Material	Thickness, mm	D (x10^{-6}), cm^2/s			J (x10^{-13}), mol/(cm^2 s)		
w/c ratio		0.4	0.5	0.6	0.4	0.5	0.6
Mortar	10		1.3	1.7		5.2	6.8
	20		2.1	3.0		4.3	6.0
	30		2.4	3.2		3.2	4.3
	50		3.2	3.8		2.6	3.0
	70		3.4	4.3		1.9	2.5
Concrete	10	2.1	2.5	3.7	8.4	10.0	14.8
	20	3.5	4.2	6.6	7.0	8.4	13.2
	30	3.9	5.2	7.9	5.2	7.0	10.6
	50	5.0	6.2	7.2	4.0	5.0	5.8
	70	5.7	6.8	11.1	3.3	3.9	6.4

It is suggested that a limiting value for the cathodic current is;

$$i_{lim} = \frac{M}{2.591 \times 10^{-6}} \qquad \textbf{EQUATION 2.28}$$

Where;

i_{lim} limiting cathodic current, A/cm^2

M molar flux of oxygen at the surface of the cathode, as adopted in an alternative model by Maruya et al. (2003), mol/(s·cm^2)

Subsequently, Song and Liu (2000) suggest that when concrete is fully saturated, oxygen-diffusion-controlled corrosion occurs, limited at the cathode by Equation 2.29, which, once rearranged, is identical to the equation proposed by Raupach (1996a; 1996b).

$$i_{lim} = n_c \cdot F \cdot D_{ox} \cdot \frac{[O_2]^0}{c} \qquad \textbf{EQUATION 2.29}$$

Where;

i_{lim} limiting cathodic current, A/m²

D_{ox} oxygen diffusion coefficient, m²/s

c concrete cover, m

F Faraday's constant, 96,500 C/mol

$[O_2]^0$ oxygen concentration on the surface, mol/m³

n_c constant (=4)

Further work by Warku, Raupach and Gulikers (2006) derive the limiting cathodic current to be;

$$i_{lim} = 3.62 \cdot 10^9 \cdot \frac{D_{ox}}{c} \cdot \frac{A_{con}}{A_{steel}}$$ **EQUATION 2.30**

Where;

i_{lim} limiting cathodic current, A/m²

D_{ox} oxygen diffusion coefficient, m²/s

c concrete cover, mm

$\frac{A_{con}}{A_{steel}}$ concrete surface to steel surface ratio (only applicable if ≤1.0)

Linking the limiting current to the oxygen diffusion coefficient assumes the cathodic reaction causing corrosion in the cell is the breakdown of oxygen and water. Should this be the case, it must be noted that the concentration of oxygen at the surface of the concrete is modelled to have no effect on the corrosion process.

For a concrete with a w/c ratio of 0.4, similar to offshore platforms, and a cover of 50mm:

$D = 5 \times 10^{-6}\ cm^2/s$

$J = \frac{5 \times 10^{-6}}{5} \cdot 1.5 \times 10^{-6} = 1.5 \times 10^{-12}\ \ mol/(cm^2 s)$

The limiting cathodic current is calculated using the methods in the discussed models and is presented in Table 2.15.

TABLE 2.15 LIMITING CATHODIC CURRENTS AS DETERMINED BY VARIOUS DISCUSSED MODELS

Model	Limiting current, μA/cm²
Raupach, 1996	0.58
Song and Liu, 2000	0.58
Warku, Raupach and Gulikers, 2006	3.62

The difference between the Warkus, Raupach and Gulikers (2006) model and the other two is significant, although all results do not limit the corrosion current substantially in oxygen-saturated water for the given exposure conditions. Due to the rapid diffusion of oxygen through water and concrete in an oxygenated environment such as the North Sea, the mechanism is unlikely to be substantially restricting the corrosion rate within the concrete.

Experimental work by Hussain (2011) explores the effect of moisture variation on the consumption of oxygen in the cathodic reaction of corroding steel. Results show that a limiting current density of 0.04μA/cm² is achieved for completely submerged concrete. This is in contradiction with previous studies (Raupach, 1996; Warkus, Raupach and Gulikers, 2006), where the limiting currents are more than an order of 10 greater.

Additionally, this does not appear to take into account any variations in the oxygen content of the water surrounding the specimen. If the corrosion current is limited by oxygen consumption, this, in turn, will then be limited by oxygen diffusion and the surface concentration of oxygen. The research makes no reference to, nor does it appear to control, the concentration of oxygen in the water.

It is stated that this low value is "actually of not much significance" (*Hussain 2011*). This is a crude judgement, as the research does not take into account the possibility of large cathodes in relation to small anodes and, therefore, the possibility of large corrosion currents still occurring in the concrete.

Contradictory research, conducted by Toro et al. (2011), concludes that although negligible oxygen concentrations were recorded in a calcium hydroxide solution, corrosion still occurred at significant rates of up to 5μA/cm². It is suggested that the chloride content and roughness

of reinforcing steel surface are the critical components of corrosion in these environments with low oxygen availability.

As this topic of research is vital, an in-depth understanding of the corrosion rates in sub-sea low-oxygen environments is required. There is currently no further work either to support, or oppose the belief of insignificant corrosion in submerged low-oxygen concrete environments. This is due to the majority of research concentrating on the splash and tidal zones, rather than the submerged area of concrete specific to a subsea structure. For this reason, it is imperative that corrosion in low-oxygen environments with a controlled oxygen concentration is the subject of investigation.

2.6.2.3 Effects of pore saturation and resistivity

Bertolini et al. (2013) indicate that corrosion currents are a balance between current flowing through the metal and concrete and the exchange currents of the anodic and cathodic processes (Figure 2.13). These currents will both be limited by the resistance of each process. The metallic resistance is extremely low and, consequently, is unlikely to be rate controlling. Depending on the nature of the exposure and resistivity of the concrete, the exchange rate at the anode or cathode could be limiting, but the resistivity is more commonly described as the limiting factor. As a result, research has often focussed on the relationship between resistivity and corrosion rate (Hornbostel, Larsen and Geiker, 2013).

Pore saturation, driven predominantly by moisture content at the surface of the concrete, is the most significant influence on the corrosion propagation rate assuming a chloride-saturated concrete. Pore saturation reduces the resistivity and, in turn, increases the corrosion rate of the steel (Warkus and Raupach, 2008). A clear indication of the dominating effect of resistivity is shown in Figure 2.14.

The ionic resistivity is an important factor influencing the potential for macrocell corrosion. In HPC concretes where the ionic resistivity is high, a very low macrocell to microcell corrosion ratio has been observed and this suggests that, although the rates were small, only microcell corrosion was occurring (Hansson, Poursaee and Laurent, 2006).

Although the resistivity has a significant effect on corrosion rate, the spread of results from 'real world' and laboratory studies is large (Figure 2.15). Due to this spread in results, the author believes that resistivity measurements could be used to identify structures that could be at risk of corrosion, allowing further investigations to be carried out.

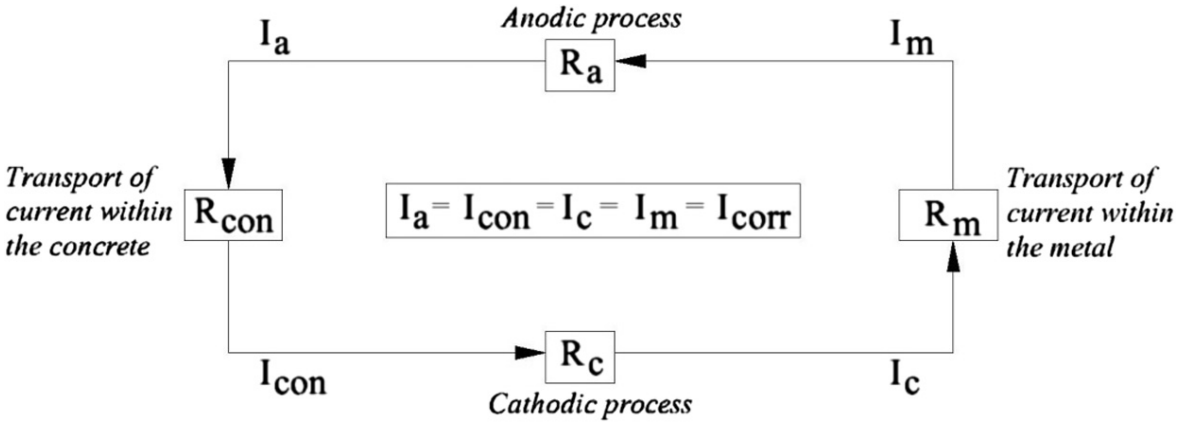

FIGURE 2.13 ELECTROCHEMICAL MEHANISM OF REINFORCEMENT CORROSION (HORNBOSTEL, LARSEN AND GEIKER, 2013; BERTOLINI ET AL., 2013.)

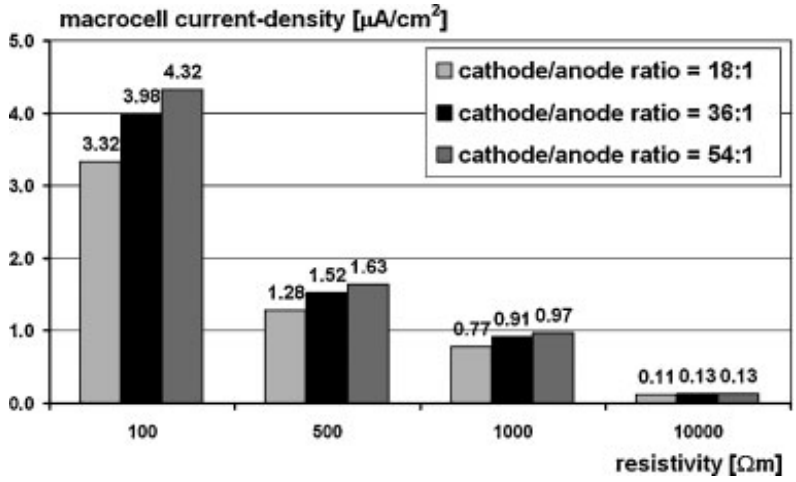

FIGURE 2.14 EFFECT OF RESISTIVITY ON MACROCELL CORROSION RATE (EXTRACT FROM WARKUS AND RAUPACH, 2008)

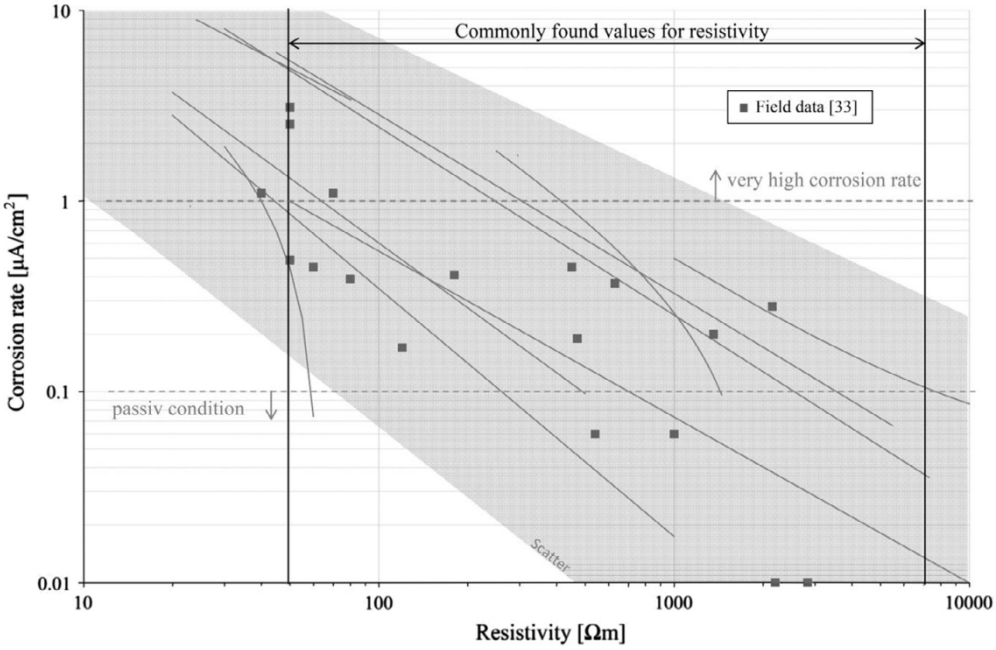

FIGURE 2.15 MEASURED RESISTIVITY AND CORROSION RATES (HORNBOSTEL, LARSEN AND GEIKER, 2013)

2.6.2.4 EFFECTS OF LOADING AND CRACKS

Offshore structures are subjected to severe wind, wave and tidal loading. These regular loading patterns can cause large bending moments in structures, which may result in cracking. These cracks, under serviceable limit states, are designed to be restricted to 0.3mm, as discussed in Section 2.5.2.4.

Cracking can accelerate corrosion by increasing the ingress of water, chlorides and oxygen (Scott, 2007; Subramaniam and Bi, 2010). Sections of concrete structures in flexure will crack, with surface crack widths that can be significantly large and allow for water and ions to penetrate to the steel surface. Any increase in the rate of this ingress will increase the rate of corrosion.

Cracking occurs due to tensile strains in the concrete cover, which are commonly caused by flexural loading, build-up of corrosive products, or freeze-thaw. Usually, in conditions where oxygen is available, the product formed due to corrosion is ferric oxide, Fe_2O_3. Ferric oxide, commonly known as 'red rust', has a crystal density roughly four times that of a steel compound with equivalent mass. This expansive product causes localised tensile strains around the reinforcement, resulting in cracking of the cover and subsequent spalling.

When cracking occurs from the reinforcement out through the cover, the transport properties of the concrete are affected in a detrimental way, allowing an accelerated flow of chlorides, oxygen and water along the crack to the reinforcing steel. The fib Model Code 2010 asserts that, for crack widths of up to around 0.2 to 0.4mm, there will be no significant effect on the rate of corrosion due to accelerated transport mechanisms. This is disputed in section 2.4, where it appears that cracking, along with loss of the aggregate-cement matrix bond in the concrete in tension, has a significant effect on corrosion by means of faster transport of chlorides to the steel.

In CEM I concrete with covers of both 20 and 40mm, Scott and Alexander (2007) recorded an increase in corrosion current of around 20% as the surface crack width was increased from 0.2 to 0.7mm. Although there was an increase, the difference between the recorded values is insignificant when compared to the influence of supplementary cementitious materials or cover depth.

Where a flexural crack is formed, the relationship between the macrocell corrosion current and measured potential can be estimated by the polarization responses of the anodic steel at the crack and passive steel elsewhere in the concrete. The macrocell current density is 31 times the microcell current and is therefore the dominant mechanism in cracked concrete (Subramaniam and Bi, 2010).

Contradicting the above views, research carried out by Dang and François (2013) concluded that corrosion appeared heterogeneous in distribution along the perimeter and length of reinforcing bars with the initial crack pattern having no bearing on long term corrosion. Corrosion was shown to occur across the majority of the section; however, in the environmental conditions of the specimens, it is likely that general corrosion would have occurred during duration of the experiment.

Considering the evidence presented, the author has no doubt that cracking increases the corrosion rate. There is, however, minimal information on the dynamics of this relationship and experimental work should be carried out with the aim of quantifying the expected increase in corrosion rate.

2.6.3 MEASURING CORROSION PROPAGATION

2.6.3.1 HALF-CELL POTENTIAL

Using half-cell measurements can be a fast and effective method for providing an indication of the likelihood of corrosion within concrete. This is performed by connecting one lead of a high impedance voltmeter to the steel and the other to a reference electrode placed on the concrete surface (Figure 2.16) (BRE, 1998). Different standard reference electrodes can be used, with readings taken on an electrode referred back to a standard hydrogen electrode, as shown in Figure 2.17.

Simplistically, the measurements can be evaluated using Table 2.16, where the likelihood of corrosion is presented for various half-cell potential measurements. These have been developed through data collected from bridges subjected to de-icing salts in the United States and, as a result, are unlikely to be representative of all structures.

It is noted that readings from areas of low resistivity can affect the results of half-cell measurements because an electrical conductivity exists between corroding and non-corroding environments (BRE, 1998). Furthermore, areas where oxygen is restricted can lead to very negative readings that are not necessarily indicative of corrosion. Typical ranges of half-cell potentials are shown in Table 2.17 (RILEM TC 154-EMC, 2003). Although these are typical of concrete in the given conditions, the effects of further factors that could affect submerged concrete half-cell measurements are outlined in Table 2.18 (Gu and Beaudoin, 1998). Therefore, half-cell potentials should be used with other tests (i.e. linear polarisation resistance) to evaluate the likelihood and rate of corrosion.

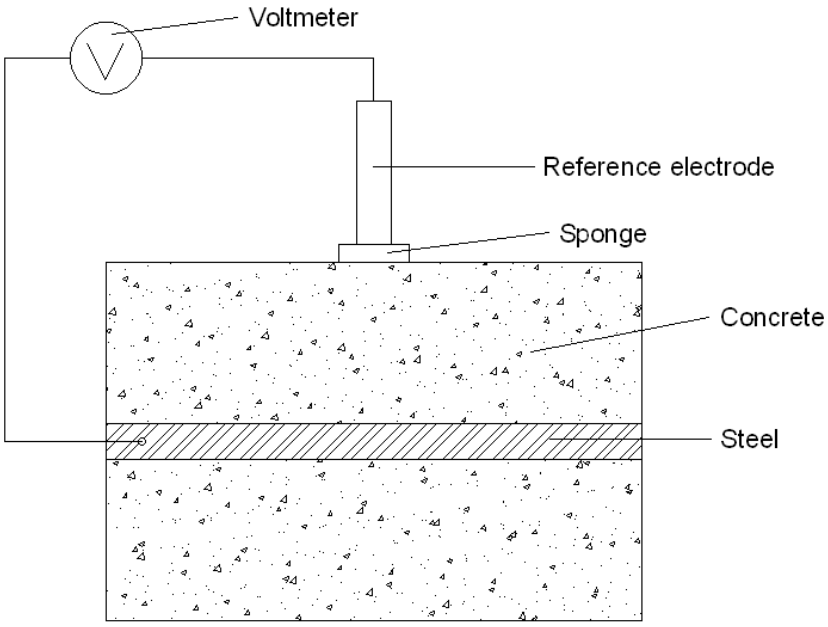

FIGURE 2.16 SCHEMATIC OF A HALF-CELL MEASUREMENT

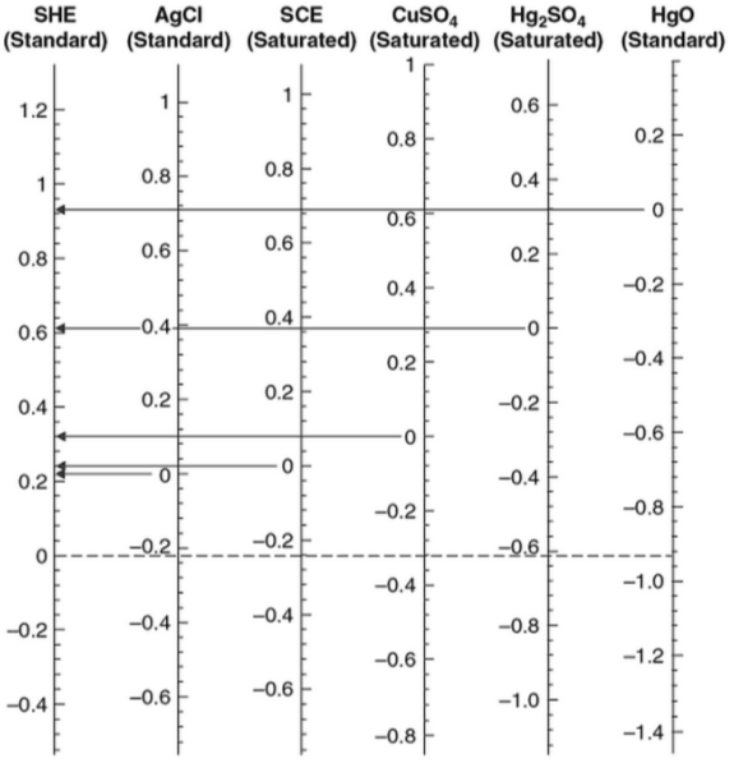

FIGURE 2.17 GRAPHICAL REPRESENTATION OF A COMPARISON OF TYPICALLY USED REFERENCE ELECTRODES

TABLE 2.16 INTERPRETATION OF HALF-CELL POTENTIAL MEASUREMENTS

Half-cell potential[#] (vs $Cu/CuSO_4$)	Half-cell potential (vs Ag/AgCl)	Half-cell potential (vs SCE)	Likelihood of corrosion
E > -200mV	E > -109mV	E > -154mV	<10%
-200 < E < -350mV	-109 > E > -259mV	-154 > E > -314mV	Uncertain
E < -350mV	E < - 259mV	E < - 314mV	>90%

[#] obtained from Gu and Beaudoin, 1998

TABLE 2.17 TYPICAL RANGES OF HALF-CELL POTENTIAL MEASUREMENTS IN CONCRETE (RILEM TC 154-EMC, 2003)

Condition	Potential, V vs. CSE
Water saturated concrete w/o oxygen	-0.9 to -1.0
Wet, chloride contaminated concrete	-0.4 to -0.6
Humid, chloride free concrete	+0.1 to -0.2
Humid, carbonated concrete	+ 0.1 to -0.4
Dry, carbonated concrete	+ 0.2 to 0
Dry concrete	+ 0.2 to 0

TABLE 2.18 POTENTIAL EFFECT OF SOME FACTORS ON HALF-CELL MEASUREMENTS (GU AND BEAUDOIN, 1998)

Situation	Half-cell potential shift	Corrosion of reinforcement
Decrease in oxygen concentration	Negative	May not increase
Carbonation, decrease in pH	Negative	Increase
Increase in chloride concentration	Negative	Increase
Epoxy-coated rebar	Positive	Not related
Dense concrete cover	Negative	Not related
Dry concrete	Positive	Not related

2.6.3.2 LINEAR POLARIZATION

Linear polarization analysis is a three-electrode method using reference, working and counter electrodes. A galvanostatic method, whereby a current is applied and the potential recorded, or a potentiostatic method, where a potential is applied and the current monitored, is used to determine the polarization resistance with Equation 2.31 (Stern and Geary, 1957).

$$R_P = \frac{\Delta E}{\Delta I} \qquad \text{EQUATION 2.31}$$

Where;

ΔE change in potential, mV

ΔI change in current, mA

R_P polarization resistance, Ω

The change in potential must be small, between 10 and 30mV about the open circuit potential, to fall in the linear Stearn-Geary range (Enos and Scribner, 1997; Song and Saraswathy, 2007).

$$i_{corr} = \frac{B}{R_P}$$ **EQUATION 2.32**

Where;

i_{corr} corrosion current, mA

B Stearn-Geary constant, mV

R_p polarization resistance , Ω

B is often simplified as 26mV for active corrosion and 52mV for passive conditions; however, this value has been reported to be between 75-278mV (Poursaee, 2010b). From experimental results, B can be determined through Equation 2.33.

$$B = \frac{\beta_A \cdot \beta_C}{2.303 \cdot (\beta_A + \beta_C)}$$ **EQUATION 2.33**

Where;

B Stearn-Geary constant, mV

β_A Anodic tafel slope, mV

β_C Cathodic tafel slope, mV

From the determined corrosion current (Equation 2.32), Faraday's laws of electrolysis can be applied to determine the mass loss of the steel due to corrosion:

$$m = \frac{Q}{F} \cdot \frac{M}{z}$$ **EQUATION 2.34**

Where;

m mass loss of metal, g

Q total charge passed $\left(= \int_0^T I \cdot dt\right)$, C

M molar mass of the metal, g

F Faraday's constant ($= 96{,}485\ C\ mol^{-1}$)

z valency number

If the polarization area is known, the corrosion current is commonly divided by the polarization area and presented in the form $\mu A/cm^2$. Interpretation of the results is shown in Table 2.19.

TABLE 2.19 INTERPRETATION OF CORROSION CURRENTS (MCCARTER AND VENNESLAND, 2004)

Corrosion current, $\mu A/cm^2$	Corrosion condition
< 0.1	Passive
0.1 - 0.5	Low to moderate
0.5 - 1.0	Moderate to high
> 1.0	High

Care must be taken when determining the polarization area, as results will vary significantly if the wrong area is used. Employing embedded electrodes with known area will allow for a known polarized area and should provide an accurate estimate of the corrosion rate. A schematic for measuring the resistance is shown in Figure 2.18.

Millard et al. (2001) investigated the effects of environment, temperature and humidity, on LPR measurements. It was concluded that the LPR measurements are insignificantly affected by short-term drying, while the concrete solution resistance is greatly affected by this process. The effects of temperature were, however, observed to be significant, albeit with a large scatter in the measured results. The authors reported that a number of LPR measurements should be taken over time to provide a reliable average corrosion current estimate.

2.6.3.3 POTENTIODYNAMIC POLARIZATION SCAN

A potentiodynamic polarization scan can be used to determine the corrosion rates, pitting potential, passivity and cathodic behaviour of metals (Enos and Scribner, 1997). The experimental setup for measurements is identical to that used for linear polarization (Figure 2.18).

The Tafel slope for the anodic and cathodic polarization can be obtained from the slope of the linear section of the curves (Figure 2.20). Extrapolating back along the slope to the point at

which the cathodic and anodic currents are equivalent will provide both the corrosion potential, E_{corr}, and current density, i_{corr}.

Results obtained can be sensitive to the applied potential scan rate (Poursaee, 2010a). If the scan rate is too rapid, it is possible to misinterpret the results as suggesting a lack of corrosion. If the scan rate is too slow, however, corrosion could significantly change during the course of the testing. According to the ASTM G5-94 (ASTM, 2004) standard, the recommended scan rate for concrete is 0.166mV/s; however, a faster rate may be used to prevent concrete samples from drying or altering their corrosion behaviour, as discussed in Chapter 3.

2.6.3.4 GRAVIMETRIC

Weight loss measurements can be useful for laboratory studies but are impractical for work on operational structures. This method determines the weight loss of the steel through the use of Equation 2.35.

$$m_{loss} = m_{initial} - m_{final} \qquad \textbf{EQUATION 2.35}$$

Where;

m_{loss} loss of mass, g

$m_{initial}$ measured mass prior to corrosion, g

m_{final} measured weight after corrosion, g

Inaccuracies can arise due to the difficulty in removing all hydrated cement from the reinforcement after destructive testing. Due to the small nature of the weight loss and the difficulty with cleaning the bars, this method is more suitable for estimating the losses due to intense corrosion.

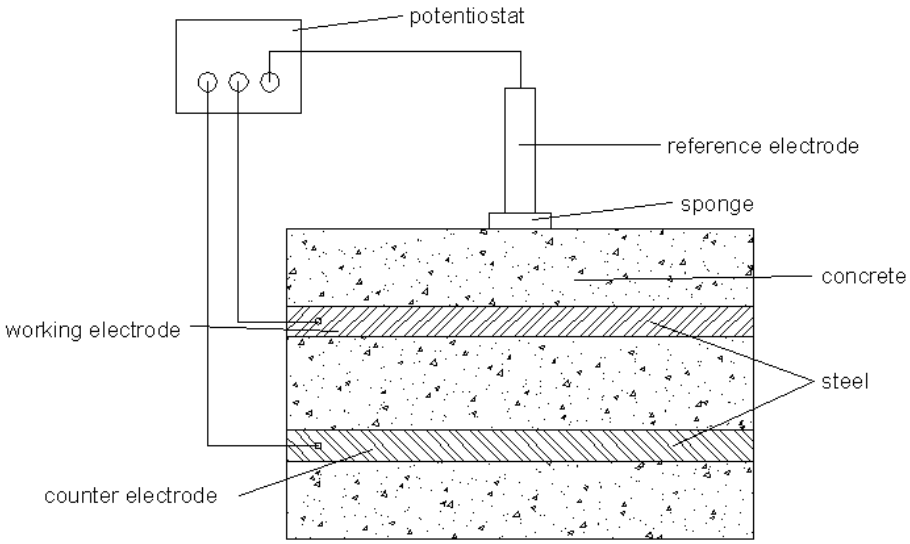

FIGURE 2.18 SCHEMATIC OF A LINEAR POLARIZATION RESISTANCE AND POTENTIODYNAMIC METHOD

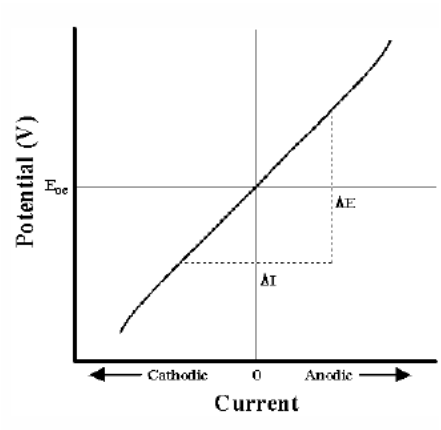

FIGURE 2.19 LINEAR POLARIZATION TECHNIQUE (ENOS AND SCRIBNER 1997)

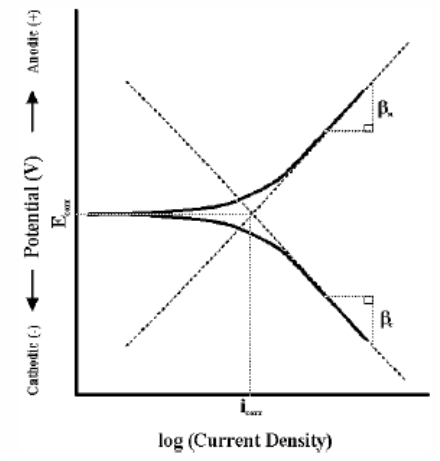

FIGURE 2.20 CALCULATION OF TAFEL SLOPES (ENOS AND SCRIBNER 1997)

2.6.3.5 ELECTRICAL RESISTANCE

After depassivation, a relationship can be expected between the resistance of the concrete and the rate of corrosion (Polder, 2001). On-site measurement of concrete resistance is often achieved through the use of a Wenner (4-point) probe (Figure 2.21). The relationship between the potential drop and induced current is used to determine the resistance. Alternatively, disc methods with one, two or four electrodes can be used.

Due to the inhomogeneity of the concrete, care must be taken when predicting corrosion rates through the use of resistance. Measurements must be sufficiently far away from any reinforcement or other forms of disturbance to the concrete. A dry surface layer of the concrete may also provide artificially low corrosion rates, particularly if the concrete around the reinforcement is most saturated.

A simple relationship developed as a guideline to estimate the risk of corrosion is shown in Table 2.20 (McCarter and Vennesland, 2004).

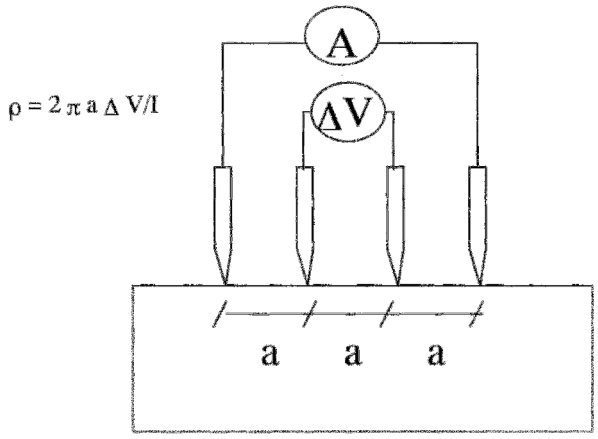

FIGURE 2.21 WENNER (4-POINT) PROBE SCHEMATIC (POLDER, 2001)

TABLE 2.20 RISK OF CORROSION DUE TO MEASURED RESISTIVITY (POLDER, 2001)

Concrete resistivity, kΩ·cm	Risk of corrosion
< 5	Very high
5-10	High
10 – 20	Low to moderate
> 20	Low/negligible

2.6.4 MODELLING OF CORROSION PROPAGATION RATES

In practice, corrosion is typically modelled in two phases: initiation and propagation (Tretheway and Chamberlain, 1988; Bertolini, 2004; and Böhni, 2005). The propagation period has been extensively modelled and previously reviewed by Raupach (2006), followed by work on the theoretical background and a regeneration of models carried out by a number of researchers (Warkus, Raupach and Gulikers, 2006; Gulikers and Raupach, 2006).

Otieno, Alexander and Beushausen (2011) are highly critical of accelerated laboratory testing and suggest that corrosion modelling should be validated through investigations on 'real world' structures. While their point is valid, the use destructive testing to further understanding of the development of anodic and cathodic areas, actual corrosion rates and the effects on structures is unfeasible. For this reason, a compromise must be achieved between these two methods of investigation.

Work using resistivity to model propagation has yielded estimates for the corrosion rate at certain levels of resistivity. Those specimens with a high resistivity will have low corrosion rates and vice versa.

Raupach (2006) explores work completed by Takewaka, Yamaguchi and Maeda (2001) in which a model is developed for the deterioration of steel due to chloride attack. Propagation is said to be limited by the slower of the anodic and cathodic reactions taking place. However, should the cathodic reaction be slower, it is likely there will be a rebalance of anodic and cathodic areas to maintain a balanced rate of corrosion.

Empirical methods involving experimental work in many conditions were used to assess the impact of these conditions on the corrosion of steel plates. Factors for each variable could then be applied and combined to provide an estimation of the rate of corrosion. One such proposed model uses three applied factors; cement content, w/c ratio and chloride content;

$$I_{corr} = 37.726 + 6.120C + 2.231\,A^2B + 2.722\,B^2C^2 \qquad \textbf{EQUATION 2.36}$$

Where;

A, B, C factors depending on w/c ratio, cement content and chloride content of concrete

This methodology is extremely simplistic because corrosion propagation rates are dependent on environmental conditions as much as, if not more than, the concrete properties. Alternative models require the use of engineering experience, using previous cases of

corrosion, to determine how future corrosion will occur. The practicality of these models is diminished by the large variations in environment and material properties and the size of the database of previous cases that would be required (Raupach, 2006).

For a predictive method to provide a reasonably accurate estimation of corrosion rate, the cathodic and anodic regions must be estimated, together with the flux of oxygen to the cathode. This, as with any method, has limitations because the cathodic and anodic areas cannot be defined as specific areas. Laboratory work can, however, be used to visually determine the formation of anodes and cathodes by destructively testing concrete that has been corroding.

More recently, Beck and Raupach (2012) developed a simplified model for determining the propagation of corrosion (Equation 2.37).

$$i_{corr} = \frac{1}{A_A}\left[\frac{E_{0,C} - E_{0,A}}{\frac{r_{p,A}}{A_A} + \frac{r_{p,C}}{A_C} + k_c \cdot \rho_c} + I_{self}\right] \qquad \textbf{EQUATION 2.37}$$

Where;

i_{corr} corrosion current density, A/m^2

A_A anode area, m^2

A_C cathode area, m^2

$E_{0,C}$ resting potential of cathode, V

$E_{0,A}$ resting potential of anode, V

$r_{p,C}$ specific integral polarization resistance of cathode, Ωm^2

$r_{p,A}$ specific integral polarization resistance of anode, Ωm^2

k_c geometry constant of macrocell, m^{-1}

ρ_c resistivity of concrete, Ωm

I_{self} self-corrosion current of macrocell, A

As with the majority of modelling techniques, although the method is simplistic, information must be gained from the structure in question. Data from an offshore structure is often

extremely difficult to determine and, for this reason, engineering estimates are often used, giving results that are extremely unreliable.

Simplifying Equation 2.37, Osterminski and Schießl (2012) provide a more simplified method for corrosion rate estimation (Equation 2.38). Although the method is relatively simple, values must be estimated or derived for individual structures.

$$i_{corr} = \frac{1}{A_A}\left[\frac{\Delta \mathrm{E}}{\mathrm{A} \cdot (C + \rho_c) \cdot \mathrm{G}}\right] \cdot f_{eigen} \qquad \textbf{EQUATION 2.38}$$

Where;

i_{corr} corrosion current density, A/m^2

A_A anode area, m^2

$\triangle E$ driving voltage, V

A anode factor

C cathodic resistivity, Ωm

ρ_c resistivity of concrete, Ωm

G geometry factor, m^{-1}

f_{eigen} eigencorrosion factor

Jiang and Yuan (2012) provide a model of corrosion propagation wherein the corrosion rate is controlled by activation polarizations, provided oxygen is easily accessible to the cathode. In saturated concrete with high concentrations of dissolved oxygen, there will be sufficient oxygen available at the cathode to render such a model useful. As shown previously, sufficient oxygen is available in a submerged North Sea environment to justify the modelling of corrosion with Jiang's method.

2.6.5 SUMMARY

Corrosion is likely to have initiated and be propagating in structures where cracking has allowed chlorides to penetrate the cover to the depth of the reinforcement. A large array of variables have been shown to be critical to the corrosion process; therefore, experimental work to determine estimates for the rate of corrosion on specific structures will be considered.

Although the propagation of corrosion within concrete structures is complex, using a combination of experimental research techniques may yield a reasonable estimation of long-term corrosion. To ensure that the conditions are representative of a real structure, consideration of the environment, concrete type and test methodology is vital (Poursaee and Hansson, 2009).

While a number of mathematical methods for the prediction of corrosion rates are available, the author believes that, due to the heterogeneous and complex structure of concrete and the inability of mathematical models to account for all variables, corrosion rates should be determined through on-site measurements. If on-site information is unavailable, as with large offshore submerged concrete structures, corrosion rates should be determined through measurements taken from experimental work carried out in laboratories.

2.7 STRUCTURAL CAPACITY OF CONCRETE

2.7.1 SCOPE

The structural capacity of a concrete structure will ultimately determine the time-to-failure of that structure under a given set of loading conditions. Taking theoretical, experimental and observed rates of corrosion and modelling the effects on the capacity of a section is difficult, owing to the complexity of the structure.

Corrosion can cause a reduction in the cross-section of the steel, a loss of bond between the concrete and the steel, a loss of ductility in the steel and, potentially, an internal stress that may lead to cracking, depending on the products formed through the corrosion process as previously discussed.

The effect of corrosion on the service and ultimate life is reviewed, assessing the links between laboratory results and 'real world' data. Additionally, methods are evaluated for prediction of the structural degradation caused by corrosion under different exposure conditions.

2.7.2 EFFECTS OF CORRODED REINFORCEMENT

2.7.2.1 REDUCED CROSS SECTION OF STEEL

It is reported that, due to the localized nature of the steel strain, reduction of the cross sectional area of steel is not the most significant factor affecting the serviceability of a concrete section. Localized losses of up to 30% did not have an effect on the mid-span deflection (Zhang, Castel and François, 2009b). Furthermore, it is noted that if corrosion propagates in a

general manner, the stiffness and, by extension, the serviceability can be dramatically reduced (Zhang, Castel and François 2009a). Ultimate strength, however, is only significantly lowered by a localised loss in the cross-sectional area of steel and the reduction in steel capacity that results.

While in partial agreement with Zhang, Castel and François, further experimental work by Dang and François (2013) concluded that the yielding moment and ultimate capacity are both reduced by the loss of cross sectional area where pitting has occurred. The reduction in yield strength will cause larger deflections at reduced loading, thus reducing serviceability. Ultimately though, the conditions at high corrosion levels still allowed for maximum moments and deflection limits to be met. The corrosion caused the reinforcing bars to fail serviceability limits through the lack of ductility and ultimate elongation.

Ultimate flexural capacity of a steel beam is directly proportional to the product of the area of reinforcing steel and the yield strength, both of which are affected by corrosion (Stewart, 2009). Evidence provided by Stewart also suggests that yield stress declines linearly with corrosion, (Equation 2.39). To allow for pitting, a factor can be included to increase the corrosion loss as appropriate.

$$f_y(t) = \left(1 - \alpha_y Q_{corr}(t)\right) f_{y0} \qquad \textbf{EQUATION 2.39}$$

Where;

$f_y(t)$ yield stress of steel at time, t, N/mm^2

f_{y0} yield stress of un-corroded steel, N/mm^2

t time of propagation, s

α_y empirical coefficient

$Q_{corr}(t)$ percentage corrosion loss, % wt. steel

Results presented by Torres-Acosta, Navarro-Gutierrez, and Terán-Guillén (2007) show a loosely linear trend between the pit depth ratio and the remaining ultimate capacity. These test methods, which use a three-point loading schedule, could yield artificially high estimates of remaining capacity if the maximum loss of cross sectional area is not at the section of maximum moment.

Chlorides will reach hoop reinforcement earlier due to the shallower cover concrete and mass loss percentages can be greater on smaller hoop reinforcing bars. Ou, Tsai and Chen (2012) showed that, due to the extreme corrosion of hoop reinforcement, the tested beams began to exhibit flexural-shear failure rather than flexural failure. The ability for the transverse reinforcement to restrain shear stresses was significantly reduced and the beam fractured when it failed in flexural-shear.

Modelling structural damage can be achieved by estimating the remaining cross-sectional area through corrosion propagation models and then calculating the ultimate capacity of this reduced section (Melchers, Li and Lawanwisut, 2006).

2.7.2.2 BOND LOSS

Reduction in bond strength has been comprehensively studied (e.g. Lundgren, 2007) and it is accepted that corrosion causes damage to the steel/concrete bond, effectively reducing the section stiffness of reinforced concrete (Zhang, Castel and François, 2009b). This will cause larger deflections and increased cracking, causing further corrosion to the steel. Bond loss occurs in the early stages of cracking, for widths up to 1mm, causing the subsequent increase in the mid-span deflection of beams.

Ouglova et al. (2008) conducted pull out testing of plain steel reinforcement in concrete samples. For percentage corrosion values up to around 0.4%, the data collected suggest a slight increase in the bond strength. In contrast, for percentage corrosion values between 0.4% and 0.76%, the data indicate a significant loss of bond strength. More recent experimental work by Yalciner (2012) supports earlier research by Chung, Najm and Balaguru (2008) showing that corrosion of up to roughly 1% can increase the bond strength but that large reductions in strength are observed with more advanced corrosion. Although these are reported results, the methodology for calculating percentage corrosion loss of the steel is inconsistent and could be larger than reported.

Pedziwiatr (2009) concludes that, contrary to common belief, it is myth that the bond has a major effect on the stiffness. This assertion is contradicted by further research where the stiffness of a section is observed to decrease most rapidly during the early stages of corrosion (5-8% mass loss) before becoming more constant at higher levels of corrosion (Malumbela, Moyo and Alexander, 2012b).

The majority of research considers unconfined pull-out testing to effectively determine bond strength. It is important to note, however, that 'real world' structures are commonly confined through stirrups and transverse reinforcement. Fang et al. (2004) showed that for deformed steel reinforcement, corrosion has little effect on the bond strength. In contrast, for plain bars with up to 5% corrosion, they observed that the bond strength continued to increase in confined concrete.

2.7.2.3 INTERNAL CRACKING OF CONCRETE DUE TO CORROSION

Although cracking is commonly initiated by external loading or early age shrinkage, the concrete cover will continue to crack, after significant propagation of corrosion, due to internal stresses caused by corrosive process. This will significantly affect the steel/concrete bond and accelerate further corrosion rates.

Internal cracking, owing to the increased interconnectivity between areas of the bar, can cause a shift in the corrosion pattern from macrocell corrosion to microcell corrosion and can also provide greater access to the steel surface for oxygen and chlorides (Zhang, Castel and François, 2009b). This change to microcell corrosion is only likely to occur should the chlorides reach all areas of the steel surface, a likely outcome with internal cracking caused by corrosion.

2.7.2.4 STRESS REDISTRIBUTION

Stewart (2009) concludes that the length of reinforcement required to distribute loads from corroded reinforcement to adjacent reinforcement has a large effect on the reliability of a given structure. Little research is available on the redistribution of stresses, with the majority of research concerned with bond loss or cracking caused by corrosion.

Investigations into the overall structural capacity with a reduced cross-sectional area in individual bars, multiple bars and in various locations are required and will be completed in this research project.

2.7.2.5 TENSION STIFFENING

Although it is commonly assumed that concrete carries no tensile stress, major experimental investigations by the University of Durham and the University of Leeds have detailed the effects of the bond stress on both the stiffness and deflections of concrete sections (Beeby and Scott, 2005).

Through the use of axially loaded reinforced beams, it was shown that the strain in the concrete around a crack is reduced to zero and the strain in the steel reinforcement is equivalent to the applied axial force over the area of steel reinforcement. The increase in strain will be linear between the crack and a distance from the crack, S_0 (Figure 2.22).

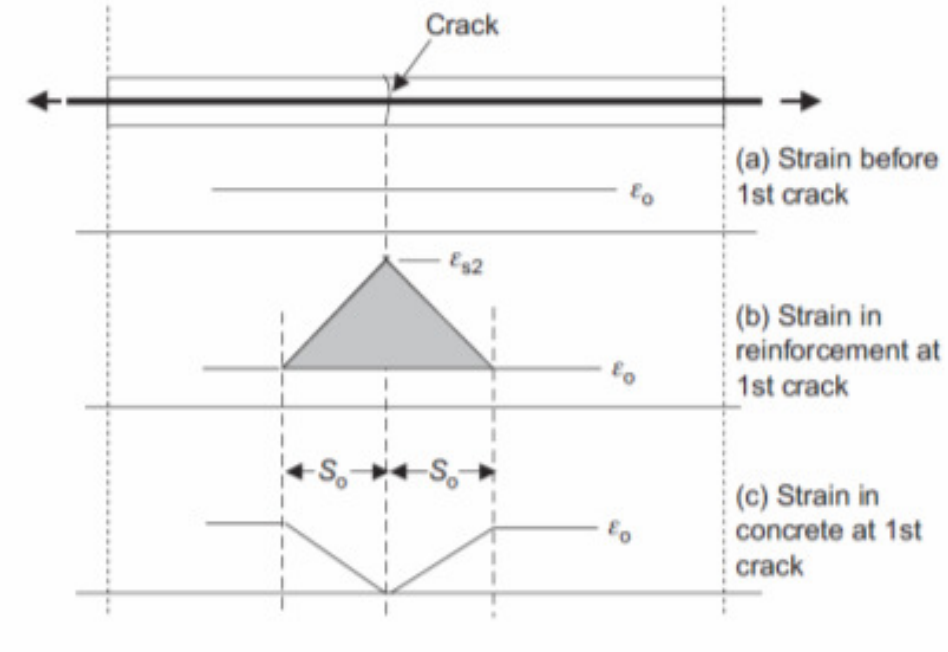

FIGURE 2.22 STRAIN DISTRIBUTION AROUND A CRACK (BEEBY AND SCOTT, 2005)

It is shown that the crack width can be determined from the product of the length, S_0, and strain of the reinforcement at the crack. Additionally, the length, S_0, is directly proportional to the cover thickness. Therefore, the crack width at a given steel strain can be estimated, (Equation 2.40).

$$w = 3.05c \cdot \varepsilon_{s2} \qquad \textbf{EQUATION 2.40}$$

Where;

w crack width, mm

c cover thickness, mm

e_{s2} steel reinforcement strain at crack

Weckenbach (2008) shows that the concrete-steel bond is acting elastically at low loading conditions, with no bond stress measured immediately adjacent to the crack. At higher

stresses, the bond is damaged and this allows slip to be possible. Crack patterns and distance of strain gauges from the major cracks will be taken into consideration throughout experimental works.

Although tension stiffening has a significant effect on crack widths and serviceability of concrete sections, the author believes that, when considering ultimate failure, the effects of tension stiffening could be ignored.

2.7.3 Effects of corroded reinforcing laps

Laps are vital for the transfer of stress along the beam, allowing the beam to continue to maintain its capacity. Should the bond capacity be lost in these sections, the ultimate capacity will reduce significantly. Although experimental results achieved in research by Chung, Najm and Balaguru (2008) indicate that the remaining bond capacity is the most important factor influencing the remaining capacity of a structure, the experiments were not directly related to fully lapped sections in structures.

In large structures with complex arrangements of vertical and loop reinforcing steel, together with vertical pre-stressing steel, the author believes that the transfer of stresses between reinforcing bars cannot be reliant on bond capacity alone. Although there are large areas of research required on lapped sections, this research will look at the initial effects of simply supported beams with lapped reinforcement.

2.7.4 Summary

Corrosion, as commonly accepted, reduces the bond strength and ultimate capacity of concrete structures through long-term exposure to chloride environments. In a large-scale concrete structure, however, the author believes the effects of bond strength on the ultimate capacity to be relatively insignificant in comparison with those of a reduced cross-sectional area of reinforcing steel. It is acknowledged that further research is required to bridge the gap between the currently available knowledge on ductility, bond strength and loss of cross-sectional area in steel and the overall structural capacity of offshore structures. Engineering solutions are required to aid the estimation of the longevity of structures, combining empirical data obtained from laboratory results and 'real world' structures, mathematical modelling and engineering judgement.

2.8 ESTIMATION OF SERVICE AND ULTIMATE LIFE

2.8.1 SCOPE

British Standards Institution (2002b) states the design working life should be specified as 50 years for 'building structures and other common structures' and 100 years for 'monumental building structures, bridges, and other civil engineering structures'. Service life is commonly defined as the time to the onset of corrosion (Siemes and Polder, 1998; Shim, 2005; Gjørv, 2010).

Corrosion initiation due to chloride ingress commonly occurs within 50 years of exposure in sound, un-cracked concrete (Gjørv, 2010). If the working life (service life) is defined as the time to the onset of corrosion, the majority of large structures will not achieve the desired working life.

The definition of service and ultimate life will be considered and assessed for suitability with regards to offshore structures. Some structures have already exceeded the intended service life and a subset of these have done so in a a decommissioned state. For this reason, the extended service life will need to be redefined.

Probabilistic and deterministic modelling currently used is reviewed and its relevance to offshore structures evaluated. The limit states for the existing offshore platforms are subsequently defined.

2.8.2 DETERMINISTIC MODELLING

Deterministic modelling, the basis for all modelling techniques, is commonly a variation of initiation modelling using a combination of transport mechanisms of chlorides, as highlighted in Section 2.5.5.

Service life is commonly defined as the time-to-initiation of corrosion, with diffusion coefficients determined from natural diffusion test results at 90 days (e.g. British Standards Institution, 2010) or migration testing over a day. Extrapolation of these diffusion coefficients, in combination with changes in environment, ageing factors and other influencing parameters, is then carried out using Crank's solution to Fick's Second Law as discussed previously. Extrapolating in such a manner on a complex heterogeneous material has the potential to cause gross errors in determining the service life of a given structure, especially when using a deterministic methodology.

2.8.3 PROBABILISTIC MODELLING

Structures will fail when the load exceeds the structural capacity (Sarja, 2000; Quillin, 2001). Equation 2.41 and Equation 2.42, or alternative adaptations, are commonly used as the basis for probabilistic models of the failure of a structure.

$$\{failure\} = \{R < S\} \quad \textbf{EQUATION 2.41}$$

$$P_f = P\{R < S\} \quad \textbf{EQUATION 2.42}$$

Where;

R response variable

S load variable

P_f probability of failure

Both the capacity of the concrete and loading conditions of offshore structures will vary with time, suggesting that a probabilistic method of service and ultimate life estimation is appropraite. Predicting the loading conditions throughout the life of the structure is relatively reliable; however, the remaining capacity of the structure and effects on ultimate life are much less well understood.

Service period design and lifetime design have been conducted previously and can be achieved with reasonable success (Figure 2.23). Increasing the reliability of the modelling should be the focus of further research, with a key priority being a reduction in the estimated variability of input parameters for the remaining capacity of sub-sea concrete.

The fib model code applies a design equation in which serviceability is lost when the probability of depassivation occuring is below a target failure probability. As with the fib model, modelling by Saassouh and Lounis (2012) applies a probabilistic approach to diffusion equations, showing corrosion is likely to initiate when the probability that the chloride concentration at the steel surface exceeds a threshold as highlighted in Figure 2.24.

Although methods utilising diffusion coefficients are suitable for estimating the time-to-corrosion in fully-saturated submerged concrete structures which are under no loading and exposed to NaCl exposures, the author believes that the importance of deterministic or probabilistic determination is overstated. Unless the environment and loading of structures,

along with the structural response of a given structure, are considered, the service and ultimate life predictions made through modelling will be insufficient.

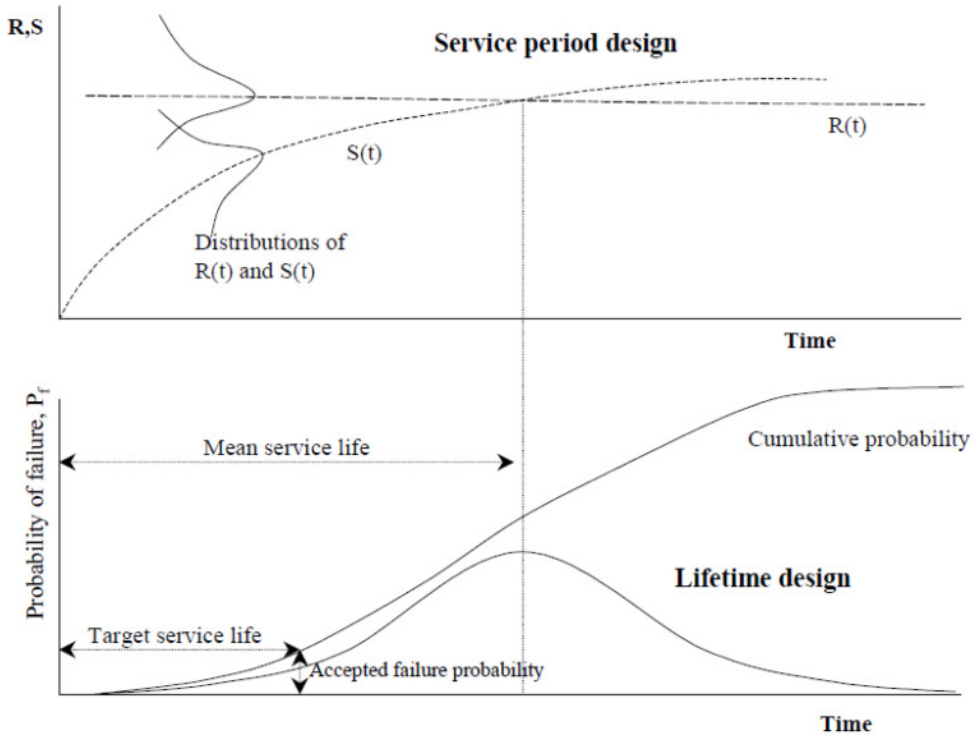

FIGURE 2.23 SERVICE AND ULTIMATE LIFE DESIGN (QUILLIN, 2001)

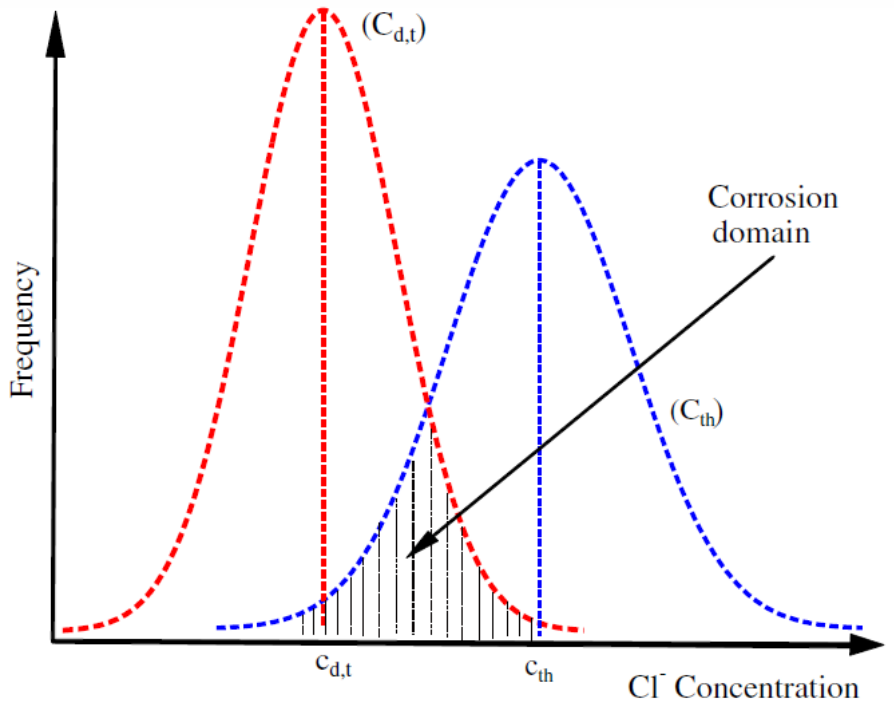

FIGURE 2.24 DETERMINISTIC VS. PROBABILISTIC PREDICTIONS OF CORROSION INITIATION (SAASSOUH AND LOUNIS, 2012)

2.8.4 'REAL WORLD' STRUCTURES

Ovstaas and Morgan (1999) investigate chloride-induced corrosion in cracked concrete due to shrinkage cracking, a process which originates at the steel surface. Although cracking sustained in loading initiates at the outer concrete surface, similar transport properties are likely in each scenario. Over each crack, chloride ions have penetrated deeper than 50mm to the steel reinforcement. Predicting chloride ingress in the sound concrete, corrosion would initiate in 42 years at 50mm deep, with a further 3.1 years to crack initiation due to corrosion. It is suggested that the cover thickness should be reduced to 20mm to take into account damage by cracking and this gives a service life is prediction of 7.2 years. This suggests that the serviceability of this structure would be breached, although the steel is epoxy coated and this will retard the process of corrosion.

Arskog, Ferreira and Gjørv (2004) reviewed samples taken from a relatively new harbour structure of 80 m in length and constructed from a high performance Portland cement with silica fume with a maximum w/c ratio of 0.45. This concrete exceeds serviceability within 10 years at a 10% probability, where serviceability is defined as the onset of corrosion.

Helland, Aarstein and Maage (2010) compiled reported data from offshore structures of chloride ingress. Profiles were obtained from multiple levels and locations from the concrete superstructures. The diffusion data obtainedwas used to predict time to initiation of corrosion due to chloride ingress and it was found that 20% of the samples from Oseberg A and Brent B would cause initiation within 40 years of exposure. Additionally, diffusion coefficients from Oseberg A show inconclusive effects of ageing within the first 18 years of exposure and suggest ageing effects should be ignored when modelling CEM I concretes.

Owing to the paucity of samples from existing offshore and marine structures, prediction of behaviour must be carried out in the laboratory and, where possible, validated against structures in situ. The author believes that the focus on chloride profiles to model 'real world' structures is inadequate and that further data on corrosion rates, steel potentials and resistivity are required to further understand the variations observed between laboratory works and the structures.

2.8.5 SUMMARY OF REMAINING LIFE ESTIMATION TECHNIQUES

The understanding of service or ultimate life determination for concrete in a subsea environment is limited predominantly to the period of initiation of corrosion, with the majority of current modelling techniques being based on chloride diffusion. Although diffusion of chlorides through sound concrete will influence the ultimate life, the effects of cracking on the rates of corrosion will be the predominant factor influencing the ultimate life of offshore structures.

Failure models taking propagation into account are often defined as the time taken to lose a certain percentage of the cross-sectional area of steel due to corrosion. Although this has the potential to provide a reasonable estimation of structural longevity, the structural behaviour and response to corrosion should also be taken into account.

2.9 SUMMARY OF LITERATURE

Although various large scale research projects over the decades have aimed to understand the degradation of concrete structures, there are considerable variations between predicted degradation and actual 'real world' degradation. As further data becomes available with the ageing of concrete structures, further laboratory-based research programmes and the improvement of on-site non-destructive testing mechanisms, there is much scope to improve the overall understanding of the complex failure mechanisms resulting from concrete degradation.

Having reviewed the available literature, the author believes that more knowledge required for the effective estimation of the remaining longevity of offshore concrete. The gaps in the literature identified and described by the author to be further investigated are summarisedin Table 2.21.

TABLE 2.21 BRIEF SUMMARY OF AREAS OF RESEARCH REQUIRING FURTHER INVESTIGATION

Research Area	Comments
Effect of alternative ions on the initiation of corrosion in concrete	Seawater comprises a number of ions, and although research continues to use NaCl solutions, the effects of alternative ions on corrosion in concrete requires further research.
Corrosion in a low oxygen/ submerged environment	Contradictory evidence has been presented by researchers suggesting that corrosion may or may not occur at significant rates in low oxygen environments. Experimental work will be aimed at determining any effects of these environments on corrosion rates.
Influence of cracking on the rate of corrosion (all environments)	It is widely accepted that cracking increases the risk and rate of corrosion. However, there is disputed research on the effects of autogenous crack healing, crack widths and corrosion in submerged, low-oxygen environments. Research is required on the corrosion in submerged conditions with controlled dissolved oxygen concentrations.
Large scale corrosion damage to concrete structures	The effect of corrosion on service life has been studied, with research predominantly focussing on reduction in stiffness and increases in crack widths. The ultimate life of a structure, however, is considered less frequently due to the importance of service life.
Effects of corroded lapping on structural capacity	Research into the effects of corrosion on lapping and remaining capacity is limited and experimental work often uses pull-out testing of lapped reinforcement in an attempt to determine remaining bond strength. Experimental work will be aimed at improving the understanding of pitting and general corrosion on the bond between lapped sections and the subsequent effect on the ultimate structural capacity.

CHAPTER 3

3 EXPERIMENTAL DETAILS AND PROGRAMME

3.1 INTRODUCTION

Substantial experimental works were carried out in four phases as outlined in Figure 3.1. Two project groups were set up to enable multiple experimental programmes to be run simultaneously. Project Group 1 (PG1) consisted of four students; Horne, Robinson, Yun and Khosravi, and carried out works on Phase II experiments. Work on experimental Phases III and IV were distributed between members of Project Group 2 (PG2); Robinson, Hope, McKenzie, McKinley, and Loh. Works were split this way to allow for extensive experimental work to be achieved in a limited timescale.

Due to lack of information on offshore concrete modelling reported in literature reviewed in Chapter 2, experimental methodologies were designed to investigate the effects of the source chlorides (NaCl or seawater), environmental exposure conditions (submerged, deoxygenated), and cracking (static, dynamic) on the rate of degradation (corrosion of reinforced steel) of submerged reinforced concrete samples. Further works were carried out to determine the effects of the chloride source on the transport of chlorides through the cover, and the consequential effects of corrosion rates remaining cross sectional area of reinforcing bars.

Additional experimental programmes were undertaken in an attempt to further understand the remaining life implications of advanced corrosion. Beams with various reinforcement setups (individual bars, lapped reinforcement, location of artificial pits) were used to evaluate overall structural response under extreme pitting and general corrosion conditions.

Individual experimental phases are discussed in detail throughout this chapter.

3.1.1 SPECIMEN PROCUREMENT

All aggregates used are quarried locally in Fife. The coarse aggregates consist of 4/10mm and 10/20mm grade and are rounded, relatively smooth edged gravel. The fine aggregates are up to 4mm in size. The aggregates were tested for absorption and particle density in accordance with BS EN 1097-6:2000. The water absorption allows for the total water of the mix to be determined, which produces the correct free water/cement ratio as specified in the mix design.

The Portland cement is of grade 52.5 cement conforming to BS EN 197-1:2000. The fly ash used for certain mixes has a category S fineness and category B loss on ignition, conforming to BS EN 450-1:2012.

Due to the relatively low water/cement ratios of the concrete mixes, a high range water reducing admixture of Glenium Sky 544, complying with BS EN 934-2:2009.

Concrete specimens are mixed in accordance with BS 1881-125:1986 with the use of laboratory dried aggregates at room temperature with added water content to adjust for the water absorption of the aggregates. The fresh properties of slump and plastic density were determined in accordance with BS EN 12350-2:2009 and BS 12350-6:2009 respectively to ensure consistency of the mix.

Once cast, concrete is left to cure for 24 hours in the moulds, covered with damp hessian and plastic sheeting. After 24 hours, the samples are de-moulded and submerged in curing tanks at room temperature for a further 27 days (Figure 3.2). After a total of 28 days, two cubes are tested for cube strength using a standard calibrated cube crusher in accordance with BS EN 12390-3:2002. Wherever possible, experimental work was carried out using concrete at an age of 28 days, unless stated otherwise.

Material details are listed in full in Appendix A.

3.1.2 CONCRETE MIXES

Experimental works were carried out on 19 different mix designs, including the use of silica fume and fly ash additives. These replicate a range of mixes that cover common mix designs among offshore structures within the North Sea. The concrete mixes, as shown in Table 3.1, were all tested in Phase I. Mixes CTBD and CTN are estimated from real offshore structures constructed in the 1970s (International Association of Oil and Gas Producers, 2003; 2012).

Mix CT07 was chosen for use in Phases II and III, as this mix is vital when determining the longevity of a specific structure of interest (Tegelaar, 1975). Although the mix design specifies a Norfolk coast flint, gravel and limestone aggregates are used in this study due to the unavailability of a suitable flint. The two aggregate types are used with this mix for Phase II of experimental work to provide a comparison between commonly used aggregates in concrete. Phase III continues to use mix CT07, however solely with gravel aggregates.

In Phase IV, concrete was precast and fabricated externally. C35/40 concrete was specified using only a CEM I mix. High cement contents were used as the procuring company was

producing self-compacting concrete at the time. For the nature of these experiments, self-compacting concrete is deemed suitable.

3.1.3 ENVIRONMENTAL EXPOSURE CONDITIONS

Chlorides are commonly applied to concrete in laboratory experiments by exposing to sodium chloride solutions, either in a tidal, spray or submerged setup. By applying chlorides using an artificial seawater solution with additional ions, Red Sea Salts®, a more realistic marine exposure condition was achieved. The composition of salts was previously determined by Atkinson and Bingman (1996). To achieve consistent chloride concentrations, synthetic sea salt and NaCl were each produced to contain 1M chloride concentration; 58.44g/L NaCl and 66.1g/L artificial seawater.

Phase I considered two sets of experiments concerned with determining chloride diffusion coefficients in varying exposures and quantifying the difference between diffusion of chlorides from pure NaCl solutions (Set I) or artificial seawater exposures (Set II). Phase II and Phase III will include exposure in artificial seawater as well as pure NaCl solutions.

Phase IV beams will be saturated through submersion in galvanised steel outdoor tanks where corrosion currents will be applied, thus accelerating corrosion. These specimens will then be exposed to the atmosphere during strength testing, as the effects of exposure conditions are inconsequential during this experimental phase as the structural response will be similar in or out of the water.

As the effects of temperature on diffusion and corrosion have been previously investigated (Pour-Ghaz, Isgor and Ghods, 2009; Bertolini et al., 2013), the exposed temperature is specified as room temperature, and was measured to be within the range of 20±2°C. Corrosion rates can then be adjusted for North Sea temperatures for use in service and ultimate life estimations.

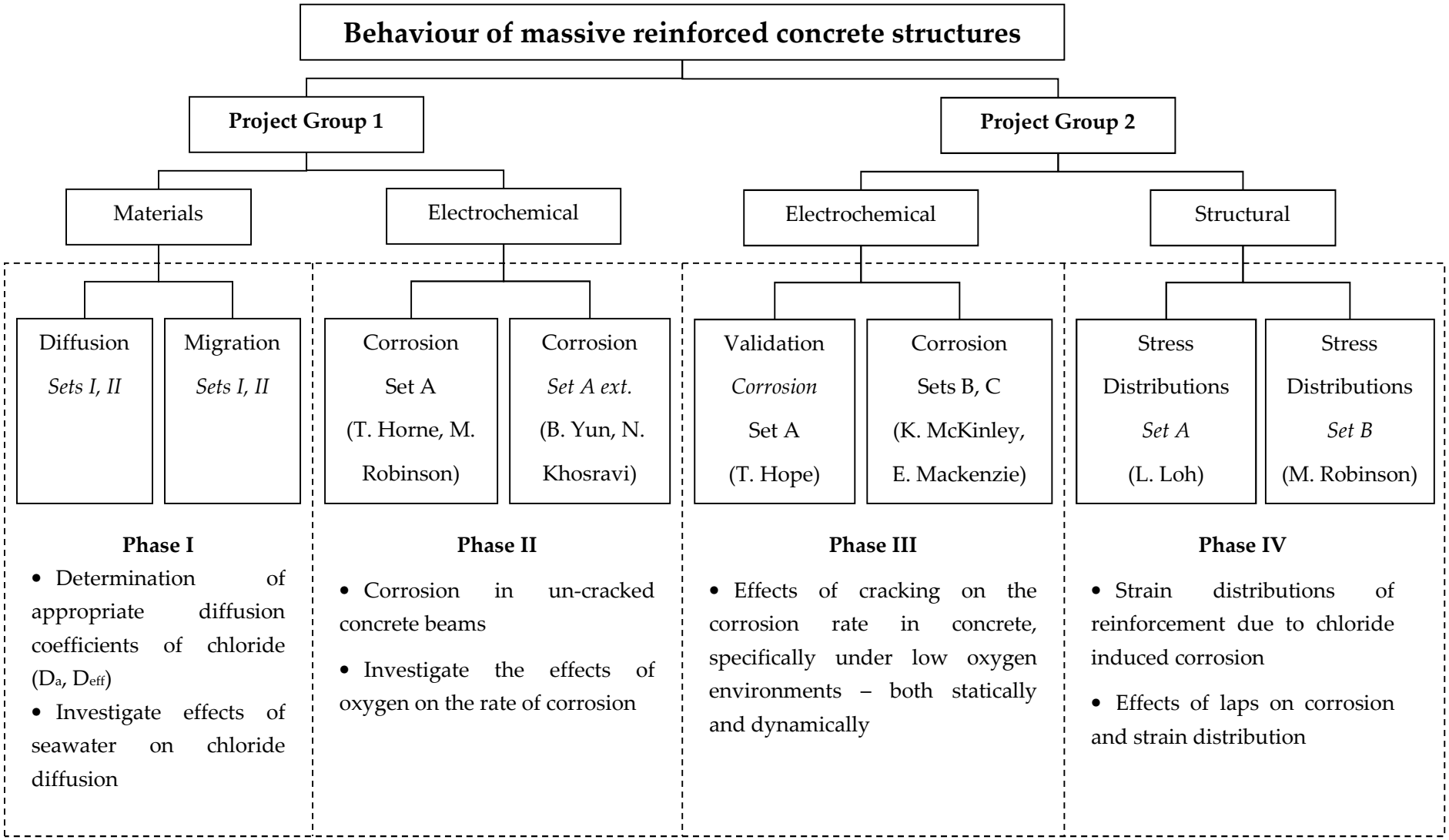

FIGURE 3.1 OVERVIEW OF RESEARCH PROJECT

TABLE 3.1 CONCRETE MIXES FOR PHASE I

Reference	w/c	Water	Binder			Aggregates			Admixtures	Slump	Strength
			PC	FA	SF	Fine	10/4	20/10			(28 days)
		kg/m³	kg/m³			kg/m³	kg/m³	kg/m³	kg/m³	mm	N/mm²
CT01	0.35	135	380			795	385	710	2.45	160	70.45
CTBD	0.39	175	450			860	245	720	1.17	190	64.10
CT02	0.4	150	380			785	380	705	1.25	70	63.20
CTN	0.4	210	405	105		685	340	685	0	85	54.90
CT03	0.4	150	265	115		745	370	745	0.78	75	48.92
CT04	0.4	150	190	190		745	370	745	0.33	70	29.56
CT05	0.4	160	380		20	735	370	735	1.18	75	63.85
CT06	0.4	160	360		35	740	370	740	1.57	110	67.20
CT07	0.42	158	375			745	370	745	0.88	75	46.21
CT08	0.45	170	378			730	365	735	0.3	65	53.65
CT09	0.45	170	265	115		730	365	735	0.53	80	42.18
CT10	0.45	170	190	190		730	365	735	0.18	90	24.84
CT11	0.45	175	370		20	725	365	725	0.37	110	55.85
CT12	0.45	180	360		35	720	360	720	0.38	100	52.75
CT13	0.5	180	360			730	365	730	0.0	85	48.98
CT14	0.5	180	250	108		730	365	730	0.0	80	34.80
CT15	0.5	180	180	180		730	365	730	0.0	160	20.01
CT16	0.5	190	360		20	720	360	715	0.23	100	51.94
CT17	0.5	190	350		35	715	355	715	0.50	115	51.89

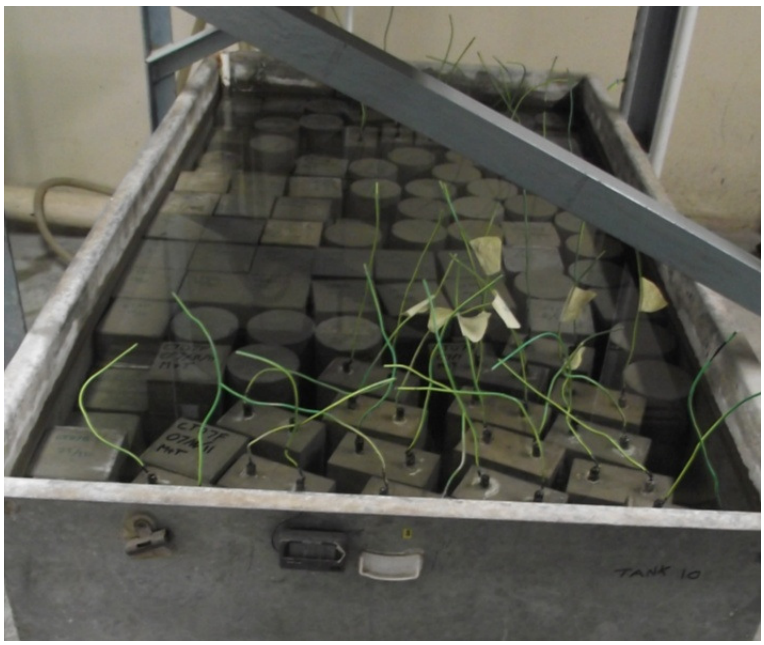

FIGURE 3.2 CURING OF CONCRETE SPECIMENS

3.2 PHASE I: DETERMINATION OF APPROPRIATE DIFFUSION COEFFICIENTS OF CHLORIDE INGRESS

3.2.1 NATURAL DIFFUSION TESTING

As is common practice, modelling of service life is dependent on the use of a measured diffusion coefficient. Through the application of Fick's Law or other transport mechanisms, the onset of corrosion could then be predicted through the use of existing models. To determine a suitable diffusion coefficient for use in modelling, natural diffusion tests were carried out. Although modelling through this method provides extremely vague and variable results as highlighted in Chapter 2, a general idea of the performance characteristics of the concrete is required.

3.2.1.1 SPECIMEN SPECIFICATIONS AND EXPERIMENTAL SETUP

Cubes of all mixes were cast and tested in a method similar to DD CEN/TS 12390-11:2011 and NT Build 443. In addition to the specified exposure of NaCl solution, a seawater solution was used. Each solution contained chlorides of 1M concentration of chlorides (35.5ppt) as previously defined.

The samples were not cut, which would allow for the bulk transport properties to be measured, and were therefore replicating 'real world' structures more appropriately. As

large offshore and marine structures are often slip formed, a cast surface is more applicable than a cut surface.

3.2.1.2 MEASUREMENTS

Three specimens were tested after 90 days exposure using a grinding method followed by x-ray fluorescence (XRF) and water soluble titration to determine the total and approximate free chloride concentrations at 8 different depths (Figure 3.3). Further samples were exposed for longer durations and are to be tested by a research group in the future to gather data on the ageing effects of concrete under laboratory conditions along with further effects of additional ions contained in seawater solutions.

Analysis of surface skin effects caused by the ions in seawater in comparison to NaCl solutions and ageing effect of concretes on chloride diffusion in a submerged environment will be undertaken through the use of x-ray diffraction (XRD) and XRF. The repeatability of the test methods and sampling techniques were reviewed and values were determined for a probabilistic approach to service-life modelling of offshore submerged concrete. Empirical methods provide sufficient data to allow for a more reliable estimation of time to initiation, as recommended by the author in Chapter 2.

a) profile grinding

b) heating and stirring

c) measuring

d) titration

FIGURE 3.3 GRINDING AND TITRATION EXPERIMENTAL METHOD AND APPARATUS

3.2.2 MIGRATION TESTING

3.2.2.1 SPECIMEN SPECIFICATIONS AND EXPERIMENTAL SETUP

100mm cylinders were cast of three realistic offshore concrete mixes; CTN, CTBD and CT07. Two methods of migration testing were carried out; the first method being NT Build 492, and the second a Multi-Regime (MR) method outlined in Section 2.5.4.2 (Castellote and Andrade, 2006). As per the natural diffusion testing, an artificial seawater solution was used in addition to a pure NaCl solution.

3.2.2.2 MEASUREMENTS

The collection of results allowed for the analysis of steady and non-steady state diffusion of chlorides through offshore concretes, the suitability of migration testing with the use of artificial seawater solutions, and the provision of further data for a probabilistic approach to service life estimation. Care must be taken when using these measurements for modelling purposes as results from such testing can differ greatly due to the applied electrical field throughout.

3.3 PHASE II: CORROSION PROPAGATION IN UN-CRACKED CONCRETE

As propagation of corrosion has been shown to be the predominant cause of failure for offshore concrete structures, experimental work was completed to determine likely corrosion rates of steel for use in predicting ultimate longevity of specific concrete materials. The method used in this study has been developed using adaptations of experimental works carried out by other researchers previously (Castellote, Andrade and Alonso, 2002; Hussain, 2011).

3.3.1 SPECIMEN SPECIFICATIONS AND EXPERIMENTAL SETUP

The specimens used for this test are beams of length 300mm, width 75mm and depth 125mm. These contain 2 no. 10mm diameter (ϕ) steel reinforcing bars (f_y = 500N/mm^2) spaced with 25mm cover from each surface (Figure 3.4).

The steel reinforcement is cleaned prior to casting using a grit blasting technique until visibly a consistent colour (Figure 3.5a). Holes of 4mm (ϕ) are drilled and then tapped into one end of the steel to allow for copper wire to be attached using stainless steel screws. Black epoxy (Elctrolube low viscosity epoxy resin) was then applied to define an exposed area of steel, important when calculating the corrosion current density from the total measured current.

Beams were cast in bespoke steel moulds (Figure 3.5b), with reinforcement out of the end of each beam allowing for monitoring of the connection between the copper wire and steel bar. Having cured for 28 days, the faces are sealed with wax and ponding is applied to the hand troweled surface (Figure 3.6).

Sample references and variables are shown in Table 3.2.

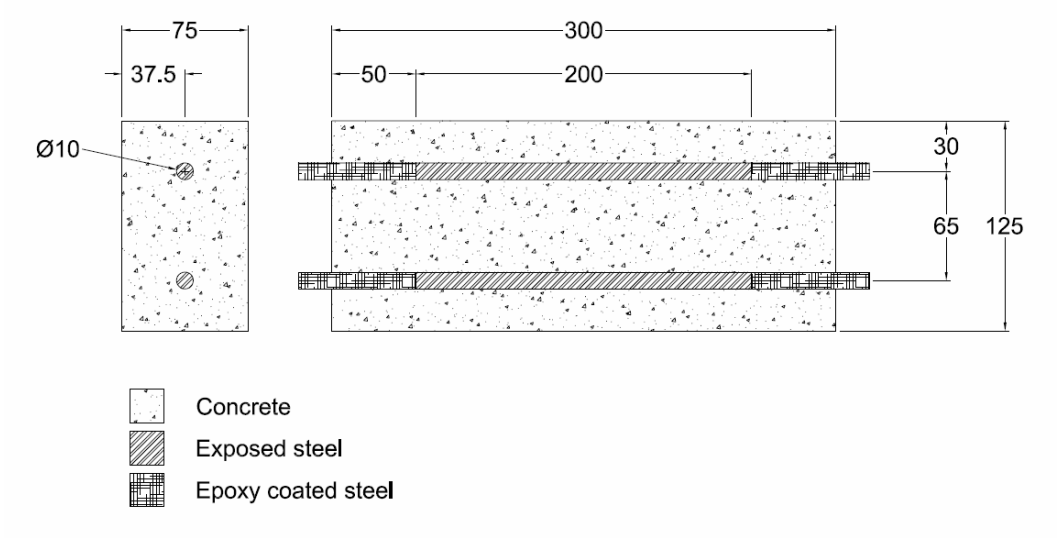

FIGURE 3.4 BEAM SECTION DETAILS

a) grit blasted reinforcing bar

b) casting in bespoke moulds

FIGURE 3.5 CASTING OF CONCRETE IN BESPOKE MOULDS

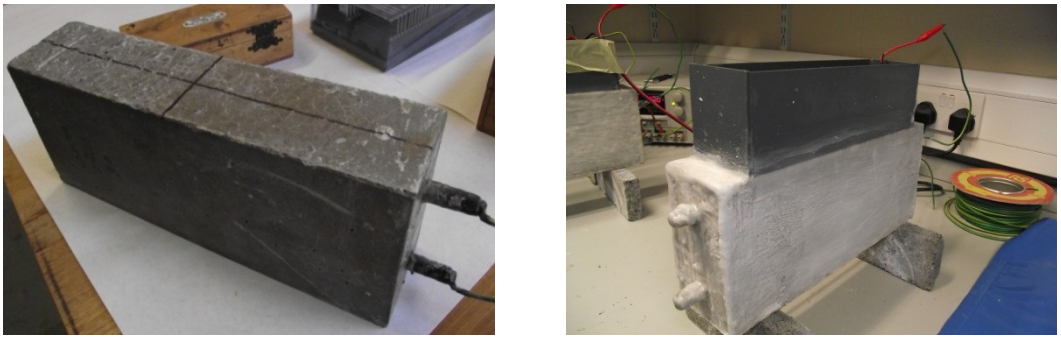

a) cured beam

b) ponding applied to upper surface and waxed

FIGURE 3.6 CURED BEAMS

TABLE 3.2 EXPERIMENTAL REFERENCE TABLE FOR LOW OXYGEN CORROSION EXPERIMENTS

	A:C	O2, ppm	Cube Strength, N/mm²		A:C	O2, ppm	Cube Strength, N/mm²		A:C	O2, ppm	Cube Strength, N/mm²		A:C	O2, ppm	Cube Strength, N/mm²
7C-1		~0		**7D-1**		~0		**7E-1**		~0		**7F-1**		~0	
7C-2		4		**7D-2**		4		**7E-2**		4		**7F-2**		4	
	1		58.8		1		57.1		1		59.3		1		59.4
7C-3		8		**7D-3**		8		**7E-3**		8		**7F-3**		8	
7C-4		Air		**7D-4**		Air		**7E-4**		Air		**7F-4**		Air	
7G-1	1			**7H-1**	1			**7I-1**	1			**7J-1**	1		
7G-2	0.5			**7H-2**	0.5			**7I-2**	0.5			**7J-2**	0.5		
		~0	58.5			4	55.9			8	55.9			Air	59.1
7G-3	0.3			**7H-3**	0.3			**7I-3**	0.3			**7J-3**	0.3		
7G-4	0.1			**7H-4**	0.1			**7I-4**	0.1			**7J-4**	0.1		
7K-1		~0		**7L-1**		~0		**7M-1**		~0		**7N-1**		~0	
7K-2		4		**7L-2**		4		**7M-2**		4		**7N-2**		4	
	1		70.3		1		64.7		1		70.0		1		67.9
7K-3		8		**7L-3**		8		**7M-3**		8		**7N-3**		8	
7K-4		Air		**7L-4**		Air		**7M-4**		Air		**7N-4**		Air	

3.3.1.1 VARIATION OF OXYGEN CONCENTRATIONS

Oxygen concentrations were controlled using water in shallow plastic trays, exposing the face closest to the cathodic bar in the water. An Oakton dissolved oxygen meter (Acorn Series DO6 Dissolved Oxygen Meter) was used to measure the dissolved oxygen concentration in the trays, with target concentrations of 4 and 8 ppm, as shown in Figure 3.7. Nitrogen is used to purge oxygen from the water to reduce the concentration from saturated (~8.5/9ppm) to the desired value.

Preliminary experiments showed that, with a small surface area to volume ratio, oxygen completely diffused into a water sample within 2 days. For larger surface area to volume ratios, with little or no disturbing currents within the water, oxygen saturation of the water was achieved within 12 hours. Nitrogen was therefore bubbled to purge oxygen from the water, controlling the concentration, every 8 hours from the commencement of the experiment. Although a constant measuring system with an automated oxygen controlled tank would be preferable, logistics of such a system were unachievable.

Due to the rapid oxygen dissolution, controlling oxygen into the tanks proved difficult (Figure 3.8). As the surface area to volume of water ratio was high, oxygen diffused into the water rapidly. The target value of 4ppm was exceptionally difficult to achieve, and average values of this tank were measured to be around 5ppm. However, for the purposes of this experiment, there is still a significant variation between the two tanks to make a comparison between environments.

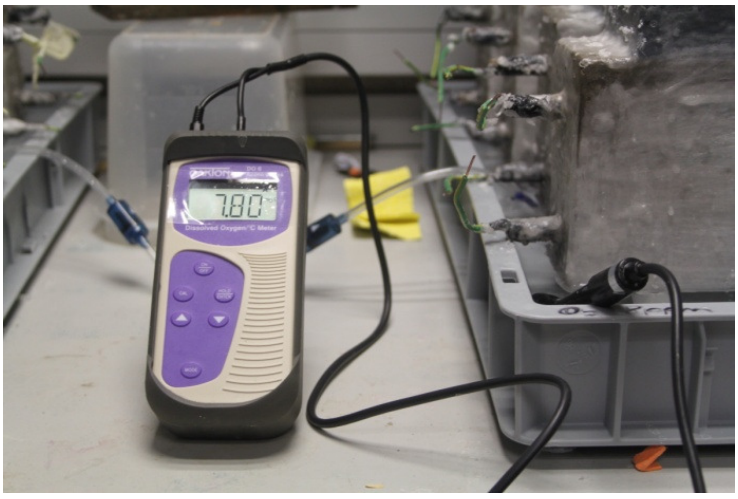

FIGURE 3.7 OXYGEN CONCENTRATION MEASUREMENTS

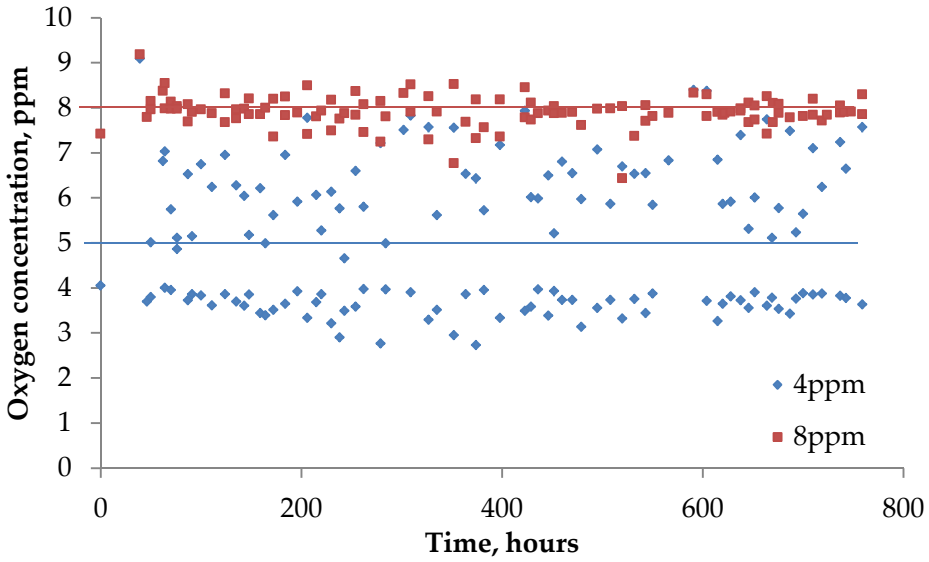

FIGURE 3.8 EXAMPLE OXYGEN CONCENTRATION READINGS FROM AN EXPOSURE TANK

3.3.1.2 ANODE/CATHODE RATIO VARIATIONS

Four anode/cathode ratios were cast into the concrete using epoxy to define the exposed reinforcement surface. These ratios were 1, 0.5, 0.25 and 0.05 with a fixed cathode size of 200mm length. Corrosion measurements were taken in the centre of the specimen above the anodic area of steel.

3.3.1.3 VARIATION OF AGGREGATE TYPE

Predominantly, gravel is used for the experimental works. However, a set of concrete beams with limestone aggregates were procured to provide a comparison between the effects of two aggregate types on corrosion currents.

3.3.2 INITIATION OF CORROSION

There are three commonly used methods of initiating corrosion in concrete specimens:

- Cast-in chlorides – mixing the concrete using chloride contaminated water.
- Potentially driven-in chlorides – applying a potential difference between the external solution and the steel reinforcement.
- Chloride exposed natural diffusion – applying a chloride source to the surface of the concrete and allowing natural transport mechanisms to take chlorides to the steel surface.

Each method has limitations, but due to the extent of initiation times due to natural diffusion, corrosion will be artificially accelerated using an applied potential difference technique. Using cast in chlorides was omitted due to the binding of chlorides and probable detrimental effects on cement paste caused by this methodology.

3.3.3 MEASUREMENTS

3.3.3.1 OXYGEN CONCENTRATIONS

Oxygen concentrations are taken with a dissolved oxygen meter calibrated through a two point calibration in zero oxygen solution and exposure to atmosphere.

3.3.3.2 HALF-CELL POTENTIAL

Using a digital multi-meter with the negative lead connected to the reference electrode (Ag/AgCl reference electrode) and the positive connected to the corroding bar, the potential difference was initially measured daily, as shown in Figure 3.9. Using the measured voltage, the likelihood of corrosion was assessed in accordance with Section 2.6.3.1. When the probability of corrosion was deemed to exceed 90%, the applied potential was removed and corrosion was allowed to propagate freely.

3.3.3.3 LINEAR POLARIZATION

Linear polarization measurements (Figure 3.10) were carried out to determine the open circuit potential and polarization resistance (Figure 3.11). By applying the Stearn-Geary equation to the measured values an estimated corrosion current is obtained.

3.3.3.4 POTENTIODYNAMIC MEASUREMENTS

To provide an estimation of the macrocell corrosion current, the Tafel slopes and coefficients of the anodic and cathodic reinforcement are obtained using potentiodynamic scans (Figure 3.12). Coupling these measured coefficients with Equation 3.1, a further estimate of the total corrosion macrocell current was determined.

$$R_P = \frac{\Delta E}{\Delta I} \qquad \textbf{EQUATION 3.1}$$

Where;

R_P Polarization resistance, Ω

E Potential, mV

I Current, mA

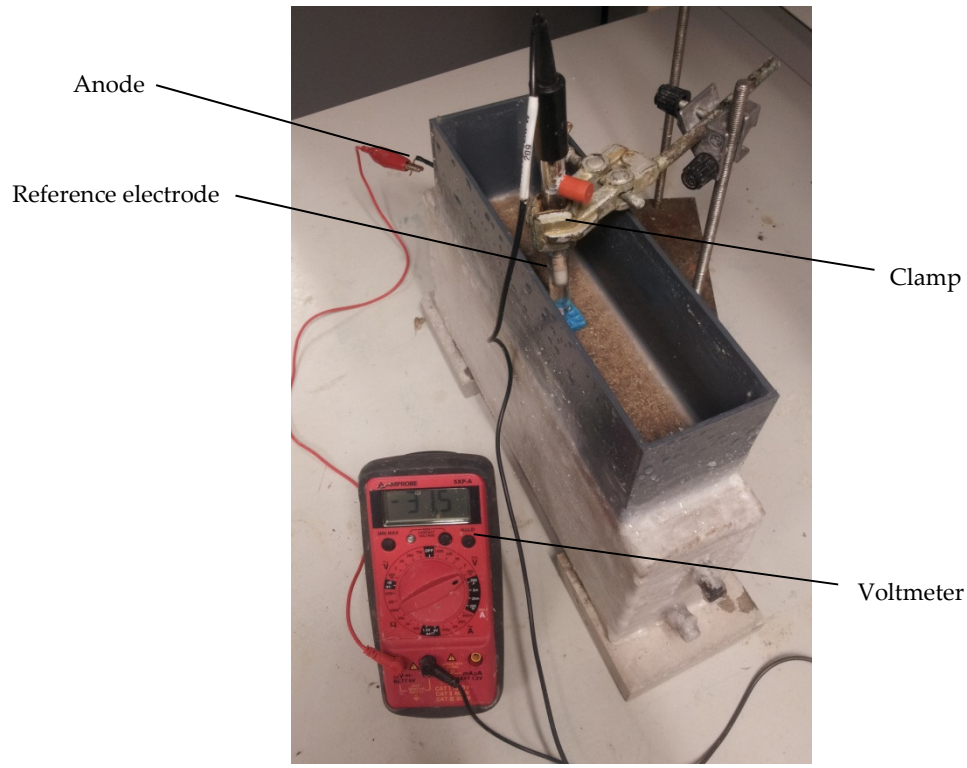

FIGURE 3.9 EXAMPLE HALF-CELL MEASUREMENT SETUP

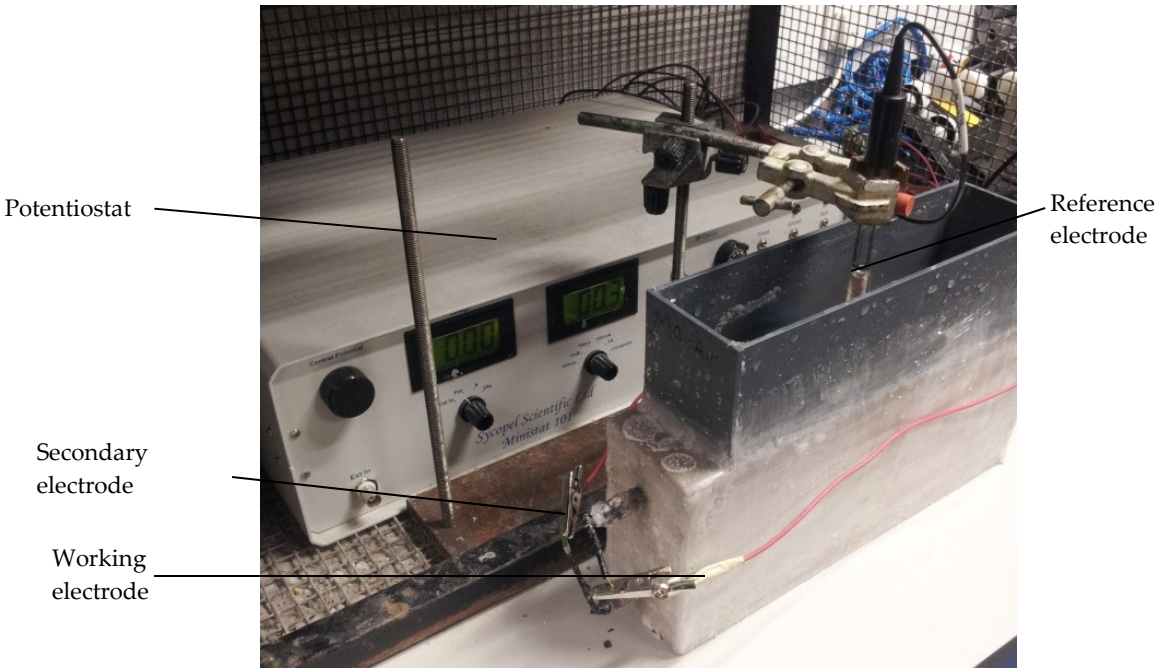

FIGURE 3.10 LINEAR POLARIZATION RESISTANCE AND POTENTIODYNAMIC SETUP

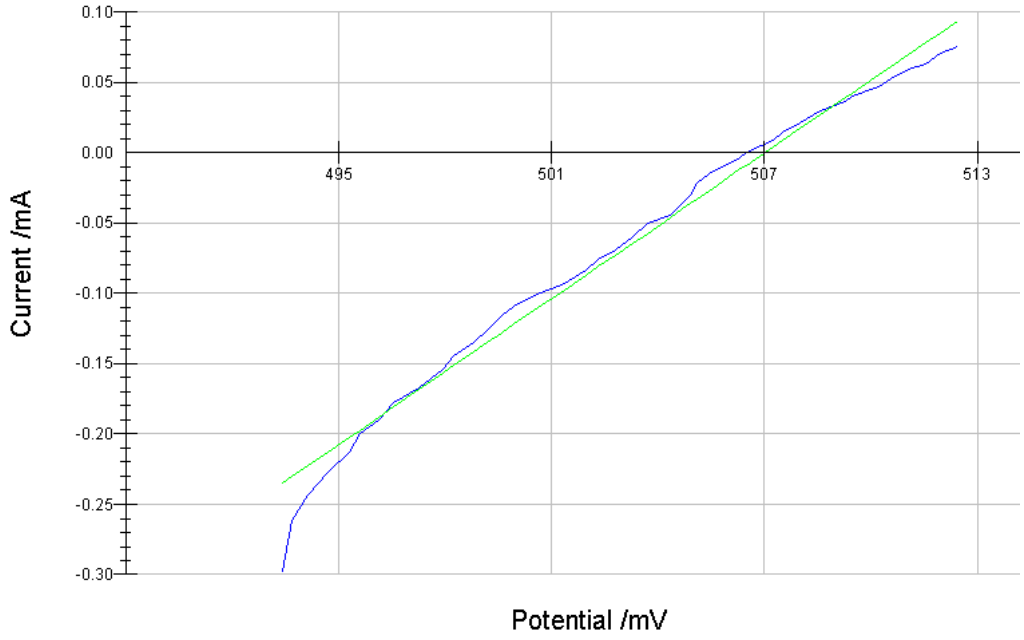

FIGURE 3.11 TYPICAL OUTPUT FROM A LINEAR POLARIZATION SCAN

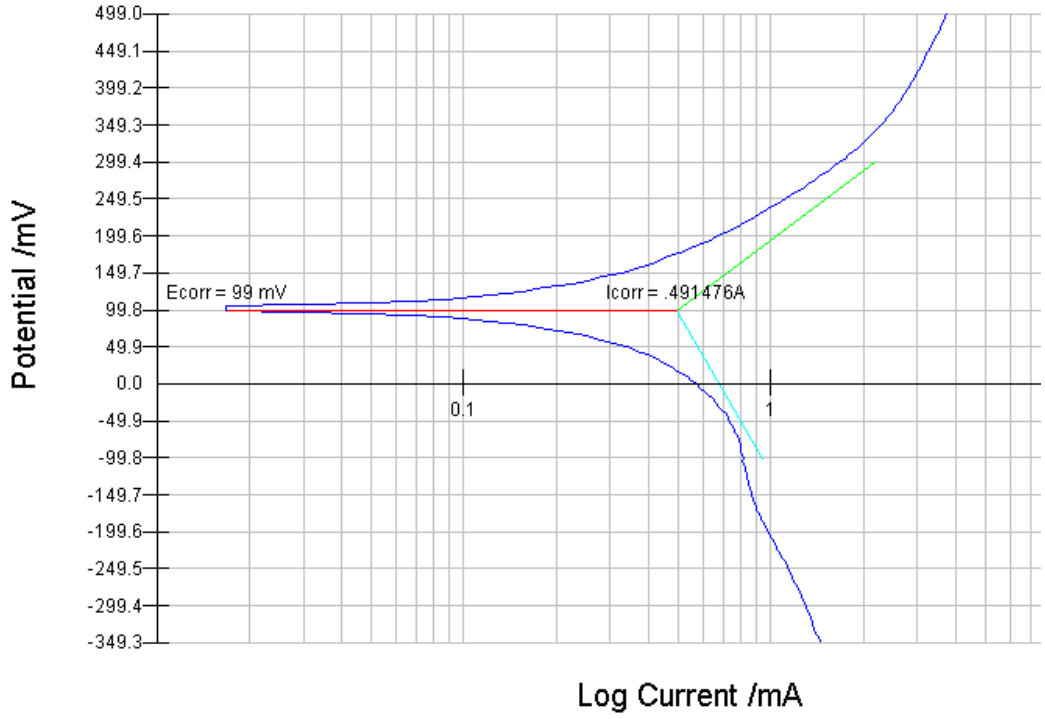

FIGURE 3.12 TYPICAL OUTPUT FROM A POTENTIODYNAMIC SCAN

3.4 PHASE IIIA CORROSION PROPAGATION IN UN-CRACKED CONCRETE VALIDATION

The follow up to Phase II involved reproducing the experiments using a different casting and exposure technique in an attempt to validate the previous findings. As there were concerns over the availability of oxygen within the system and the speed at which oxygen dissolves into exposed water, a more controlled and sealed system was set up in an attempt to restrict this availability of oxygen.

3.4.1 SPECIMEN SPECIFICATIONS AND EXPERIMENTAL SETUP

Specimens were cast in clear plastic containers of height 200mm with sections of 110x80mm at the top and 100x70mm at the base. The concrete was cast up to a depth of 150mm. This allows for a sealed pond of 50mm depth confined between the lid of the container and the surface of the concrete, thus preventing access for oxygen into the system as shown in Figure 3.13.

Two large sealed containers of dimensions 670x520x200mm are filled with distilled water and sealed (Figure 3.14). 12 holes are cut in the top of the lids to accommodate the concrete specimens. Once the specimens are in situ, silicone sealant is used to prevent oxygen seeping through the joint.

Experimental variables are shown in Table 3.3.

3.4.1.1 VARIATION OF OXYGEN CONCENTRATIONS

Initially oxygen concentrations of negligible, 2ppm, 6ppm and atmospheric exposure were to be used in accordance with the experiments run in Phase II. However, due to leakage of oxygen through the lid, oxygen saturated water exposure replaced the intermediary values (Table 3.3). Direct comparison between the results with Phase II can be completed to confirm the previous findings.

3.4.1.2 VARIATION OF WATER/CEMENT RATIO

Two differing water/cement ratios are used, 0.42 and 0.5, to evaluate the variation in corrosion rate of oxygen depleted concrete due to differing diffusion coefficients. As the pore structure is more interconnected due to a higher w/c ratio, the movement of chlorides, water and oxygen should be faster and therefore increasing the corrosion rate.

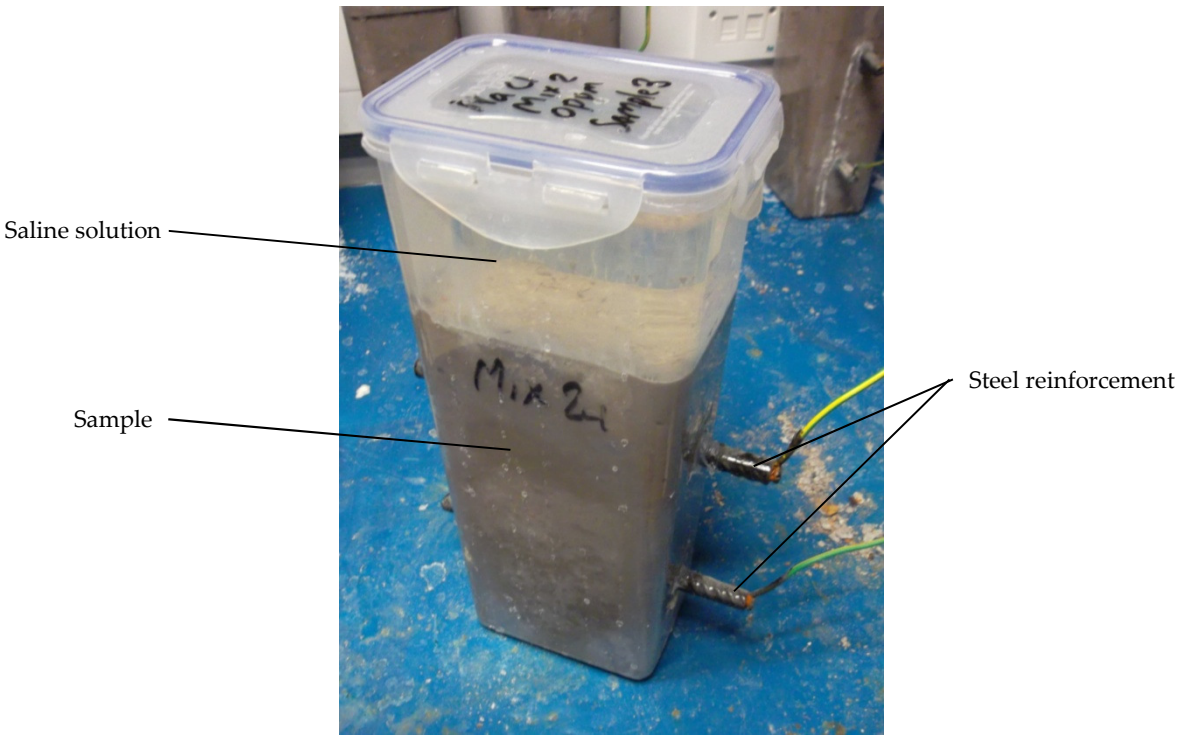

FIGURE 3.13 CAST SPECIMEN FOR LOW OXYGEN CONCENTRATION VALIDATION

FIGURE 3.14 EXPOSURE SETUP FOR OXYGEN VARIATION

3.4.2 INITIATION OF CORROSION

Initiation was achieved using a 10V potential difference applied between the pond solution and the reinforcing bar as per the method in Phase II, Section 3.3.2.

3.4.3 MEASUREMENTS

Measurements of oxygen concentration, half-cell potential, linear polarization resistance and potentiodynamic scans will all be carried out as described in Section 3.3.3.

TABLE 3.3 EXPERIMENTAL REFERENCE TABLE FOR LOW OXYGEN CORROSION VALIDATION EXPERIMENTS

Reference	Mix	No.	Solution	Oxygen, ppm
ASW0		3	seawater	Negligible
ASW3		3		3ppm¤
ASW6		3		6ppm¤
ASWA	A	3		Atmospheric
ANACL0	(CT07)	3	NaCl	0ppm
ANACL3		3		3ppm¤
ANACL6		3		6ppm¤
ANACLATM		3		Atmospheric
BSW0		3	seawater	0ppm
BSW3		3		3ppm¤
BSW6		3		6ppm¤
BSWATM	B	3		Atmospheric
BNACL0	(CT13)	3	NaCl	0ppm
BNACL3		3		3ppm¤
BNACL6		3		6ppm¤
BNACLATM		3		Atmospheric
Total		48		

¤ change of exposure to oxygen saturated water (~8ppm O_2)

3.5 PHASE IIIB CORROSION INITIATION AND PROPAGATION IN CRACKED CONCRETE

As discussed in Chapter 2, cracking can have a significant effect on corrosion initiation and propagation. However, the corrosion due to cracks in sub-sea concrete is generally inadequately researched and continually ignored in industrial applications.

Experimental work throughout this phase will allow for the investigation of the effects of seawater composition, crack widths, and static and dynamic loading conditions on the rate of corrosion. Close attention was paid to any evidence of self-healing effects and any potentially subsequent change in corrosion rate.

3.5.1 SPECIMEN SPECIFICATIONS

Beams of mix CT07 (Table 3.1) were cast in pairs in wooden formwork. Steel reinforcing bars of 6mm diameter were located at 25mm cover and 40mm cover to the top and bottom surfaces respectively. Cross-sectional dimensions and details of the beam setup are shown in Figure 3.15 and Figure 3.16.

Preliminary experiments where loading of control beams to failure using three-point bending at 28 days were carried out (Figure 3.17). Results of this are shown in Table 3.4.

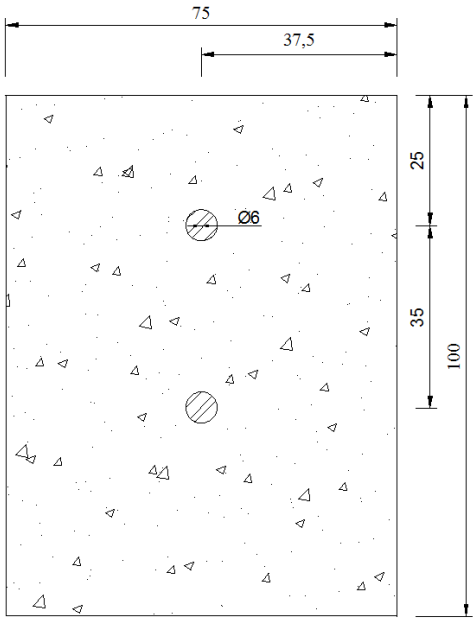

FIGURE 3.15 CROSS-SECTIONAL AREA OF BEAMS

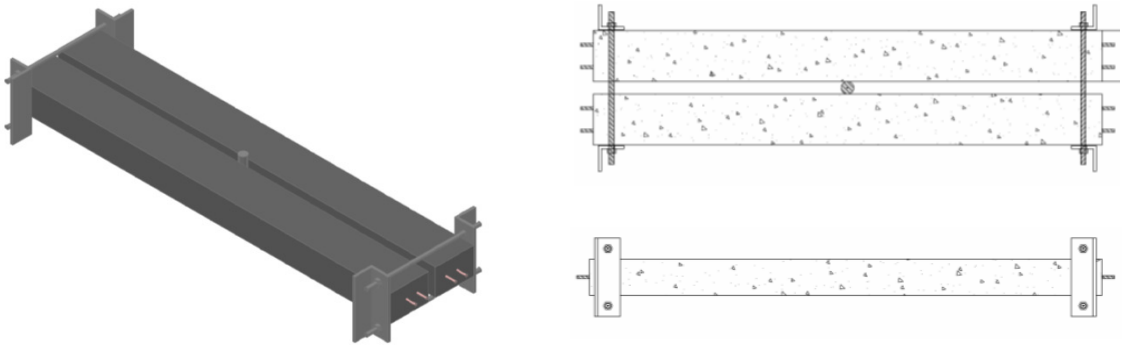

FIGURE 3.16 EXPERIMENTAL LOADING SETUP FOR STATIC CRACKING

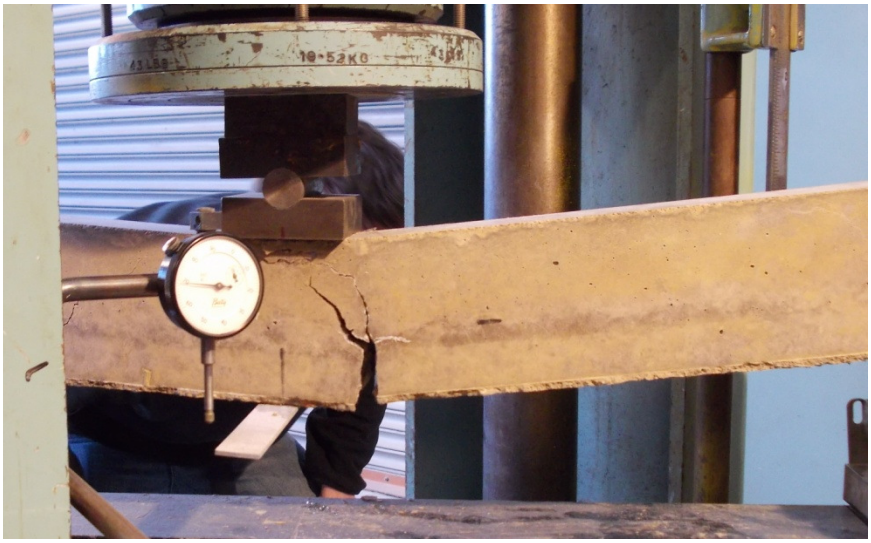

FIGURE 3.17 3-POINT BENDING TEST TO ULTIMATE FAILURE

TABLE 3.4 PRELIMINARY BEAM LOADING

Load, kN	Deflection, mm	Crack width, mm
0.0	0.00	0.0
1.1	0.06	0.0
2.0	0.14	0.0
2.7	0.22	0.0
3.5	0.64	0.15
4.1	1.27	0.25
4.9	1.60	-
5.8	2.54	1.00
6.7	5.03	2.00
7.3	7.37	2.50

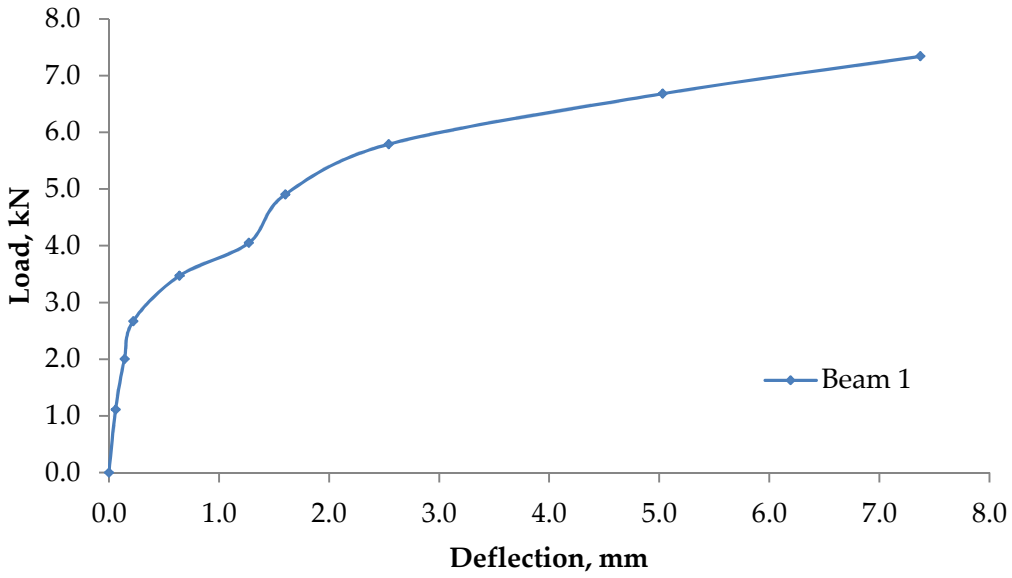

FIGURE 3.18 LOAD DEFLECTION PLOT FOR UNCORRODED BEAM UNDER THREE-POINT BENDING

3.5.2 STATIC CRACKING

3.5.2.1 EXPERIMENTAL SETUP

The static cracking experimental setup is a variation of a similar experimental cracking technique carried out by Jaffer and Hansson (2009). It was decided to bend the beams with one reinforcing bar in tension, acting as a working electrode, thus allowing for corrosion to initiate on this outer bar rather than over a combination of two bars.

Cracking is to be induced in a three-point loading rig comprising two stainless steel brackets and a round stainless steel rod as a fulcrum. Two beams are configured back to back with cracking located on the outer surface of each beam where the 40mm cover is located, as shown in Figure 3.19 and Figure 3.20.

The beams are then continuously submerged in either a sodium chloride solution or an artificial seawater solution (1M concentration of chlorides) (Table 3.5). Submerging all beams limits the oxygen available to the steel reinforcement to below 9ppm while keeping the beams saturated.

3.5.2.2 INITIATION OF CORROSION

Corrosion initiation is achieved using two methods; artificially induced through the use of an applied potential difference, and naturally induced through the diffusion of chlorides through the crack. With crack widths of 0.2mm and above, initiation of corrosion was found to occur extremely quickly and therefore there is no real requirement for artificial initiation.

Artificial initiation, however, was applied to validate results obtained in Phase II, whereby all experimental programmes used a potential driven initiation due to time constraints. By comparing the differences between the two initiation methods, the results from Phase II can be evaluated.

3.5.2.3 LOADING SCHEDULE

Loading for the static beams is achieved manually through tightening the bolts across one end of the beam sets creating a three-point bending setup. Loads are applied after 28 days of curing and transferred to submerged exposure in tanks. The crack widths are controlled by monitoring with a crack-width microscope routinely and loading adjusted accordingly.

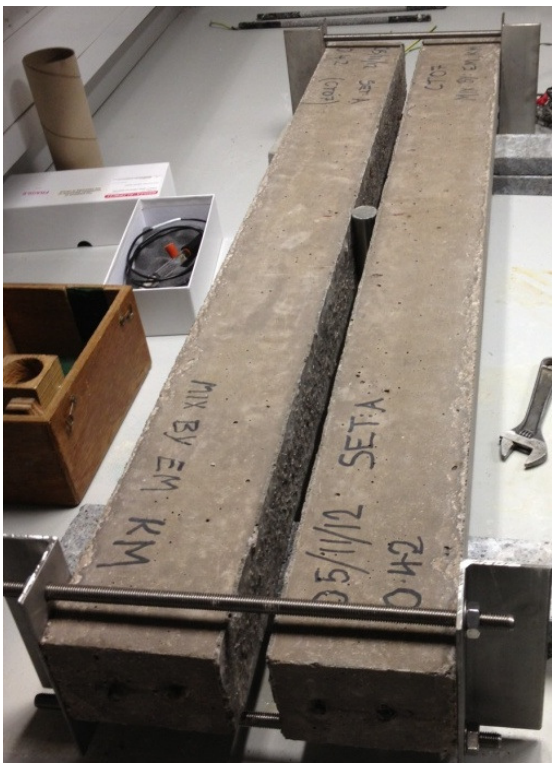

(a) loading brackets

(b) formation of a crack at centre of beam

FIGURE 3.19 LOADING SETUP

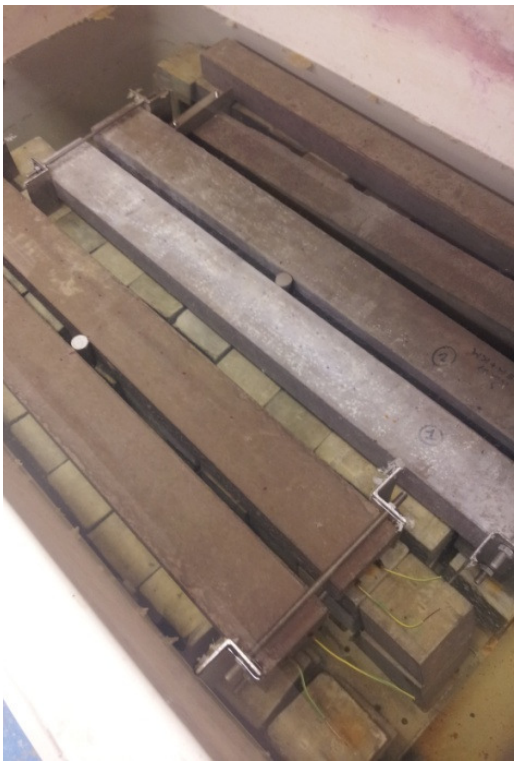

(a) seawater exposure

(b) NaCl exposure

FIGURE 3.20 SUBMERSION OF CRACKED BEAMS IN TANKS

TABLE 3.5 STATIC CRACKING EXPERIMENTAL SETS

Reference	Set	28 day cube strength,˘ N/mm²	Crack width, mm		Exposure solution[ς]	Initiation method
			Beam 1	Beam 2		
NACL02N	A	58.50	0.2	0.2	NaCl	Natural
NACL07N	B	61.70	0.7	0.7	NaCl	Natural
SW02N	C	58.45	0.2	0.2	Artificial Seawater	Natural
SW07N	D	59.30	0.7	0.7	Artificial Seawater	Natural
NACL005N	E	52.90	0.01	0.02	NaCl	Natural
NACL05N	F	56.55	0.5	0.5	NaCl	Natural
NACL02A	G	55.95	0.2	0.2	NaCl	Accelerated
SW02A	H	61.90	0.3	0.2	Artificial Seawater	Accelerated

˘ Mix design CT07 used for all beams

ς Submerged in solution at room temperature (20±2°C)

3.5.3 DYNAMIC CRACKING

3.5.3.1 EXPERIMENTAL SETUP

Complete exposure conditions and loading schedule for the dynamic cracking beams are reported in Table 3.6. The setup allows for up to four beams, sitting vertically, being submerged in aqueous sodium chloride solution and loaded horizontally using a combination of manual loading through threaded bolts and a variable actuator with a 50mm stroke and maximum force 6kN (RoboCylinder RCP2-RFA-I-PM-5-50-P1), shown in Figure 3.21. All beams are loaded with a variable repetitive load applied through the actuator to increase cracking up to desired widths and then reduce to an unloaded state.

The framework, constructed from scaffold tubes, angular steel and steel sheets have been configured to support up to four beams (Figure 3.22 and Figure 3.23). Steel, susceptible to rusting, was sprayed and the joints wrapped to assist in protecting from corrosion. To decrease the payload due to bending and friction of the loaded angle, the beams were completely unloaded, allowing for relaxation of the framework.

TABLE 3.6 DYNAMIC CRACKING EXPERIMENTAL SETS

Reference	28 day cube strength,ˇ N/mm²	Loading schemeˆ	Crack widths, mm¬	Exposure solutionˢ
NACL01D-1	57.55	0-7mm	0.15 (0.2)	NaCl
NACL02D-2	57.55	0-7mm	0.1 (0.2)	NaCl

ˇ Mix design CT07 used for all beams

ˆ 7mm final deflection at the loaded end

¬ Reported crack widths were measured in an unloaded condition after initial loading at 91 hours (final crack width due to deflection of the beam)

ˢ Submerged in solution at room temperature (20±2°C)

FIGURE 3.21 ROBOCYLINDER RCP2 ACTUATOR

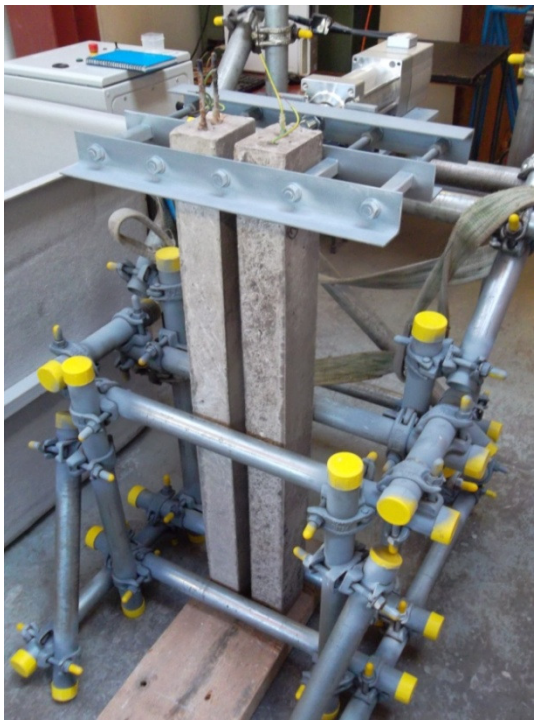

FIGURE 3.22 OVERVIEW OF FRAMEWORK FOR DYNAMIC CRACKING OUTSIDE THE TANK

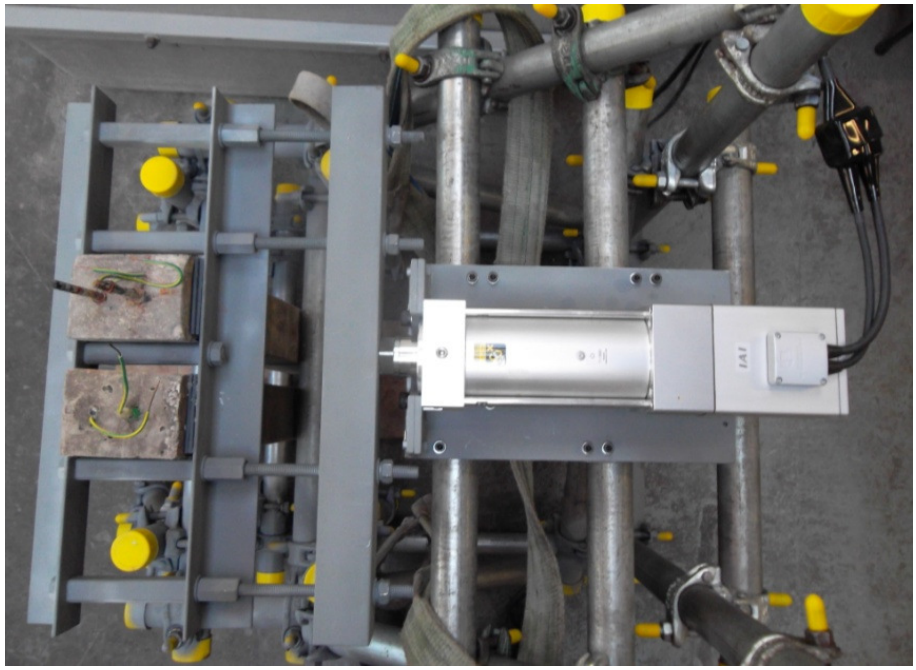

FIGURE 3.23 PLAN OF EXPERIMENTAL SETUP

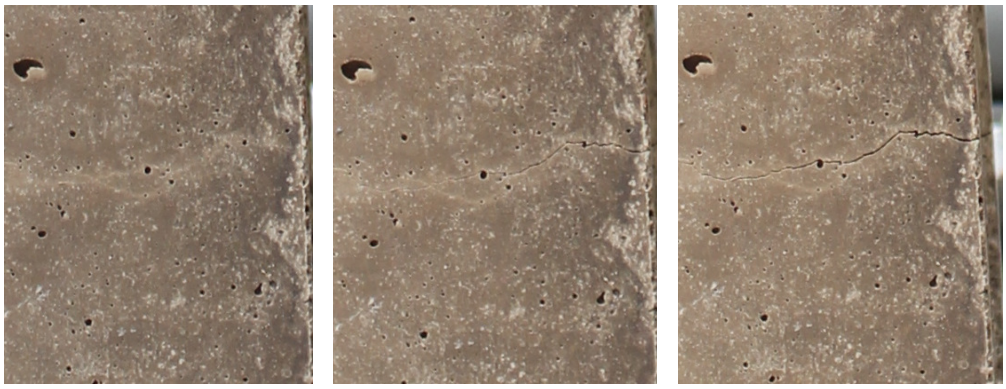

FIGURE 3.24 DYNAMIC CRACK GROWTH

FIGURE 3.25 SETUP OF DYNAMIC BEAM LOADING IN SUBMERGED ENVIRONMENT

3.5.3.2 INITIATION OF CORROSION

Similarly to static cracking experimental work, Section 3.5.2.2, initiation of corrosion was achieved using natural diffusion. Artificial acceleration of initiation through application of a potential difference was omitted during dynamic loading as corrosion occurs when chlorides reach the steel almost instantaneously through the crack, causing significant corrosion propagation at an early age.

3.5.3.3 LOADING SCHEDULE

Data were achieved on two beams by using the program, ROBO Cylinder PC Software Version 7. The beams were loaded to desired crack widths and unloaded back to an unloaded displacement with a frequency of around 0.14Hz (1 cycle every 7 seconds). The actuator was controlled by displacement rather than load, with the displacement cycling from 6mm to 22mm at the tip of the beam as shown in Figure 3.26.

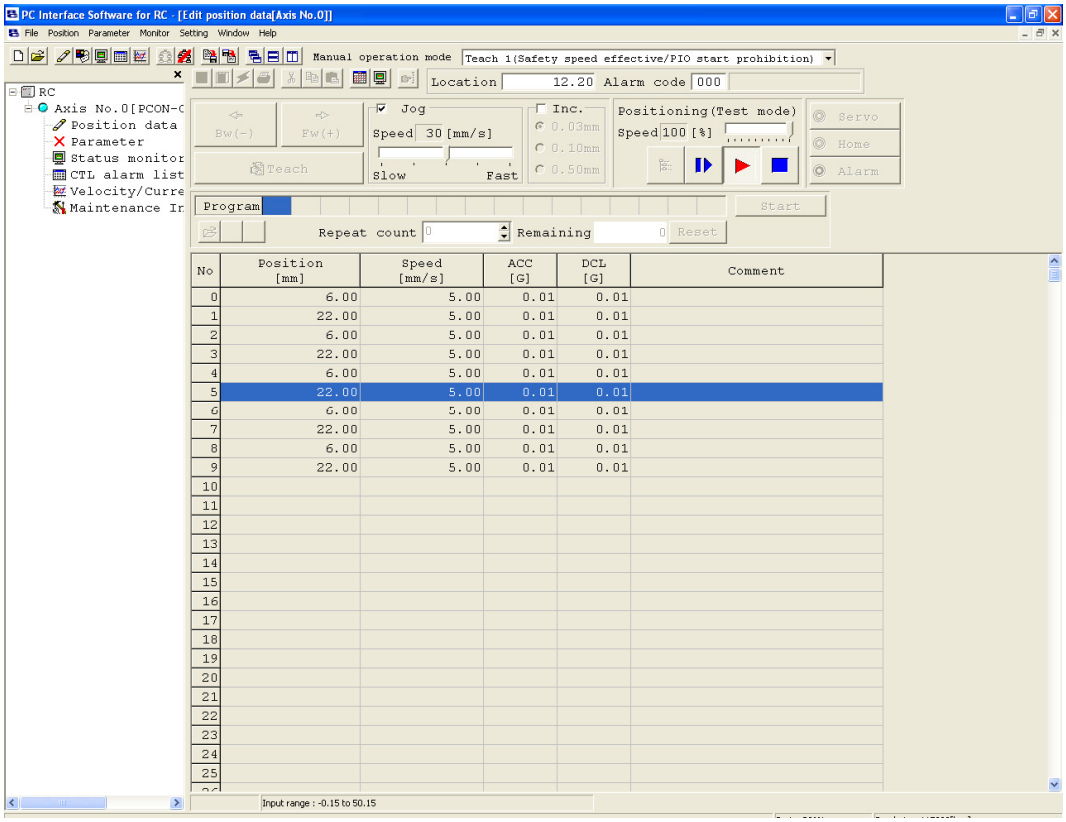

FIGURE 3.26 EXAMPLE LOADING SETUP FOR A SIMPLE CYCLIC LOADING

3.5.4 MEASUREMENTS

3.5.4.1 CORROSION MEASUREMENTS

Potentiodynamic, linear polarisation, and half-cell potential measurements were completed in an identical manner to the methods used in Sections 3.3.3.

Potentiodynamic scans were applied at a rate of between 1 and 10mV/s due to the rapid drying of the concrete under testing conditions. A balance was struck between the requirement for consistent measurements and a changing environment. The results were carefully examined with the use of LPR and HC measurements to determine suitable predictions of corrosion rates. HC potentials were measured 5 minutes after retrieving from the tanks.

Measurements continued up to 3 months or until corrosion rates stabilised.

3.5.4.2 CRACK WIDTHS

Crack width measurements were taken periodically to determine if the crack width varies over time. These crack widths, however, could only be determined once the loading has been removed, preventing the maximum crack width measurement from being precisely known. Dynamic loading will cause the crack widths to increase over time without the effect of corrosion, however as the deflection remains constant, the loading force may be reduced and crack widths maintained as constant. Corrosion will, subsequently, decrease the tensile capacity of the steel and possible bond loss will reduce the stiffness of the section. Combining these effects will increase the deflection and the crack width of the beams.

3.6 PHASE IV STRUCTURAL EFFECT OF CORROSION OF REINFORCEMENT

Phase IV is an additional set of experiments aimed at defining the effects that pitting and general corrosion has on structural capacity of beams with straight reinforcement and lapped reinforcement. This work was undertaken with Robinson (2013) and Loh (2013), with the majority of lapping experiments completed by Robinson (2013).

3.6.1 SPECIMEN SPECIFICATIONS

Concrete was cast by an external supplier using a CEM I concrete mix with a target characteristic strength of 35/40 (Table 3.7). The manufacturing plant were trialling SCC (self-compacting concrete) and therefore provided high cube strengths, which was reflected in the maximum bending strength of the beams. The mix design was as follows:

Free water/cement ratio	0.48
OPC (CEM I 52.5N)	465 kg/m^3
Cambusmore washed concrete sand	950 kg/m^3
Cambusmore 20-6mm coarse aggregate	950 kg/m^3
ADVA 576 super plasticiser	0.8% wt. cement

Cubes of side 150mm were cast with corroded and un-corroded reinforcement of length 300mm. Each end of the reinforcement was coated with epoxy, leaving 100mm exposed to the interior of the concrete allowing a bond to develop (Figure 3.27). The bar schedule and sample references are shown in Table 3.8.

Beam Set A (Table 3.9), 20 beams with dimensions 200mm x 150mm x 1500mm, were procured as shown in Figure 3.28. Artificial pitting corrosion at varying locations of the three steel bars was done prior to the application of four strain gauges located in the constant moment area of the beams as detailed in Section 3.6.3.2.

Beam Set B (Table 3.10), 20 beams also with dimensions 200mm x 150mm x 1500mm, were procured as shown in Figure 3.29. Three strain gauges are attached to each steel bar located at 125mm centres throughout the lapped area of reinforcement.

TABLE 3.7 DENSITY AND STRENGTH DATA FOR BEAM SETS A AND B

Mix date	Beams	Density, kg/m^3	Strength, N/mm^2
14 Dec 12	A1, A2, A7, A8, A14	2460	66
17 Dec 12	A5, A6, A15, A16	2480	71
18 Dec 12	A3, A10, A19, A20	2470	65.5
19 Dec 12	A4, A11, A17, A18	2480	63
20 Dec 12	A9, A12, A13	N/A	N/A
22 Apr 13	-	2470	64
23 Apr 13	-	2490	65
24 Apr 13	-	2480	67.5
25 Apr 13	-	2480	68.5

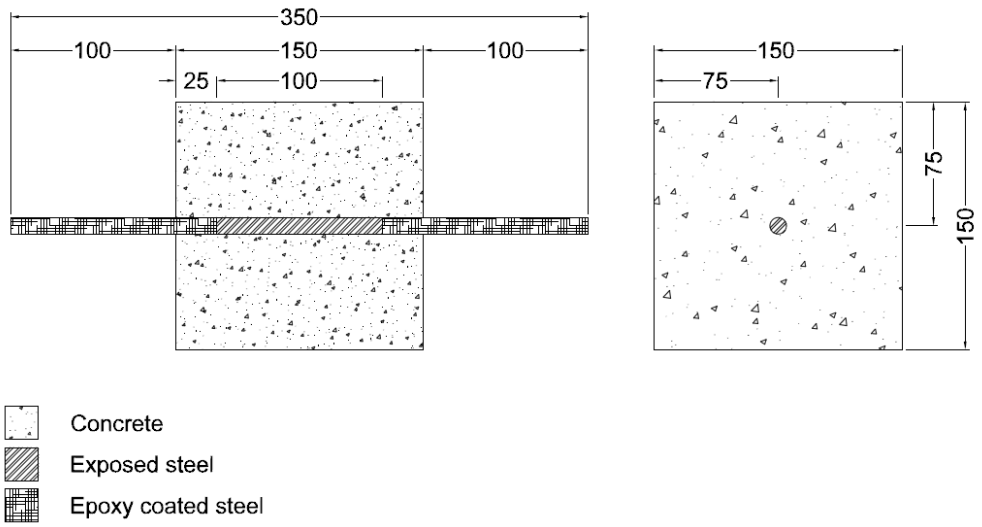

FIGURE 3.27 CUBE DIMENSIONS FOR PULL-OUT TESTING

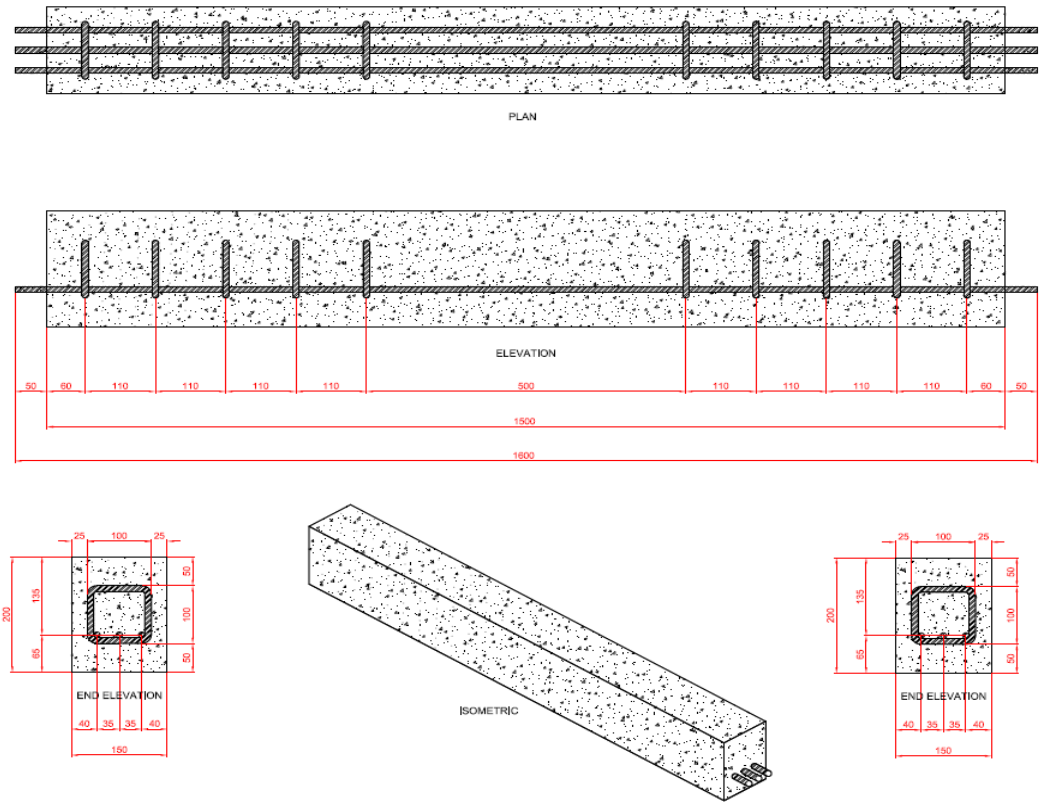

FIGURE 3.28 BEAM SET A DETAILS (ROBINSON, 2013)

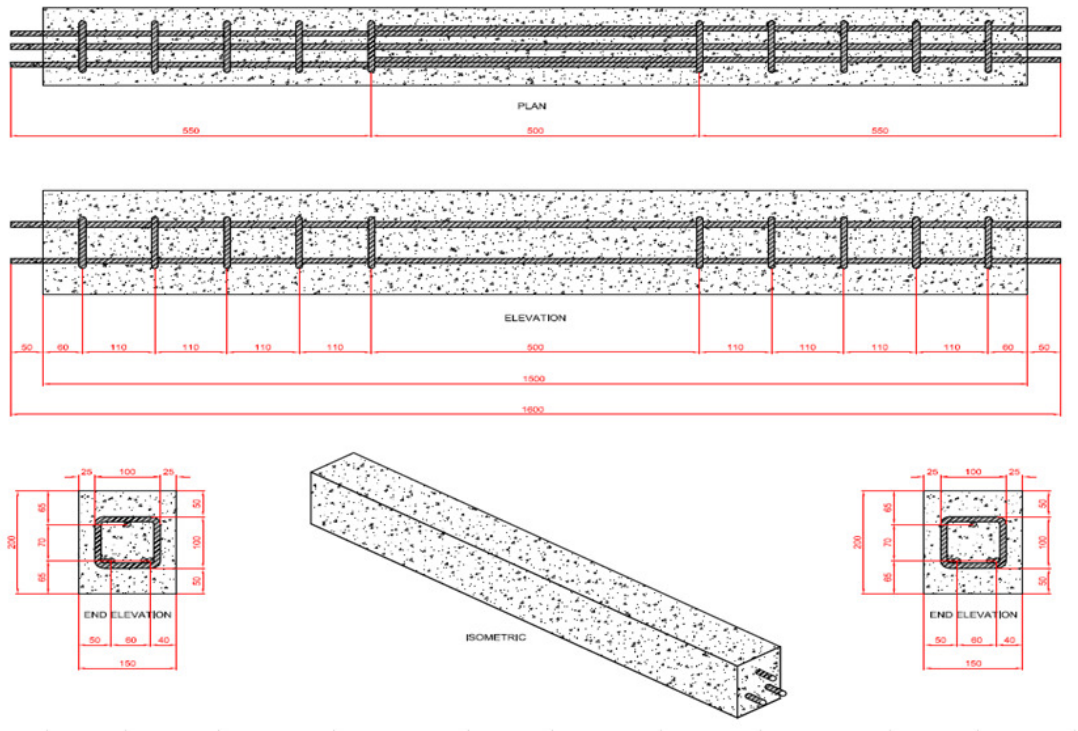

FIGURE 3.29 BEAM SET B DETAILS (ROBINSON, 2013)

TABLE 3.8 PULL-OUT BAR SCHEDULE

Reference		Description
PO1	1	Uncorroded bar - control
PO1	2	Centre 25mm ground and glued (replicating gauge attachment)
PO1	3	Centre 100mm ground and glued (replicating gauge attachment)
PO2	1	Uncorroded bar – control
PO2	2	2.5% corrosion – cast in
PO2	3	5% corrosion – cast in
PO2	4	7.5% corrosion – cast in
PO2	5	2.5% corrosion – bar cast in and forced corrosion
PO2	6	5% corrosion – bar cast in and forced corrosion
PO2	7	7.5% corrosion – bar cast in and forced corrosion

TABLE 3.9 BAR DETAILS FOR GENERAL AND PITTING CORROSION – BEAM SET A

Beam	General Corrosion, % wt. steel			Pit depths, mm								
				Bar 1			Bar 2			Bar 3		
	Bar 1	Bar 2	Bar 3	L	C	R	L	C	R	L	C	R
1	0	0.0	0.0									
2	0	9.0	0.0									
3	0	9.0	0.0					1.03				
4	0	11.0	0.0					0.78	1.36			
5	0.0	10.0	0.0				1.6	1.12	1.15			
6	5.6	5.6	5.6									
7	12.0	0.0	0.0		0.74							
8	12.0	0.0	0.0		0.93	1.08						
9	10.0	0.0	0.0	1.1	0.75	1.09						
10	9.0	9.0	9.0									
11	9.8	9.8	0.0		1.4			1.52				
12	20.0	20.0	0.0		1.11	0.79		0.85	1.18			
13	8.0	8.0	0.0	1.35	1.17	1.21	1.14	1.38	0.98			
14	13.5	13.5	13.5									
15	8.2	8.2	8.2		0.88			1.18			1.19	
16	2.5	2.5	2.5		1.05	0.94		1.01	0.88		1.27	1.45
17	9.8	9.8	9.8	1.00	1.21	0.74	1.03	1	1.1	1.49	0.87	1.24
18	Taped	0	0		Taped							
19	0	Taped	0					Taped				
20	Taped	Taped	0		Taped			Taped				

TABLE 3.10 BAR DETAILS FOR GENERAL AND PITTING CORROSION – BEAM SET B

Beam		General Corrosion, % wt.	Pitting, mm							
		All bars	Bar 1a		Bar 1b		Bar 2a		Bar 2b	
			A	B	A	B	A	B	A	B
1	A	0								
	B	0								
2	A	5								
	B	5								
3	A	10								
	B	10								
4	A	20								
	B	20								
5	A	5	X							X
	B	5	X							X
6	A	5		X					X	
	B	5		X					X	
7	A	10	X							X
	B	10	X							X
8	A	10		X					X	
	B	10		X					X	
9	A	20	X							X
	B	20	X							X
10	A	20		X					X	
	B	20		X					X	

3.6.2 PULL-OUT TESTING

Pull-out testing was completed using the setup shown in Figure 3.30. Measurements of force against displacement were recorded and plotted to compare the effects of corrosion on concrete/steel bond. This testing was aimed at providing information for the further experiments by providing an insight into the effects of corrosion on bond loss, as well as any loss of bond due to the gluing of strain gauges onto the bars.

Alterations to the schedule were made after the initial cubes were tested due to the lack of bond movement (measured using LDVTs) at corrosion levels of up to 7.5%, and updated schedules are discussed in Chapter 7.

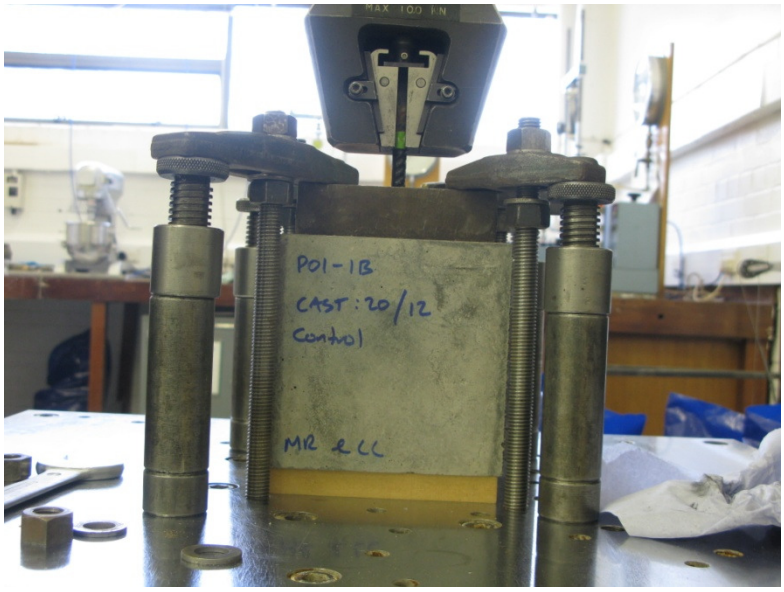

FIGURE 3.30 PULL-OUT TEST EXPERIMENTAL SETUP

3.6.3 STRAIN DISTRIBUTIONS OF CORRODED REINFORCED BEAMS

3.6.3.1 EXPERIMENTAL SETUP

Four-point bending tests were conducted on all beams after corrosion, loading to ultimate failure while measuring deflections, strains and crack patterns (Figure 3.31).

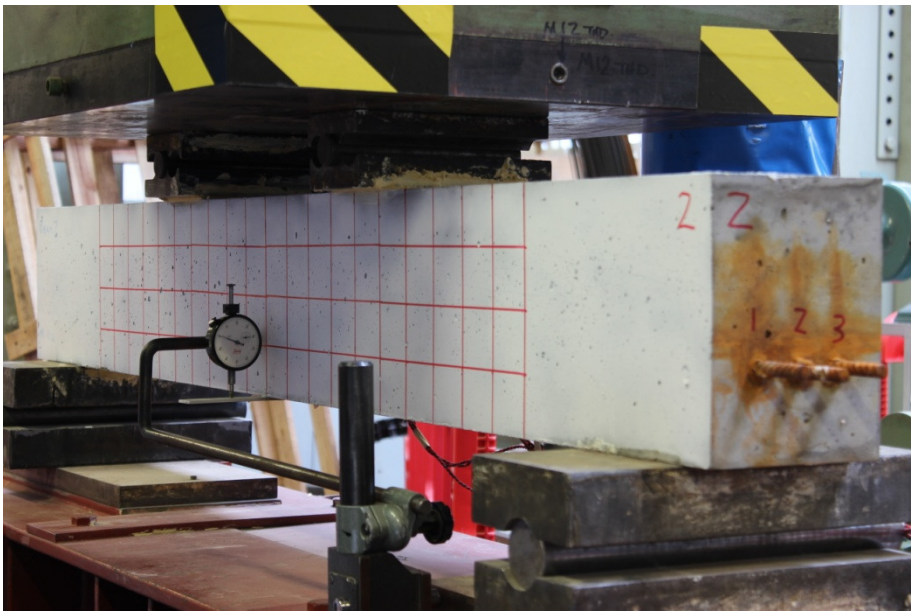

FIGURE 3.31 FOUR-POINT BENDING TESTING WITH DEFLECTION AND STRAIN MEASUREMENTS

3.6.3.2 CORROSION OF REINFORCEMENT

Prior to casting, pitting corrosion was induced using a potential difference of 12V between a copper wire cathode above a wet sponge electrolyte and the steel reinforcement. Electrical tape limited the area of steel in connection with the electrolyte, causing an artificial square pit of target depth 1mm (Figure 3.32). The depths of induced pits were then measured using callipers with the potential difference removed when the pit depth reaches 1mm.

After casting, a positive terminal is connected to the corroding bars and the negative terminal to a cathode located in a pond setup on the top of an inverted beam (Figure 3.33 and Figure 3.34) a direct electric current was applied forcing a generalised corrosion of the steel. The percentage mass loss of the steel was then estimated from the averaged current and time.

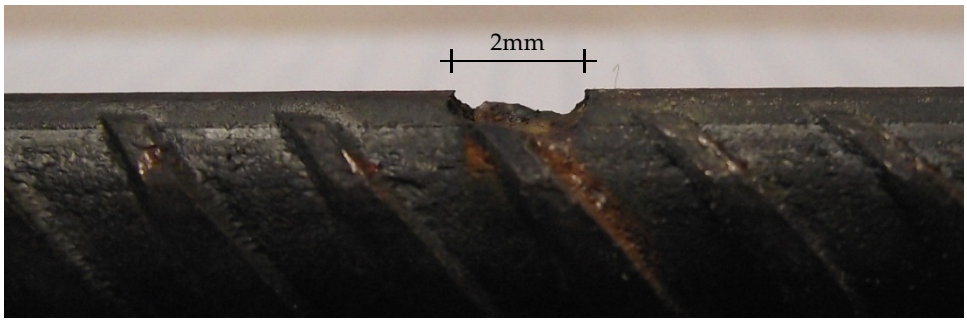

FIGURE 3.32 ARTIFICIALLY INDUCED PITTING CORROSION

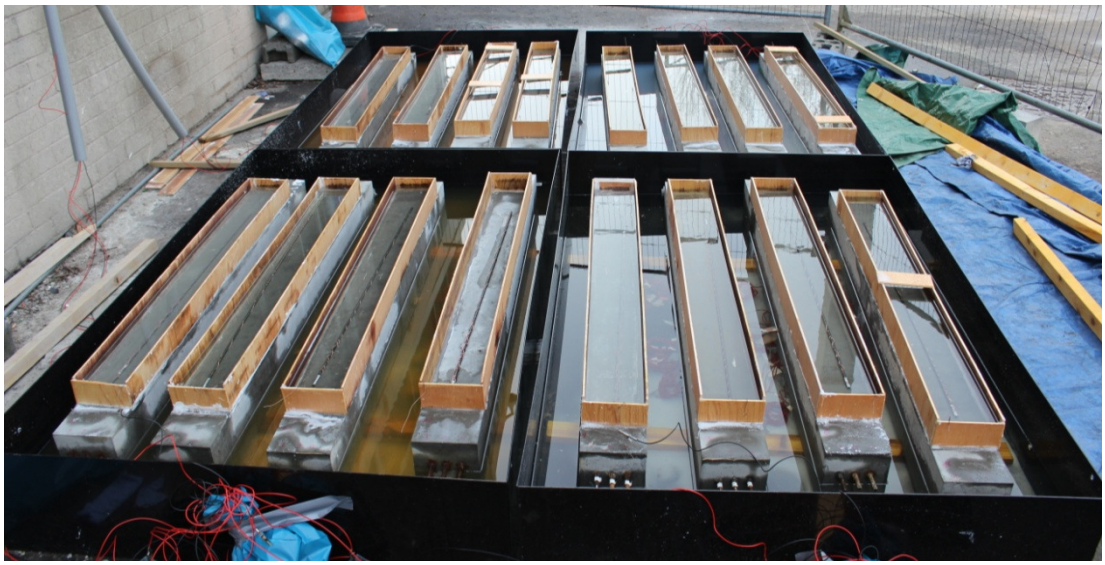

FIGURE 3.33 OVERVIEW OF BEAMS DURING CORROSION

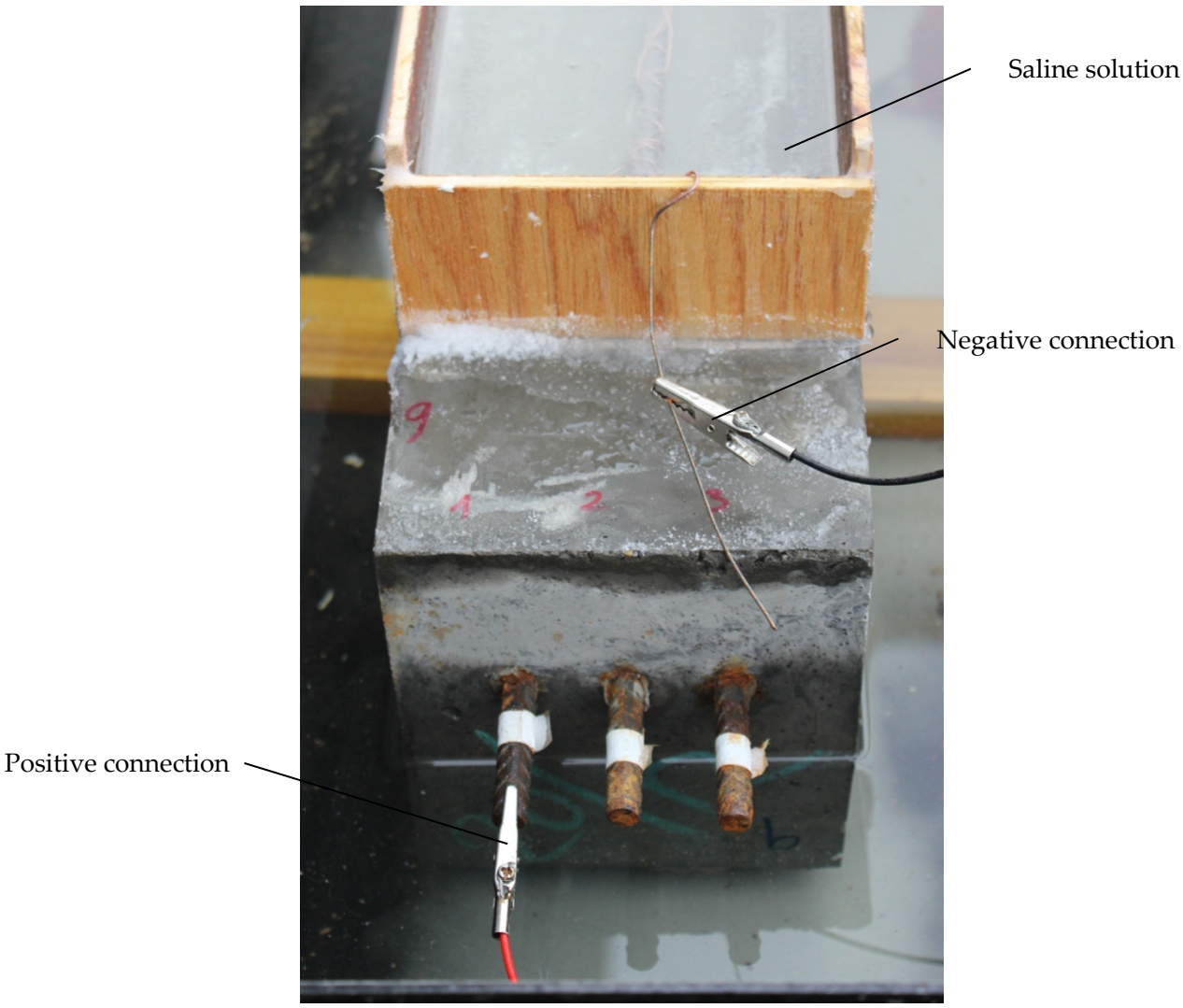

FIGURE 3.34 CONNECTION OF BEAM 1 BAR 9 DURING THE APPLICATION OF A CORROSION CURRENT

3.6.3.3 LOADING SCHEDULE

Loading was completed at a rate of 10kN/min using a 4-point loading setup, up to ultimate failure whereby the peak load cannot be sustained. Deflection measurements were made every 2kN increments, with strain readings being logged through a Microlink data logger once per second.

Cyclic loading of lapped sections consisted of 4 cycles to 10kN then 1 cycle to 60kN, repeated then loaded to failure.

CHAPTER FOUR

4 EFFECTS OF THE SOURCE OF CHLORIDES ON THE INITIATION OF CORROSION IN REINFORCED CONCRETE

4.1 INTRODUCTION

As results reported in literature and measured during previous research carried out in the Concrete Technology Unit (CTU) at the University of Dundee (e.g. Abu Hassan, 2012) show there are significant discrepancies between expected chloride concentrations and actual chloride concentrations in marine and offshore structures.

From laboratory measurements, and cores from marine structures, several researchers have attempted to explain the differences between observed chloride profiles and profiles obtained from the laboratory through the application of an ageing factor, which reduces the chloride diffusion rate exponentially over time for a fixed number of years (Thomas and Bamforth, 1999; Helland, 2008; Andrade, Castellote and d'Andrea., 2011). Other researchers have noted that alternative mechanisms in the surface layer of the concrete may be critical in the apparently slower diffusion rates noted in real structures (Mohammed, Yamaji and Hamada, 2002b).

Laboratory methodologies to study chloride diffusion and migration commonly use sodium chloride solutions (NT Build 443, ASTM C1202, CEN TS 12390-11). Use of pure solutions may lead to an unrealistic interpretation of chloride movement through concrete exposed to seawater if other components of seawater play an active part in influencing diffusion. In order to assess the influence of other components in the seawater on chloride diffusion, experimental work was carried out in an attempt to further understand the transport of chlorides through concrete and attempt to quantify differences between results when exposed to the more complex environment that seawater presents.

The study comprised a number of samples with varying mix designs (see Table 3.1) submerged in seawater and sodium chloride solutions, with chloride measurements and recordings taken in accordance with CEN TS 12390-11. Migration experiments (MR and NTBuild 492) were carried out on CEM I concrete to evaluate the suitability of these methods with the use of artificial seawater, and determine if short term experiments yield equivalent,

reduced, or increased chloride diffusion coefficients compared to the use of sodium chloride solutions.

From the measurements, estimates of diffusion coefficients suitable to model the submerged concrete in specific offshore structures are obtained. These provide a mean and standard deviation for use in deterministic and probabilistic modelling and allow for the time to initiation to be determined and assessed.

4.2 SUBMERGED NATURAL DIFFUSION

Although there are potentially a number of different transport mechanisms of chlorides, in submerged concrete it can be assumed that diffusion is the predominant, if not the only, transport mechanism acting prior to corrosion initiation. Diffusion coefficients were determined for all mixes at an age of 90 days, as shown in Table 4.1.

Chloride diffusion coefficients for all mixes correspond to values expected for concretes of those qualities as reported in literature and extensively researched (eg. Abu Hassan 2013).

Results from artificial seawater experiments at an age of 90 days show little or no diffusion of chlorides into the concrete, even though there are significant concentrations of chlorides in the surface layer of the concrete up to 1mm depth. This supports a view by Abu Hassan (2013) that alternative chemical interactions between the concrete matrix and alternative ions present in seawater are having a reducing effect on chloride transport. At 180 days, CEM I concretes continued to show no further ingress of chlorides from artificial seawater exposure.

Typical chloride profiles showing the variation between seawater and NaCl solutions is shown in Figure 4.1. Samples shown, CT01B and CT08B, contain negligible concentration of chlorides deeper than 3mm into the concrete.

TABLE 4.1 AVERAGED DIFFUSION COEFFICIENTS AT 90 DAYS

Reference	NaCl				Seawater
	D_{app} x10^{-12}, m^2/s		C_s, % wt. concrete		D_{app} x10^{-12}, m^2/s
	μ	σ	μ	σ	
CT01	1.81	0.30	0.45	0.05	
CT02	2.29	0.20	0.33	0.06	
CT03	0.91	0.20	1.42	0.19	
CT04	1.17	0.13	1.52	0.14	
CT05	0.19	0.05	1.45	0.20	
CT06	0.54	0.18	0.70	0.10	
CT07	1.32	0.39	1.20	0.16	
CT08	2.82	0.63	0.41	0.03	
CT09	1.18	0.15	1.53	0.22	Due to no significant ingress of chlorides, diffusion coefficients could not be determined.
CT10	1.45	0.56	1.98	0.21	
CT11	0.52	0.13	0.93	0.06	
CT12	1.65	0.21	1.69	0.16	
CT13	1.84	0.57	0.46	0.05	
CT14	1.42	0.08	1.70	0.13	
CT15	1.91	0.02	1.98	0.09	
CT16	1.02	0.37	1.02	0.06	
CT17	1.97	0.19	1.46	0.11	
CTBD	0.99	0.20	1.32	0.18	
CTN	1.93	0.60	0.36	0.10	

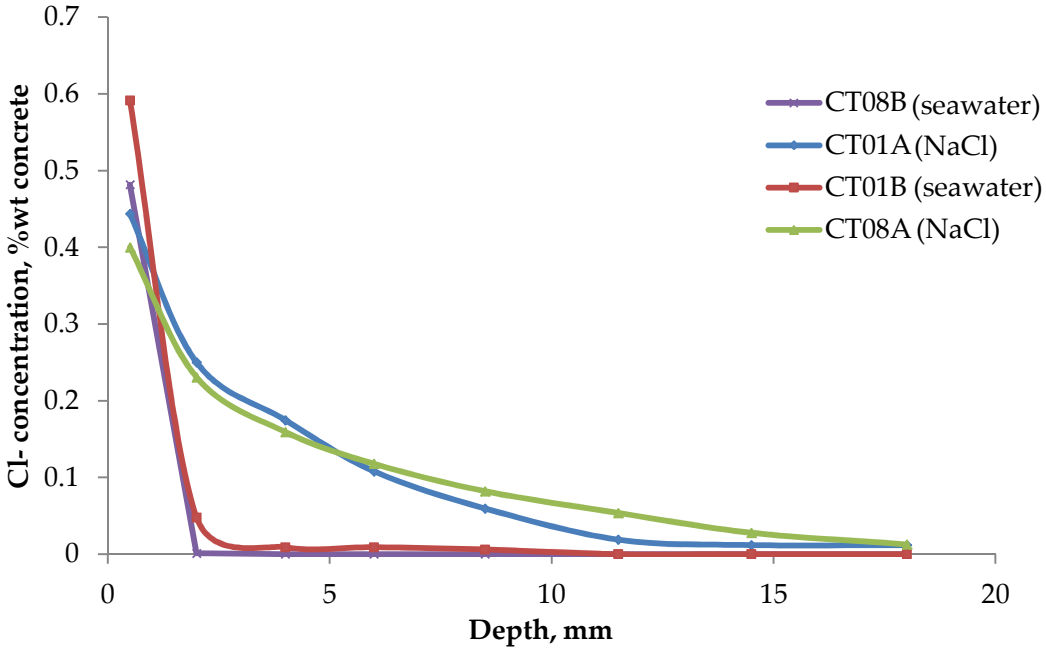

FIGURE 4.1 TYPICAL CHLORIDE PROFILES FOR CEM I CONCRETES IN NACL AND SEAWATER SOLUTIONS (AFTER 90 DAYS)

4.3 CHLORIDE MIGRATION

Chloride migration test methods are rapid but use an externally applied electric potential across the specimen. Multi Regime (MR) tests and NT Build 492 were carried out on 5, CEM I concrete types; 02, 07, 08, N and BD.

4.3.1 MULTI-REGIME (MR) TEST

Results from the MR test methods show no correlation between results from sodium chloride (NaCl) or seawater exposure as shown in Figure 4.2. Measured diffusion coefficients are unpredictable with large variations between results. The method of measuring the conductivity of the downstream cell is suitable for the use of NaCl, as only the chloride ion will influence the conductivity due to the absence of alternative anions in the solution. The transport of additional ions, most notably sulphates, will cause an increase in conductivity leading to incorrect chloride measurements. Therefore, the MR test should not be used to evaluate transport of chlorides from a seawater solution.

4.3.2 NT BUILD 492

When exposed to NaCl solution, NT build results are in agreement with trends seen using natural diffusion test methods, producing diffusion coefficients that are up to twice as large as those measured with exposure to seawater, as shown in Figure 4.3. As the measurement

technique determines the chloride concentration only, the results are more reliable than those from the MR test.

The difference is observable throughout a 24 hour test, suggesting that competition between sulphate and chloride ions through the pore structure could be a contributing factor. It is likely that due to the potential difference applied and short duration of the testing, a pore blocking mechanism is unlikely to have established fully. However, it is possible that physical blocking mechanisms through either the deposition of brucite on the surface, or constriction of the pores due to a rapid reaction of sulphates with the cement paste causing a build-up of gypsum or ettringite, could prevent further chloride ingress.

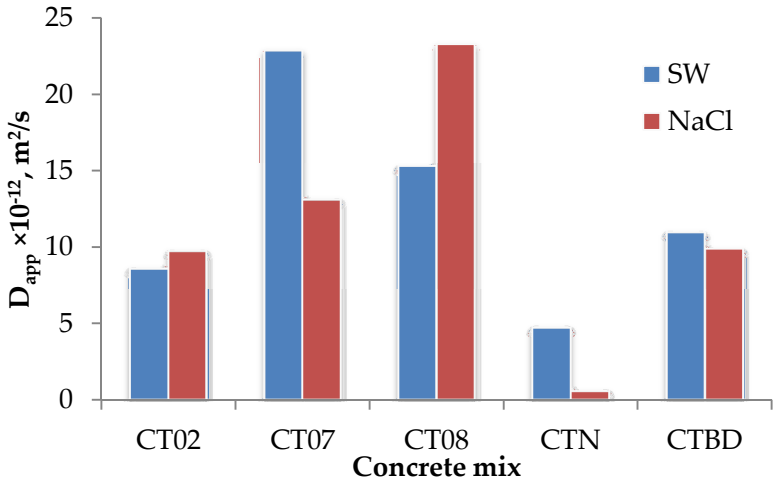

FIGURE 4.2 MR TEST RESULTS FOR 5 CEM I CONCRETE MIXES

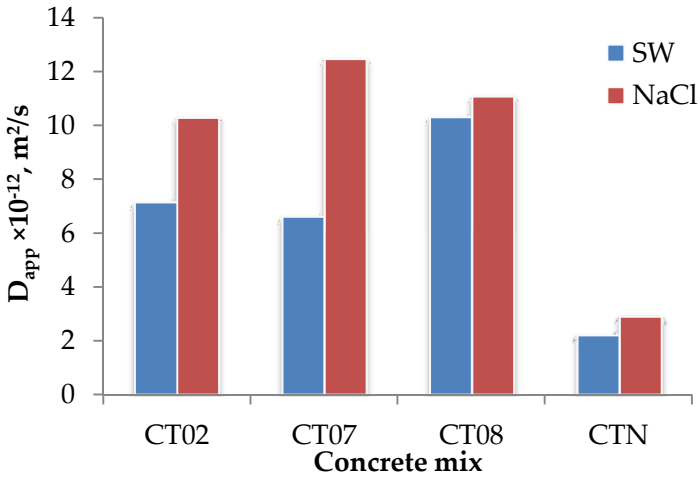

FIGURE 4.3 NT BUILD 492 TEST RESULTS FOR 4 CEM I CONCRETE MIXES

4.4 COMPARISONS BETWEEN TIDAL AND SUBMERGED CHLORIDE INGRESS

4.4.1 ARTIFICIAL SEAWATER

Results obtained by Abu Hassan (2013) of tidal exposure experiments using artificial seawater, as described in Chapter 3, of 1M chloride concentration are summarised in Table 4.2. Typical profiles are shown in Figure 4.4.

Care must be taken when utilising D_{app} and C_s values obtained through the use of fitting Crank's solution to the measured values obtained from concrete profiles where seawater was the exposure solution. Measured diffusion values remain artificially high when using common practice and ignoring the first measured point, and in contrast C_s is much lower than the first measured point.

By calculating the diffusion coefficients using all points produces Cs values much larger and much reduced D_{app} values (Table 4.3). Although the profiles shown in Figure 4.5 appear to show that ignoring the first point provides a better fit, regression analysis proves that including all points for this type of exposure provides a slightly better fit when maximising R^2.

TABLE 4.2 DIFFUSION RESULTS OF CONCRETE EXPOSED TO TIDAL SEAWATER OBTAINED BY ABU HASSAN (2013)

Concrete mix	**w/c ratio**	**D_{app} ($x10^{-12}$), m^2/s**	**Cs,** %wt. concrete
CEM I	0.35	1.23	0.106
CEM I	0.4	3.45	0.086
CIII/A	0.5	0.56	0.153
CV/A-M (S-LL)	0.55	0.44	0.141
CIII/B	0.5	0.92	0.614
CII/B-V	0.5	2.42	0.080
CIV/B-V	0.5	4.18	0.636

TABLE 4.3 CALCULATED VALUES FOR TIDAL EXPOSURE SAMPLE ZD1.35 7/4 S2 22/6 XS (ABU HASSAN 2013)

	C_s, %wt. concrete	D_{app} (x10^{-12}), m^2/s	R^2
Ignoring first point	0.110	1.27	0.990
All points	0.602	0.08	0.991

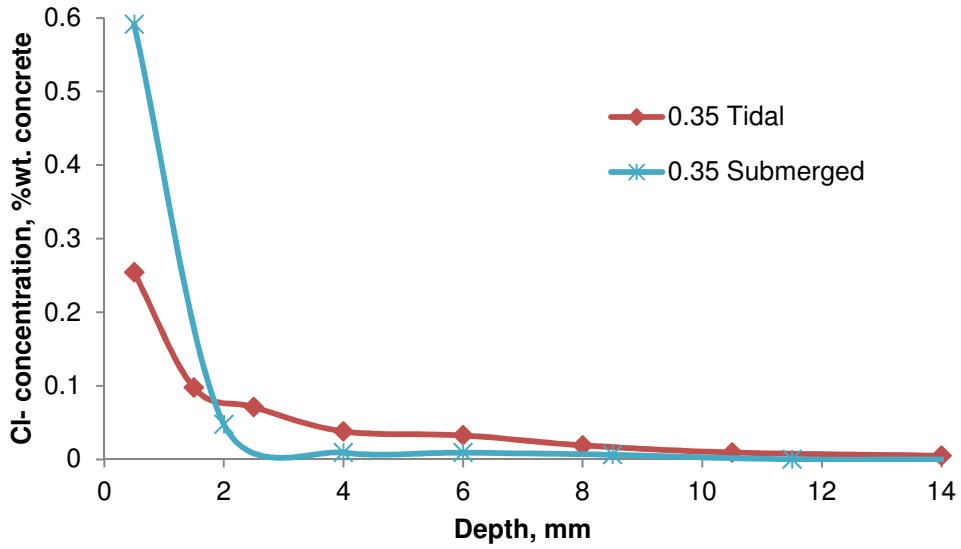

FIGURE 4.4 TYPICAL MEASURED PROFILES OF TIDAL AND SUBMERGED ARTIFICIAL SEAWATER EXPOSURE

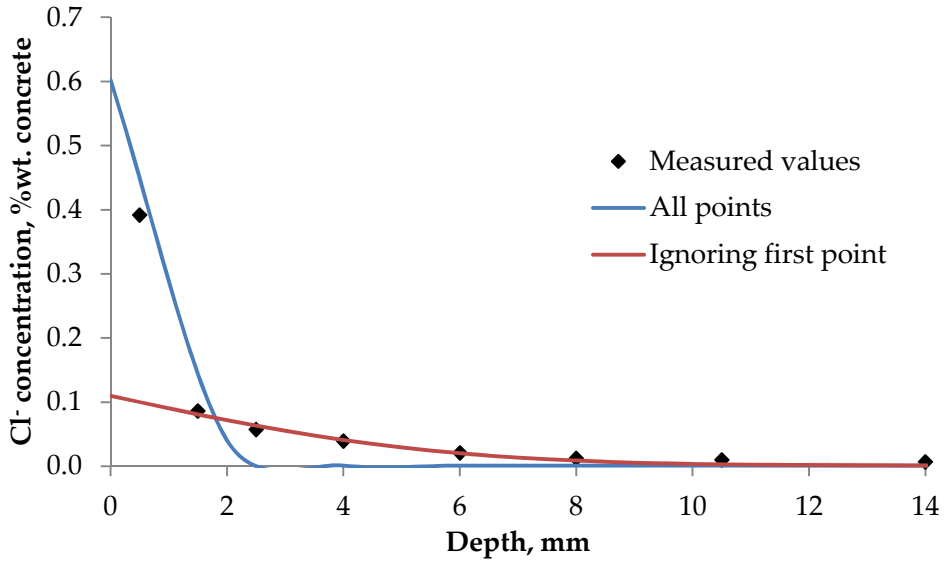

FIGURE 4.5 TYPICAL BEST FIT UTILISING DIFFERENT MEASURED VALUES (SUBMERGED)

4.5 SURFACE SKIN ANALYSIS

X-ray diffraction (XRD) analysis was carried out on a selection of samples of the concrete surface layer. XRD results, typical example shown in Figure 4.6, show no significant differences between concrete exposed to sodium chloride or seawater solutions when analysed qualitatively. Although peaks are slightly differing in magnitude, no significant variations in XRD response were noted.

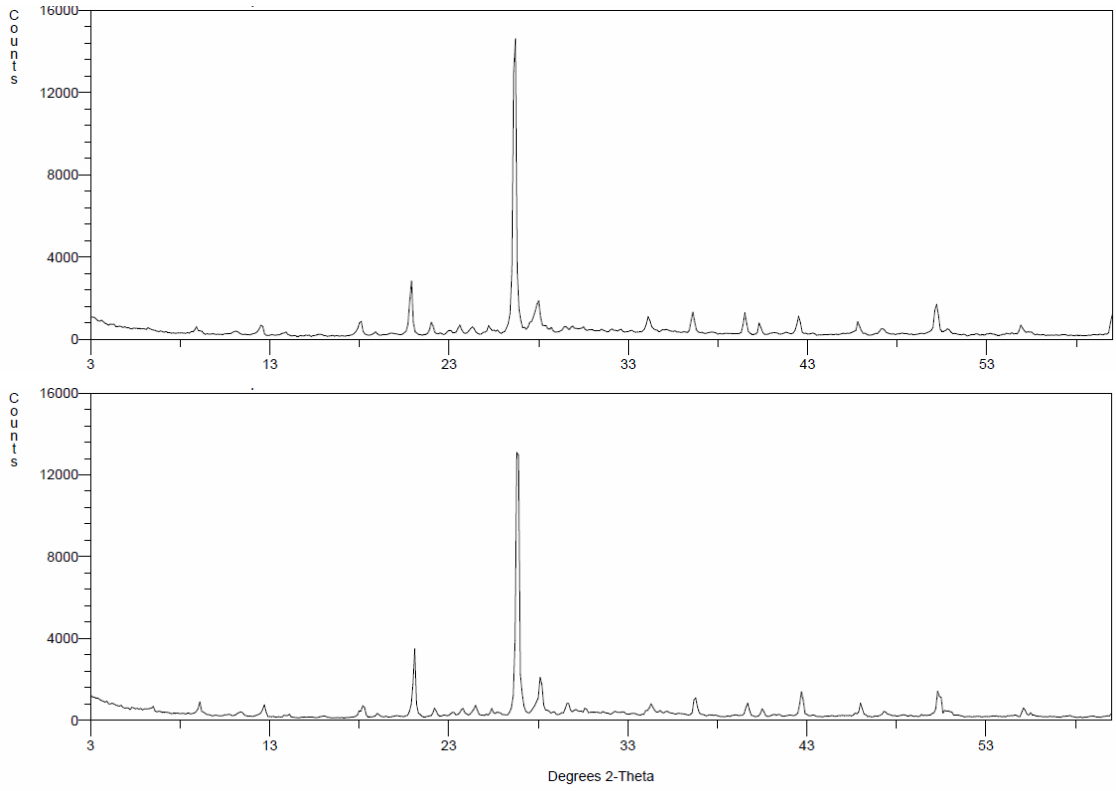

FIGURE 4.6 EXAMPLE XRD PLOTS FOR SURFACE LAYER ANALYSIS OF SUBMERGED SAMPLE CT07A (TOP) AND CT07B

XRF results comparing the surface layers of samples in seawater and sodium chloride are shown in Table 4.4.

TABLE 4.4 AVERAGE RATIOS BETWEEN CONCENTRATIONS OF IONS IN THE SURFACE LAYERS OF CEM I CONCRETES EXPOSED TO NACL AND SEAWATER

	Ca	Si	Al	Fe	Mg	Mn	Ti	K	Na	P	S
μ	0.97	1.02	1.00	1.01	1.00	0.99	1.01	1.00	0.82	1.01	0.95
σ	0.06	0.02	0.05	0.08	0.10	0.05	0.08	0.05	0.11	0.06	0.08

Sodium is the only element to show a significant difference between the concentrations within the surface layers of the two sample sets. The samples immersed in a sodium chloride solution being 18% lower than in artificial seawater. Although there is an apparently significant difference, it is unlikely this contributes to the reduction in chloride ingress observed. This could be due to the deposition of sodium sulphates from seawater into the surface layer, which are less soluble than sodium chloride and may remain in the surface layer more readily.

Other researchers (Buenfeld and Newman, 1984; Santhanam, Cohen and Aloek, 2006) had identified a difference between ions present in surface layers of concrete exposed to differing solutions, however the lack of observed or measured differences in this experiment may be due to the depth of surface layer being 1mm. If brucite is only evident in the outer 35μm as reported in literature (Chapter 2), it would be extremely difficult to determine any differences with such large layers.

4.6 EFFECT OF THE METHOD OF DETERMINATION OF D_{APP}

Determining D_{app} from chloride profiles using a least-square non-linear regression analysis is common practice (CEN TS 12390-11), although the application of this technique varies depending on researcher. Currently, CEN TG5 (unpublished) are investigating and the differences between techniques to determine a consistent D_{app} for use in service-life modelling of un-cracked concrete structures. Service life being defined as the time to initiation of corrosion due to the ingress of chlorides through diffusion based transport mechanisms.

Four methods of determining an appropriate D_{app} have been carried out on multiple profiles from samples contained within this research. All profiles are from experimental cubes carried out in accordance with CEN TS 12390-11 using only CEM I concrete with a cast surface and submerged in 1M NaCl solution. Non-linear regression analysis was used with the following variations in methodology:

- Method 1 – the outermost measured point is ignored due to variability in surface layer properties
- Method 2 – all measured points are included
- Method 3 – only D_{app} is variable with C_s fixed at the maximum measured chloride concentration ignoring first point
- Method 4 – D_{app} is variable with C_s fixed at the maximum measured chloride concentration including all measured points

Commonly, chloride profiles are of varying shape, with profiles often having a higher concentration of chlorides at the second layer than the first (Figure 4.7). Profiles obtained on CEM I concretes in this study consistently have the most concentrated chloride content in the surface layer. The discrepancy is most likely due to the use of a cut surface for the standardised test method, CEN TS 12390-11. For measured profiles where the chloride concentration is largest in the second layer, applying Method 1 would cause an artificially high C_s and a lower D_{app}.

As the chloride content of the exposed solution is kept constant throughout all samples, a fixed value for C_s would be more realistic. When predicting service life of concrete using a relatively low calculated D_{app} and an artificially increased C_s, the estimated life could be significantly overestimated.

Assuming a 50mm cover, C_{crit} of 0.07% wt. concrete, and C_s as determined for individual methods, the time to initiation of corrosion (assumed service life by many researchers) for a concrete mix was calculated using each of the stated methodologies (Table 4.5).

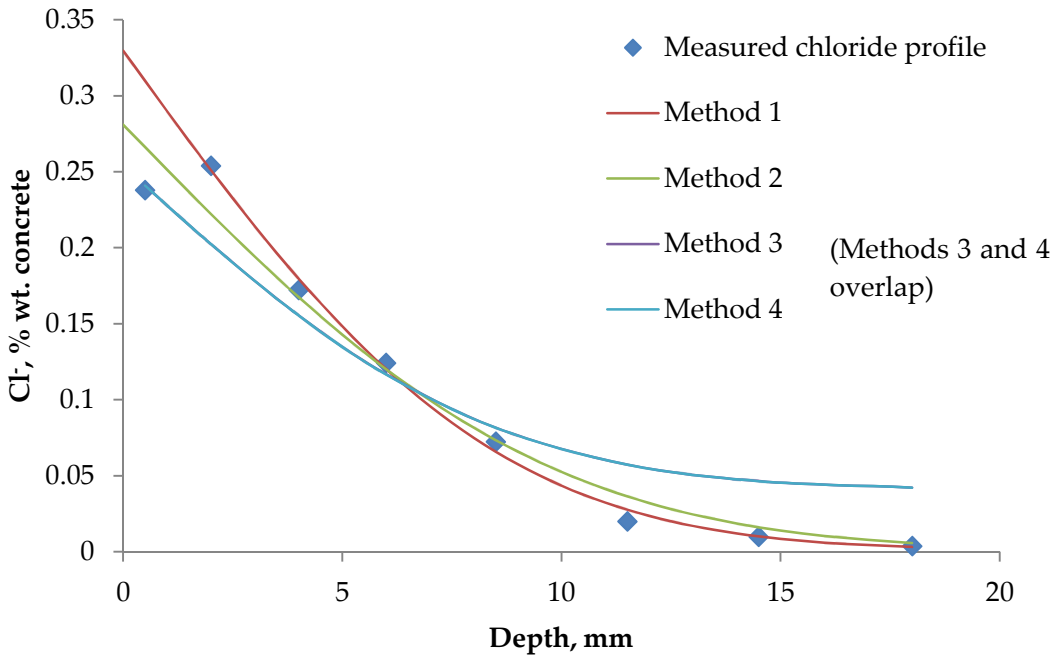

FIGURE 4.7 MEASURED CHLORIDE PROFILE AND COMPARISON OF METHODS OF DETERMINATION OF DIFFUSION COEFFICIENT AND CHLORIDE SURFACE CONCENTRATION

TABLE 4.5 EXAMPLE OF CALCULATED DIFFUSION COEFFICIENTS, SURFACE CHLORIDE CONCENTRATIONS AND TIME TO INITIATION

Method	D_{app} ($x10^{-12}$), m^2/s	C_S, % wt. concrete	t_i, years
1	2.79	0.330	9.1
2	3.64	0.281	8.2
3	2.71	0.254	12.3
4	2.71	0.254	12.3

For the purposes of long term modelling, as required for existing offshore structures, it is recommended curve fitting for chloride profiles obtained from standardised submerged testing should be achieved through Method 4. Although the R^2 coefficient is not always the best, taking into account all measured data is important whilst fixing the surface chloride concentration to either the highest value or an agreed constant as determined by the exposure conditions. Fixing this surface concentration will provide a more realistic determination of diffusion into the concrete as diffusion is driven by a concentration gradient. It should be noted that this method of curve-fitting and determination of D_{app} should be used for profiles obtained from laboratory methods in a submerged environment and not structures in the tidal, atmospheric or splash zones. At these locations alternative chloride transport mechanisms, such as absorption or convection, can significantly influence the obtained profiles, and therefore fitting an error function curve assuming a diffusion-based transport mechanism may be erroneous.

Although it is suggested that these diffusion coefficients could be used in predicting initiation time if necessary, extrapolating data from laboratory testing at 90 days to decades of exposure is extremely unreliable. As there is large variability between results obtained from different experimental procedures and calculations, diffusion coefficients should be used as a guideline to assist in concrete mix designs.

4.7 KEY OBSERVATIONS

4.7.1 EFFECTS OF ALTERNATIVE IONS FROM SEAWATER SOLUTIONS

Difficulty in predicting the initiation of corrosion due to chloride ingress from exposure to seawater solutions remains because of the inability to single out one mechanism causing the prevention of chlorides through short term testing. The combination of the large number of alternative ions appears to cause an observed reduction in the chloride ingress, although this is unquantifiable from short term exposure.

Currently ageing factors are applied to concrete structures to explain frequent variations between measured diffusion coefficients using laboratory testing and 'real world' profiles after natural exposure including additional ions. Although there is evidence of ageing in laboratory studies, the discrepancy between some measured diffusion coefficients can be explained through a 'seawater effect' (i.e. the difference in composition between NaCl solutions and seawater)

Sampling of further concrete specimens submerged for a longer duration is likely to provide diffusion coefficients for seawater exposure, which will allow for a coefficient to be applied to measured diffusion coefficients from NaCl solutions, and is recommended in Chapter 9.

Migration testing methods commonly applied through the use of NaCl are unsuitable for using seawater solutions. MR testing produces artificially high diffusion coefficients due to conductivity measurements being affected by multiple ions, and other experimental methods do not allow for the formation of any blocking mechanisms, which are apparently present in natural diffusion tests.

4.7.2 DETERMINATION OF D_{APP} FROM OBSERVED PROFILES

The method for determining D_{app} from chloride profiles can have a significant effect on estimated service life should it be defined as the time to initiation due to chloride diffusion. Values for C_s and D_{app} currently being used for long term modelling are inconsistent causing large errors in estimations of time to initiation.

It is recommended that determination of values for use in long-term modelling should be calculated using sound engineering judgement from a number of profiles collected from concrete with an identical, or at least similar, concrete mix exposed to similar conditions. Natural diffusion experiments should be used to gather chloride data, before assessing

diffusion using a value of C_s not exceeding results found on 'real world' structures when used for modelling purposes.

4.7.3 EVALUATION OF THE USE OF D_{APP} AND C_s FOR SERVICE-LIFE MODELLING

Although these diffusion coefficients are commonly used to predict the onset of corrosion, a number of variables are often omitted through the use of this technique alone.

Early age shrinkage or loading can cause cracking which can rapidly decrease the initiation period due to an increased rate of chloride ingress. Cracks are generally ignored when determining initiation times, even though life estimates ignoring cracking can be significantly higher than for cracked concrete. Additionally, ignoring alternative ions in the exposed saline solution could provide unrealistically conservative estimates for the initiation time causing concrete to be over specified.

Although determining a diffusion coefficient provides a comparative evaluation between different concrete qualities, which can be extremely useful when used in conjunction with condition surveys of existing structures, a more comprehensive modelling technique is required to provide a realistic estimate of long-term service or ultimate life. Consideration must be taken of the effects of cracking, environment, and concrete quality on the initiation period as well as the propagation of corrosion and associated damage.

Additionally, due to the heterogeneous nature of concrete, initiation of corrosion should be modelled spatially as well as temporally.

CHAPTER FIVE

5 CORROSION PROCESSES IN UN-CRACKED CONCRETE

5.1 INTRODUCTION

Experimental results from Phase II and Phase IIIA are presented and reviewed to provide analysis on the effect of submerged oxygen concentrations on corrosion rates. Tafel coefficients, corrosion potential, linear polarization resistance and corrosion currents were measured over a period of up to 6 months, which allowed for corrosion rates to settle and consistently stable rates to be measured.

48 concrete specimens were used to test differing oxygen controlled environments; sealed concrete, a single face exposed to 4ppm, 8ppm and the atmosphere. 32 beams contained gravel aggregates and the remainder contained limestone aggregates.

Validation experiments were then completed using 48 samples cast in plastic with continuous sealed ponds, to provide a variation and validation on the methodology for oxygen control. Experimental methods meant the reduced variables tested were oxygen saturated water, atmospheric exposure and sealed face.

Accelerated corrosion methods were used to initiate corrosion, which is taken into consideration when using measured rates for future remaining life calculations. Results from completed experimental work laid the foundations for cracking experiments reported in Chapter 6.

5.2 VARIABLE OXYGEN CONCENTRATION OF EXPOSED SURFACE

5.2.1 RATE OF CORROSION

The rate of corrosion is commonly reported as a corrosion rate per area of steel surface, $\mu A/cm^2$. Both current density and total current are used throughout this chapter when reporting results. The polarized area of steel, which impacts upon the severity of corrosion and the depth of penetration into the reinforcement, is important when determining the remaining cross-sectional area. In order to exercise due diligence, both units of corrosion are used and appropriate units are selected dependent on the environments and methods being investigated. This approach was used due to the variations in the cathodic and anodic areas

experienced in different environments, and assumptions are often made in order to utilise certain units which may be unrepresentative of the actual conditions.

Figure 5.1 shows the development of corrosion current density over time up to a period of 6 months. These values are the average readings of four samples (A, B, C, D) in each given exposure condition. Although Figure 5.1 suggests there is no significantly discernible difference between measured corrosion rates observed under low oxygen environments, upon removal of the steel reinforcement there was visible evidence that the corrosion mechanisms occurring are dissimilar. Care must be taken analysing results as reported in Figure 5.1 as the measured corrosion current was divided by the assumed anodic area of corroding steel.

To make a direct comparison between corrosion on each anodic bar, Figure 5.2 shows the total corrosion current of anodic bars in beams D1, negligible oxygen exposure, and D4, atmospheric exposure. In this instance, both values of i_{corr} appear to decrease as the oxygen within the system is diminished and the external perturbances are equilibrated. These currents then converge at roughly 0.2mA. This suggests that the corrosion process is limited, in this case, by the resistivity of the concrete or the oxygen availability at the cathode, as chlorides are freely accessible throughout. However, if the oxygen concentration was the predominant limiting factor, the anode to cathode ratio would be required to be much smaller for the corrosion rate to remain identical. Further investigation of the corrosion product was carried out to determine the effect of oxygen concentration on polarization areas and provide a more in-depth explanation of converging corrosion rates.

In Figure 5.1 and Figure 5.2, the lines serve to illustrate the observed trend. Current densities in Figure 5.1 are calculated assuming a polarized length of 200mm defined by the experimental methodology.

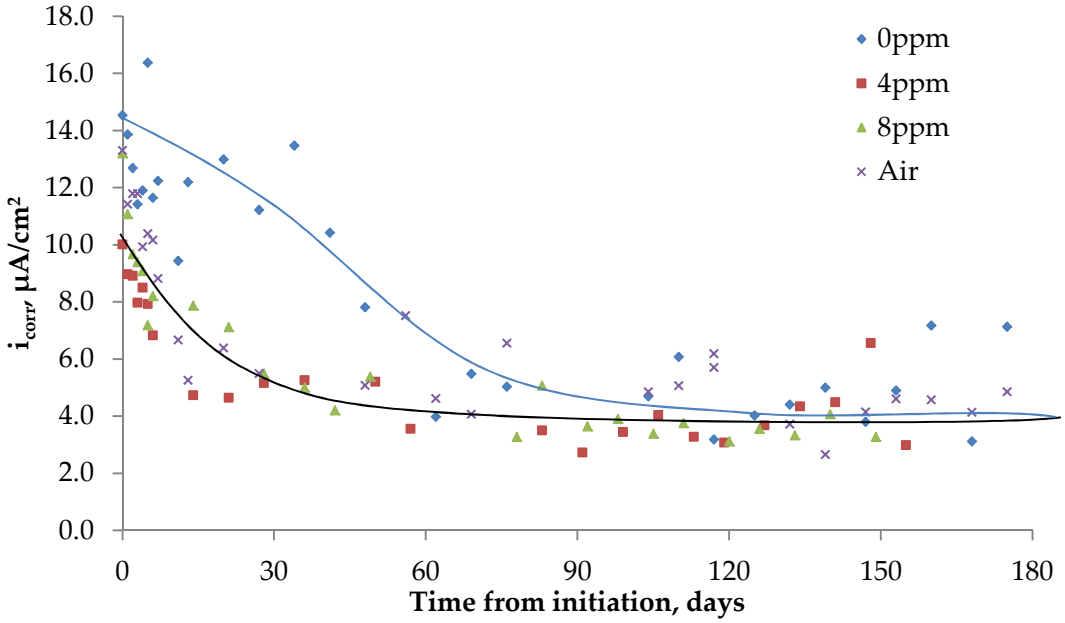

FIGURE 5.1 EFFECT OF SURFACE OXYGEN CONCENTRATION ON CORROSION CURRENT DENSITY

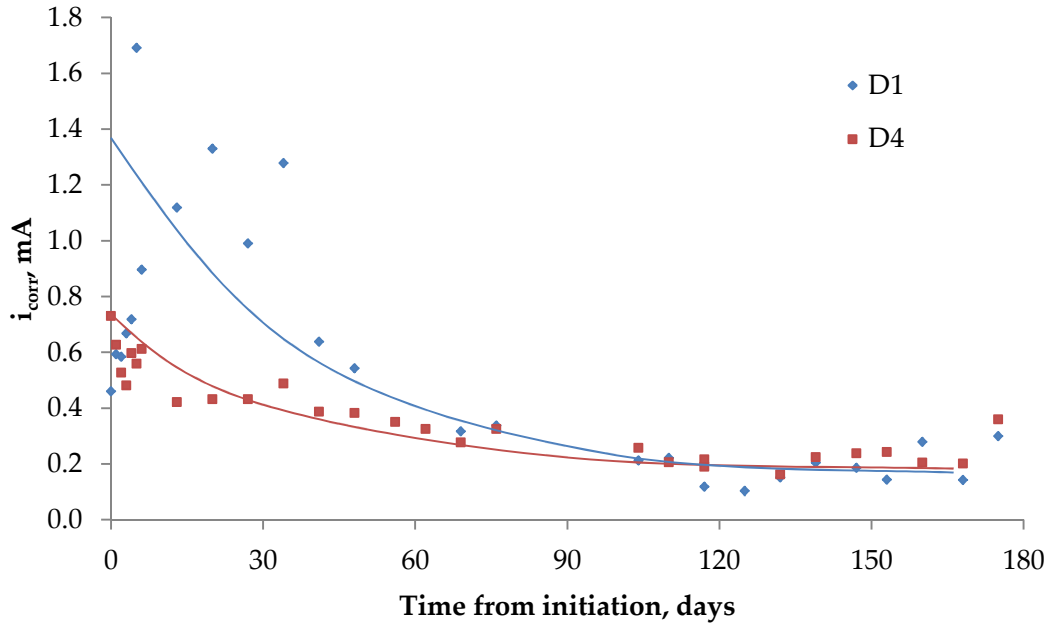

FIGURE 5.2 MEASURED CORROSION CURRENT OF BEAMS D1 AND D4

5.2.1.1 Effect of the proportionality coefficient

The proportionality coefficient commonly used to calculate corrosion currents was determined from the Stearn-Geary equation using the measured coefficients from the corresponding Tafel slopes. Averaged coefficients for each exposure condition are shown in Figure 5.3.

Poursaee (2010b), among others, suggest that for passive bars a value of 52mV should be used, depicted by the green line, and for active bars a coefficient of 26mV should be used, red line. Results suggest coefficient values lie around a value of 100mV, and therefore using 26mV as the coefficient could underestimate the corrosion current by a factor of four. Underestimating corrosion rates will significantly overestimate the life of a reinforced structure. Observed coefficients are similar to other reported values previously highlighted by the author.

5.2.1.2 Predicting the corrosion current from open circuit potentials

The open circuit potentials, or half-cell measurements, provide an indication of the expected corrosion current and can be estimated for these laboratory conditions using results shown in Figure 5.4. This method of predicting the likelihood of corrosion through quick OCP measurements can often be sufficient, however only a rough estimation of the corrosion rate is possible due to the large scatter of results. Although there is a reasonable visible correlation, the author believes a line of best fit be drawn as shown. When the OCP readings are above around 350mV, corrosion rates are extremely high and further investigation into the corrosion damage of such a structure should be carried out.

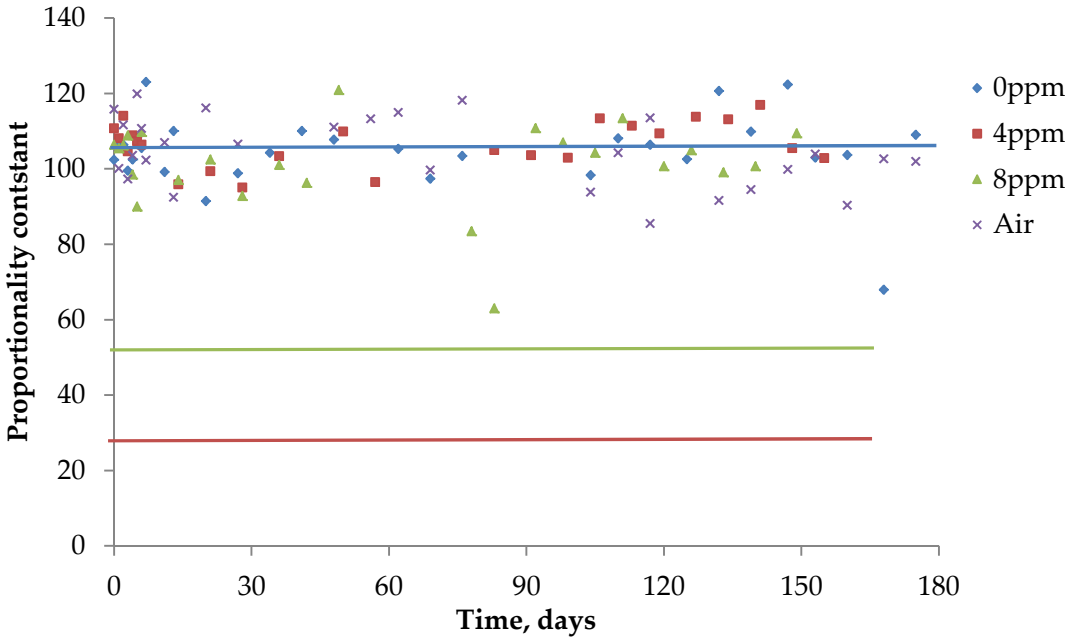

FIGURE 5.3 PROPORTIONALITY COEFFICIENT FOR CORRODING BEAMS UNDER LOW OXYGEN SUBMERGED ENVIRONMENTS

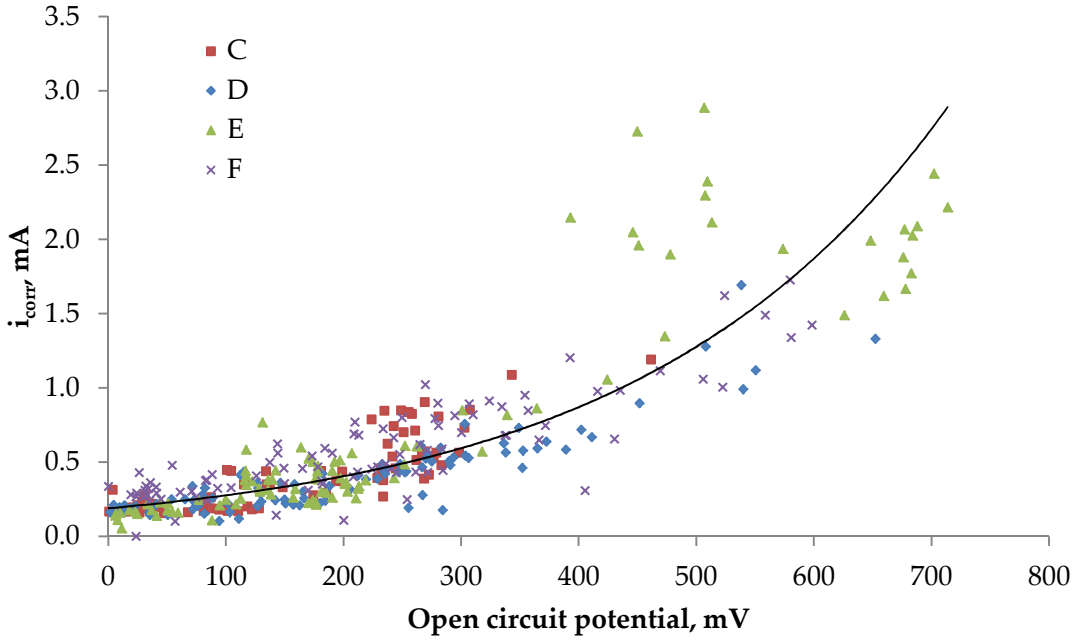

FIGURE 5.4 ESTIMATION OF I_{CORR} FROM OPEN CIRCUIT POTENTIAL MEASUREMENTS FOR DATA SETS C, D, E AND F

5.2.2 CORROSION PRODUCTS

Corrosion can cause different products at the steel concrete interface depending on exposure conditions, most notably 'red rust', commonly forming with an abundance of oxygen, and 'black rust', which occurs whereby a limited oxygen supply is available.

Figure 5.5 highlights a variation in the perceived colour of corrosion product, suggesting the beam exposed to atmospheric conditions at the surface (D4) has a mechanism of corrosion producing Iron (III) Hydroxides. Under conditions of limited oxygen availability at the surface (D1), the corrosion product will be a form of Iron (II) Oxide such as magnetite, Fe_3O_4. Iron hydroxides have a crystal density roughly four times that of steel, whilst magnetite only has a crystal density around twice that of steel. More expansive corrosion products, such as iron hydroxides, cause increased tensile strains in the concrete leading to cracking and spalling. The extent of cracking is dependent on spacing of bars, pore structure and the tensile strength of the concrete.

Not only do the corrosion products differ under varying oxygen exposures, the polarized area (area of steel whereby ion exchange is occurring) of the anodic bars are evidently different. While beam D1 has two small patches of corrosion, D4 has a much larger corroding area.

As these differing polarized areas have been measured, corrosion current densities can be recalculated. These suggest that the corrosion at the anode in a low oxygen environment can be more intense than in an atmospheric environment. The observation of this macro effect occurring on one bar suggests that the earlier belief of corrosion being limited by the cathodic corrosion current and resistivity to be limiting to be correct. In the case of a sealed environment, oxygen may seep in at extremely low rates through the wax, ponding setup or any minor gaps in the sealant.

Due to the cathodic current density being lower than the density at the anode, a balanced system whereby the anodic current density is much higher over a small area is established. Estimated anodic corrosion current densities were recalculated using Equation 5.1, with units of $\mu A/cm^2$, as is the common practice, and are reported in Table 5.1.

$$v = 0.0116 \frac{i_{corr}}{A_A} \qquad \textbf{EQUATION 5.1}$$

Where;

v corrosion rate, mm $year^{-1}$

i_{corr} corrosion current, μA

A_A area of anode, cm^2

Although there is a lack of oxygen availability in beam D1, the real corrosion current density of the patchy areas is calculated to be in the region of 60μA/cm^2, which is equivalent to an approximate cross-sectional area loss of 0.74mm/year. This is consistent with the apparent condition of the reinforcing bar after 6 months of exposure.

FIGURE 5.5 COMPARISON BETWEEN CORROSION PRODUCTS ON ANODES IN BARS D4 (TOP) AND D1

TABLE 5.1 ESTIMATED CORROSION DENSITIES IN BEAMS D1 AND D4

Beam	Corrosion current ($i_{corr,total}$), μA	Polarized area, % total steel¤	Current density (i_{corr}), μA/cm^2	Diameter loss, mm/year˜
D1	200	5	64	0.7
D4	200	50	6.4	0.07

¤ estimated from visual inspection of both cathodic and anodic bars

˜ 1000μA/cm^2 is equivalent to roughly 11.6mm/year (derived from Equation 3 in Poupard et al., 2006)

The transport of oxygen plays a major role in the corrosion of reinforcement as has been proved. The concentration of oxygen at the steel reinforcement in atmospheric and submerged atmospheres will vary, but not as significantly as initially expected. The transport of oxygen through the pore restricts the ability for atmospheric exposure to supply oxygen to the steel (Figure 5.6).

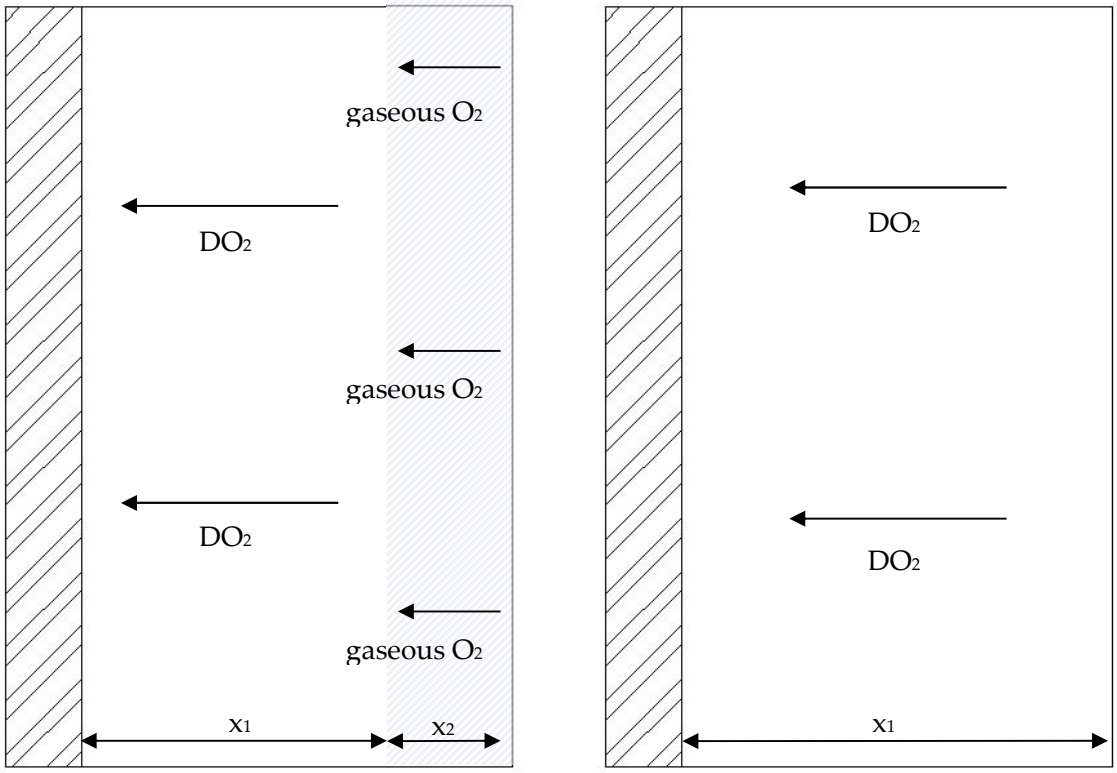

(a) atmospheric exposure **(b) submerged exposure**

FIGURE 5.6 EFFECT OF EXPOSURE ON OXYGEN TRANSPORT

In atmospheric conditions, gaseous oxygen can diffuse through the convection/dry zone of the concrete pores reaching depth x_2 rapidly. Diffusion through the saturated zone, x_1, is independent of exposure and will be the rate at which dissolved oxygen can diffuse to the steel surface. In submerged exposure conditions, x_1 is further than for atmospheric conditions, therefore reducing the supply of oxygen to the reinforcement sufficiently to alter the anode to cathode ratio on the bars.

Corrosion densities in the submerged exposure condition exceed those found in atmospheric saturated concrete. Although this is not the commonly held view of worst case corrosion conditions in the tidal/splash zone, under these given conditions it would be expected. Due to the application of a potential difference between the surface and the reinforcement, chlorides were allowed to rapidly saturate the entirety of the concrete cover, thus allowing initiation of reinforcement corrosion along its entire exposed length. This allowed corrosion to propagate along the majority of the length of the bar as oxygen was more freely available, producing much smaller cathodic areas.

The total mass loss may have been equivalent across both exposure conditions, however due to the larger cathode required for submerged concrete, the apparent current density appears much larger. In practice though, chlorides would only reach certain parts of the reinforcement due to the heterogeneous nature of the concrete cover. Initiation would then occur at various sections along the bar and propagate at total corrosion rates similar to those measured, causing much larger localised current densities. The water saturation of the cover concrete, and therefore resistivity of the concrete will be the predominant factor in determining the corrosion rate.

5.3 VARIATION IN ANODE TO CATHODE RATIO

Hansson, Poursaee and Laurent. (2006) previously show that the anode to cathode area has a pronounced effect on the rate of corrosion. In a corrosion cell, the anodic reaction and cathodic reaction balance. When the reaction is limited by the rate of cathodic reaction, a larger cathodic area of steel will be evident as suggested by the corrosion in Figure 5.7.

Corrosion rates of beams with varying anode to cathode ratios in all exposure conditions are shown in Figure 5.8 and Figure 5.9. The total corrosion current (Figure 5.8) varies depending on the anodic polarized area, with the smaller anode causing a reduced total corrosion current suggesting a chloride or resistivity limiting corrosion mechanism.

When the corrosion current density is determined (Figure 5.9) there is no apparent difference between any of the four corrosion currents measured suggesting the previously held theory of resistivity limited corrosion is supported when a rebalance of the anodically and cathodically polarized areas is not possible.

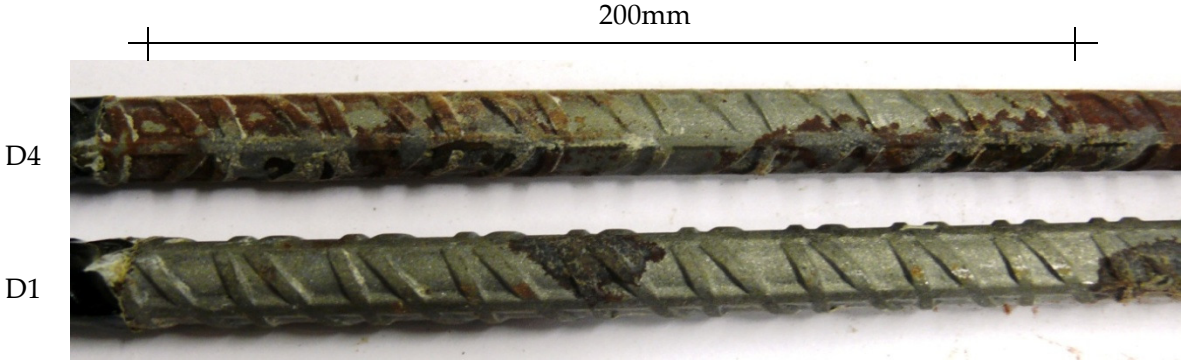

FIGURE 5.7 VARIATION IN PROPORTION OF POLARIZED ANODIC AREAS IN BEAMS D4 (TOP) AND D1

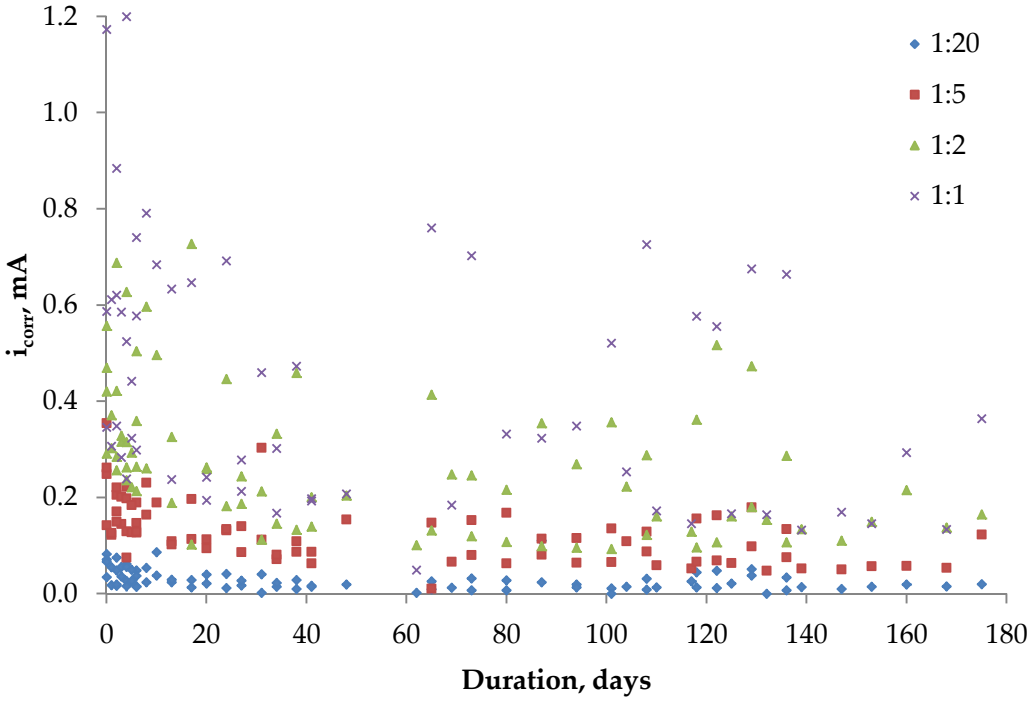

FIGURE 5.8 EFFECT OF ANODE TO CATHODE RATIO ON TOTAL CORROSION CURRENT

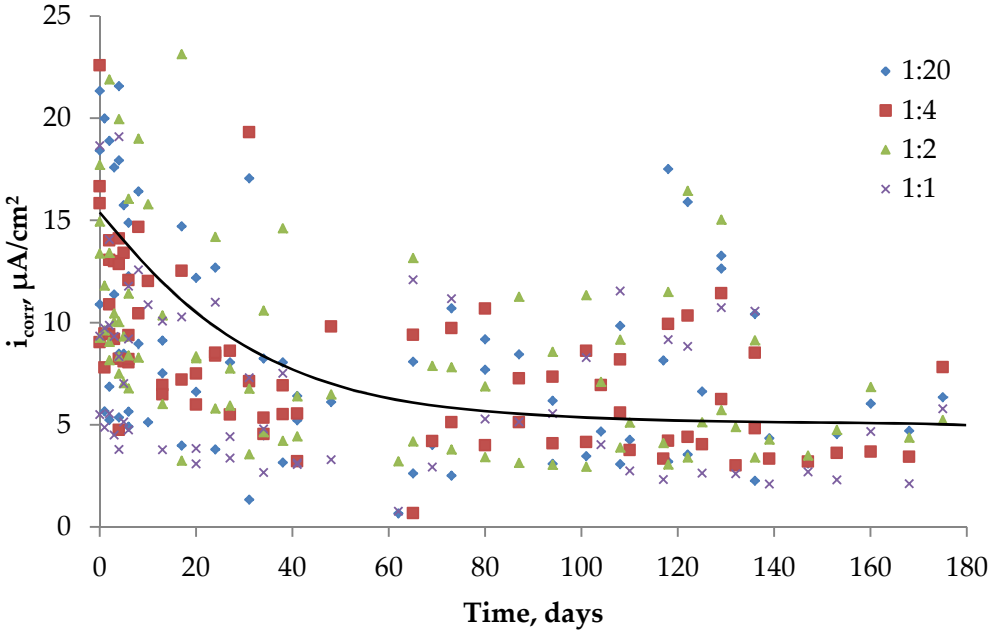

FIGURE 5.9 EFFECT OF ANODE TO CATHODE RATIO ON CORROSION CURRENT DENSITY

5.4 EFFECT OF AGGREGATE TYPE

Although the aggregate has an effect on the concrete strength, no discernible difference between the corrosion currents between the two mixes was observed. Average corrosion currents in oxygen saturated water for gravel and limestone aggregate mixes are shown in

Figure 5.10. Although the strength has increased, the limiting area for the diffusion of chlorides and oxygen is through the cement paste and the interfacial transition zone (ITZ). As the cement paste is likely to be the same in both concrete mixes and the aggregate sizes are similar, no difference between corrosion rates is expected.

5.5 VARIATION OF WATER/CEMENT RATIO

5.5.1 INITIATION

Typically, initiation occurred faster for Mix 2 (0.5 w/c ratio) than Mix 1, supporting the well-established theory that the more open pore structure allowed for a faster transport of chlorides. This trend was observed for seawater exposure in all oxygen concentrations and atmospheric environments for NaCl solutions. However the exposure to oxygen depleted NaCl solution caused a reversal of results, which is likely to be due to poor compaction of concrete on these samples. Air voids between the plastic and concrete will cause an accelerated transport of chlorides.

5.5.2 PROPAGATION

Measured corrosion currents between concrete with varying water cement ratios confirm that as the cement matrix becomes denser (lowering w/c ratio) the corrosion propagation rates decrease by between 30-40% in negligible oxygen environments, as shown in Figure 5.11. Corrosion rates of concrete in a negligible oxygen environment with varying w/c ratios and those in atmospheric conditions are shown in Figure 5.11 and Figure 5.12.

Samples tested in atmospheric conditions have reduced corrosion rates in comparison to submerged samples in all cases. In a scenario where one face of the concrete is exposed to the atmosphere there is a decrease in the water saturation of the concrete. This in turn causes an increase in resistivity which can limit the corrosion rate. As results show the decrease in measured currents between the samples, the corrosion rate in such environments is limited by the resistivity of the concrete.

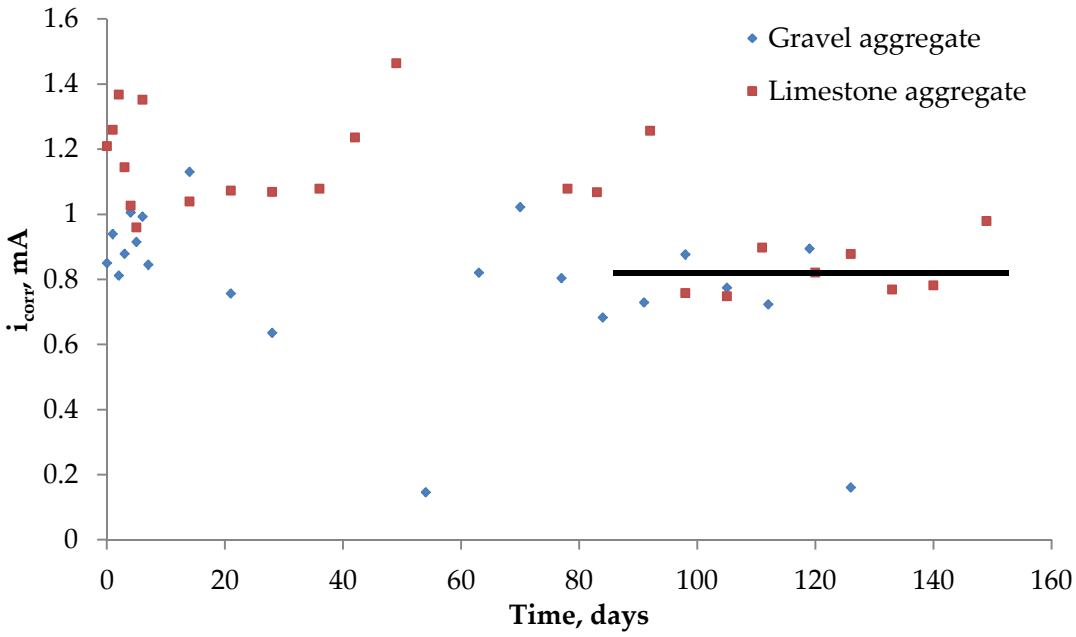

FIGURE 5.10 VARIATION OF I_{CORR} DUE TO VARIATION IN AGGREGATE TYPE

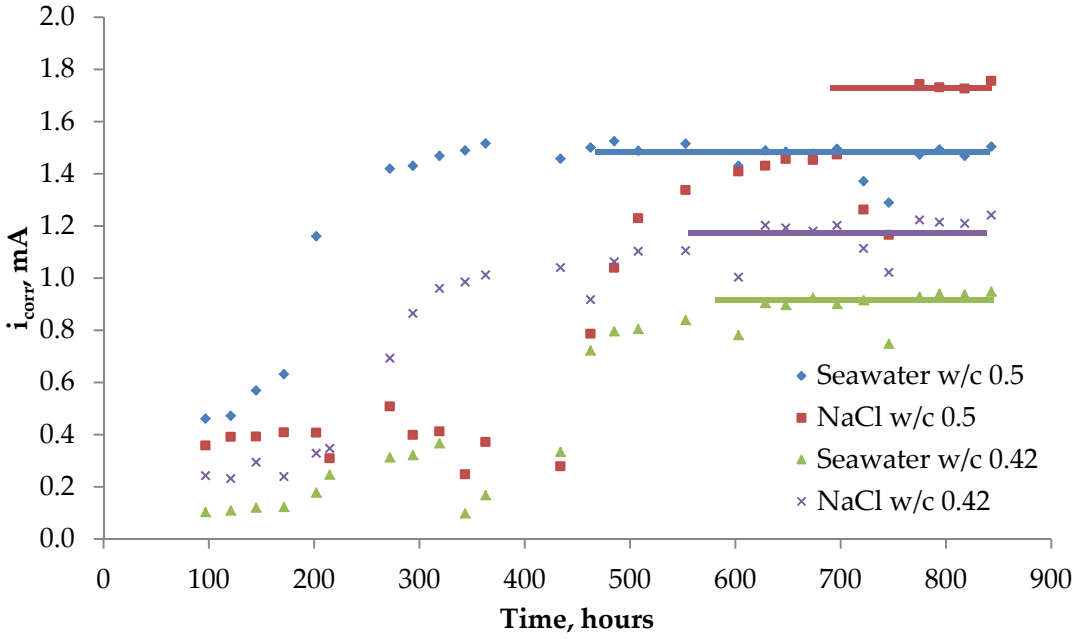

FIGURE 5.11 CORROSION RATES OF CONCRETE IN A NEGLIGIBLE OXYGEN ENVIRONMENT WITH VARYING W/C RATIOS

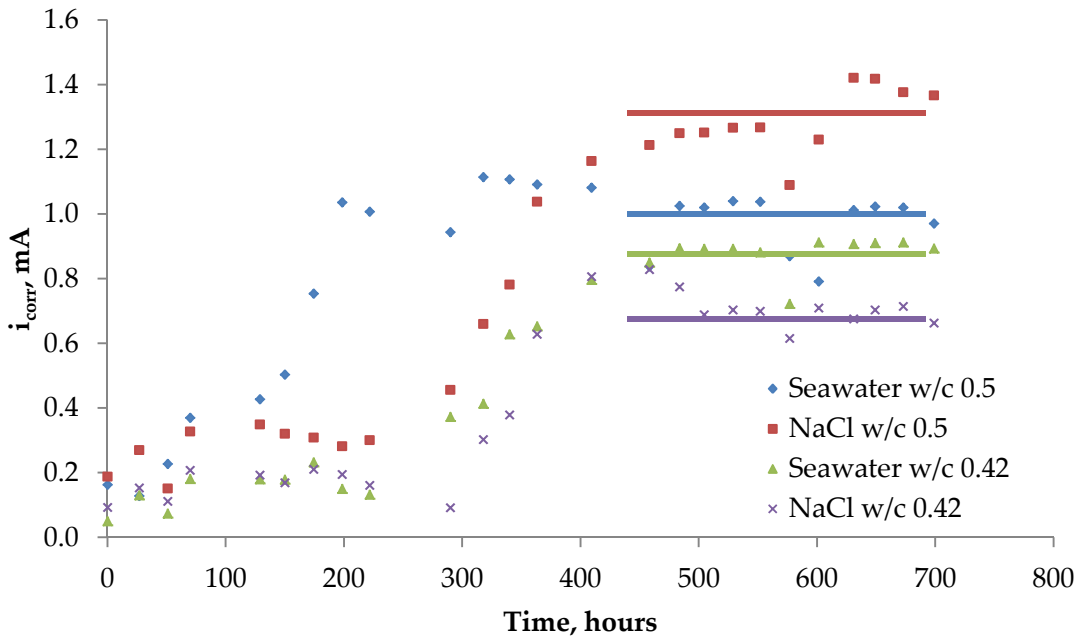

FIGURE 5.12 CORROSION RATES OF CONCRETE IN AN ATMOSPHERIC EXPOSURE ENVIRONMENT WITH VARYING W/C RATIOS

5.6 EFFECT OF SEAWATER ON CORROSION INITIATION AND PROPAGATION

Interestingly, seawater exposure causes a faster initiation of chlorides when applying this method of initiation acceleration. This is contradictory to results from Phase I, where it is suggested in natural and accelerated conditions the transport of chlorides from seawater exposure is retarded in comparison with those from NaCl solutions. This is due to one of two reasons, neither of which is known to have a more dominating effect on the initiation time. The two possible reasons are:

- decreased resistivity due to alternative ions, specifically sulphates in the pore solution
- decrease in the chloride threshold when Mg^{2+} and Ca^{2+} chloride cations are present, as theorised by (Jiang et al. 2012)

Propagation of seawater exposed concrete was predominantly lower than that of concrete exposed to NaCl. As the corrosion is limited by the resistivity of the concrete cover, a reduction in resistivity will cause an increased propagation rate in such samples. It is probable, however, that due to a shorter initiation time, the resistivity of the concrete in these samples is higher and therefore propagation is slower. Although, during propagation the external current is removed, protection of the concrete may be achieved through a skin or pore blocking mechanism or competition of ions through the concrete pore structure causing a reduced propagation rate.

5.7 VALIDATION OF EXPERIMENTAL PROCEDURE AND RESULTS

Validation experiments using a different method of oxygen control as discussed in Chapter 3, confirm initial findings on the continuation of the propagation of corrosion in low oxygen environments. Although similar initiation and measuring techniques were used, the experiments were run with new mixes and a redesigned control system for oxygen concentration.

Initial setup and results proved the setup to control the oxygen concentration successfully was difficult, therefore the variables were adapted to expose the concrete to three environments; negligible oxygen, oxygen saturated water and the atmosphere.

5.7.1 LOW OXYGEN CORROSION

Figure 5.13 and Figure 5.14 show that there is significant measured corrosion in all environments, supporting results from Phase II showing that the oxygen concentration is not the critical influencing factor on the rate of corrosion propagation. The figures show there is a difference between the two mixes: specifically that there are higher corrosion rates in concrete with a higher w/c ratio as supported previously. However, there are some outlying results that are of interest.

Results from water saturated exposure of Mix B (CT13, Table 3.1) suggest erroneous readings were measured and initiation disabled too early. As the Linear Polarization Resistance (LPR) results dropped below 200Ω, corrosion was assumed to have initiated, however subsequent measurements of LPR remained relatively high in the context of other samples exposed to the same environment. Results from this test provides further evidence that corrosion in these conditions is not oxygen limited.

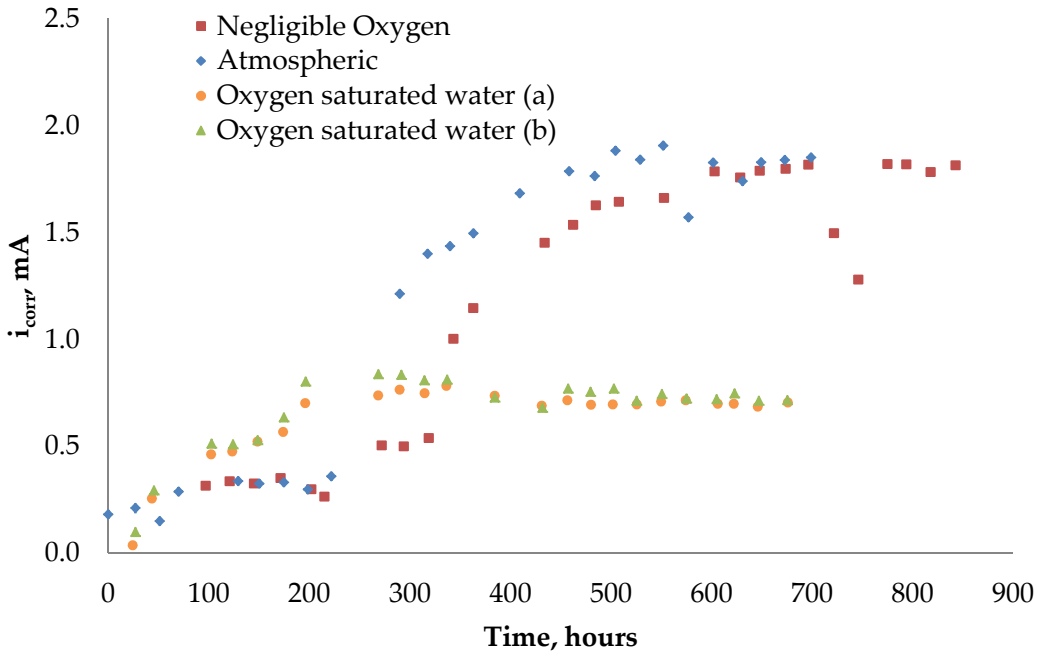

FIGURE 5.13 CORROSION CURRENTS OF NACL MIX B IN MULTIPLE ENVIRONMENTS

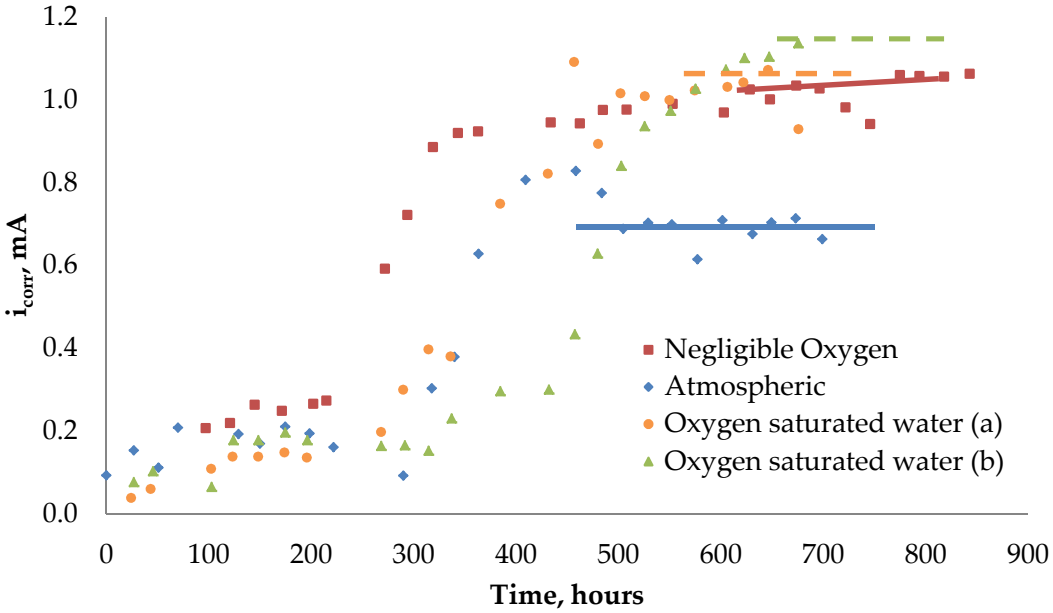

FIGURE 5.14 CORROSION CURRENTS OF NACL MIX A IN MULTIPLE ENVIRONMENTS

5.7.2 CORROSION PRODUCTS

Corrosion products formed across the entire exposed section in almost all conditions. Examples of corrosion products for negligible oxygen, oxygenated water and atmospheric are shown in Figure 5.15 to Figure 5.19.

Rust staining through the concrete was observed to be more prominent for corrosion under low oxygen environments, Figure 5.18. As iron is oxidised from the steel, iron chlorides

transport the iron through the pore structure before reacting with available hydroxyl ions, oxygen and/or water to form iron oxides. Where the availability of hydroxyl ions and oxygen is limited, iron is transported further from the steel/concrete interface before forming the iron oxides, as seen in the rust staining.

For samples exposed to atmospheric conditions, the minimal rust staining will be due to more freely available hydroxyl groups formed through a standard cathodic reaction and transported through the pore solution to the anode.

FIGURE 5.15 VARIATION IN PROPORTION OF POLARIZED ANODIC AREAS IN BEAMS D4 (TOP) AND D1

FIGURE 5.16 BLACK CORROSION PRODUCT (NEGLIGIBLE OXYGEN)

FIGURE 5.17 RED/BLACK CORROSION PRODUCT (OXYGENATED WATER)

FIGURE 5.18 MINIMAL RUST STAINING (ATMOSPHERIC)

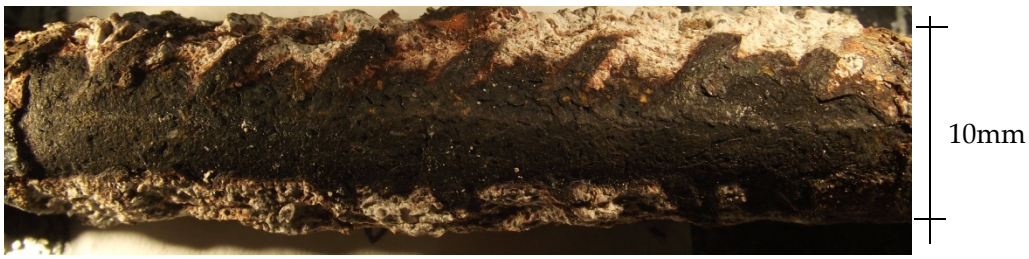

FIGURE 5.19 BLACK AND RED CORROSION PRODUCT

5.8 KEY OBSERVATIONS AND DISCUSSION

5.8.1 CORROSION PRODUCTS

The type and location of corrosion products vary between the concrete exposed to various exposure conditions. With a lack of oxygen, magnetite, Fe_3O_4, is deposited. When oxygen is readily available, either through dissolved oxygen from the sea water or from the atmosphere, ferrous or ferric hydroxides are formed.

Iron hydroxides have a unit mass of around four times larger than that of iron, whilst magnetite only around twice that of iron. Corrosion is more likely to be reported to occur on structures in the splash and tidal zones because an increased incidence of cracking and spalling in those areas. The oxygen available in this exposure causes more expansive corrosion products, which in turn create tensile strains in the concrete. This tensile strain causes the cracking and spalling of cover concrete, which is easily detectable and therefore likely the reason for being more reported. Time to the occurrence of this cracking or spalling could be significantly shorter for oxygenated corrosion due to these more expansive products of iron hydroxides in comparison with steel or magnetite. Additionally, access for inspection is easier for concrete in a splash or tidal zone, allowing for more frequent observation of corrosion.

5.8.2 EFFECTS OF LOW OXYGEN CONCENTRATIONS

Low oxygen concentrations appear to have little or no effect on the measured corrosion current using the available methods of detection. However, the location and apparent size of polarized areas of steel appear significantly affected.

As reported by Hussain (2011), the limiting cathodic current in submerged concrete was around 0.04μA/cm^2 for the setup and concrete mix used. If the anodic area was one hundredth the size of the cathode, the total anodic current would be 4μA/cm^2 assuming a

cathodically limited corrosion rate. Results have shown that cathodic areas of steel increase in size to provide an electrical current that balances with the anodic current. Furthermore, as reviewed previously, limiting current models suggest that corrosion can propagate at significant rates even with low dissolved oxygen concentrations. Validation experiments confirmed the initial findings showing significant corrosion currents in negligible oxygen concentrations, forming a similar black corrosion product.

Alternatively the reinforcement from beam C1, subjected to low oxygenated exposure, has large areas of obvious corrosion damage but with no apparent corrosion product on the surface of the steel. The iron oxidized from the surface of this steel is likely to have formed iron chlorides and been transported elsewhere in the cement matrix leaving a heavily pitted bar in comparison to an initial clean bar shown in Figure 5.20 and Figure 5.21. Pitting has occurred on the corroded reinforcement, and although there was no rust staining, there is a visible loss of steel.

FIGURE 5.20 UNCORRODED REINFORCEMENT

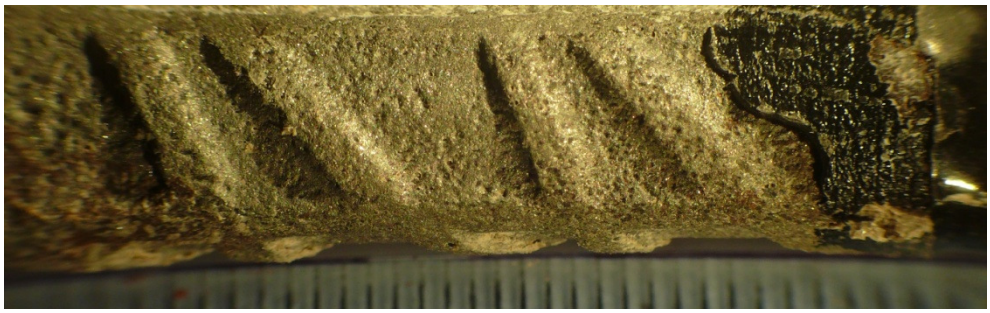

FIGURE 5.21 CORRODED REINFORCEMENT FROM BEAM C1

5.8.3 CORROSION PROCESSES

Evidently, as shown in the previous two subsections, under the low oxygen environments the corrosion processes continue. The reactions at the anode appear to be in agreement with previously observed reactions and are variable dependent on the availability of hydroxyls at the anode (Rosenberg et al., 1977; Böhni, 2005). The availability of hydroxyls is dependent on the rate of cathodic reaction as well as the hydroxyls already present in the pore solution. However, the iron continues to oxidise from the steel with or without the hydroxyls and will be transported throughout the pore solution as Iron Chloride complexes (Figure 5.22 and Figure 5.23).

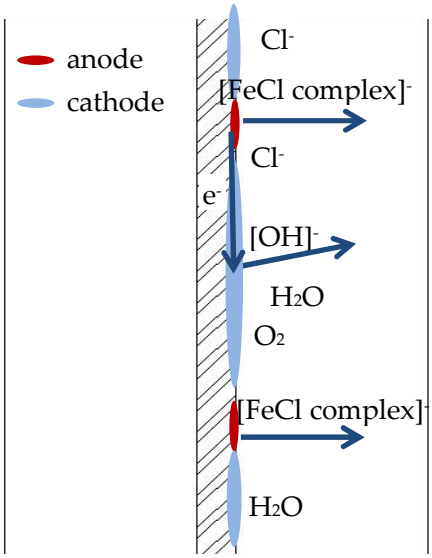

Comments

- Chloride saturated environment initiating corrosion at any location
- Low availability of oxygen restricting the cathodic current density
- Water saturated concrete due to submerged exposure
- At anode, chlorides act as a catalyst to form transient FeCl complex e.g. $FeCl_3$ (aq)
- At cathode, oxygen and water form hydroxyl ions, $[OH]^-$
- Anode:cathode area is small due to restricted cathodic reaction
- Aqueous iron chlorides travel further from anodic site causing staining through the concrete cover

FIGURE 5.22 LOW OXYGEN AVAILABILITY CORROSION DIAGRAM

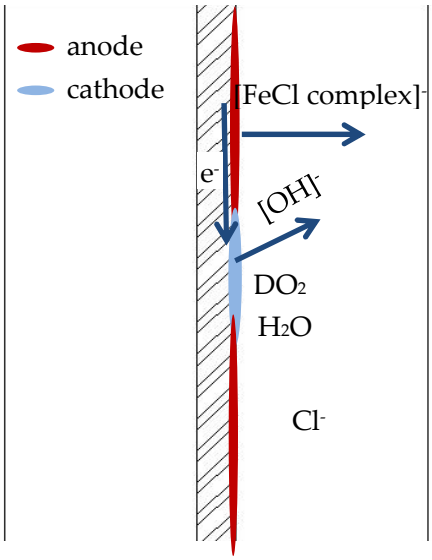

Comments

- Chloride saturated environment initiating corrosion at any location
- High availability of oxygen
- Water saturated concrete due to submerged exposure
- At anode, chlorides act as a catalyst to form transient FeCl complex e.g. $FeCl_3$ (aq)
- At cathode, oxygen and water form hydroxyl ions, $[OH]^-$
- Anode:cathode area is high due to availability of oxygen and water at cathodic region

FIGURE 5.23 HIGH OXYGEN AVAILABILITY CORROSION DIAGRAM

5.8.4 CORROSION MEASUREMENT INTERPRETATION

Measuring the corrosion rates of concrete should be done with care due to the complex nature of the environment. Half-cell (HC) or open circuit potential (OCP) measurements provide a good indication of whether corrosion is occurring and there was a correlation between the measured potential and the measured rate of corrosion. Caution must be used when taking measurements on 'real world' structures, as knowledge of anodic or cathodic bars can be crucial in interpreting these measured half-cell potentials due to the influence of water saturation and oxygen depletion.

LPR and PD measurements also provide a good indication of the rates of propagation, with measured values corresponding well to visibly recorded corrosion products on the surface of the reinforcement. Although these measured rates are often expressed in $\mu A/cm^2$, it is extremely unlikely that the size of the anodic area of reinforcement can be determined due to the nature of concrete structures. As the size of the anode and cathode vary dramatically in differing environments, an estimate of the total corrosion rate could provide an indication of corrosion, but engineering judgement is required when estimating the potential anodic and cathodic areas. Introducing a total corrosion rate into a probabilistic model that accounts for observed variations in polarized areas could provide a more realistic indication of corrosion damage.

Corrosion products are much more difficult to determine due to the complex nature of iron. Results have shown a marked difference between low oxygen and oxygen rich environments, with less expansive corrosion occurring in the submerged section. Further evidence has shown loss of steel cross section with no evident corrosion product build up.

5.8.5 EFFECTS OF ARTIFICIAL SEAWATER

Artificial seawater decreases the initiation time of corrosion through accelerated testing, although apparently effective at reducing initiation times of corrosion due to natural chloride diffusion. After initiation, there is no consistent relationship between the corrosion rates and type of chloride cation. Effects of seawater on corrosion propagation should be ignored for propagation models, although the measured effects on resistivity of concrete could be included. Although this is conservative, the use of sodium chloride for corrosion testing is therefore adequate when predicting corrosion rates.

5.8.6 IMPACT FOR ASSESSMENT OF OFFSHORE CONCRETE STRUCTURES

Corrosion occurred in all environments, but the rate and polarized areas of corrosion however is dependent on exposure to chlorides, water and oxygen. Offshore structures should therefore be modelled in separated areas dependent on exposure conditions, such as per the commonly used exposure areas; submerged, splash/tidal, and atmospheric.

Rates of corrosion in chloride saturated submerged concrete can be estimated and are significant, as shown in Table 5.2. Although the corrosion rates discussed are rapid, it should be noted that the use of an accelerated corrosion technique, high chloride concentrations, room temperatures and low concrete cover are not representative conditions for a submerged North Sea offshore platform and this must be taken into account when modelling remaining ultimate life.

TABLE 5.2 ESTIMATED RATES OF CORROSION FOR SUBMERGED CONCRETE OF 0.42 W/C RATIO WITH 25MM COVER

Exposure O_2 concentration	Corrosion rate,¤ $\mu A/cm^2$	A/C ratio~	Comments
Negligible	65	0.05	Extremely high observed corrosion currents over small areas.
5ppm DO	16.25	0.2	No observed variation between samples exposed to dissolved oxygen, similar polarised areas.
8ppm DO	16.25	0.2	
Atmospheric	6.5	0.5	Expansive corrosion product with freely available oxygen. Large anodic areas causing low corrosion current densities.

¤ estimated through division of total corrosion current by observed polarised area

~ estimated from visual observation of measured bars

Consideration must be taken for changes in exposure, such as the structure of a platform with an operational drawdown during its working life. A large oxygen concentration in a humid environment will be available on one face of the concrete and a completely saturated chloride environment with relatively high concentrations of dissolved oxygen on one face. The operational history of the platform can be used to estimate the condition of the structure at a predicted decommissioning date before extrapolating continuing damage in the updated environment post decommissioning.

CHAPTER SIX

6 EFFECTS OF CRACKING ON CORROSION PROCESSES IN SUBMERGED CONCRETE

6.1 INTRODUCTION

As corrosion has been shown to continue propagation in submerged conditions, attention now focusses on cracking formed under flexural loading and its subsequent effects on corrosion rate. Static cracking experiments were carried out in submerged conditions with crack widths ranging from 0.1 to 0.7mm. Sodium chloride and artificial sea water solutions were used as exposure environments, with accelerated and natural diffusion techniques used for initiation. Half-cell and corrosion rate measurements, using linear polarization and potentiodynamic scans, were taken weekly to evaluate the effects of crack width on corrosion rates.

Finally, a control beam and a selection of corroded beams were broken apart to evaluate the type and location of corrosion products, as well as to carry out a visual inspection of anodic and cathodic areas. Anodic areas were then estimated from visual inspections and results are used in assessing corrosion current densities for ultimate life modelling.

Previous research on dynamic cracking caused by continuous repetitive loading is deemed insufficient by the author, therefore an experimental rig was designed and setup to allow for submerged and semi-submerged dynamic cracking to columns/beams. Experiments focused on repetitive loading from unloaded up to a maximum width of 0.2mm were carried out, and a range of experiments to continue these studies are proposed in Chapter 9.

6.2 STATIC CRACKING

6.2.1 GENERAL DEVELOPMENT OF HALF-CELL POTENTIALS

As would be expected, half-cell potential measurements along the reinforcement reduce over time due to the ingress of chlorides. More negative values of steel potential are expected where corrosion has initiated due to the breakdown of the passive layer of the steel. At the location of the cracks, transport of chlorides to the steel will have occurred in a relatively short time-frame. Chloride ingress through bulk diffusion in the un-cracked section will not have occurred, causing the variation in steel potential.

Figure 6.1 shows a typical development of measured half-cell potentials of reinforcing steel in a cracked bar over time. The readings taken prior to exposure in the sodium chloride solution are consistent along the length of the beam. This is due to no chlorides being present in the concrete and therefore no significant variation of potential along the beam.

Half-cell readings for the 40mm cover and 25mm cover reinforcement of beams NACL05N after 43 days exposure are shown in Figure 6.2. The 40mm readings are in the region predicting a 90% probability of corrosion initiation; however the 25mm bars are more negative than the bars with a larger cover suggesting initiation has occurred. As corrosion is unlikely to be occurring due to a lack of access to chlorides, the low potentials are due to the reduction of oxygen at the cathodic bar, 25mm depth, causing a lack of oxygen at the steel surface. A reduced oxygen environment causes a significant drop in the potential of the steel without necessarily indicating on-going corrosion of the bar.

Development of half-cell potential at the location of the crack is shown for beam SW07N-1 in Figure 6.3. Initially, as the chlorides penetrate the crack, the half-cell potential of the 40mm steel decreases before settling at between -400 and -500mV vs. Ag/AgCl. The 25mm reinforcement remains at values more positive than the 40mm bar, before dropping significantly to values more negative than -700mV. This drop is attributed to the low oxygen environment of the submerged concrete. Half-cell potentials of concrete exposed to seawater show a more positive reading at the site of the cracking (Figure 6.4) opposite to results from exposure to NaCl solutions.

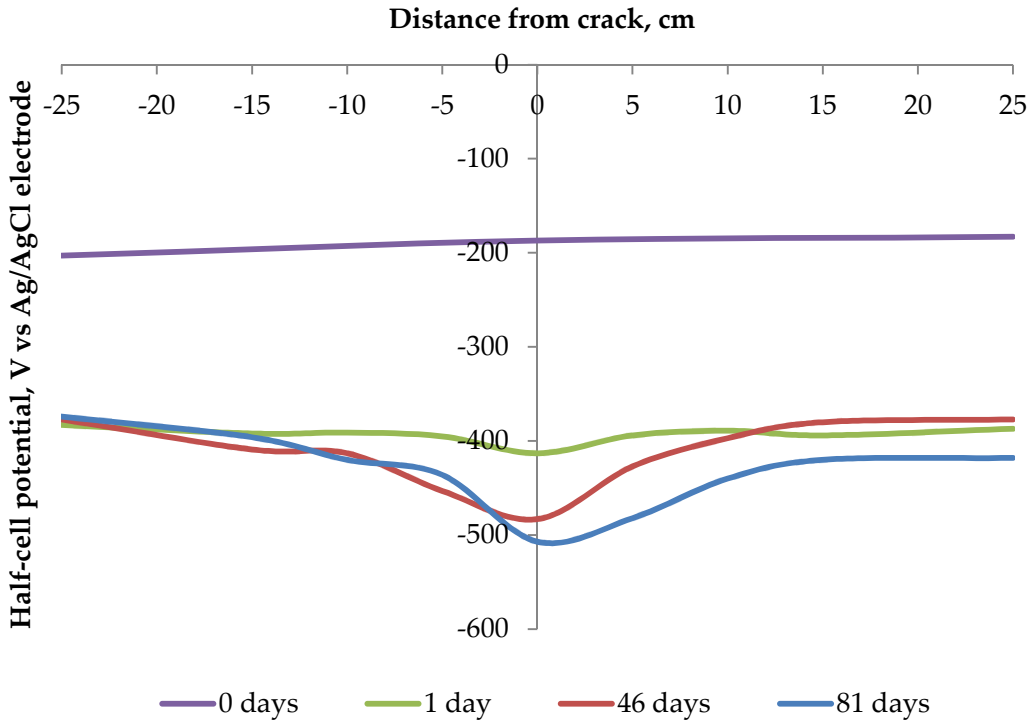

FIGURE 6.1 DEVELOPMENT OF HALF-CELL POTENTIALS ON BEAM NACL07N-1 UP TO 81 DAYS EXPOSURE

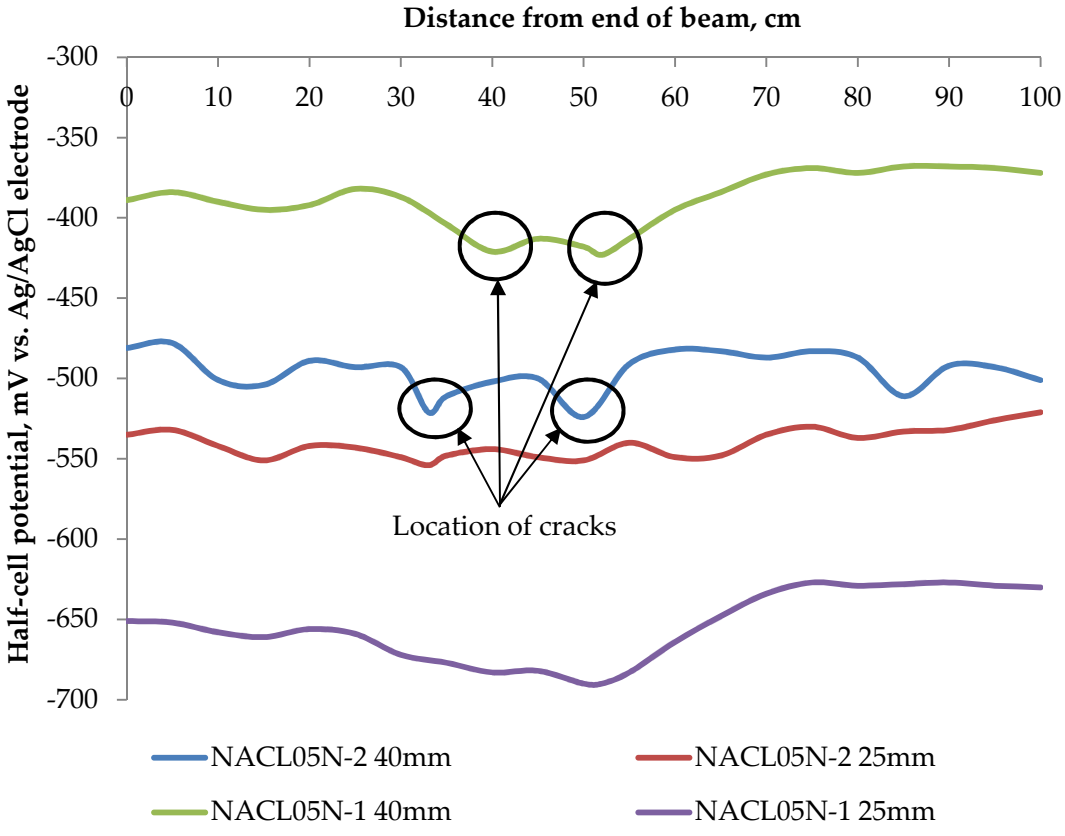

FIGURE 6.2 HALF-CELL POTENTIAL MEASUREMENTS OF BEAMS NACL05N-1 AND 2 AFTER 43 DAYS EXPOSURE

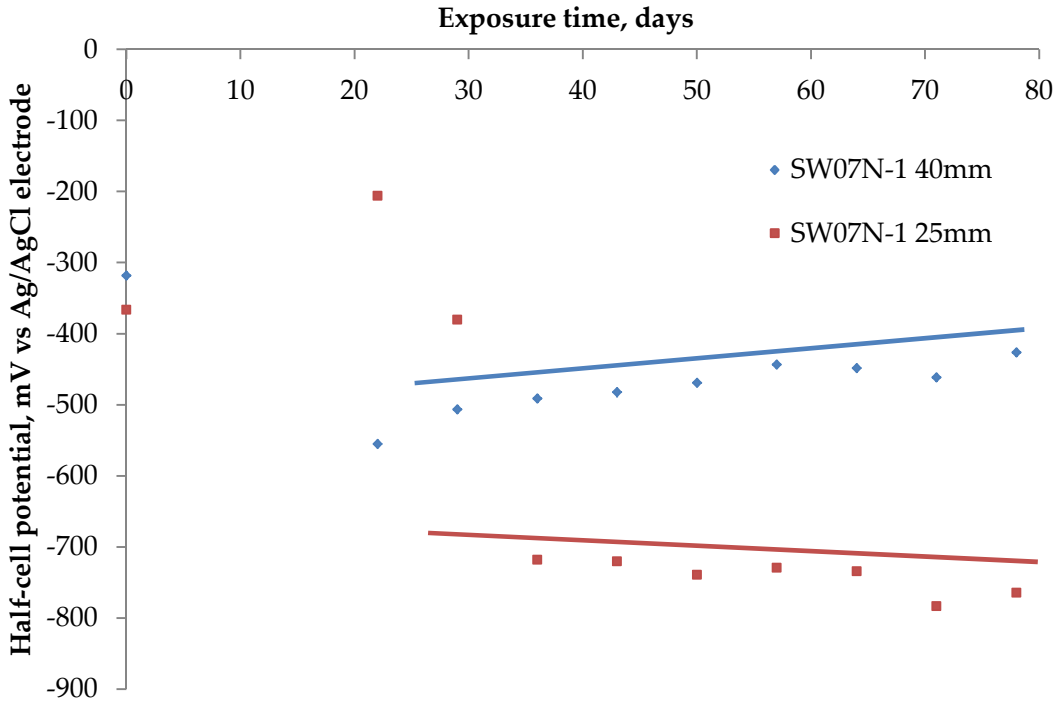

FIGURE 6.3 DEVELOPMENT OF HALF-CELL POTENTIALS OVER 78 DAYS EXPOSURE ON BEAM SW07N-1

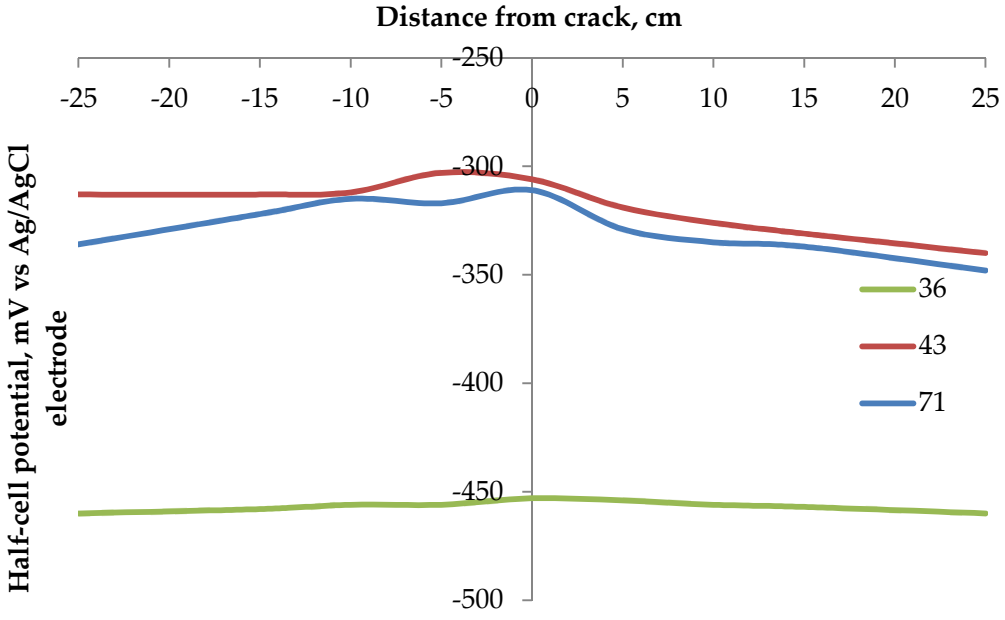

FIGURE 6.4 DEVELOPMENT OF HALF-CELL POTENTIAL OF SEAWATER EXPOSURE

6.2.2 General development of linear polarization resistance of anodic steel

The rapid transport of chlorides at the crack causes a rapid decrease of the linear polarization resistance (LPR) of the steel due to initiation of corrosion. Typical results for linear polarization measurements over the crack are shown in Figure 6.5. For cracks of width greater than 0.2mm, LPR results become consistent after 30 to 40 days with larger cracks causing lower stable LPR results. This is due to the further ingress of chlorides into the concrete reducing the resistivity of the concrete in and around the crack.

6.2.3 Effects of seawater solution

Corrosion rates for small cracks (<0.3mm) appear to show no variation between immersion in seawater or sodium chloride solutions, as shown in Figure 6.6. For cracking of 0.7mm, corrosion rates appear between around five times higher when exposed to sodium chloride solutions. Crack widths of 0.7mm in seawater were increased to 1.5mm on day 80 accounting for the steep rise in corrosion rate. This increase in crack width was an unsuccessful attempt to take a sample of any apparent crack sealing material.

The cracks of beams exposed to seawater appear visibly different to cracks exposed to NaCl (Figure 6.7). Crack sealing by reactions of magnesium with the calcium hydroxide to form brucite could cause sealing of the crack, as supported in works by Sibbick, Fenn and Crammond (2003). Other mineral deposits, such as Friedel's salts, gypsum, ettringite or magnesium carbonate could cause reduced chloride ingress by the process of crack self-healing. Further mineral deposits were evident after breaking open beam D2 (Figure 6.8). Retrieving a useful sample of this apparent material proved impossible.

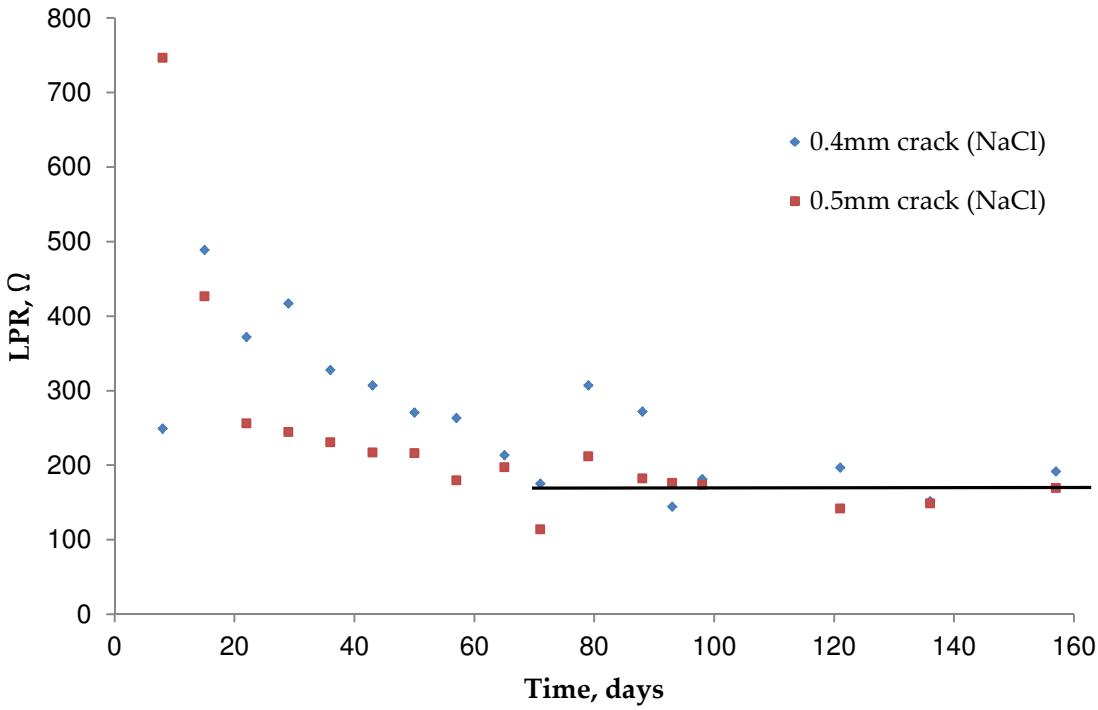

FIGURE 6.5 VARIATION OF LINEAR POLARIZATION RESISTANCE OVER TIME

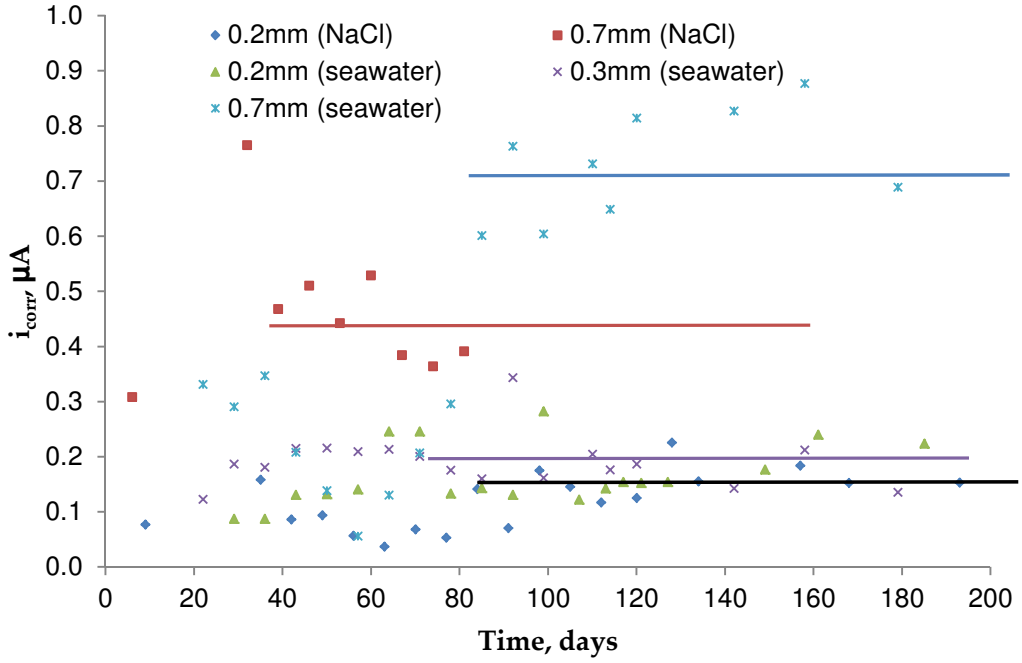

FIGURE 6.6 COMPARISON BETWEEN AVERAGED CORROSION RATES WITH VARYING CRACK WIDTHS IN NACL AND SEAWATER SOLUTIONS

a) sealed crack (seawater) b) open crack (NaCl)

FIGURE 6.7 CRACKS FROM BEAMS EXPOSED TO SEAWATER (BEAM A1) AND NACL (BEAM D2)

FIGURE 6.8 MINERAL DEPOSITS THROUGHOUT THE CRACK IN BEAM D2

Although apparent sealing of cracks is more evident on samples exposed to seawater solutions, sealing apparently also occurs within crack widths up to 0.2mm for concrete immersed in NaCl solution. Currently no observed decrease in corrosion current is noted, most likely due to the sealant in the crack being much more porous than the cement matrix as well as incomplete, leaving voids for rapid chloride ingress. Additionally, sealing of the cracks is extremely unlikely to be homogenous and therefore passage of ions to the steel is still extremely fast. Once the corrosion has initiated, corrosion will continue to propagate, therefore self-healing/sealing of cracks should be ignored in long-term degradation modelling.

6.2.4 CRACK WIDTHS

Increasing crack widths lead to increased measured rates of corrosion (Figure 6.9 and Figure 6.10). The increase in corrosion rate is shown as linear with increase in crack width, proving proportionality between cracking at the surface and damage to the steel. This is either due to the diffusion of oxygen and chlorides through a given aperture, through an increase in polarization area due to a larger crack width at reinforcement level as well as at the surface, or a combination of both effects.

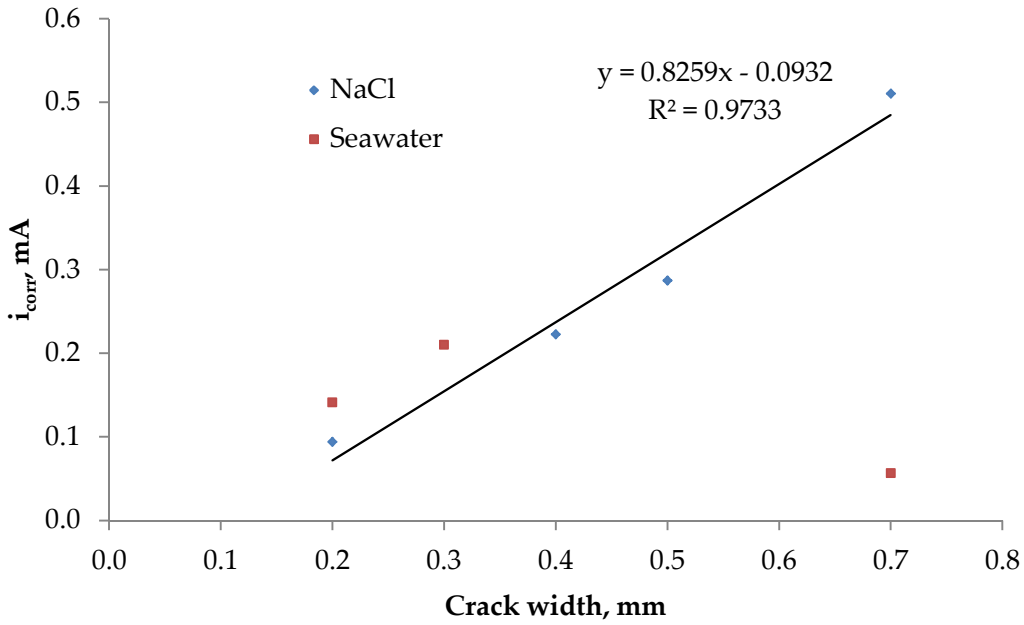

FIGURE 6.9 EFFECT OF CRACK WIDTH ON CORROSION RATE

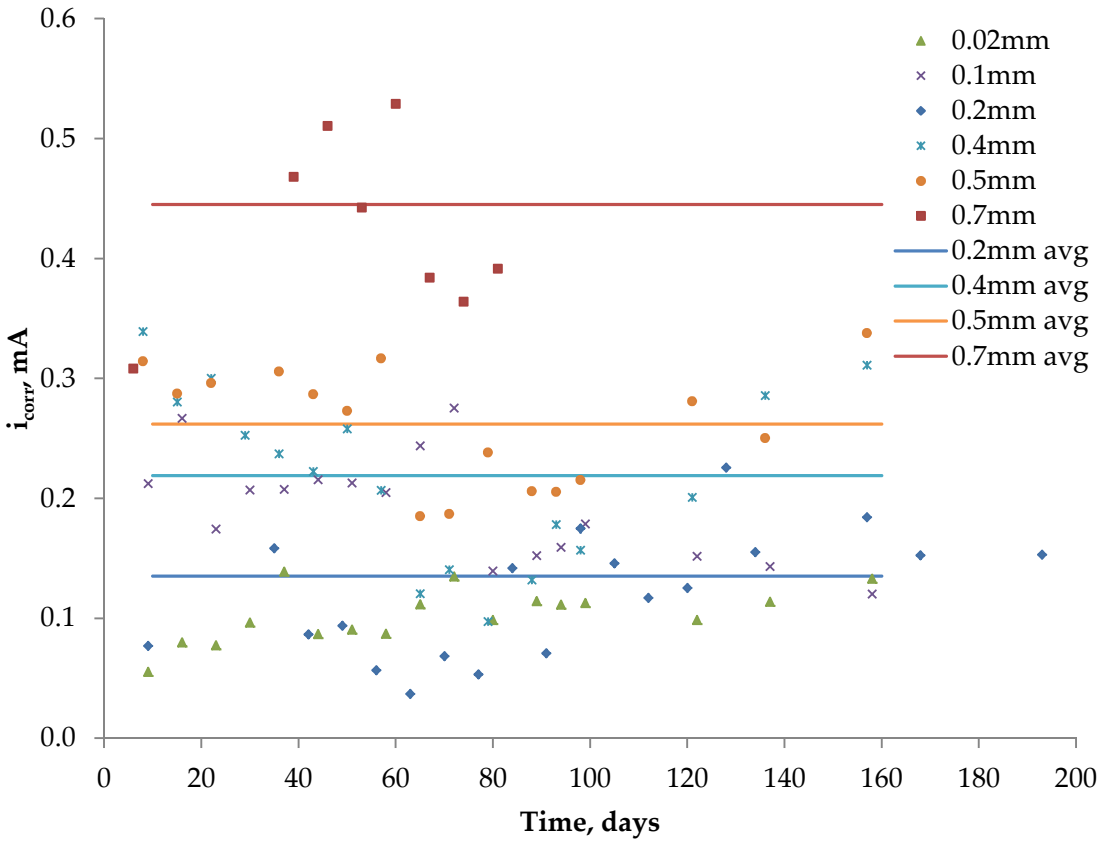

FIGURE 6.10 VARIATION IN CORROSION CURRENT DUE TO CRACK WIDTHS

6.2.5 ACCELERATED AGAINST NATURAL INITIATION

Accelerating corrosion causes large fluctuations in measured corrosion currents within the first 30 days for sodium chloride and 80 days for seawater (

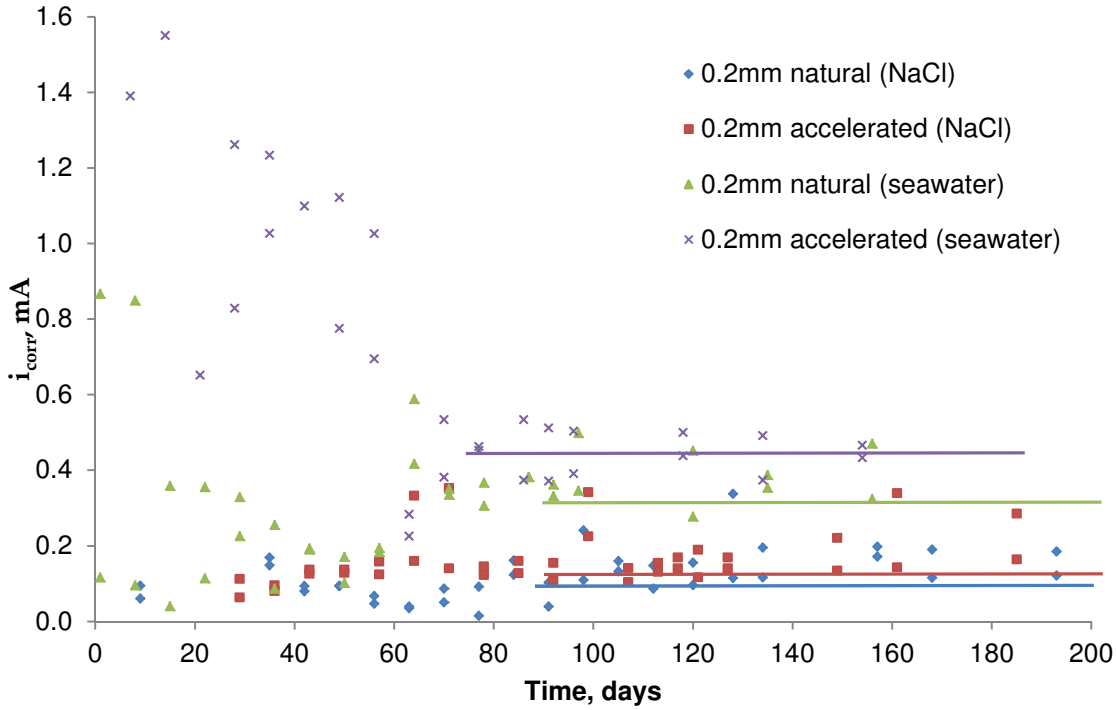

Figure 6.11). Results in chapter 5 show corrosion currents are stable after around 60 days using sodium chloride solutions, which is in agreement with results from cracking experiments. Results obtained from LPR and potentiodynamic scans show, although the rates are remaining relatively stable, the variability of readings on accelerated beams is large.

When corrosion is initiated using an external potential difference, chlorides are expected to saturate the concrete, reducing the resistivity of the concrete along the length. Corrosion rates are then higher, supporting the hypothesis that the corrosion in this scenario is resistivity limited and not oxygen limited.

Comparing like-for-like crack widths, corrosion measured through accelerated techniques is 2.9 times faster in NaCl solutions and 2.6 times faster in seawater solutions, where measurements are more variable (Table 6.1). For modelling purposes a conservative estimate of 3 should be used as a dynamic factor to adjust corrosion rates.

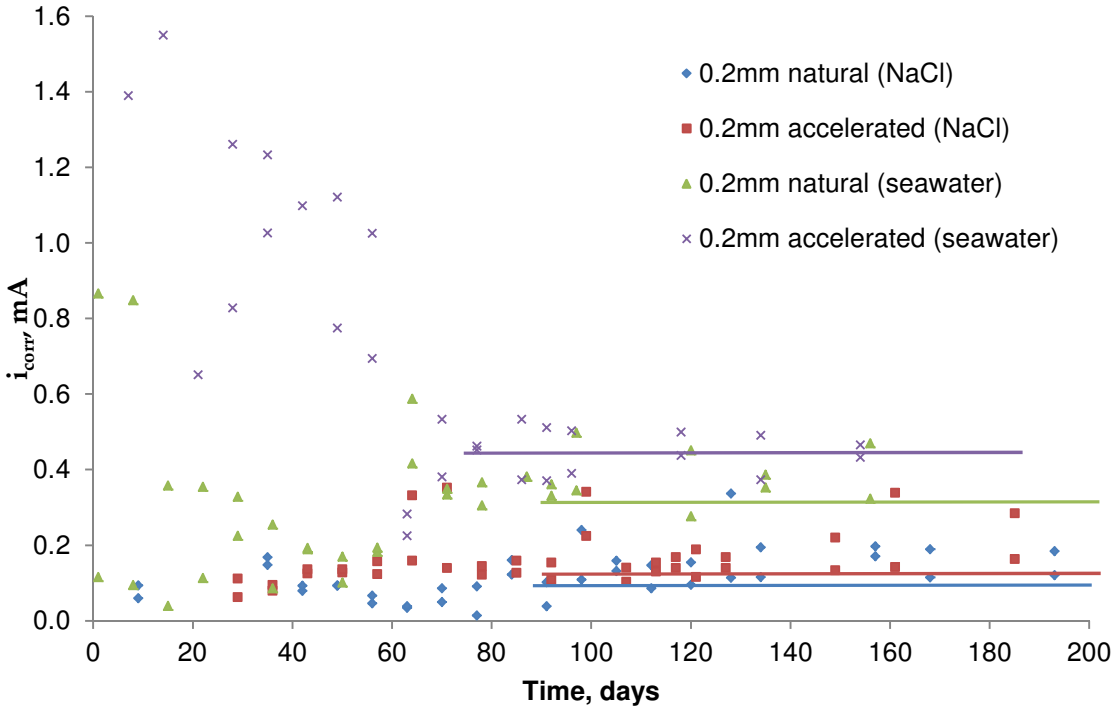

FIGURE 6.11 EFFECTS OF INITIATION ACCELERATION ON CORROSION RATES

TABLE 6.1 DIFFERENCES BETWEEN MEASURED CORROSION RATES FOR ACCELERATED AND NATURAL INITIATION

	A1	A2	G1	G2	C1	C2	H1	H2
i_{corr}, mA	0.103	0.145	0.389	0.342	0.174	0.185	0.524	0.420
	0.124		0.365		0.180		0.472	
Difference	2.9†				2.6§			

† Sodium chloride solutions with identical crack widths

§ seawater solution with identical crack widths

6.2.6 ANODIC POLARIZATION AREA

After 82 days, two beams of type NACL07N were broken open to observe any corrosion of the steel and analyse the actual polarization area and corrosion products. Corrosion had occurred with an area of visible pitting and black/red rust. After a short period of time exposed to the atmosphere, the product altered through further oxidation causing a more prominent expansive corrosion product. Figure 6.12 clearly shows this corrosion covering an area of

approximately 3cm long, with the majority of corrosion evident on the upper surface of the steel. Figure 6.13, of beam D2 after 180 days exposure, shows similar corrosive product along a length of roughly 3cm, similar to that after 82 days.

Additionally, the area along the crack was sprayed with 0.1M silver nitrate, $AgNO_3$, as per the NT Build 443 methodology to determine the chloride penetration front. As a consequence, silver chloride, AgCl, precipitated on the entire sprayed surface of the cover indicating chlorides were present throughout the entire sample. This quick transfer of chlorides to the surface of the steel was expected due to the nature of the crack, backing up the hypothesis stating crack widths as being critical, contradicting research that suggested minimizing the diffusion coefficient as a priority to increase service, or ultimate, life.

Instead of considering the polarization area to be the entire length of the bar, as is common practice throughout experimental result reporting, using the actual polarization area will increase the accuracy of expected corrosion damage. Beam set B, with crack widths up to 0.7mm, was broken open after 3 months of exposure to assess for corrosion damage to the bar. Around the cracked area, corrosion had appeared to have occurred over a polarized area of 3cm, with larger cathodic areas either side of the anodic area. As the area was shown to be 3cm, as opposed to 80cm, the corrosion current density will be roughly 27 times as large (Table 6.2).

High rates of corrosion are still likely, even in the submerged state, due to similar localized corrosion mechanisms as reported in Chapter 5 (Figure 6.14). Rather than limiting the area of anodic polarization due to a limiting cathodic reaction, the corrosion areas and therefore densities are limited by the availability of chlorides to break down the passivity of the steel around the base of the crack. Additionally, resistivity of the concrete between the anode and cathode could limit the corrosion current, however as the chlorides penetrate into the paste from the crack, the resistivity will decrease thus increasing the corrosion rate.

FIGURE 6.12 CORROSION OF 40MM REINFORCEMENT FROM BEAM B1 (0.7MM CRACK WIDTH) AFTER 82 DAYS EXPOSURE

FIGURE 6.13 CORROSION OF 40MM REINFORCEMENT FROM BEAM D2 (0.7MM CRACK WIDTH) AFTER 180 DAYS EXPOSURE

TABLE 6.2 EFFECT OF POLARIZED AREA AND CRACK WIDTH ON CORROSION RATES

Crack width, mm	Polarized length, cm	Corrosion rate[#], $\mu A/cm^2$
0.2	3	16.8
0.2	80[¬]	0.63
0.3	3	25.5
0.4	3	37.2
0.5	3	51.8
0.7	3	89.1
0.7	80	3.34

[¬] assumed polarization across entire length of the bar

[#] Calculated from observed polarized areas after 90 days of corrosion

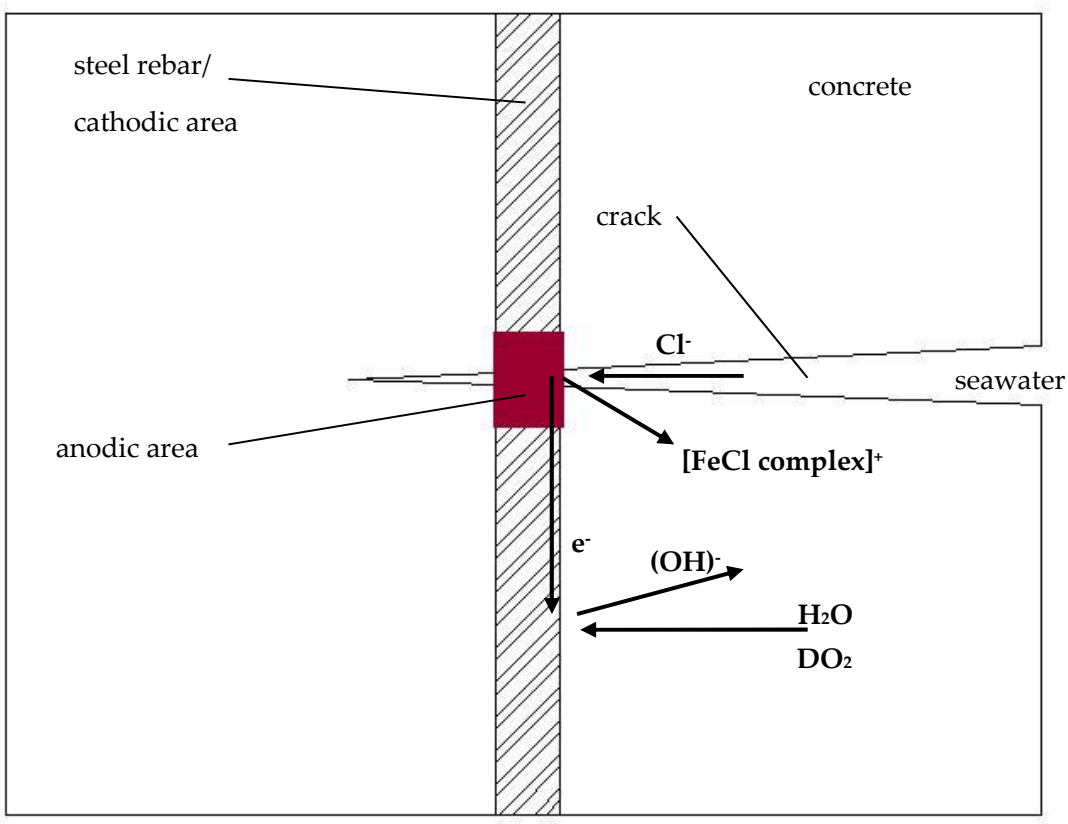

FIGURE 6.14 CORROSION MECHANISM AROUND CRACK

6.3 DYNAMIC CRACKING

6.3.1 0.2MM MAXIMUM CRACK WIDTHS

Short term testing of up to three months was completed on beams in a submerged environment. Loading was consistent throughout with beams being loaded from an unloaded state to an extension of the actuator to 22mm at the top of the beams, causing cracking of 0.1 and 0.15mm, increasing to 0.2mm at maximum deflection. Unloading the beams causes the cracks to reduce in width initially, although crack widths remain at 0.2mm in the unloaded state after around 30 days of loading. Total corrosion currents measured for 0.2mm maximum crack widths are shown in Figure 6.15. The solid black line represents the mean corrosion current of 0.97mA, with the grey lines show the 95% confidence of measured rates.

Up to 30 days, the crack depths continue to propagate up to a depth of 90mm before becoming consistent. Corrosion rates quickly become consistent around 13 days into the loading schedule, continuing at the same propagation rate for the remainder of the experiment.

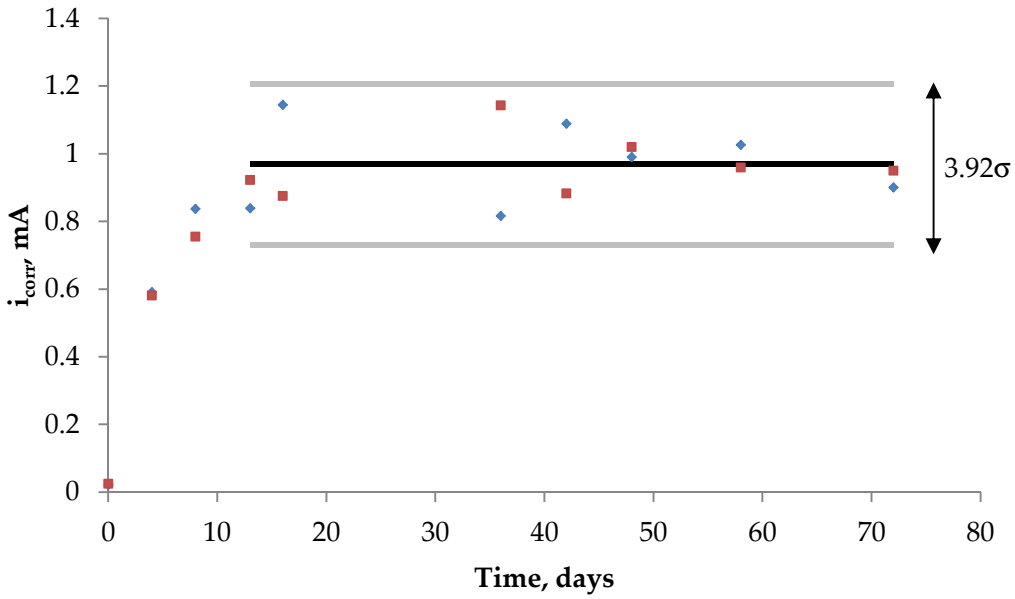

FIGURE 6.15 CORROSION RATES OF CRACK WIDTHS 0.2MM UNDER DYNAMIC LOADING

As the current methodology and equipment has been setup in the laboratory, further dynamic loading experiments to be carried out by future researchers are outlined in Chapter 9.

6.4 KEY OBSERVATIONS

6.4.1 EFFECTS OF CRACK HEALING

Physical crack healing is visually evident with apparent self-healing occurring in the concrete exposed to artificial seawater (Figure 6.16).

Crack widths of 0.2mm and wider are visually clear of healing product, however as the crack width decreases towards the neutral axis, mineral deposits are visible, supporting previous research that suggested cracks of around and under 0.1mm are conducive to healing (Reinhardt and Joos, 2003; Sahmaran, 2007).

There is no evidence of crack healing preventing the propagation of corrosion after initiation has occurred. Additionally there is no evidence of crack healing reducing the detrimental effects of corrosion in a dynamic loading condition as would be expected due to pumping of water throughout the crack. Corrosion rates are faster due to dynamic loading, although it is unlikely because of crack healing in the statically cracked sections and more likely due to increased ingress of chlorides, water and oxygen.

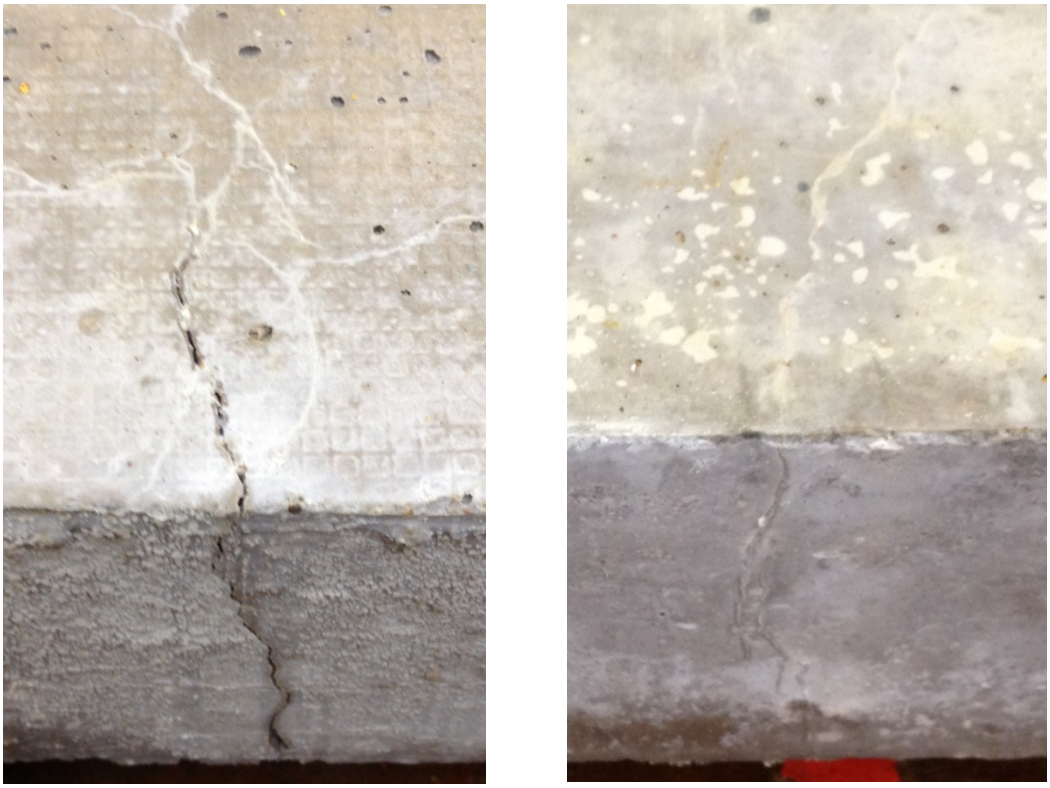

a) 0.7mm crack in seawater b) 0.2mm crack in seawater

FIGURE 6.16 APPARENT SEALING OF CRACKS

6.4.2 EFFECTS OF SEAWATER ON MEASURED RATES OF CORROSION

Although healing is visibly more apparent on seawater samples, corrosion currents are similar to measured currents in NaCl solution. As no significant variation between the two solutions is apparent, corrosion experiments can be conducted using either solution. This supports the use of on-site measurements on existing structures to determine the actual corrosion rate occurring as the effects of alternative ions in seawater will not cause erroneous readings.

In cases where concrete has been submerged in seawater for long durations, it is possible a reduction in concrete resistivity associated with multiple ionic species from seawater could increase the actual corrosion propagation rates.

6.4.3 EFFECT OF ACCELERATED CORROSION

Accelerating corrosion rates drawing chlorides in from the surface causes a sustained increase in measured propagation rates by roughly 3 after 180 days. Should accelerated corrosion methods for determining corrosion propagation rates be used, careful consideration of the choice of the method of acceleration is required. Driving chlorides into the concrete through

the use of an external potential difference can cause artificially low corrosion densities as chlorides will reach the entirety of the steel, which is unlikely to occur simultaneously in 'real world' structures.

6.4.4 CORROSION PRODUCTS

Corrosion products on the steel surface immediately after removal from the concrete are a black rust and did not expand. No visible rust staining of the concrete through the crack is evident, in line with the expected corrosion mechanisms. Initially, when removing steel from the concrete around cracked areas, visible pitting with black corrosion product is visible, before oxidizing further to 'red rust' when exposed to the atmosphere.

Due to the nature of the observed corrosion in submerged cracked concrete, loss of bond is unlikely to be an issue for overall structural capacity. Failure of the structure due to cross sectional area loss is likely to occur prior to spalling or bond loss due to the lack of expanding solid corrosion product.

6.4.5 SUMMARY OF DATA FOR MODELLING

For the purposes of modelling, a crack width factor, k_w, was applied to a reference corrosion current obtained through the experiments carried out (Equation 6.1). When the factor was applied to the corrosion current, the predicted current increased proportionally with the crack width as determined through experimental results,

$$k_w = 11.47(w_{max} - 0.2) + 1 \qquad \textbf{EQUATION 6.1}$$

Where;

k_w crack width factor

w_{max} maximum crack width, mm

For a structure with maximum crack width of less than 0.12mm, it is recommended that corrosion currents are similar to un-cracked sections with a reduced initiation time.

The reference corrosion rate was determined to be a normal distribution with a mean of 120μA and a standard deviation of 30μA. This is applicable to CEM I concrete of water/cement ratio of around 0.4 with a cover of 40mm, however, experimental testing should be carried out on the concrete mix prior to being modelled.

CHAPTER SEVEN

7 REDUCTION IN STRUCTURAL CAPACITY OF BEAMS DUE TO REINFORCEMENT CORROSION

7.1 INTRODUCTION

Having observed corrosion continuing under low oxygen environments and through cracked concrete, understanding its effects on the structural capacity of concrete sections are vital in modelling the remaining life of structures.

An experimental programme was designed as an additional phase to the project to help determine the relationship between corrosion and loss of structural strength. This phase ran three sets of experimental work:

- Pull-out testing involving cast-in corroded bars and corrosion to bars after casting were undertaken to determine effects on bond strength due to corrosion of steel.
- Stress redistribution in pitted and corroded reinforcement in beams containing multiple reinforcing bars.
- Investigation of the effects of corrosion on reinforcement in lapped sections.

Although strain gauges were applied to the external surface of the steel, results on strains were gathered along with corrosion damage, deflections and crack patterns as beams were loaded to ultimate failure. Structural response in terms of stiffness and ultimate capacity were determined and analysed.

7.2 PULL-OUT TESTING

Load displacement graphs of the control cube (Figure 7.1) show no bond slip between the steel and concrete, instead the loading represents the typical results expected for steel. Results of up to 5% corrosion show similar results, indicating that no bond loss has occurred due to corrosion.

Yield of the steel occurs outside the cube between the vice and the top surface, suggesting the restraint of the cube on the steel is sufficient to prevent yield of the steel within the concrete. This suggests the pull-out test method is not representative of the bond in structural members.

Pre-corroded or corrosion in situ appears to have no effect on the pull-out testing, with the ribbed reinforcement keeping bond well with the concrete.

Because the initial results of the testing schedule did not show any pull-out, the corrosion experiments were altered in an attempt to determine the amount of corrosion damage that is required to cause bond slip prior to yielding of the steel.

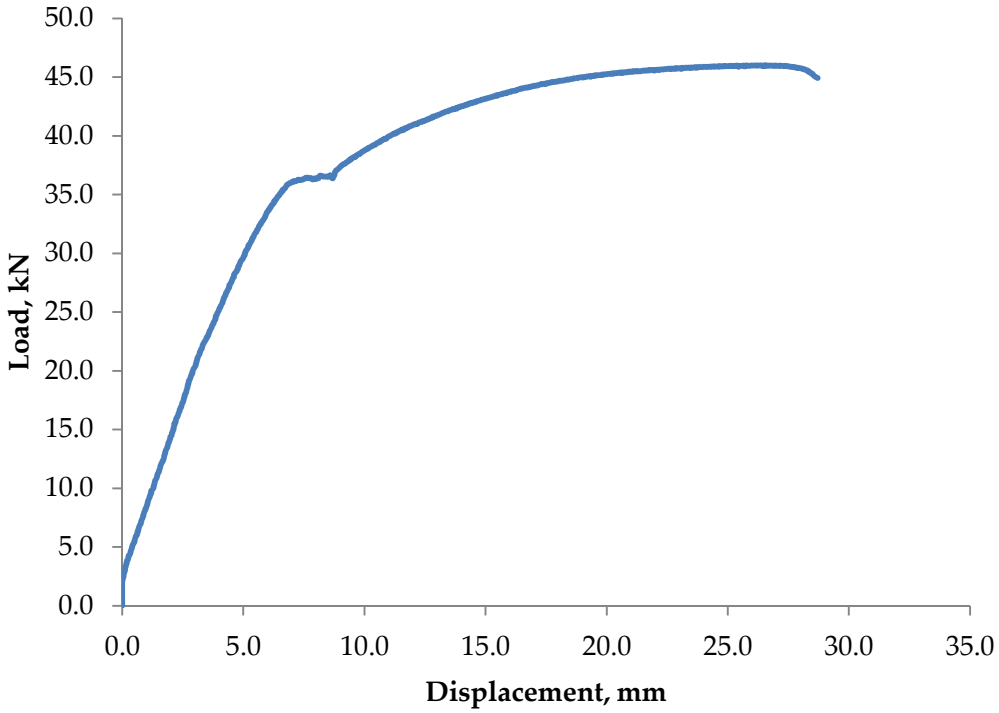

FIGURE 7.1 EXAMPLE LOAD DISPLACEMENT GRAPH WITH NO BOND SLIP (SAMPLE PO1-1B)

Table 7.1 shows the new test schedule for cubes with reinforcement corrosion up to 20%, using an applied current of up to 1000 μA/cm^2 corrode the reinforcement. Although it is reported that a current density of greater than 200μA/cm^2 causes additional crack damage to the concrete that is not as realistic as would be found with naturally occurring corrosion (Malumbela, Moyo and Alexander, 2012), for the purposes of this work where extensive damage is to be created in a short timescale, electrical current is increased above this limit to accelerate the corrosion.

All samples with corrosion up to 14% loss of steel showed no bond slip, and the maximum force was equivalent to the capacity of the steel (Figure 7.2). Final results show that the cube with 20% corrosion damage to the reinforcement caused slip of the bond, reducing the

ultimate force to approximately 15kN (Figure 7.3). Bond slip was only evident in this high strength concrete with modern steel bars at general corrosion loss of between 14 and 20%.

As bond loss is deemed to be of little significance on the total failure capacity of the structure, experimental work was carried out on beam sections to determine how general and pitting corrosion affects the overall structural integrity of rectangular beam sections.

TABLE 7.1 UPDATED PULL-OUT TESTING SCHEDULE

Sample	Corrosion, % mass loss	Maximum Force, kN	Comments
PO1-1B	0	40.65	Control
PO1-2A	0	45.12	25mm gauge replication
PO1-3C	0	47.36	100mm gauge replication
PO2-1B	20	15.02	Pull out failure
PO2-2A	15	36.18	Steel failure within cube
PO2-2C	2.5	45.92	Steel failure outside cube
PO2-3B	5	47.95	Steel failure outside cube
PO2-4C	10	46.90	Steel failure outside cube
PO2-5A	2.5	46.39	Steel failure outside cube

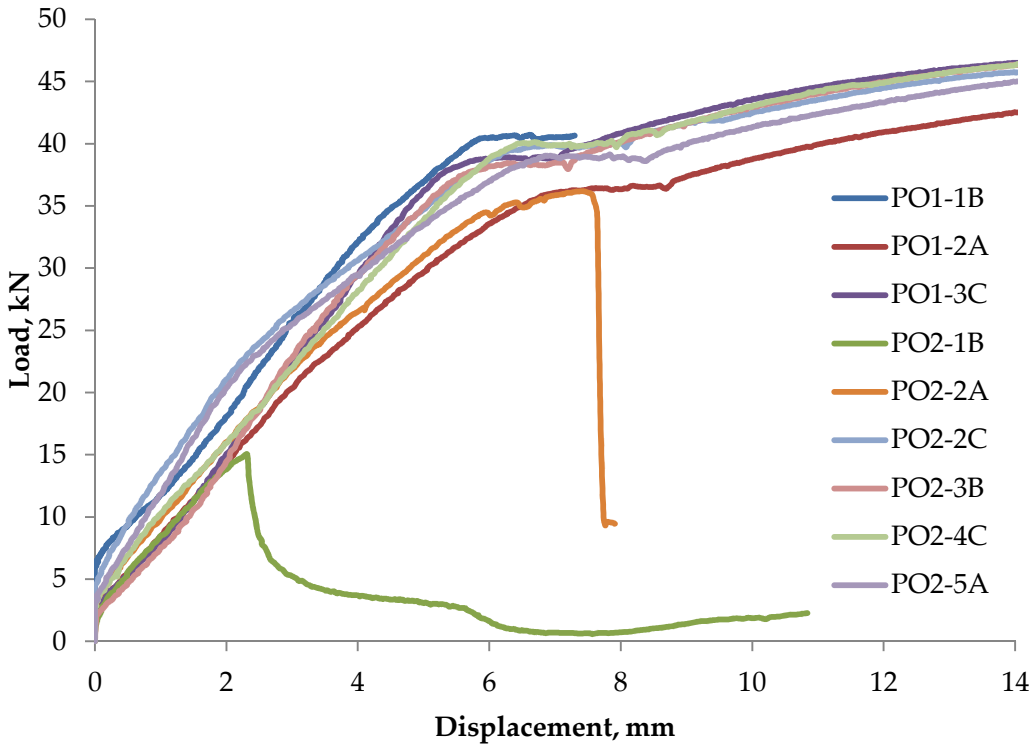

FIGURE 7.2 LOAD-DISPLACEMENT GRAPH OF BARS UP TO 20% CORROSION

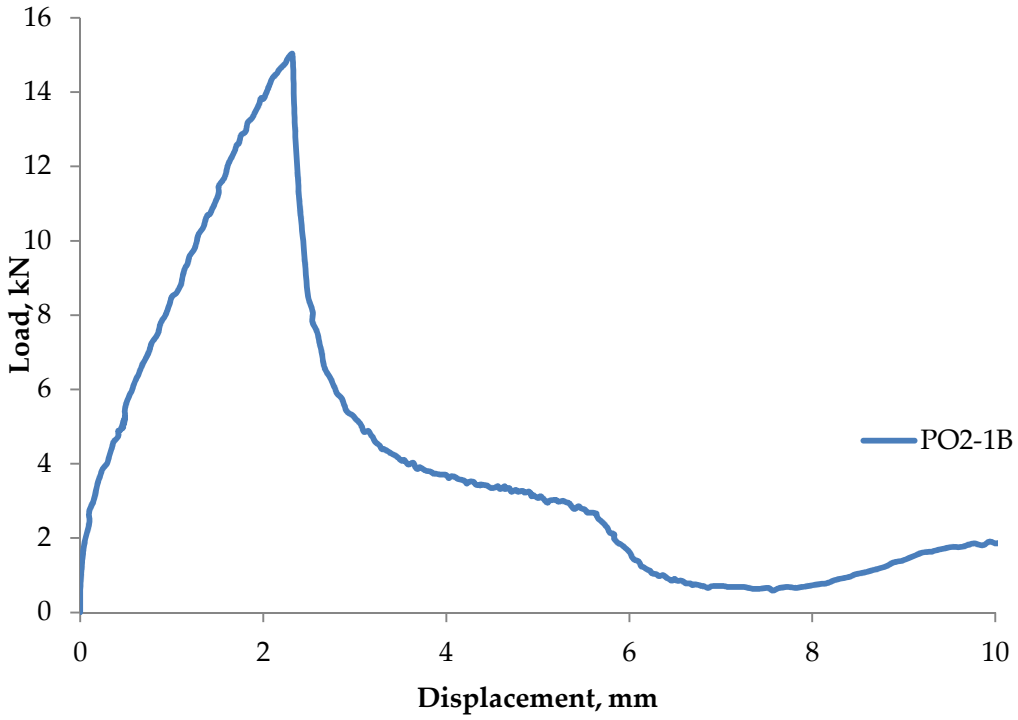

FIGURE 7.3 LOAD-DISPLACEMENT OF BAR AT 20% CORROSION

7.3 CORROSION OF REINFORCEMENT OF SINGLE BARS

7.3.1 CONTROL BEAM ANALYSIS

The control beam was loaded, at a rate of around 0.1kN/s, to failure providing results for an un-corroded beam section. Maximum loading achieved was 104.0kN with first visible cracks appearing at 23.5kN. Stress in the steel bars was determined from strain data acquired every second (Figure 7.4) and cross-referenced with loading data to provide load-stress data (Figure 7.5). Stress appears to increase significantly around 10.3kN suggesting cracking occurs although not visible.

Up to first cracking the strain distribution across the gauges is consistent with an almost uniform stress distribution through the steel reinforcement. Once cracked, the bars are then unrestrained allowing for the bars to elongate as the loading is increased causing large curvature and widening cracking.

Although Beeby and Scott (2005) advocate the use of internal strain gauges along the entire length of the reinforcing bars, the practicalities of using smaller bars, shorter beams and high levels of corrosion make this unfeasible. It is acknowledged that the use of the strain gauges on the surface of the reinforcement may provide strain measurements of steel and concrete combined and results from the strain gauges are therefore carefully utilised.

Where strain gauges are in line with cracking, the strain in the steel will increase and the readings will be high. This is due to the entire load being transferred as stress in the steel, with the concrete taking no tensile stress around the crack. Where the stresses are measured in an un-cracked area, the measured strains will be representative of the overall strain in the concrete and steel combined due to a composite bond action.

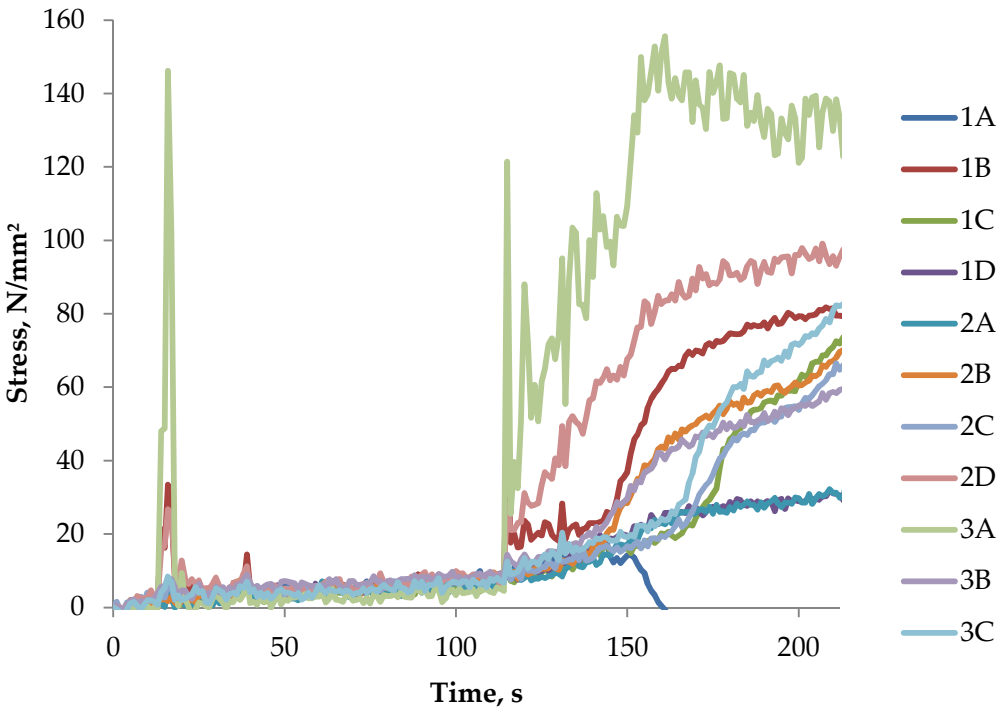

FIGURE 7.4 CONTROL BEAM - EXAMPLE STEEL STRESS AGAINST TIME

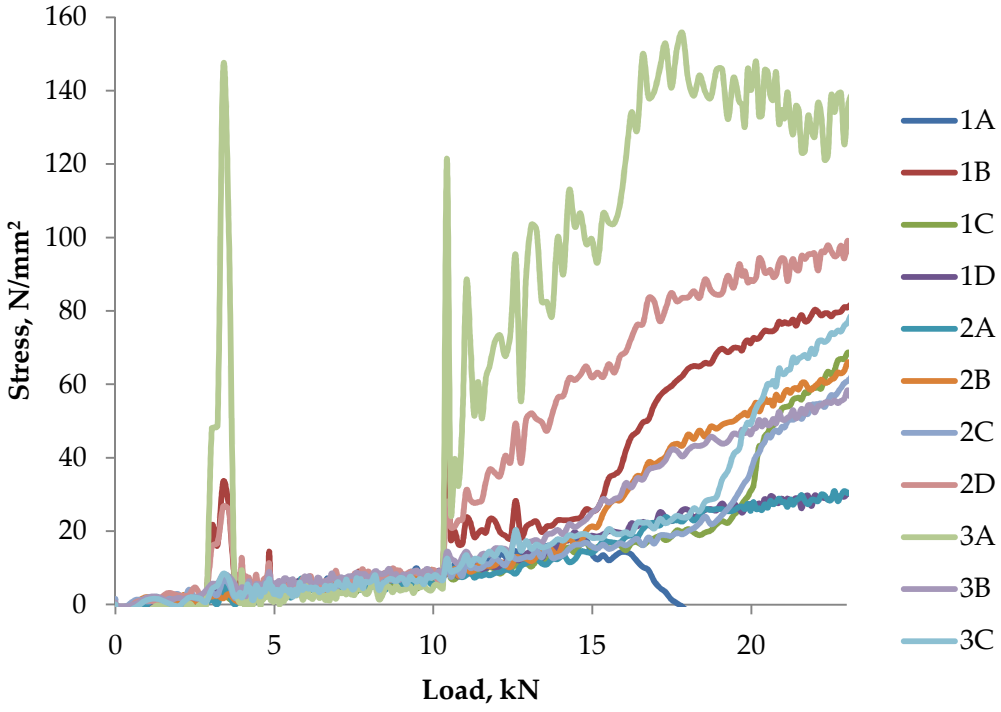

FIGURE 7.5 CONTROL BEAM - STEEL STRESS AGAINST LOAD

7.3.2 EFFECTS OF BOND LOSS ON SERVICEABILITY

With the general corrosion of steel, the bond between the reinforcement and the concrete was affected causing the composite action of the beam to be altered. The stiffness of the section decreases with the loss of bond (Figure 7.6). Bond loss was determined through the general corrosion loss to each bar, with a bar with more than 2% corrosion assumed to have lost complete bond. Although this is not supported through pull-out testing carried out previously, Chung, Najm and Balaguru (2008) suggest that a bond loss occurs at more than 1% corrosion mass loss. Although there is a significant scatter, the general trend shows a significant reduction of stiffness.

The loss of bond therefore has a pronounced effect on serviceability, with the load at which first visible cracking occurs following a similar pattern to the stiffness (calculated from load/deflection curves).

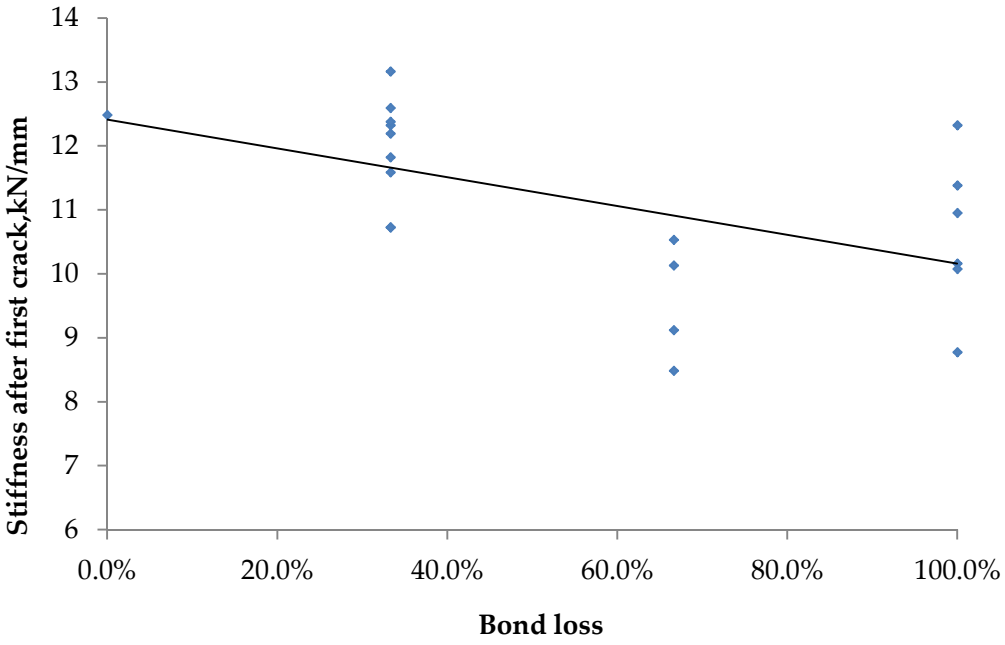

FIGURE 7.6 REDUCTION IN STIFFNESS DUE TO BOND LOSS

7.3.3 EFFECTS OF GENERAL CORROSION ON STRUCTURAL CAPACITY

Beams with no artificially induced pitting showed a reduced stiffness with increased general corrosion, even though pull-out testing suggested that with up to 14% corrosion the bond should not be affected by corrosion.

Ultimately the corroded beams had a reduced capacity, however the beam with potentially less corrosion damage (Beam 6) had a similar capacity to the more damaged beam (Beam 10)

(Table 7.2). Due to the induced corrosion technique and the variability in material properties between bars, some variability in ultimate capacity results was expected.

TABLE 7.2 EFFECT OF GENERAL CORROSION ON STRUCTURAL RESPONSE

Beam	Maximum load, kN	First visible crack, kN	Deflection (first crack), mm	Stiffness after cracking, kN/mm	Corrosion, %wt. steel		
					Bar 1	Bar 2	Bar 3
1	104.0	23.5	0.76	12.5	0.0	0.0	0.0
6	94.2	19.6	0.61	11.4	5.6	5.6	5.6
10	95.6	17.7	0.74	8.8	9.0	9.0	9.0

7.3.4 EFFECTS OF PITTING CORROSION ON STRUCTURAL CAPACITY

Pitting corrosion reduces the remaining cross sectional area at a given location where chlorides have reached the steel first, commonly at the base of a flexural crack. To simulate pitting corrosion and cross sectional area loss, pits were created at predetermined locations prior to casting.

Comparisons between beams 3/7, 4/8 and 5/9 (Table 7.3) show that regardless of the bar within the structure being damaged, the stiffness and ultimate capacity are only affected by the loss of overall bond or total steel area respectively.

7.3.5 SUMMARY OF BEAM TESTING

Although the stiffness reduces due to the loss of bond, causing increased deflections and earlier cracking, overall ultimate capacity can be directly predicted through the loss of cross sectional area (CSA) of the steel section. Figure 7.7 highlights the observed linear trend between remaining cross sectional area and ultimate failure load. As the cross sectional area decreases, the ultimate failure load of the concrete decreases approximately linearly (Table 7.4).

Extrapolating the line of best fit suggests that an unreinforced beam of identical dimensions would support an ultimate load of around 10kN. Although it is common to discuss bond loss when determining service life of a structure, either when corrosion is severe enough or the concrete reaches an ultimate limit state, the quality of bond has no significant influence on ultimate capacity.

TABLE 7.3 COMPARISON BETWEEN EFFECTS OF DAMAGE TO CENTRAL OR EDGE REINFORCEMENT

Beam	Maximum load, kN	First visible crack, kN	Deflection (first crack), mm	Stiffness after cracking, kN/mm	Corrosion, %wt. steel		
					Bar 1	Bar 2	Bar 3
3	101.5	-	-	11.8	0.0	9.0	0.0%
4	103.0	19.6	0.59	12.3	0.0	11.0	0.0
5	93.2	19.6	0.43	10.7	0.0	10.0	0.0
7	102.0	15.7	0.38	12.2	12.0	0.0	0.0
8	96.1	19.6	0.38	11.6	12.0	0.0	0.0
9	98.1	20.6	0.44	12.6	10.0	0.0	0.0

A simplified load-deflection graph shows the generalised response of all beams with Beam 5 highlighted to provide an example (Figure 7.8). From left to right the beams had a reduced stiffness causing larger deflections at lower loading. When responding plastically up to ultimate failure the graph becomes horizontal to failure, with the beams that have reduced cross sectional areas failing at lower loading. Complete load-deflection graphs are found in Appendix H.

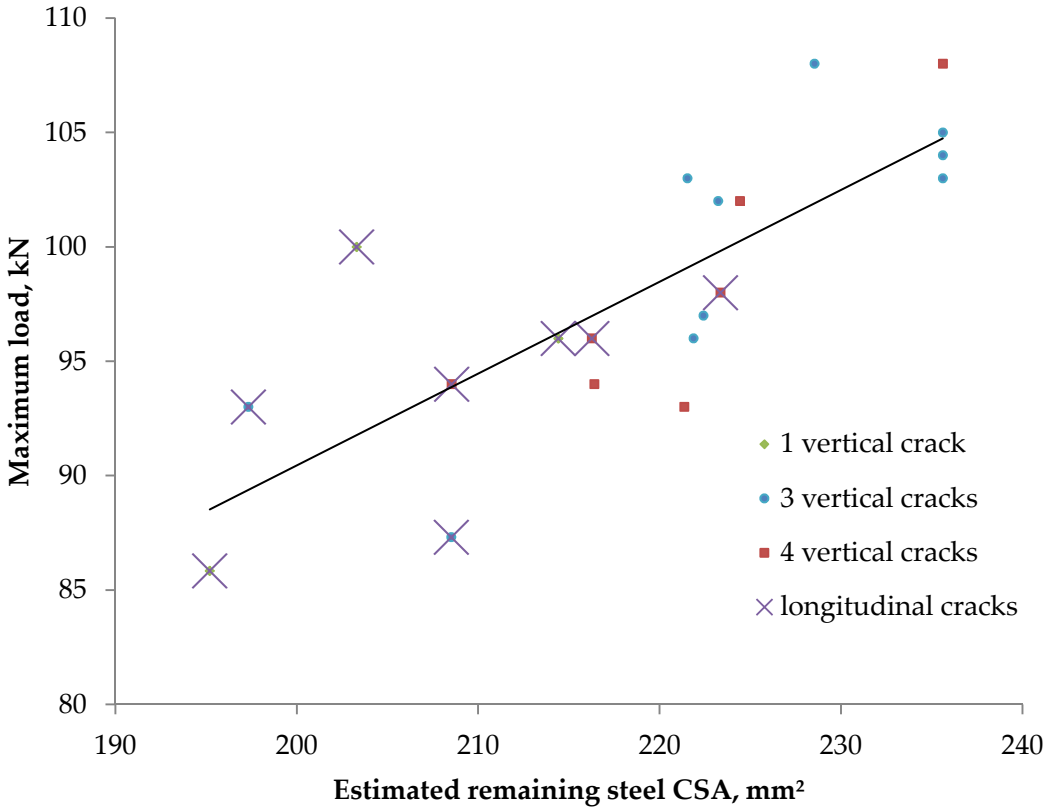

FIGURE 7.7 MAXIMUM LOAD AND CRACKING DUE TO LOSS OF STEEL CROSS SECTIONAL AREA

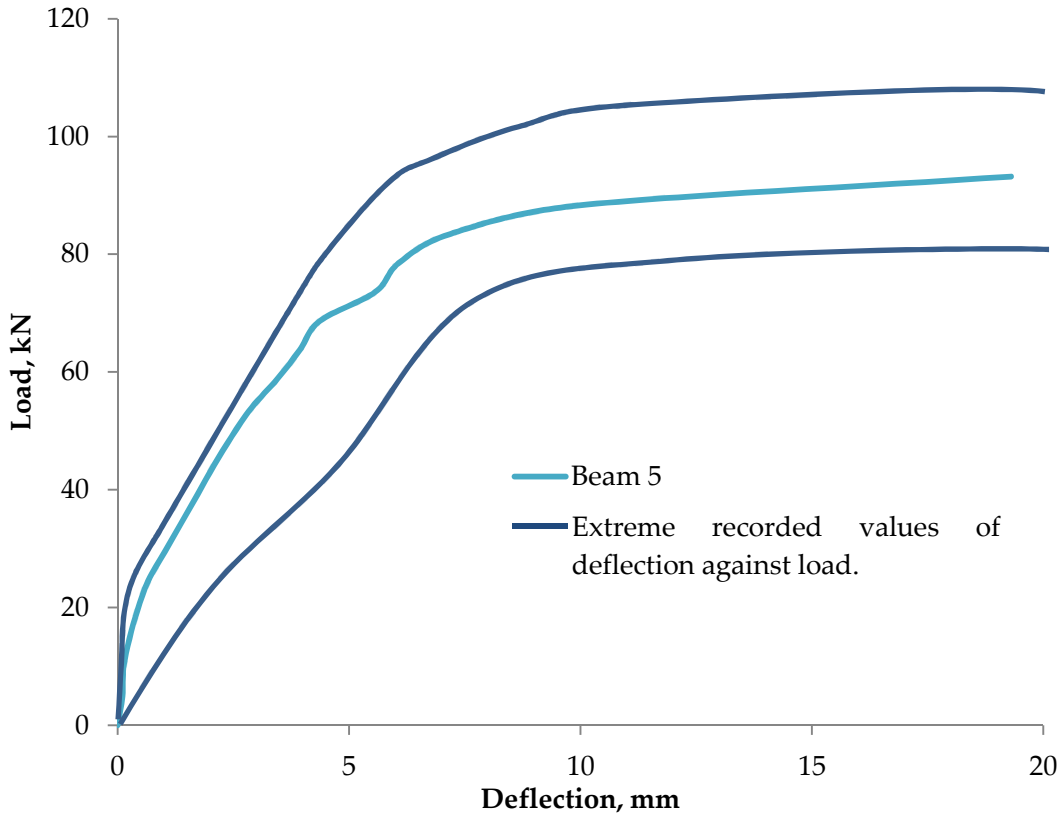

FIGURE 7.8 LOAD – DEFLECTION OF BEAM SET A

TABLE 7.4 SUMMARY OF BEAM SET A RESULTS

No.	Maximum load, kN	First visible crack, kN	Deflection first crack, mm	Stiffness after cracking, kN/mm	CSA, mm²	General Corrosion, % wt. steel	Bond loss, %
1	104.0	23.5	0.76	12.48	235.6	0.0	0.0
2	107.9	29.4	0.69	13.17	228.6	3.0	33.3
3	101.5	-	-	11.82	224.8	3.0	33.3
4	103.0	19.6	0.59	12.33	222.1	3.7	33.3
5	93.2	19.6	0.43	10.73	222.0	3.3	33.3
6	94.2	19.6	0.61	11.38	222.4	5.6	100.0
7	102.0	15.7	0.38	12.20	223.6	4.0	33.3
8	96.1	19.6	0.38	11.59	222.4	4.0	33.3
9	98.1	20.6	0.44	12.59	223.8	3.3	33.3
10	95.6	17.7	0.74	8.78	214.4	9.0	100.0
11	94.2	17.7	0.51	10.53	209.7	6.5	66.7
12	85.8	7.8	0.43	10.95	195.9	13.5	100.0
13	94.2	17.7	0.36	10.13	213.0	5.3	66.7
14	87.3	17.7	0.53	8.49	205.8	12.7	66.7
15	100.1	13.7	0.46	10.16	204.4	8.2	100.0
16	94.2	27.5	0.81	10.08	216.0	2.5	100.0
17	92.7	19.6	0.25	12.33	198.8	9.8	100.0
18	107.9	24.5	0.91	12.38	235.6	0.0	33.3
19	103.0	29.4	1.02	10.73	235.6	0.0	33.3
20	105.5	-	-	9.12	235.6	0.0	66.7

7.4 CORROSION OF REINFORCEMENT IN LAPPED SECTIONS

7.4.1 THEORETICAL BEHAVIOUR

As lapped reinforcement is sometimes seen as a source of weakness in reinforced concrete, theoretical evaluation of remaining capacity was carried out. Corrosion due to chlorides in a submerged marine environment has little effect on the bond between steel and the concrete, and therefore lapping will be unaffected by bond loss.

Assuming pitting corrosion occurs at any of 5 locations on the bottom bar (Figure 7.9), the effects of pitting will have a varied effect on total capacity of the section. Considering a unit force acting on each bar with a unit area, the maximum stress would therefore be a unit stress.

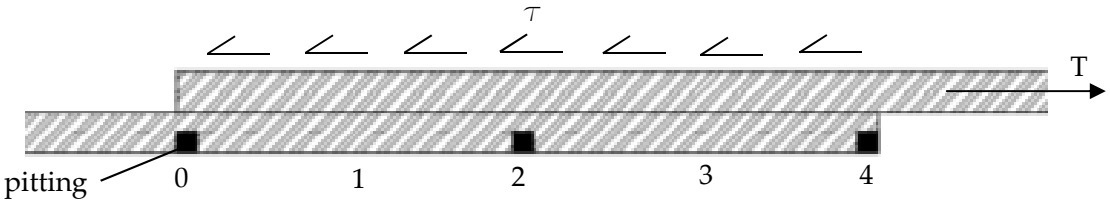

FIGURE 7.9 EFFECT OF CORROSION ON LAPPED REINFORCEMENT

As the force is gradually transferred between the bars due to the resistance of the bond, the location of the pit is critical to the overall strength of the section (Figure 7.10). As pitting occurs locally at a given location on the bottom bar, the stress is increased due to loss of CSA (Figure 7.11). At location 3 it is evident that 75% loss of CSA could occur before stress limits are exceeded, similarly at location 2, 50% loss of CSA is critical. This critical loss of CSA decreases linearly to location 0 whereby any corrosion would cause excess stress. Therefore, at location 0, corrosion is most critical, which is identical to a scenario at a location within the concrete where there is no lapping, thus showing that lapping is inconsequential when considering submerged corrosion.

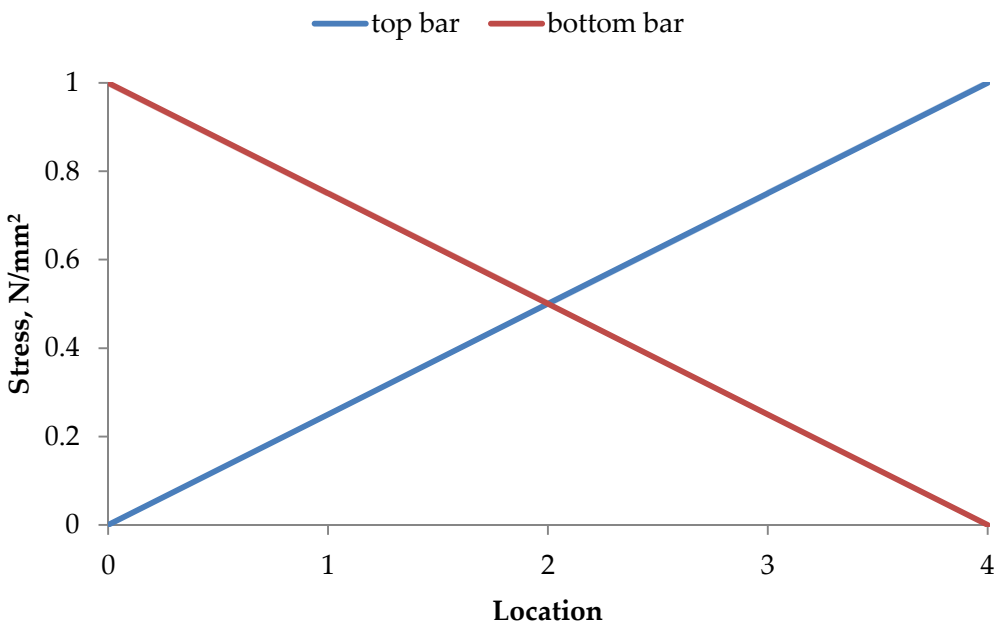

FIGURE 7.10 STRESS AGAINST LOCATION FOR UNCORRODED LAPPED SECTION

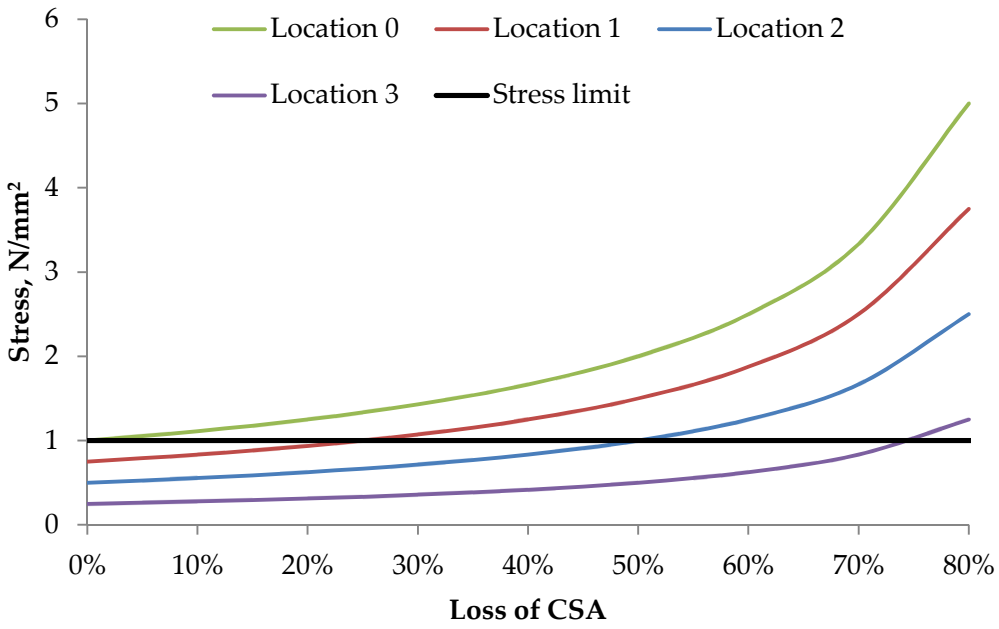

FIGURE 7.11 STRESS DUE TO LOSS OF CSA AT LOCATIONS 0-3

7.4.2 CONTROL BEAMS

The control beam showed crack patterns that would be expected from a lapped section in an area of constant moment. Cracking occurred at either end of the lapped section, where the section capacity reduces by a half due to the decrease in steel from 2 bars to 1 (Figure 7.12).

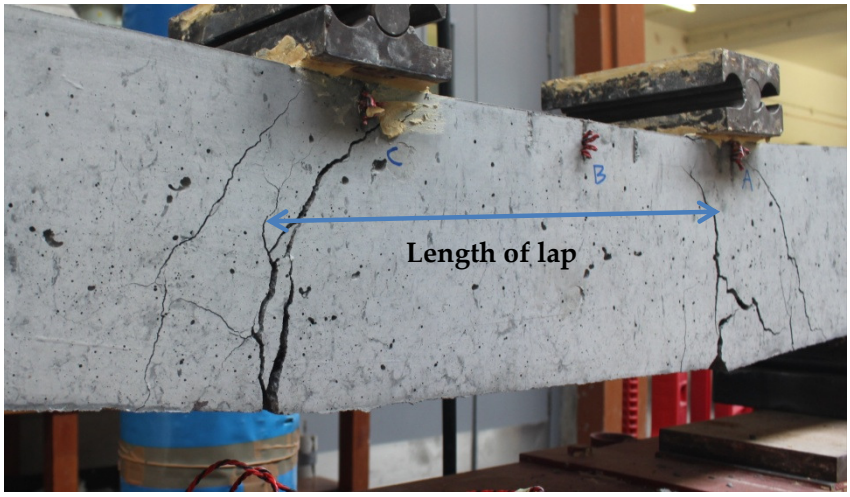

FIGURE 7.12 CRACK PATTERN ON SET B CONTROL BEAM

Control Beam A was loaded directly to failure, whilst Control Beam B was loaded to 10% capacity 4 times and then to 75% capacity, repeated twice before loading to failure (Figure 7.13).

After the first set of cyclic loading to 10% capacity, the stiffness didn't change and the beams acted elastically. After first cracking, the stiffness reduced by 50%. When unloaded, the deflection returned to initial values before stiffening slightly over the next 5 cycles. Deflection then increased linearly to failure at an increased stiffness.

Both control beams ultimately failed at the same loading, as would be expected from similar beams, showing no deterioration from 10 cycles.

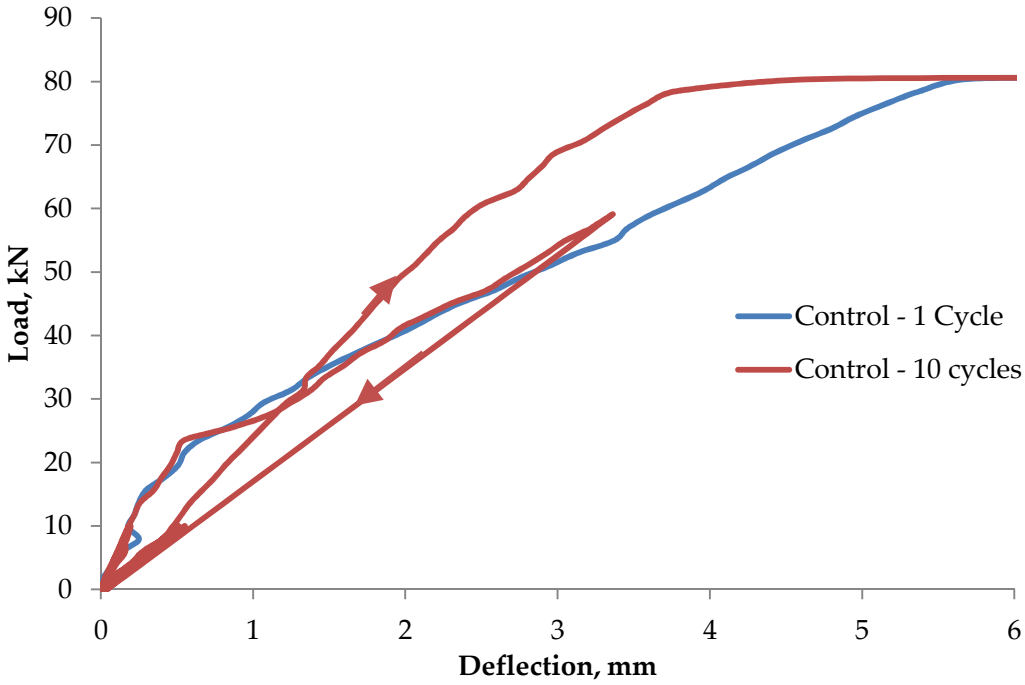

FIGURE 7.13 LOAD-DEFLECTION OF SET B CONTROL BEAMS

7.4.3 EFFECTS OF GENERAL CORROSION

General corrosion causes a reduction in the ultimate capacity due to the loss of CSA of the steel. The ultimate capacity decreases roughly proportionally with around a 10% loss of capacity with 10% general corrosion, similar to results obtained in sections with individual lapped bars (Figure 7.14).

After corrosion, the stiffness of the section is reduced both prior to and post cracking, although this is likely due to the reduced CSA of steel than a large bond loss.

7.4.4 EFFECTS OF CYCLIC LOADING ON CORRODED SECTIONS

Cyclic loading of corroded sections showed a similar behaviour to the control beam through initial loading up to 60kN (Figure 7.15). When unloaded however, the beam remained at over 1mm deflection, expected due to the irreversible behaviour of reinforced concrete. Reloading to 10kN cyclically caused no stiffening as seen with the control beam due to the ability for the reinforcement to slip due to loss of bond, although only over small lengths.

Cyclic loading, however, appeared to have no effect on the ultimate capacity of the section, however only a small number of cycles were used.

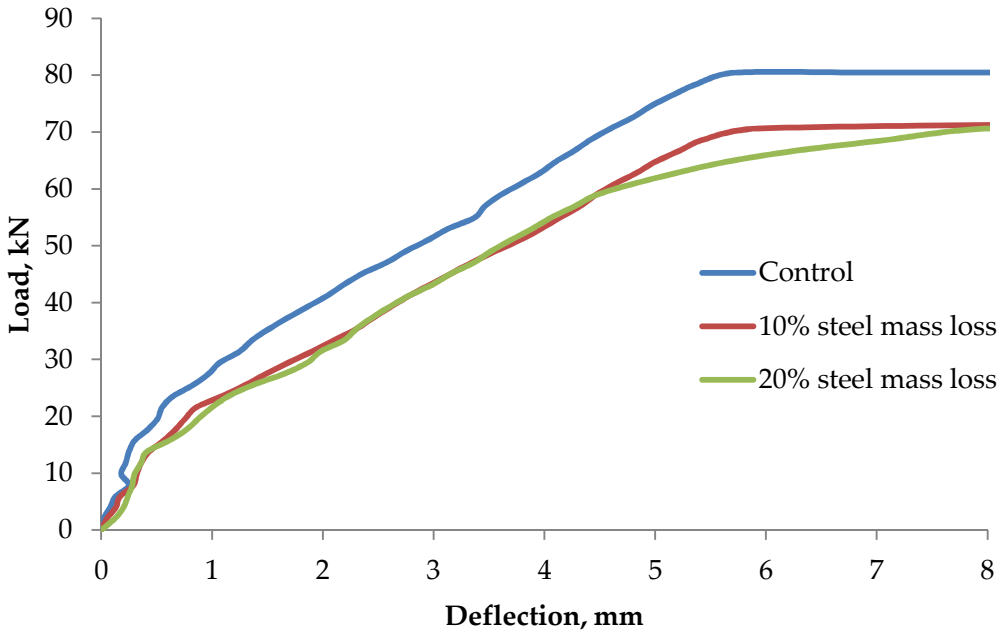

FIGURE 7.14 LOAD-DEFLECTION FOR CORRODED LAPPED SECTIONS

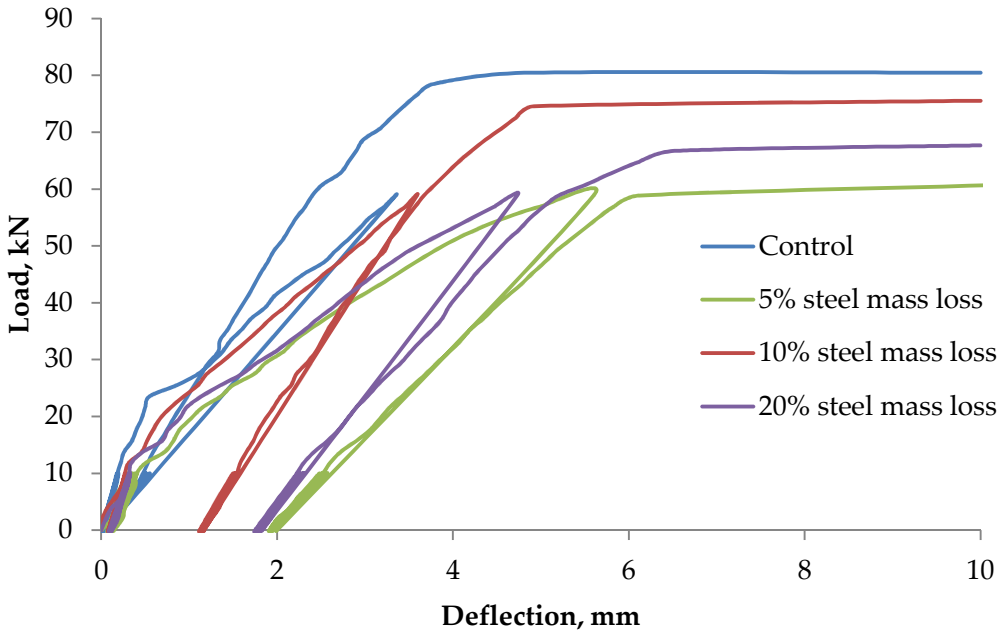

FIGURE 7.15 LOAD-DEFLECTION FOR CYCLIC LOADING OF CORRODED LAPPED SECTIONS

7.4.5 EFFECTS OF PITTING CORROSION

Pitting corrosion within the lapped section appeared to have no influence on the stiffness or the ultimate capacity as the beams still failed at a location outside the lapped area. This supported theoretical behaviour with the lapped section having a larger capacity due to the increased steel.

7.5 KEY OBSERVATIONS

7.5.1 ULTIMATE CAPACITY

The ultimate capacity of beams can be predicted through the use of structural analysis considering the beams to consist of concrete in compression and the steel acting alone in tension. Reducing the steel cross sections depending on corrosion rates and predicted damage to the bars, an estimate for the remaining ultimate capacity can then be achieved.

7.5.2 SERVICEABILITY

Serviceability of structures is commonly defined through maximum deflections or maximum allowable crack width. Results have shown that with increased bond loss due to corrosion, first visible cracking occurs at a reduced loading limiting service life defined by allowable crack widths. Additionally, the stiffness of a section is reduced due to bond loss causing larger deflections under similar loading.

The reduction in stiffness between an undamaged section and a section with an averaged corrosion mass loss of 12.7% was in the region of 30% (Table 7.5). This caused an increase in additional deflection by 43%.

TABLE 7.5 EXAMPLE SERVICEABILITY CALCULATION

Beam	**Stiffness, kN/mm**	**ΔF, kN**	**Δd, mm**
Undamaged	12	10	0.83
12.7% mass loss	8.4	10	1.19
% change	- 30%	-	43%

7.5.3 PREDICTING REMAINING STRUCTURAL CAPACITY OF COMPLEX MARINE STRUCTURES

Lapped sections appear to have no significant effect on the ultimate capacity, as in submerged corrosion mechanisms bond loss is insignificant. As lapped sections have increased steel, the worst case section remains a regular cross section with individual bars.

Predicting the remaining capacity of beams can therefore be estimated using a simple loss of steel CSA due to corrosion propagation. By combining the mass loss expected from measured rates with a loss of diameter, estimating the remaining CSA is straightforward and is completed in Chapter 8.

CHAPTER EIGHT

8 REMAINING LIFE MODELLING OF MARINE AND OFFSHORE CONCRETE

8.1 INTRODUCTION

Predicting the remaining ultimate life of a reinforced concrete structure in a marine or offshore environment is extremely complex and a function of a large number of variables, which have been discussed throughout this thesis. To completely model the type of failure mechanisms and time to failure, structures will need to be analysed as a whole and not just in terms of materials of construction.

Offshore structures have undergone a variety of loading conditions and will continue to experience varying conditions over the coming decades. To complete a structural analysis, the loading history is as important as any future loads. Historical loading, including construction and operational loads, and future loading, including decommissioned loading, must be determined and analysed at a macro level.

The structural response to loading will be significantly affected by the material properties, including the continued degradation of the materials due to environmental and physical loading. Due to the nature of this research, modelling will focus on the degradation of the reinforcing steel, along with a simplified approach to ultimate failure.

Deterministic methods of modelling are reviewed and utilised for an equivalent concrete for offshore structures taking into account the most significant degradation variables as perceived by the author (Table 8.1). Throughout this modelling process, a submerged CEM I concrete section with w/c ratio of 0.42 and a cover of 50mm will be applied to existing techniques to assess the remaining life of these structures. Application of experimental results obtained throughout this research is achieved, enhancing the remaining life estimations.

An estimated remaining ultimate life is predicted due to the combination of corrosion initiation and propagation, with a probabilistic model allowing for the variability of inputs. Probable scenarios are investigated, taking into account the most significant variables.

TABLE 8.1 VARIABLES TO BE CONSIDERED DURING MODELLING

	Variable*	Effect on concrete deterioration	Importance Rating§
Exposure	Humidity	High humidity reduces resistance and can increase corrosion	High
	Oxygen availability	Decrease could potentially decrease the corrosion rates	High
	Additional ion availability	Can reduce resistivity increasing corrosion	Low
	Temperature	Decrease causes a decrease in corrosion by twofold per 10^{o}C	Medium
	Chloride concentration	Surface concentration can increase diffusion rates causing reduced service life	Medium
Construction	Cover depth	Increased cover reduces chloride access to steel increasing service life	Medium
	Steel composition	Stainless steel or other alloy reduces susceptibility to corrosion	High
	Lapping		X
	Compaction	Good compaction reduces the voids preventing easier transportation of chlorides	High
	Coatings	Prevent ingress of water/chlorides into the concrete	Medium

TABLE 8.1 CONT'D

	Variable*	Effect on concrete deterioration	Importance Rating§
Material properties	Water/cement ratio	Reduced w/c ratio decreases pore size and restricts movement of chlorides, water and oxygen	Medium
	Aggregates	Aggregates have a pronounced effect on strength, but minimal on corrosion rate	Low
	Binders	FA, GGBS and LS can reduce permeability of the concrete, thus reducing chloride ingress	Medium
	Age	Ageing is shown to reduce chloride ingress, more pronounced in ggbs and fa concretes	Medium
Loading	Magnitude	Larger crack widths increase corrosion rates	High
	Frequency	Increased frequency may increase the flow of chlorides, water and oxygen to the steel surface through hydraulic pumping	Average
	Extreme	Extreme loading will cause failure when wave/tidal impact load exceeds remaining ultimate capacity	High

* variables of most importance as determined by the author

§ importance rating defined by the author and described as high, medium or low

Combining predicted corrosion mechanisms with an overall structural response is complicated, therefore where available, empirical data was used to numerically attempt to quantify the ultimate life. Possible failure mechanisms are described, with this research suggesting an expected failure mode, with estimated time to ultimate failure.

8.2 PROBABLE CORROSION MECHANISMS

Predicting this time to ultimate failure of such a complex structure accurately must be undertaken using considerable engineering judgement. In this case, consideration is taken of all corrosion mechanisms and the most likely are outlined. The scenarios of the three probable corrosion mechanisms are summarised in Table 8.2 and detailed throughout this section.

TABLE 8.2 SUMMARY OF PROBABLE CORROSION SCENARIOS

Scenario	Summary of corrosion mechanism
IA	Chloride initiates corrosion in weak areas of concrete, however not in a single cross section, as would be found in cracking mechanisms. Corrosion propagation will increase gradually as the conductivity of the concrete increases and more chlorides become available at the anode.
IB§	Chloride saturated concrete would cause anodes and cathodes to form freely and with ratios depending on the oxygen availability at a cathode. Low resistivity allows for a speedy transfer of charge through the concrete, causing propagation to be limited by the oxygen rate and exchange at the cathode.
IIœ	Cracking causes almost instantaneous initiation due to the rapid transport of chlorides to the steel, especially when crack widths are above 0.1mm. Macrocell effects will occur with small anodes and large cathodes, with the resistivity of the concrete between the areas limiting the corrosion current achievable.

§ defined in Chapter 5 and highlighted through experimental results obtained in Phases II and IIIA

œ described in detail and shown by results in Phase IIIB experimental work, Chapter 6

8.2.1 SCENARIO IA: UN-CRACKED CONCRETE (RANDOM CHLORIDE PROFILES)

Chlorides will reach the steel in various locations throughout the structure due to poor workmanship, variable cover depths, and variations in exposure. Corrosion will then initiate where chloride is present, most probably the hoop reinforcing steel that is located closer to the surface. During the initial phase where drawdown is operational, macrocell corrosion will occur with the internal reinforcement becoming a cathode with continuous replenishment of oxygen at the steel surface. Corrosion currents will be limited by the resistance through the concrete between the cathode and anode, limiting the flux of hydroxyl ions completing the electrochemical cell.

8.2.2 SCENARIO IB: UN-CRACKED CONCRETE (CHLORIDE SATURATED CONCRETE)

Assuming chlorides penetrate the concrete uniformly because of the homogenous material properties, concrete will be saturated with chlorides causing a lower cover resistivity. Initiation can occur on any area of the steel surface, likely to be where steel is highly stressed,

oxygen is readily available or there are defects on the steel surface. The anode to cathode ratio is then naturally balanced, depending on the ability for the charge to be transmitted through the concrete pore structure. If oxygen becomes more readily available, corrosion will propagate over a larger anodic area, and should oxygen become less readily available, the anodic area will decrease, as shown in Chapter 5.

Once propagation has begun to occur, the rate can be altered due to environmental changes, however, because of a likely decrease in pH at the steel surface and the continued presence of chlorides, corrosion will continue to propagate.

8.2.3 SCENARIO II: CRACKED CONCRETE

Statically and dynamically cracked concrete will cause almost instantaneous corrosion at crack widths above 0.1mm, lower than commonly modelled. As chlorides, water and oxygen all reach the concrete/steel interface through the crack opening, corrosion will initiate in the region where the cracking intercepts the steel. Up to around 3cm of steel was shown to begin to corrode, whereby the anodic exchange current density will limit the corrosion due to the large cathodic areas within the un-cracked concrete and the relatively low resistivity of the concrete in the region.

As cracks increase in width, the corrosion rate appears to increase linearly for statically cracked concrete. As cracks are increased, the transport of chlorides, water and oxygen increase due to a larger surface area through which to dissolve.

8.2.4 CONCLUSION

As each mechanism is likely, Scenario II will occur first due to the rapid ingress of chlorides through a crack. As massive offshore structures are difficult to assess for cracking due to marine growth and lack of ability to inspect, initially the designs were carried out to standards, and therefore within the service life period cracks up to 0.2mm are expected. As corrosion in submerged, low oxygen environments will not lead to expansive cracking and spalling, the loss of CSA will still occur.

8.3 PROBABLE OVERALL FAILURE MECHANISMS

As with the corrosion mechanisms, there are a number of possible failure mechanisms for the entire structure. Utilising literature and results reported in Chapter 7, five probable failure mechanisms are considered likely and are described throughout this section (Table 8.3).

TABLE 8.3 SUMMARY OF PROBABLE OVERALL FAILURE MECHANISMS

Scenario	Summary of corrosion mechanism
I	Flexural failure of a section will occur when the capacity of the section is reduced to below the loading and can simply be caused by a reduction in the cross sectional area of the steel. As an assumption, the section capacity of the concrete can be modelled as proportional to the steel cross sectional area.
II§	Corrosion of the steel lateral reinforcement will cause a reduced ability to withstand shear stresses, causing a possible shear failure before the vertical reinforcement has reduced in cross section significantly.
III	Large reduction in stiffness caused by bond failure causing no stress to be transferred from the steel to the concrete. As the deflection increases, the compressive zone will reduce in size causing increased stress and crushing failure of the concrete.
IV	Loss of capacity at lapped sections will cause failure in a similar manner to Scenario I, however should the corrosive product be expansive a combination of Scenario I and III could occur. The area of loss of cross section is vital when determining capacity in a lapped section, as discussed in Chapter 7.
Vœ	Should the prestressing steel begin to corrode, rapid loss of capacity will be evident causing a likely catastrophic instantaneous flexural failure.

§ this is less likely in the decommissioned period due to the lack of expansive corrosion product in submerged corrosion observed in Chapter 5.

œ similar overall failure mechanism to Scenario I, however likely to be instantaneous

8.3.1 SCENARIO I: FLEXURAL FAILURE DUE TO LOSS OF CSA ON VERTICAL REINFORCEMENT

As reported in Chapter 2 and shown through results in Chapter 7, the cross sectional area (CSA) of steel is the dominant factor influencing the remaining ultimate capacity of reinforced concrete subjected to overturning moments. Simplistically, failure of the structure would occur when reinforcement corrosion reduces the section capacity sufficiently that applied moments would exceed this capacity.

Estimating time to such a failure could be loosely achieved by assuming corrosion at cracking occurs on each bar at a predicted propagation rate. The expected loss of CSA and therefore section capacity can be calculated, predicting the decline in structural capacity.

8.3.2 Scenario II: Flexural-shear failure due to CSA loss on lateral reinforcement

As lateral/hoop reinforcement is located closer to the surface, it is highly likely that chlorides, water and oxygen will penetrate to this steel first, initiating corrosion. With the loss of this restraining reinforcement, shear stresses could lead to failure of the structure when these bars fracture.

As highlighted by Ou, Tsai and Chen (2012), the majority of lateral reinforcement is of a smaller diameter than vertical reinforcement. This can lead to a greater percentage loss of section over the same corrosion duration as vertical reinforcement, causing a larger reduction in shear capacity. Determining the remaining shear capacity through a complex section with corroded reinforcement could be difficult due to the potential for stress transfers through a number of different mechanisms.

Nevertheless, the author believes this mechanism is highly likely due to the shallow cover to the hoop reinforcement and therefore must be considered and an attempt to model must be made in the future.

8.3.3 Scenario III: Bond failure due to general corrosion

Although unlikely, if sufficient oxygen is available general corrosion of the steel may occur, possible during an operational state. Should the bond of all bars in a section be lost, slip of the tensile reinforcement may occur, causing large deflections and increased compressive strain. When the curvature becomes excessively large, the concrete in the compressive zone crushes due to geometrical restraint.

Despite this being a theoretically possible mechanism, the author rules this out as a potential failure mode for such a structure due to the unlikely conditions that would lead to such a corrosion mechanism in a chloride laden submerged environment. Yet if deterioration of bond due to repetitive loading or alternative degradation mechanism occurs, this may require consideration.

8.3.4 SCENARIO IV: LOSS OF CAPACITY AT LAPPING OF STEEL

Lapping of steel is often considered a weak point in concrete structures, relying on the bond between the bars and concrete to maintain a continuous path for the transfer of tensile stress. General corrosion would cause a loss of bond which could lead to a reduction in the stress carrying capacity of the reinforcement. As discussed previously in Chapter 5, general corrosion is unlikely, however further research into the effect of pitting corrosion and stress transfer is required.

Location of anodic areas are critical when considering the overall capacity loss as residual capacity could be retained should corrosion occur in the centre of a lap in comparison with corrosion in the main bar the end of the lapped section as reported in Chapter 7.

Although the location of the anodic area along the length of the lap is critical for the ultimate capacity of the section, the worst case scenario occurs at the end of the lapped section whereby the structural section contains only one reinforcing bar.

8.3.5 SCENARIO V: FAILURE OF PRESTRESSING SYSTEM

Although grouted prestressing tendons are located at depths of at least 100mm, rapid corrosion of tendons could lead to an instantaneous failure. Concrete around the prestressing tendons should remain in compression, preventing any cracking and therefore can be regarded as a failure mechanism that could occur should access for seawater to the tendons be achieved.

With loss of prestress, the structure must be evaluated to determine if the reinforced structure would withstand the loading in the decommissioned state. Should the structure be able to withstand these forces, the crack widths would be increased which would lead to accelerated corrosion rates. Ignoring the effects of prestressing, the section loss and remaining ultimate capacity could be estimated as for previous mechanisms.

8.3.6 ADDITIONAL CONSIDERATIONS

Failure mechanisms described consider the ultimate failure in terms of the loading exceeding the remaining capacity. In an under reinforced concrete beam without corrosion, the steel will yield causing large cracking and increasing deflections. As the curvature continues to increase, the concrete cover in compression will proceed to crush and spall due to the reduced compressive zone. Failure in this manner absorbs energy, meaning an impact load, such as

large wave loading in a storm, may permanently disfigure the structure whilst not causing total structural collapse.

Corrosion causes a reduction in ductility of steel reinforcement due to cracking in the steel, as well as the potential for hydrogen embrittlement caused through hydrogen production in corrosion pits. Less ductile steel does not allow for as much energy to be absorbed, potentially leading to an instantaneous catastrophic failure.

8.3.7 CONCLUSION

Although any of the five scenarios are probable, it is difficult to assess which mechanism will cause failure on such a large scale and complex structure. As corrosion is likely to initiate at areas of cracking, the author believes Scenario I to be critical and therefore modelling of ultimate life of such structures should be based on the propagation of vertical reinforcement and subsequently the loss of CSA in outer vertical reinforcement.

8.4 DETERMINISTIC MODELLING OF CORROSION APPLYING VARIOUS METHODOLOGIES

8.4.1 DURACRETE

Applying the DuraCrete model (Lindvall, 1998) to submerged concrete used throughout the experimental programme, a time to corrosion initiation was determined to be 20.6 years and a corrosion propagation rate of 80.09μm/year (Appendix C). This is approximately equivalent to 12.4 years to lose 1mm of reinforcing steel diameter.

For 75mm depth of vertical reinforcement the initiation period was determined to be 59.1 years. Assuming corrosion initiates in this method, hoop reinforcement will have reduced by over 3mm in diameter before vertical reinforcement begins to corrode. It is, however unlikely the vertical reinforcement will take an additional 40 years to initiate when chlorides have reached the lateral reinforcement.

8.4.2 CONCRETE SOCIETY TECHNICAL REPORT 61

Application of methodologies in Technical Report 61 estimate the initiation period to be 53.2 years for 50mm cover and 146.6 for 75mm cover (Appendix C).

8.4.3 LIFE365

Application of Life365 models determines initiation to be only 7.4 years for 50mm cover increasing to 20.3 years for 75mm cover. No attempt was made to model propagation, which is therefore defined as 6 years before repairs are necessary (Appendix C).

8.4.4 UPDATED METHOD FOR CURRENT NORTH SEA STRUCTURE

Updating a model to incorporate a revised 'ultimate life' prediction, defined having taken into account structural response of beams due to artificially applied heavily advanced corrosion.

Corrosion propagation has been shown to continue in submerged environments, albeit at a rate that will vary slightly depending on the oxygen availability within the water. Due to there being significant concentrations of dissolved oxygen in the North Sea, corrosion propagation corrosion rates are altered to take this into account, along with the effects of cracking.

The author believes that the resistivity of the concrete between cathodic and anodic areas to be the corrosion limiting factor, rather than the rate of cathodic reaction as often stated for submerged conditions. This is due to conditions within the concrete being conducive to anodic and cathodic reactions, and the continuity of the steel reinforcement.

Three concrete systems will be considered for this modelling; sound/un-cracked, statically cracked, and dynamically cracked sections. Although initiation will take considerable time in sound concrete, corrosion will still propagate in these areas once initiation has occurred, albeit at a slower rate. Critically, the cracked area is likely to cause ultimate failure due to the increased corrosion rate.

$$i_{corr} = \frac{k_T \cdot k_D \cdot k_{Ox} \cdot k_w \cdot i_{corr,0}}{A_A} \qquad \textbf{EQUATION 8.1}$$

Where variables are as listed in Table 8.4.

TABLE 8.4 VARIABLES FOR UPDATED ULTIMATE-LIFE MODELLING OF PLAFTORM A CONCRETE

Variable	Value
Temperature factor (k_T)[#]	$k_T = 2^{\left(\frac{T-T_{ref}}{10}\right)}$
Dynamic loading factor (k_D)[†]	$k_D = 3$
Oxygen exposure factor (k_{Ox})	$k_{Ox} = 1$[~]
Maximum crack width (w_{max}), mm	$w_{max} = 0.2$[ˇ]
Crack width factor (k_w)	$k_w = 11.47(w_{max} - 0.2) + 1.0$ for $w_{max} > 0.12$mm
Reference corrosion current at crack width 0.2mm ($i_{corr,0}$), μA	120 [1/]
Diameter loss (v), mm/year	$v = 0.0116 \cdot i_{corr}$
Propagation duration (t_{prop}),years	$t_{prop} = 50$
Reinforcement diameter (d_{ref}), mm[œ]	$d_{ref} = 32$
Reinforcement diameter post corrosion (d), mm	$d = D_{ref} - k_p v \cdot t_{prop}$
Steel cross sectional area ($A_{s,0}$), mm^2	$A_{s,0} = \frac{\pi {D_{ref}}^2}{4}$
Area of anode (A_A), cm^2	$A_A = 30$
Capacity loss (R), %	$\frac{A_{s,R}}{A_{s,0}}$

[#] factor designed to increase corrosion rate by a factor of 2 every 10 degrees

[†] judged from dynamic and cracking results, Phase IIIB in Chapter 6

[ˇ] design value as visual inspection of the submerged concrete is impossible

[~] conservatively assume oxygen saturated water throughout

[1/] corrosion current for statically cracked section (w_{max} = 0.2mm) under laboratory conditions

[œ] diameter of rebar used as vertical reinforcement on offshore structures

Remaining steel CSA ($A_{s,R}$) is calculated assuming a constant corrosion current given the environmental and loading factors applied. This initial simplistic estimation assumes a worst

case corrosion and damage scenario, and will provide a basis for a lower bound estimation of longevity of the structure.

$$A_{s,t} = \frac{\pi {d_t}^2}{4}$$ EQUATION 8.2

Where;

$A_{s,t}$ remaining steel CSA, mm^2

d_t reinforcement diameter post corrosion, mm

Corrosion rates with 0.2mm dynamic cracking are estimated to be 0.046mm/year, equivalent to approximately 22 years to lose 1mm of reinforcement diameter (Appendix C). This is assuming corrosion is occurring at one crack location on an individual beam. As ultimate capacity is for all intents and purposes proportional to the remaining CSA of steel, a lower bound estimate for loss of capacity is predicted assuming every steel bar corrodes at the same section. For various dynamic crack widths, minimum remaining capacity is shown in Figure 8.1, where capacity is determined as the loss in percentage of CSA of individual reinforcing bars.

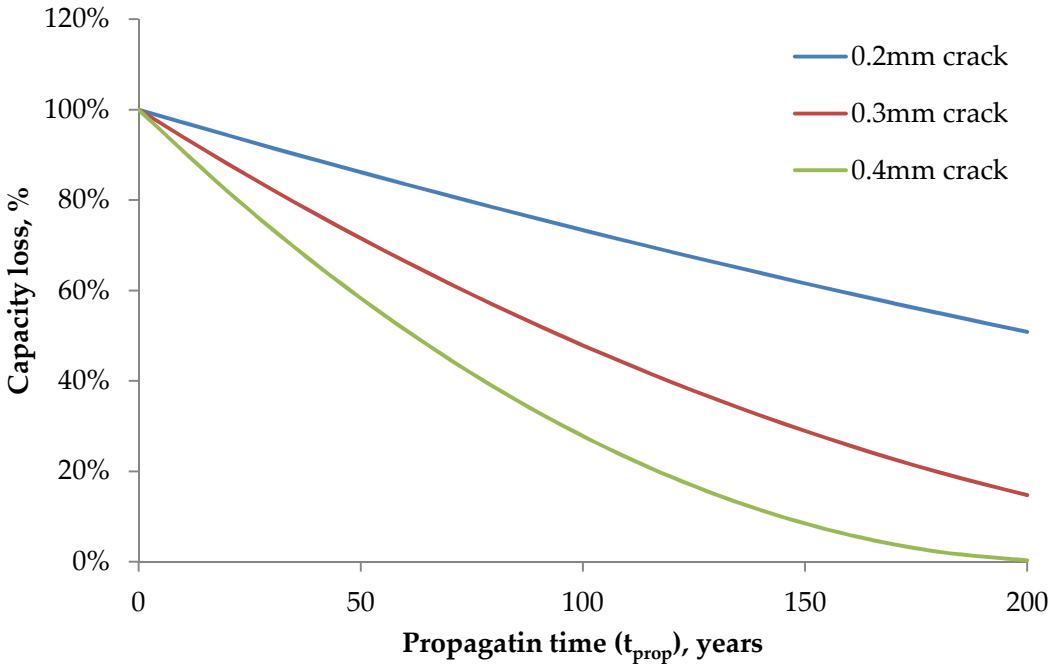

FIGURE 8.1 PREDICTED WORST CASE LOSS OF CAPACITY DUE TO VARIATIONS IN CRACK WIDTH

8.4.4.1 OPERATIONAL/WORKING STATE

Operational platforms often undergo additional physical loading through raised temperatures causing large temperature gradients and a draw-down system to reduce the internal pressure

of each leg allowing hydrostatic pressure to increase the compression in each leg. Furthermore, increased bending moments can be caused due to tall steel topsides increasing the leverage and therefore the bending moment at the base of the legs. Topsides may, however, cause legs to act as a portal frame increasing the stiffness and reducing lateral deflection of the structure.

Any area within the legs where a draw-down is effective, oxygen will be more readily available at the concrete surface causing an increased corrosion current should initiation occur during this operational state (Figure 8.2).

8.4.4.2 DECOMMISSIONED STATE

Post-decommissioned concrete GBS will have had steel topsides removed and legs flooded as shown in Figure 8.3. As the compressive loading is somewhat reduced, a large relaxation of the concrete is expected. However, bending moments are also reduced, which decrease the maximum tensile strain on the concrete counteracting the reduction due to reduced compressive payload. An increase in maximum crack width is expected however, with chloride ingress subsequently accelerated. Macrocell effects from the reduction in availability of oxygen on the internal face will reduce, thus decreasing the corrosion rate somewhat, although results in Chapter 5 prove that the effect is not significant.

8.4.5 SUMMARY

As shown for the current corrosion models, there is a large discrepancy between results, with initiation ranging from around 20 to 150 years (Table 8.5) with propagation commonly ignored or arbitrarily defined. Although models of this form are vague, experimental data must be utilised to form an empirical estimation of remaining life by defining propagation and initiation times for individual concrete types. The updated model uses similar methodology to others, however variables are populated through results obtained from the literature review and more importantly, those highlighted through Chapters 4 to 7.

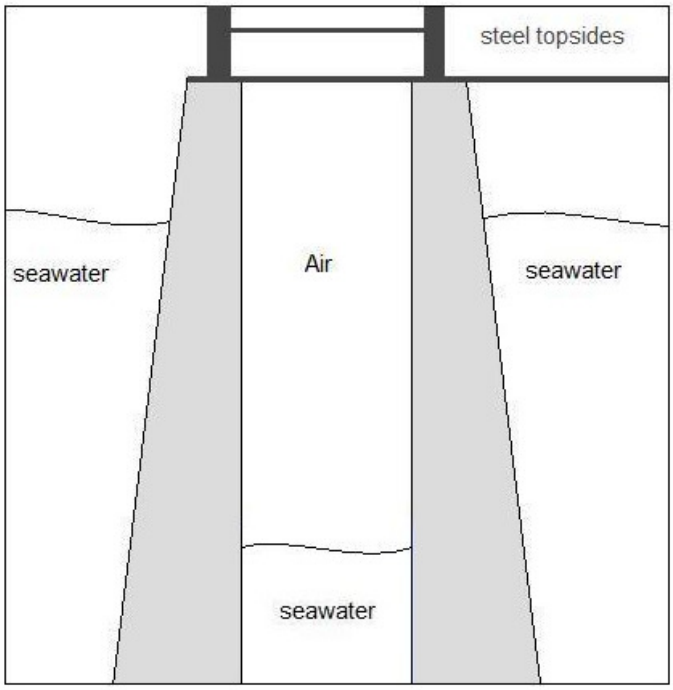

FIGURE 8.2 OPERATIONAL DRAWDOWN ENVIRONMENT WITHIN THE LEGS

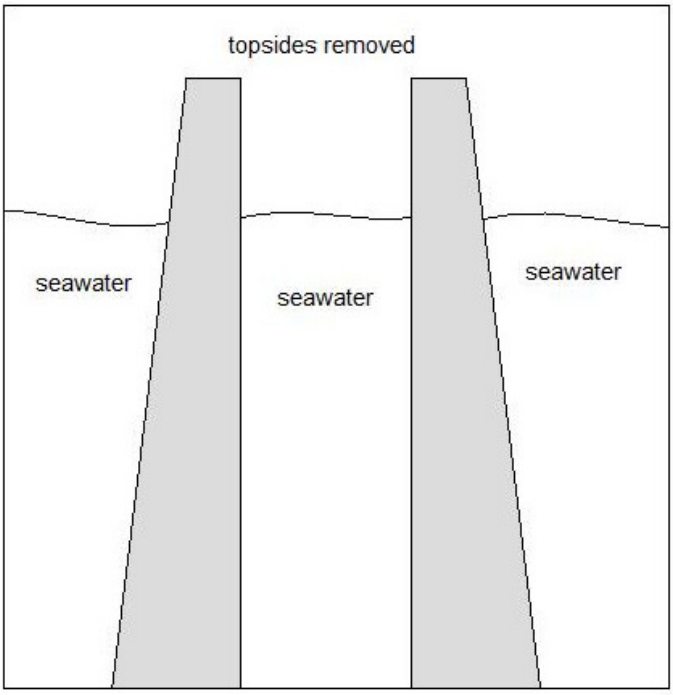

FIGURE 8.3 DECOMMISSIONED STEUP – TOPSIDES REMOVED AND LEGS FLOODED

TABLE 8.5 SUMMARY OF PREDICTED INITIATION AND PROPAGATION TIMES FOR 75MM COVER

Model	Initiation years	Propagation years	Comments
DuraCrete	59.1	12.4[#]	For 32mm diameter bars, CSA will be reduced by 50% after around 180 years from initial exposure assuming general corrosion around the entire circumference of the bar.
Concrete Society TR 61	146.6	N/A	Extremely long initiation period in which ageing has a large effect on the chloride ingress. This model suggests the structures could be left without issue.
Life 365	20.3	6	Propagation period is 'time to repair' and is constant regardless of structure. This model suggests North Sea structures should have undergone reparation works programmes in the past 20 years.
Updated	48 uncracked[¬] 0 Cracked	22.1[#]	Initiation is assuming a CEM I concrete and is calculated as a mean value. Variability in results is extremely large, with a reported standard deviation of 25 years. Propagation

[#] per loss of 1mm reinforcement

[¬] calculated using a Monte Carlo simulation with 100,000 repetitions

8.5 PROBABILISTIC MODELLING OF CORROSION RATES

8.5.1 INTRODUCTION

Applying variability to input parameters for deterministic modelling through the use of a Monte Carlo method is common practice, and is used in combination with the updated method as reported in Section 8.4.4. Expected initiation time for un-cracked sections along with corrosion rates for the operational and decommissioned states are calculated.

8.5.2 ASSUMPTIONS OF VARIABLES

Engineering values for modelling are defined through experimental results, reported data in the literature and engineering judgement by the author. Distributions of variables are determined from existing models and judgement from observed results.

Material properties used are a CEM I concrete with a 0.42 w/c ratio determined from a platform described in Tegelaar (1975). It is assumed a gravel aggregate used for testing is similar to the flint most likely used in construction.

The corrosion is assumed to be as in Scenario II, whereby corrosion propagates at the base of the cracking, with little to no expansive corrosive product, causing no cracking or spalling. Base corrosion rates are determined from Phase IIIB results assuming a crack width of 0.2mm in submerged conditions at 293K.

8.5.3 INITIATION

Time to initiation was calculated using a Monte Carlo simulation with variables determined from experimental research along with reported literature data, as shown in Table 8.6. Ageing factors are defined as zero due to the contradictory evidence reported throughout literature for CEM I offshore concrete.

TABLE 8.6 VARIABLES USED IN CALCULATING EXPECTED TIME TO INITIATION FOR CT07 CONCRETE

Variable	Distribution	Mean	StDev
D_{app} ($x10^{-12}$), m^2/s ˇ	Normal	1.3	0.4
C_s, % wt. concrete	Uniform[ƴ]	0.5	0.06[#]
C_{crit}, % wt. concrete	Normal	0.1	0.03[†]
x, mm	Normal	75	8 ˜

ˇ determined from 90 day diffusion coefficient using CEN TS 12390 methodology

˜ 95% chance of the cover being between ±20%

ƴ C_s is commonly between 0.4 and 0.6 in literature and throughout results therefore the author chose a uniform distribution

calculated standard deviation from a uniform distribution from 0.4 to 0.6

† determine from literature review, 95% confidence C_{crit} will be ±60%.

Using 100,000 repetitions of the deterministic method applying the variables listed, time to initiation can be described as a positively skewed normal distribution with mean 48 years and a standard deviation of 25 years (Figure 8.4). Cumulative probability of initiation is shown in Figure 8.5, and if allowing for a 10% chance of initiation before assuming propagation, the time to initiation would be around 24 years.

Deterministic and probabilistic modelling both suggest corrosion initiation is likely to have begun on offshore structures of this type, even when ignoring cracking. Propagation rates will determine the ultimate longevity of the structure as corrosion is the ultimate cause of failure in offshore structures.

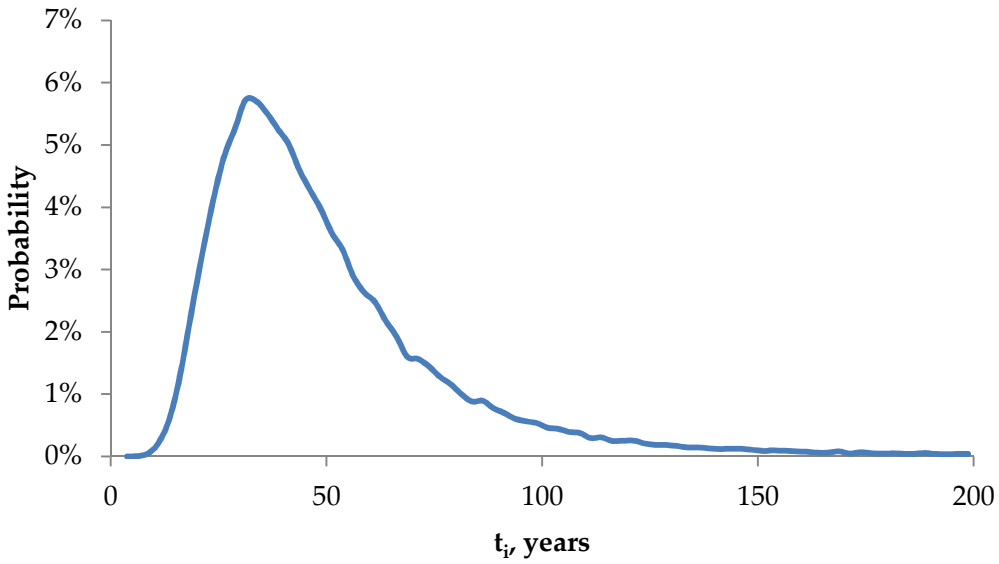

FIGURE 8.4 ESTIMATED DISTRIBUTION OF TIME TO INITIATION IN UNCRACKED CONCRETE

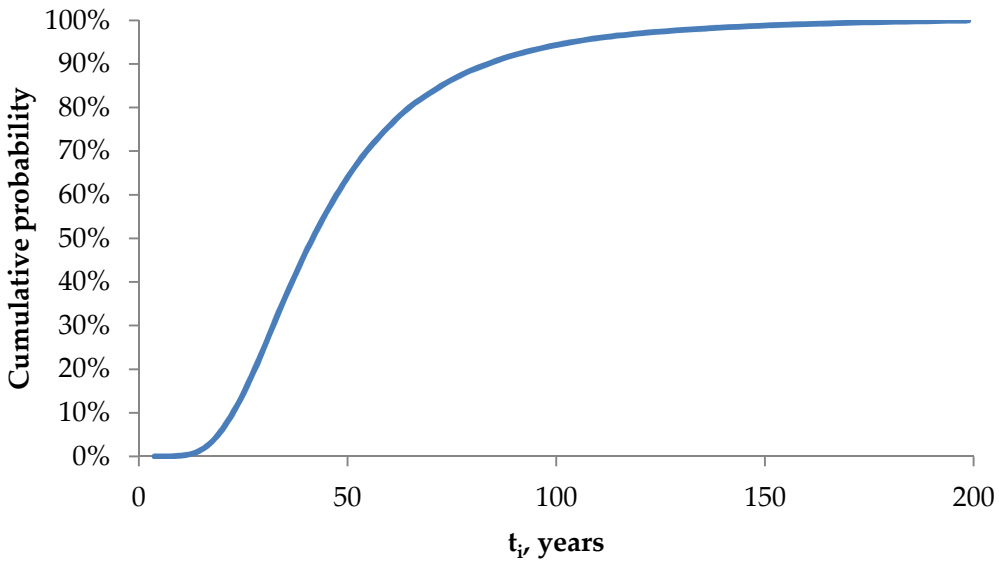

FIGURE 8.5 CUMULATIVE PROBABILITY OF CORROSION INITIATION IN UNCRACKED CONCRETE

8.5.4 OPERATIONAL PERIOD

The operational state is modelled by doubling the oxygen factor due to previous research showing corrosion continues at considerable rates in submerged environments. The availability of oxygen on the internal face of the concrete however, can increase the rate at which dissolved oxygen reaches the steel due to the convection zone, whereby gaseous oxygen will be transported faster than dissolved oxygen.

The updated deterministic methodology is applied to determine the average and mean corrosion rates expected under the given conditions. A Monte Carlo simulation was carried out with 100,000 repetitions using the variables outlined in Table 8.7.

From these calculations, i_{corr} was determined to have a mean average of 7.6μA/cm² and a standard deviation of 2.7μA/cm², which will be subsequently used for ultimate remaining life modelling (Figure 8.6).

TABLE 8.7 VARIABLES FOR OPERATIONAL CORROSION CURRENT MODELLING

Variable	Distribution	Mean	StDev
$i_{corr,0}$, µA[#]	Normal	120	30
T, K[ɣ]	Normal	8	1
w	-	0.2[˘]	-
k_d	Uniform[˜]	2.5	0.3
k_{ox}	Normal	2[†]	0.5
A_A, cm^2	-	30[˘]	-

[#] determined from results of set A, Phase IIIA, Chapter 6

[ɣ] Schlüter and Jerosch (n.d.) show temperature in the region of the platforms commonly fluctuates between around 7 and 9°C (280-282K)

[˘] no variability applied, therefore the value is not a mean but a single figure

[˜] the author defined this variable from Phase IIIB results, reported in Chapter 6

[†] the author determined a significant chance the corrosion rate will rise by a factor of 2 as experimental work supports in Chapter 5

- no value defined

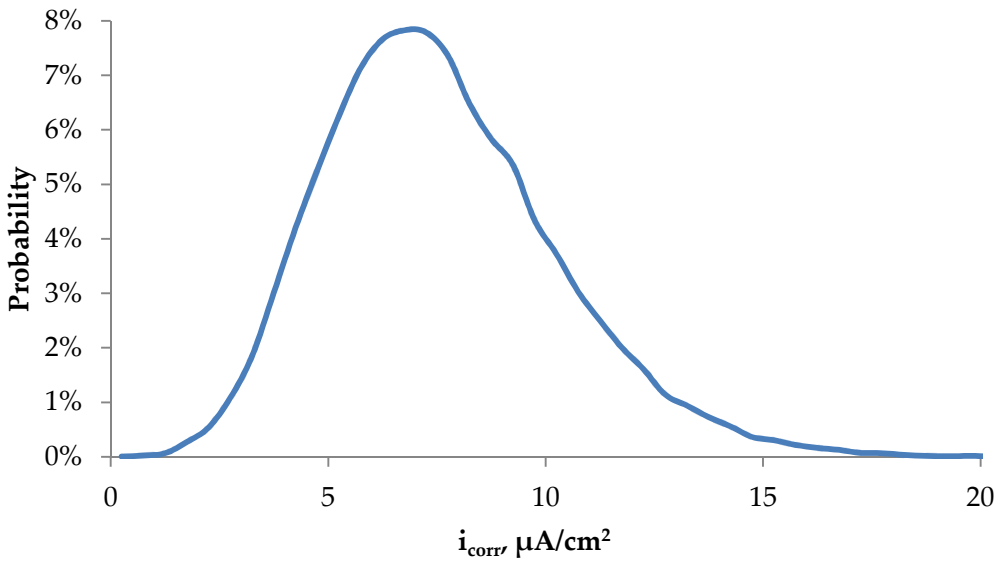

FIGURE 8.6 ESTIMATED DISTRIBUTION OF CORROSION RATE FOR OPERATIONAL CONCRETE

8.5.5 DECOMMISSIONED PERIOD

Once decommissioned, the internal face of the legs will now be exposed to seawater, at identical saturations of dissolved oxygen as the seawater. The oxygen coefficient is reduced to reflect this, with a mean value of 1, as experimental studies were carried out in submerged saturated conditions (Table 8.8).

TABLE 8.8 VARIABLES FOR DECOMMISSIONED CORROSION CURRENT MODELLING

Variable	Distribution	Mean	StDev
$i_{corr,0}$, μA[#]	Normal	120	30
T, K[ɣ]	Normal	8	1
w, mm	Fixed	0.2[˘]	-
k_d[~]	Uniform	2.5	0.3
k_{ox}	Normal	1[†]	0.1
A_A, cm^2	Fixed	30[˘]	-

[#] determined from results of set A, Phase IIIA, Chapter 6

[ɣ] Schlüter and Jerosch (n.d.) show temperature in the region of the platforms commonly fluctuates between around 7 and 9°C

[˘] no variability applied, therefore the value is not a mean but a single figure

[~] the author defined this variable from Phase IIIB results, reported in Chapter 6

[†] the author determined a variation of corrosion rate due to oxygen variation as being ±20%

- no value defined

From these calculations, i_{corr} was determined to have a mean average of 3.8μA/cm^2 and a standard deviation of 1.2μA/cm^2, which will be subsequently used for ultimate remaining life modelling (Figure 8.7).

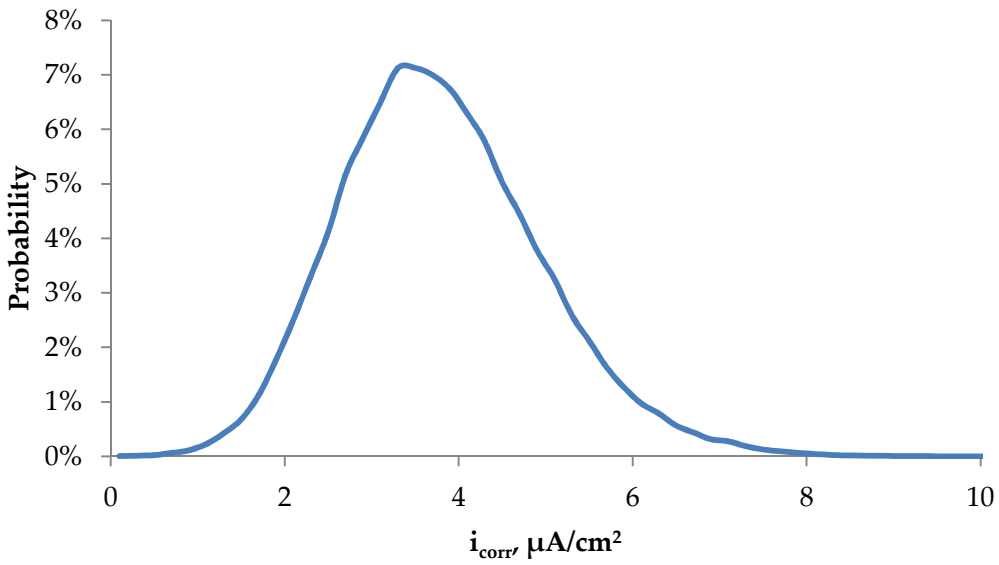

FIGURE 8.7 DISTRIBUTION OF ESTIMATED DECOMMISSIONED CORROSION RATE

8.6 REMAINING ULTIMATE CAPACITY

Remaining ultimate capacity is difficult to determine precisely, as the external vertical reinforcement will not solely determine the capacity. For the purposes of modelling however, remaining capacity of the external steel vertical reinforcement is defined as critical. When the remaining steel cross sectional area, ultimate capacity in this instance, drops below 50% the structure is assumed to have failed.

Assuming an operational duration of 45 years, and propagation between 0 and 205 years, the probability of failure was calculated through Monte Carlo simulations with 100,000 repetitions (Figure 8.8 and Table 8.9).

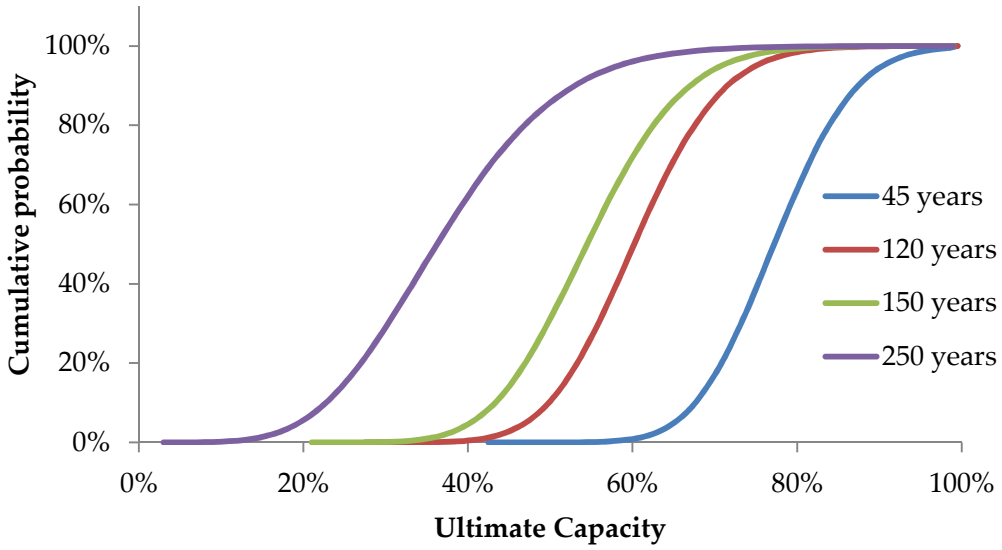

FIGURE 8.8 CUMULATIVE PROBABLITY OF ULTIMATE CAPACITY AFTER CORROSION

TABLE 8.9 PROBABILITY OF FAILURE

Age (t_{op} + t_{decom}), years	Probability of failure
45	0.002%
120	12%
150	35%
250	84%

Although simplistic and extremely conservative, results have shown that although corrosion is occurring, the large structures located in the North Sea will likely last into the next century unhindered. Taking into consideration spatial variations in corrosion, reduced crack widths, and extra remaining capacity among other factors, the structures are likely to last for centuries without becoming dangerous, supporting decommissioning through leaving the structures in situ.

8.7 SUMMARY

Due to the large variability in modelling chloride induced corrosion, it is advised that when dealing with projecting estimations of service life, experimental research is completed on the chloride diffusion coefficients of the specified concrete as well as work on corrosion rates in the environment in which the structure is exposed.

Although chloride profiling and use of diffusion coefficients are ill-advised for long-term modelling as previously recommended, understanding the type of concrete for comparison with other existing structures could provide vital insight into the long-term degradation of further structures. Building a database of existing structures and the damage caused by chloride-induced corrosion will allow for a better informed estimation of remaining service or ultimate life in future structures.

Probabilistic modelling carried out in this research, assuming a 50% loss of CSA accounts for ultimate failure conditions, suggests offshore structures will have an 11.6% chance of ultimate failure by 120 years of exposure. These estimates were based on experimental data gathered throughout, literature data where applicable and sound engineering judgement. All estimates are very conservative, supporting the belief that the structures will remain in situ with little damage for at least a century. It is therefore recommended that such structures are left in situ when decommissioning as to avoid costly removal.

Further work is recommended on the structural response of structures with heavily corroded reinforcement to provide a better understanding of the like failure mechanisms of heavily degraded offshore concrete structures. It is also suggested the response of alternative section shapes and sizes are reviewed. These recommended studies are outlined in Chapter 9.

CHAPTER NINE

9 CONCLUSIONS AND RECOMMENDATIONS

9.1 GENERAL SUMMARY

Current service-life and ultimate-life modelling of offshore concrete structures is often flawed due to the misrepresentation of the complexity of reinforced concrete structures and their exposed environments. These, along with the issue of current models using simplified diffusion equations to predict the onset of corrosion ignoring cracking and propagation rates, often cause erroneous time-to-failure predictions.

Investigative works carried out through this thesis have challenged preconceived views of submerged concrete corrosion, corrosion in cracked structures either statically, or more importantly dynamically, loaded and the remaining life of such structures. Experimental work challenged the basic methodology of modelling service life through initiation along, and important conclusions can be drawn from the works carried out with respect to ultimate life of structures in a sub-sea environment.

Structures in the North Sea environment are likely to remain unaffected for at least a hundred years, however the likelihood is the concrete will show little signs of degradation for many years after this. An area for concern remains any concrete protruding through the splash zone as expansive corrosive products will form due to the availability of excessive oxygen. Submerged concrete, without this issue is likely to continue to remain relatively undamaged for much longer.

9.2 CONCLUSIONS

The following conclusions are drawn from experimental works carried out throughout this research project and are summarised in Table 9.1.

1) Transport of chlorides will inevitably initiate corrosion in concrete structures exposed to saline solutions. The rate at which chlorides penetrate is heavily dependent on the solution of exposure, where many alternative ions are present the surface skin effects will become predominant and can have a more significant influence on initiation than alterations in water/cement ratio or additional cementitious materials. Construction quality (such as quality

of compaction) also has a very significant influence on initiation and should be modelled through conservative estimates of mean and standard deviation of variables.

Experimental works, however, showed that in structures under flexural loading whereby cracking occurs, corrosion will initiate rapidly rendering the transport of chlorides through the cover irrelevant to ultimate life estimation. It is vital that the structural response of the structure in question is well understood allowing for the number of cracks, widths of cracks and location of cracks to be known.

2) Corrosion propagates at significant rates under sub-sea conditions, wherein oxygen is limited. The anodically polarized area of the steel however alters in size depending on oxygen availability, even though chlorides are present along the entire length of the bar. Whereby cracking has occurred, the availability of chlorides at the steel surface and the resistivity of the concrete will be the limiting factors for propagation rates.

3) Flexural cracking that penetrates past reinforcement to the neutral axis causes almost instantaneous corrosion when the cracks are greater than 0.1mm. Corrosion rates then increase linearly up to measured static crack widths of 0.7mm.

At the base of the crack, 3cm of length appeared to be anodic whereby corrosion was visible after exposure to the atmosphere. Although there is evidence of pitting within the 3cm area, it can be assumed for modelling that the CSA reduces averaged over this small area.

4) When dynamically loaded, the cracks appeared to increase the corrosion rate by a factor of roughly 2.5 after taking the number of cracks in the surface and anodic areas of the bar into account. A dynamic factor was proposed to take this into account in propagation modelling. Further works on the effects of dynamic cracking on corrosion rates are required to enhance understanding of how variable frequency, variability of magnitudes with infrequent peak loads, and gradually increasing crack width and depth effect corrosion propagation rates of reinforcing steel.

5) Bond loss does not occur with modern day steel reinforcing bars up to general corrosion of around 15% in pull-out testing, supporting the hypothesis that the loss of CSA is the most important factor in the reduction of ultimate capacity. However, as the CSA was reduced and bond was deteriorating, bending tests showed a loss of stiffness of the section. In turn this caused larger deflections and greater crack widths under identical loading conditions.

6) As the CSA is reduced, the ultimate capacity is reduced proportionally. This provides the basis for predicting the ultimate capacity through the estimated loss of CSA due to corrosion at rates previously determined.

TABLE 9.1 SUMMARY OF EXPERIMENTAL FINDINGS

Phase	Conclusions
I	Initiation will occur within 50 years of exposure for sub-sea concrete of common quality to that which exists within the North Sea. Seawater causes slower diffusion of chlorides through concrete in comparison with NaCl, with diffusion coefficients unable to be obtained at early ages of exposure.
II	Corrosion continues to propagate in low oxygen environments, such as those of fully submerged concrete in the North Sea. Anodic areas are reduced due to lack of oxygen, however the overall corrosion rate remains significant.
IIIA	Reduced water/cement ratios cause longer initiation and slower propagation of steel in submerged conditions. Corrosion rates appear to continue in submerged/low oxygen environments similar to results from Phase II, thus validating previous results.
IIIB	Static cracking causes corrosion almost instantaneously, with significant rates observed for cracks of greater than 0.1mm. The corrosion rate increases linearly with increasing crack width. Dynamic cracking caused multiple cracks through three-point loading, with increasing crack depth. Corrosion rates increased by a factor of roughly 2.5.
IV	Ultimate capacity is heavily dependent on remaining cross sectional area of the tensile steel, and appears not linked to loss of bond within reinforcing beams. Lapping has an insignificant effect on ultimate capacity and is not a concern for ultimate failure of structures, as the failure of lapped sections occur where the lapping ends and the section is reduced to single bars.

9.3 RECOMMENDED FUTURE WORKS

Although steps have been taken to improve the understanding of sub-sea concrete degradation and aid in the long-term lifetime modelling of existing structures, further works should be carried out among material understanding as well as structural response of damaged structures. Along with further laboratory works and continuation of experimental methodologies carried out within this thesis, emphasis on validating results with 'real world' structures should be a priority. This is not just the case for offshore structures, but for all structures whether submerged, tidal, or in the splash zone, exposed either to marine or de-icing salts.

Measuring the rate of corrosion in existing sub-sea concrete structures is difficult as connecting cables to reinforcement would be impractical. Taking half-cell measurements would be similarly difficult, however this would be much simpler on protruding structures or land based structures. Sampling of cover concrete is easily achievable and would provide data on concrete strength, chloride ingress and ageing of the concrete.

Continuation of dynamic cracking experiments for longer exposure times, differing exposure environments. Attempt to control the pressure or oxygen concentration in the submerged environment.

Extended cracking experiments in salt water and analysis of the effect of crack self-healing, chemical determination of samples from within the crack to attempt to determine the self-healing product

9.3.1 DETERMINATION OF AN APPLICATION FACTOR TO ACCOUNT FOR THE 'SEAWATER EFFECT'

Continuation of diffusion studies started throughout this research programme by sampling concrete exposed to NaCl and seawater solutions over the following years.

Between 8 and 12 samples of 19 differing concrete mixes are exposed to each solution and currently at between 18 and 24 months exposure (Table 9.2). Profiling and determination of D_{app} values should be carried out to provide information on ageing of submerged concrete in a controlled seawater and NaCl solutions, differences between measured D_{app} in each solution and an estimation of an exposure condition factor to apply to measured coefficients for lifetime estimation.

TABLE 9.2 REMAINING EXPOSED CONCRETE SAMPLES

Mix reference	Cubes	Exposure date
CT01	8	10 August 2011
CT02	8	10 August 2011
CT03	12	5 September 2011
CT04	12	16 September 2011
CT05	12	20 October 2011
CT06	12	17 October 2011
CT07	12	5 September 2011
CT08	8	10 August 2011
CT09	12	16 September 2011
CT10	12	11 October 2011
CT11	12	22 October 2011
CT12	12	22 October 2011
CT13	8	10 August 2011
CT14	12	11 October 2011
CT15	12	20 October 2011
CT16	12	3 November 2011
CT17	12	3 November 2011
CTN	8	18 November 2011
CTBD	8	18 November 2011

The chemical interactions between seawater and the surface layer of the concrete should be investigated further, ideally through the use of a large-scale multi-variable experimental programme that could isolate the precipitation of compounds in the surface layer directly responsible for reduced chloride ingress.

9.3.2 DYNAMIC CORROSION EXPERIMENTAL WORK

Using the setup devised in Chapter 3, and following up on results in Chapter 6, experimental work is suggested for dynamic cracking to further understand the effects of dynamic loading on corrosion (Table 9.3).

TABLE 9.3 PROPOSED FUTURE DYNAMIC EXPERIMENTAL WORKS

Variable	Recommended experiments	Comments
Salt solution	NaCl and seawater	Determine if evidence of self-healing exists in either solution after multiple applied loads. Visual inspection of cracks with measurements of corrosion rate evolution over time.
Crack width	0.1-0.7mm starting widths	Investigation of the effects on dynamic crack width on corrosion rate determining if the relationship between crack width and corrosion rate is consistent with the relationship observed from static cracking experiments.
Frequency variation	1Hz, 0.5 Hz, 0.2Hz	Does the frequency of repetitive loading influence corrosion rate. Although wave frequencies are relatively consistent, loading of other structures may vary, i.e. bridge traffic.
Magnitude variation	Peak loading	Wave loading is rarely of consistent magnitude and can be extremely variable. Does extreme rare loading cause a consistently greater rate of corrosion.

Additionally, to determine the true corrosion rates of structures in the North Sea, experiments should be completed to determine how low temperatures, extruding metals, dissimilar metals and hydrostatic pressure under dynamic loading affects the corrosion rate of reinforcing steel.

9.3.3 STRUCTURAL CAPACITY UNDER EXTREME CORROSION

The ultimate capacity of concrete beams with corrosion of up to 10% loss of mass reduced proportionally. As experimental work was carried out in a relatively short 6 month period, similar experiments could be carried out to determine the effects of larger steel mass loss due to corrosion. If the ultimate capacity continues to fall proportionally to the total area of steel remaining, the remaining ultimate life of structures could remain substantially long.

9.3.4 STRUCTURAL CAPACITY OF DIFFERING CROSS-SECTIONS

Cracking in beams is relatively predictable and occurs across the entire tensile surface of the concrete. Crack patterns in circular sections are likely to be different. As the bars at the centre of the crack begin to corrode, the crack will propagate around the structure, initiating further corrosion on other bars in tension.

Loss of ultimate capacity will occur when the cross-sectional area of steel of this section sufficiently reduces the moment capacity whereby the loading will be larger than the capacity. To determine the further effects of round steel sections and crack propagation an experimental set of hollow cylinders should be cast, and cracked through a bending moment whilst submerged. As the loading rate is constant, corrosion rates of independent longitudinal reinforcement should be monitored to determine the spread of corrosion across the bars.

REFERENCES

Abu Hassan, Z.F., 2013. *Rapid assessment of the potential chloride resistance of structure concrete*. PhD. University of Dundee.

Alonso, C., Andrade, C., Castellote, M. and Castro, P., 2000. *Chloride threshold values to depassivate reinforcing bars embedded in a standardized OPC mortar*. Cement and Concrete Research, 30(7) pp.1047-1055.

Alonso, C., Castellote, M. and Andrade, C., 2004. *Chloride threshold dependence of pitting potential of reinforcements.* Electrochimica Acta, 47(21) pp.3469-3481.

Andrade, C., Castellote, M., and d'Andrea, R., 2011. *Measurement of ageing effect on chloride diffusion coefficients in cementitious materials.* Journal of Nuclear Materials, 412(1) pp.209-216.

Andrade, C., Prieto, M., Tanner, P., Tavares, F. and d'Andrea, R., 2013. *Testing and modelling chloride penetration into concrete*. Construction and Building Materials, 39(1) pp. 9-18.

Angst, U., Elsener, B., Larsen, C.K. and Vennesland, Ø., 2009. *Critical chloride content in reinforced concrete – a review*. Cement and Concrete Research, 39(12) pp.1122-1138.

Ann, K.Ann, K.Y., Ahn, J.H. and Ryou, J.S., 2009. *The importance of chloride content at the concrete surface in assessing the time to corrosion of steel in concrete structures.* Construction of Building Materials, 23(1) pp.239-245.

Årskog, V., Ferreira, M. and Gjørv, O.E., 2004. *Durability and performance of Norwegian concrete harbour structures.* In: B.H. Oh et al., eds 2004. *Concrete under Severe Conditions: Environment & Loading*. CONSEC'04, Seoul, Korea.

ASTM G5-94, 2004. Standard reference test method for making potentiostatic and potentiodynamic anodic polarization measurements.

Atkinson, M.J. and Bingman, C., 1996. *Elemental composition of commercial seasalts.* Journal of Aquariculture and Aquatic Sciences, 3(2) pp.39-43.

Bamforth, P.B., 2004. *Enhancing reinforced concrete durability: Guidance on selecting measures for minimising the risk of corrosion of reinforcement in concrete*. Technical Report No. 61. Camberley: The Concrete Society.

BE95-1347/TG7/ Report R17., 2000. *DuraCrete – final technical report: general guidelines for durability design and redesign*. Project No. BE95-1347. Brussels: Brite-EuRam.

Beck, M. and Raupach, M., 2012. *Deterioration model and input parameters for reinforcement corrosion*. Structural Concrete, 13(3) pp.145-155.

Beckman, J., n.d. *Cormorant Alpha*. [image online] Available at: <http://www.offshore-mag.com/content/dam/etc/medialib/new-lib/offshore/print-articles/2011/june/85439.res/_jcr_content/renditions/original> [Accessed 15/06/2012].

Beeby, A.W. and Scott, R.H., 2005. *Cracking and deformation of axially reinforced members subjected to pure tension*. Magazine of Concrete Research, 57(10) pp. 611-621.

Bentz, D.P., Feng, X. and Hooton, R.D., 2001. *Time-dependent diffusivities: Possible misinterpretation due to spatial dependence.* National Institute of Standards and Technology, Technology Administration, US Department of Commerce.

Bertolini, L., Elsener, B., Pedeferri, P. and Redaelli, E., Polder, R., 2013. Corrosion of Steel in Concrete / 2nd completely revised and enlarged edition. Weinheim: Wiley-VCH.

Bertolini, L. and Redaelli, E., 2009. Depassivation of steel reinforcement in case of pitting corrosion: detection techniques for laboratory studies. Materials and Corrosion, 60(8) pp.608-616.

Böhni, H., 2005. *Corrosion in reinforced concrete structures: edited by Hans Böhni*. Boca Raton: CRC Press.

BRE, 1998. *Corrosion of reinforcement in concrete: electrochemical monitoring.* Digest 434. London: Building Research Establishment.

British Standards Institution, 1986. *BS 1881-125:1986 Testing concrete – Part 125: Methods for mixing and sampling fresh concrete in the laboratory.* London: BSI.

British Standards Institution, 2000a. *BS EN1097-6:2000 Tests for mechanical and physical properties of aggregates - Determination of particle density and water absorption.* London: BSI.

British Standards Institution, 2000b. *BS EN 197-1:2000 Cement – Part 1: Composition, specifications and conformity criteria for common cements.* London: BSI.

British Standards Institution, 2000c. *BS EN 206-1:2000 Concrete specification, performance, production and conformity*. London: BSI.

British Standards Institution, 2002a. *BS EN 12390-3:2002 Testing hardened concrete – Part 3: Compressive strength of test specimens*. London: BSI.

British Standards Institution, 2002b. *BS EN 1990:2002 Basis of structural design*. London: BSI.

British Standards Institution, 2004. *BS EN 1992-1-1:2004 Eurocode 2: Design of concrete structures – Part 1-1: General rules and rules for buildings.* London: BSI.

British Standards Institution, 2009a. *BS EN 12350-2:2009 Testing fresh concrete – Part 2: Slump test.* London: BSI.

British Standards Institution, 2009b. *BS EN 12350-6:2009 Testing fresh concrete – Part 6: Density.* London: BSI.

British Standards Institution, 2009c. *BS EN 934-2:2009 Admixtures for concrete, mortar and grout. Concrete admixtures – Definitions, requirements, conformity, marking and labelling.* London: BSI.

British Standards Institution, 2010. *DD CEN/TS 12390-11:2010 Testing hardened concrete - Part 11: Determination of the chloride resistance of concrete, unidirectional diffusion.* London: BSI.

British Standards Institution, 2012. *BS EN 450-1:2012 Fly ash for concrete. Definition, specifications and conformity criteria.* London: BSI.

Brown, P.W. and Doerr, A., 2000. *Chemical changes in concrete due to the ingress of aggressive speices.* Cement and Concrete Research, 30(3) pp. 411-418.

Brown, P.W., Hooton, R.D. and Clark, B.A., 2003. *The co-existence of thaumasite and ettringite in concrete exposed to magnesium sulphate at room temperature and the influence of blast-furnace slag substitution on sulphate resistance*. Cement and Concrete Composites, 25(8) pp.939-945.

Buenfeld, N. R. and Newman, J. B., 1984. *The permeability of concrete in a marine environment.* Magazine of Concrete Research, 36 (127) pp.67-80.

Buenfeld, N.R., Newman, J.B., and Page, C.L., 1986. *The resistivity of mortars immersed in seawater*. Cement and Concrete Research, 16 (4) pp.511-524.

Castellote, M., Andrade, C. and Alonso C., 2001. *Measurement of the steady and non-steady state chloride diffusion coefficients in a migration test by means of monitoring the conductivity in the anolyte*

chamber. Comparison with natural diffusion tests. Cement and Concrete Research, 31(10) pp.1411-1420.

Castellote, M., Andrade, C., and Alonso, C., 2002. *Accelerated simultaneous determination of the chloride depassivation threshold and of the non-stationary diffusion coefficient values.* Corrosion Science, 44 (11) pp.2409-2424.

Castellote, M. and Andrade, C., 2006. *Round-robin test on methods for determining chloride transport parameters in concrete*. Materials and Structures, 39 (294) pp.955-990.

Chung, L., Najm, H. and Balaguru, P., 2008. *Flexural behaviour of concrete slabs with corroded bars.* Cement and Concrete Composites, 30(3) pp.184-193.

Coppola, L., Fratesi, R., Monosi, S., Zaffaroni, P. and Collepardi, M., 1996. *Corrosion of Reinforcing Steel in Concrete Structures Submerged in Seawater*. In: Proceedings, Third CANMET/ACI International Conference on Performance of Concrete in Marine Environment, no. SP-163.

Crank, J., 1956. The mathematics of diffusion. Oxford: Clarendon Press.

Dang, V.H. and François, R., 2013. *Influence of long-term corrosion in chloride environment on mechanical behaviour of RC beam.* Engineering Structures, 48 pp.558-568.

Det Norske Veritas., 2006. *Material risk – ageing offshore installations.* Technical Report no. 2006-3496. Norway: Petroleum Safety Authority Norway.

Dhir, R.K., McCarthy, M.J., Tittle, P.A.J. and Zhou, S., 2004. *Role of cement content in specifications for concrete durability: Cement type influences.* Proceedings of the Institution of Civil Engineers: Structures and Buildings, 157(2) pp.113-127.

Dhir, R.K., McCarthy, M.J., Zhou, S. and Tittle, P.A.J., 2006. *Role of cement content in specifications for concrete durability: Aggregate type influences*. Proceedings of the Institution of Civil Engineers: Structures and Buildings, 159(4) pp.229-242.

Edvardsen, C., 1999. *Water permeability and autogenous healing of cracks in concrete.* ACI Materials Journal, 96(4) pp.448-454.

Enos, D.G. and Scribner, L.L., 1997. *The potentiodynamic polarization scan.* Technical Report 33. Farnborough: Solartron Instruments.

Erdogdu, S., Bremner, T.W. and Kondratova, I.L., 2001. *Accelerated testing of plain and epoxy-coated reinforcement in simulated seawater and chloride solutions.* Cement and Concrete Research, 31(6) pp.861-867.

Fagerlund, G. and Hassanzadeh, M., 2010. *Self-healing of cracks in concrete long-term exposed to different types of water – results after 1 year exposure.* Lund Institute of Technology Division of Building Materials, Report TVBM-3156.

Fairfield Energy, n.d. *Dunlin Alpha Decommissioning*. [image online] Available at: <http://www.fairfield-energy.com/pages/view/dunlin-alpha-decommissioning-options-assessment-and-selection> [Accessed 15/6/2012].

Fairfield Energy, 2012. [online] *Dunlin Alpha – decommissioning programme.* Available at: <http://www.fairfield-energy.com/pages/view/dunlin-study-reports> [Accessed 13/02/2013].

Fang, C., Lundgren, K., Chen, L. and Zhu, C., 2004. *Corrosion influence on bond in reinforced concrete.* Cement and Concrete Research, 34(11) pp.2159-2167.

fib International Federation for Structural Concrete, 2006. *Model code for service life design.* Bulletin 34, Lausanne.

fib International Federation for Structural Concrete, 2010a. *Model Code 2010 – First complete draft – Volume 1.* Bulletin 55, Lausanne.

fib: International Federation for Structural Concrete, 2010b. *Model Code 2010 – First complete draft – Volume 2.* Bulletin 56, Lausanne.

Gjørv, O.E., Vennesland, O. and El-Busaidy, A. H. S., 1986. *Diffusion of dissolved oxygen through concrete.* Materials Performance, 25(12) pp. 39-44.

Gjørv, O.E. ed., 2009. *Durability design of concrete structures in severe environments*. New York: Taylor & Francis.

Gjørv, O.E., 2010. *Service life and sustainability of important concrete infrastructures.* In: Proceedings: Second International Conference on Sustainable Construction Materials and Techniques, Ancona, Italy, June 28-30.

Gjørv, O.E., 2011. *Durability of concrete structures*. Arabian Journal for Science and Engineering, 36 (1), pp.151-172.

Gowripalan, N., Sirivivatnanon, V. and Lim, C.C., 2000. *Chloride diffusivity of concrete cracked in flexure.* Cement and Concrete Research, 30(5) pp.725-730.

Grace Construction Products, 2006. *Understanding AASHTO T277 and ASTM C1202 Rapid chloride permeability test.* Technical Bulletin TB-0100. Cambridge, USA: W.R. Grace and Co.

Gu, P. and Beaudoin, J.J., 1998. *Obtaining effective half-cell potential measurements in reinforced concrete structures.* Construction Technology Update no. 18. Ottawa: National Research Council of Canada.

Gulikers, J. and Raupach, M., 2006. *Numerical models for the propagation period of reinforcement corrosion.* Materials and Corrosion, 57(8) pp.618-627.

Hansson, C.M., Poursaee, A. and Luarent, A. 2006., *Macrocell and microcell corrosion of steel in ordinary Portland cement and high performance concretes.* Cement and Concrete Research, 36(11) pp.2098-2102.

Helland, S. 2008., *Ageing factor concept.* In: Nordic exposure sites – input to revision of EN 206-1, workshop proceedings, Hirtshals, Denmark, 12-14th November 2008.

Helland, S., Aarstein, R. and Maage, M., 2010. *In-field performance of North Sea offshore platforms with regard to chloride ingress.* Structural Concrete, 11(1) pp.15-24.

Hornbostel, K., Larsen, C.K. and Geiker, M.R., 2013. *Relationship between concrete resistivity and corrosion rate – a literature review.* Cement and Concrete Composites, 39 pp.60-72.

Hussain, R.R., 2011. *Effect of moisture variation and oxygen consumption rate of corroding steel in chloride contaminated concrete.* Cement and Concrete Composites. 33 (1) pp.154-161.

International Association of Oil and Gas Producers, 2003. *Disposal of disused offshore concrete gravity platforms in the OSPAR Maritime Area*. Report no. 338. UK: OGP.

International Association of Oil and Gas Producers, 2012. D*ecommissioning of offshore concrete gravity based structures (CGBS) in the OSPAR maritime area/other global regions*. Report no. 484. UK: OGP.

Isgor, O.B. and Razaqpur, A.G., 2006. *Advanced modelling of concrete deterioration due to reinforcement corrosion*. Canadian Journal of Civil Engineering, 33 (6) p.707.

Izquierdo, D., Alonso, C., Andrade, C. and Castellote, M., 2004. *Potentiostatic determination of chloride threshold values for rebar depassivation - Experimental and statistical study*. Electrochimica Acta, 49(17) pp.2731-2739.

Jaffer, S.J. and Hannson, C.M., 2008. *The influence of cracks on chloride-induced corrosion of steel in ordinary Portland cement and high performance concretes subjected to different loading conditions*. Corrosion Science, 50(12), pp.3343-3355.

Jaffer, S.J. and Hannson, C.M., 2009. *Chloride-induced corrosion products of steel in cracked-concrete subjected to different loading conditions*. Cement and Concrete Research, 39(2) pp.116-125.

Jiang, J. and Yuan, Y., 2012. *Prediction model for the time-varying corrosion rate in rebar based on micro-environment in concrete.* Construction and Building Materials, 35 pp.625-632.

Jiang, L., Liu, R., Mo, L., Xu, J. and Yang, H., 2013. *Influence of chloride salt type on critical chloride content of reinforcement corrosion in concrete.* Magazine of Concrete Research, 65(5) pp.319-331.

Kurdowski, W., 2004. *The protective layer and decalcification of C-S-H in the mechanism of chloride corrosion of cement paste.* Cement and Concrete Research, 34(9) pp.1555-1559.

Life-365 Consortium II, 2012. *Life-365 service life prediction model and computer program for predicting the service life and life-cycle costs of reinforced concrete exposed to chlorides*. Version 2.1. [online] Available at: http://www.life-365.org/download/Life-365_Users_Manual.pdf [Accessed: 18/03/2013].

Lindvall, A., 1998. DuraCrete – probability performance based durability design of concrete structures. In: 2nd International PhD symposium in civil engineering, Budapest.

Lundgren, K., 2007. *Effect of corrosion on the bond between steel and concrete: An overview.* Magazine of Concrete Research, 59(6) pp.447-461.

Maage, M. and Helland, S., 2008. *Shore approach – 26 years experience with high quality concrete in XS3 exposure.* In: Nordic exposure sites – input to revision of EN 206-1, workshop proceedings 8, Hirtshals, Denmark, 12-14th November 2008.

Malumbela, G., Moyo, P. and Alexander, M., 2012a. *A step towards standardising accelerated corrosion tests on laboratory reinforced concrete specimens.* Journal South Africa Institute of Civil Engineering [online]. 54(2) pp.78-85.

Malumbela, G., Moyo, P. and Alexander, M., 2012b. *Longitudinal strains and stiffness of RC beams under load as measures of corrosion levels.* Engineering Structures, 35 pp.215-227.

Marchand, J. and Samson, E., 2009. *Predicting the service-life of concrete structures – limitations of simplified models.* Cement and Concrete Composites, 31(8) pp.515-521.

Maruya, T., Hsu, K., Takeda, H. and Tangtermsirikul, S., 2003. *Numerical modelling of steel corrosion in concrete structures due to chloride ion, oxygen and water movement.* Journal of Advanced Concrete Technology, 1(2) pp.147-160.

McCarter, W.J., Linfoot, T.M., Chrisp, T.M. and Starrs, G. 2008. *Performance of concrete in XS1, XS2 and XS3 environments.* Magazine of Concrete Research, 60(4) pp.261-270.

McCarter, W.J. and Vennesland, Ø. 2004. *Sensor systems for use in concrete*. Construction Building and Materials, 18(6) pp.351-358.

Mehta, P.K., 1991. *Concrete in the marine environment*. London: Elsevier Applied Science.

Melchers, R.E., Li, C.Q. and Lawanwisut, W., 2006. *Modelling deterioration of structural behaviour of reinforced concrete beams under saline environment corrosion.* Magazine of Concrete Research, 58(9) pp.575-587.

Melchers, R. E. and Wells, T., 2006. *Models for the anaerobic phases of marine immersion corrosion.* Corrosion Science, 48(7) pp.1791-1811.

Millard, S.G., Law, D., Bungey, J.H. and Cairns, J., 2001. *Environmental influences of linear polarisation corrosion rate measurement in reinforced concrete.* NDT&E International, 34(6) pp.409-417.

Mohammed, T.U., Yamaji, T. and Hamada, H., 2002a. Chloride diffusion, microstructure, and minearalogy of concrete after 15 years of exposure in tidal environment. ACI Materials Journal, 99(3) pp.256 – 263.

Mohammed, T.U., Yamaji, T. and Hamada, H., 2002b. Microstructures and interfaces in concrete after 15 years of exposure in tidal environment. ACI Materials Journal, 99 (3) pp.352-360.

Neville, A.M., 2011. *Properties of concrete. 5th ed.* Harlow: Prentice Hall.

Norwegian Petroleum Directorate, n.d. [image online] Available at: <http://www.npd.no/Global/Engelsk/3-Publications/Facts/Facts2012/Figures/Chapter-06/Fig-6-7.png> [Accessed 15/6/2012].

NT BUILD 443,1994. *Concrete, hardened: accelerated chloride penetration.*

NT BUILD 492, 1999. *Concrete, mortar and cement based repair materials: chloride migration coefficient from non-steady state migration experiments.*

OSPAR, 1998. *OSPAR decision 98/3 on the disposal of disused offshore installations.* Ministerial meeting of the OSPAR Commission, Sintra, 22-23 July.

Osterminski, K. and Schießl, P., 2012. *Design model for reinforcement corrosion.* Structural Concrete, 13(3) pp.156-165.

Otieno, M. B., Alexander, M. G. and Beushausen, H-D., 2010. *Corrosion in cracked and uncracked concrete – influence of crack width, concrete quality and crack reopening.* Magazine of Concrete Research, 62(6) pp.393-404.

Otieno, M. B., Beushausen, H. D. and Alexander, M. G., 2011. *Modelling corrosion propagation in reinforced concrete structures – a critical review.* Cement and Concrete Composites, 33(2) pp.240-245.

Ou, Y-C., Tsai, L-L. and Chen, H-H., 2012. *Cyclic performance of large-scale corroded reinforced concrete beams.* Earthquake Engineering and Structural Dynamics, 41(4) pp.593-604.

Ouglova, A., Berthaud, Y., Foct, F., François, M., Ragueneau, F. and Petre-Lazar, I., 2008. *The influence of corrosion on bond properties between concrete and reinforcement in concrete structures.* Materials and Structures, 41(5) pp.969-980.

Ovstaas, G. and Morgan, D.R., 1999. *Investigation of concrete jetties at CFB Esquimalt and prediction of future service life.* In: *Durability of Building Materials and Components 8, eds. Lacasse, M.A., and Vanier, D.J.* pp.46-55. Ottawa, Canada: Institute of Research in Construction.

Page, C. L. and Lambert, P. 1987. *Kinetics of oxygen diffusion in hardened cement pastes.* Journal of Materials Science, 22(3) pp.942-946.

Pedziwiatr, J., 2009. *The influence of the bond between concrete and reinforcement on tension stiffening effect.* Magazine of Concrete Research, 61(6) pp.437-443.

Polder, R.B., 2001. *Test methods for on-site measurement of resistivity of concrete – a RILEM TC-154 technical recommendation.* Construction and Building Materials, 15(2) pp. 125-131.

Polder, R.B. and de Rooij, M.R., 2005. *Durability of marine concrete structures – field investigations and modelling*. HERON, 50(3) pp.133-153.

Polder, R.B. and Larbi, J.A., 1995. *Investigation of concrete exposed to North Sea water submersion for 16 years.* HERON, 40(1) pp.31-56.

Poulsen, E., 2006. *Diffusion of chloride in concrete: theory and application.* London: Taylor & Francis.

Poupard, O., L'Hostis, V., Catinaud, S. and Petre-Lazar, I., 2006. *Corrosion damage diagnosis of a reinforced beam after 40 years natural exposure in marine environment.* Cement and Concrete Research, 36(3) pp.405-520.

Pour-Ghaz, M., Isgor, O.B. and Ghods, P., 2009. *The effect of temperature on the corrosion of steel in concrete. Part I: Simulated polarization resistance tests and model development.* Corrosion Science 51(2) pp.415-425.

Poursaee, A., 2010a. *Determining the appropriate scan rate to perform cyclic polarization test on the steel bars in concrete.* Electrochimica Acta, 55(3) pp.1200-1206.

Poursaee, A., 2010b. *Potentiostatic transient technique, a simple approach to estimate the corrosion current density and Stern-Geary constant of reinforcing steel in concrete.* Cement and Concrete Research, 40(9) pp.1451-1458.

Poursaee, A. and Hansson, C.M., 2009. *Potential pitfalls in assessing chloride-induced corrosion of steel in concrete.* Cement and Concrete Research, 39(5) 391-400.

Quillin, K., 2001. *Modelling degradation processes affecting concrete*. Watford, UK: BRE.

Raupach, M., 1996a. *Investigations on the influence of oxygen on corrosion of steel in concrete - part 1.* Materials and Structures, 29(187) pp.174.

Raupach, M., 1996b. *Investigations on the influence of oxygen on corrosion of steel in concrete - part 2*. Materials and Structures. 29(188), pp.226.

Raupach, M., 2006. *Models for the propagation phase of reinforcement corrosion.* Materials and Corrosion, 57(8) pp.605-613.

Reinhardt, H.W. and Joos, M., 2003. Per*meability and self-healing of cracked concrete as a function of temperature and crack width*. Cement and Concrete Research 33 (7), pp.981-985

RILEM TC 154-EMC, 2003. *Recommendations of RILEM TC 154-EMC: Electrochemical techniques for measuring metallic corrosion. Half-cell potential measurements – potential mapping on reinforced concrete structures.* Materials and Structures, 36(261) pp.461-471.

Roberge, P. R., 2008. Corrosion engineering: principles and practice. USA: McGraw-Hill Professional.

Robinson, L., 1978. *Ninian Central construction*. [image online] Available at: <http://www.oilrig-photos.com/picture/number2118.asp> [Accessed 15/06/2012].

Rosenberg, A.M., Gaidis, J.M., Kossivas, T.G. and Previte, R.W., 1977. A corrosion inhibitor formulated with calcium nitrite for use in reinforced concrete. In: D.E. Tonini and S.W.Jr. Dean eds., 1977. *Chloride corrosion of steel in concrete*. Committee G-1 on Corrosion of Metals 1977, American Society for Testing and Materials. Baltimore: ASTM.

Saassouh, B. and Lounis, Z., 2012. *Probabilistic modelling of chloride-induced corrosion in concrete structures using first- and second-order reliability methods.* Cement and Concrete Composites, 34(9) pp.1082-1093.

Sahmaran, M., 2007. Effect of flexure induced transverse crack and self-healing on chloride diffusivity of reinforced mortar. Journal of Materials Science, 42(22) pp. 9131-9136.

Sandvik, K., Eie, R., Advocaat, J-D., Godejord, A., Haereid, K.O., Høyland, K. and Olsen, T.O., 2004. *Offshore structures – a new challenge.* XIV National Conference on Structural Engineering, Acapulco.

Santhanam, M., Cohen, M. and Aloek, J., 2006. *Differentiating seawater and groundwater sulphate attack in Portland cement mortars.* Cement and Concrete Research, 36(12) pp.2132-2137.

Sarja, A., 2000. *Durability design of concrete structures – Committee report 130-CSL.* Materials and Structures, 33(1) pp. 14-20.

Schlüter, M. and Jerosch, K., n.d. *Digital atlas of the North Sea – An overview about geo-information considering the sea floor and bottom water column.* AWI [online] Available at:

<http://www.awi.de/en/research/research_divisions/geosciences/marine_geochemistry/marine_gis/digital_atlas_of_the_north_sea/> [Accessed 22/2/2013].

Scott, A. and Alexander, M. G., 2007. *The influence of binder type, cracking and cover on corrosion rates of steel in chloride-contaminated concrete.* Magazine of Concrete Research, 59(7) pp. 495-505.

Scottish Enterprise, 2009. Report in industry consultation: North Sea decommissioning supply chain steering group.

Sharp, J.V., 1980. *Constructional materials for North Sea oil platforms.* Physics in Technology, 11 (2) pp. 67-73.

Shim, H., 2005. *Design & analysis of corrosion free service life of concrete structures using Monte Carlo method*. KSCE Journal of Civil Engineering, 9(5) pp.377-384.

Sibbick, T., Fenn, D. and Crammond, N., 2003. *The occurrence of thaumasite as a product of sea water attack.* Cement and Concrete Composites, 25 (8) pp.1059-1066.

Siemes, T. and Polder, R., 1998. *Design of concrete structures for durability. Example: chloride penetration in the lining of a bored tunnel.* HERON, 43(4) pp. 227-244.

Siemes, T. 1999. *DuraCrete: Service life design for concrete structures*. In: Durability of building materials and components 8, M.A. Lacasse and D.J. Vanier eds. pp.1343-1356.

Song, H-W. and Saraswathy, V., 2007. *Corrosion monitoring of reinforced concrete structures – a review.* International Journal of Electrochemical Science, 2(1) pp. 1-28.

Song, H-W., Lee, C-H. and Ann, K.Y., 2008. *Factors influencing chloride transport in concrete structures exposed to marine environments.* Cement and Concrete Composites, 30(1) pp. 113-121.

Song, H-W., Pack, S-W. and Ann, K.Y., 2009. *Probabilistic assessment to predict the time to corrosion of steel in reinforced concrete tunnel box exposed to sea water*. Construction and Building Materials, 23(10) pp.3270-3278.

Song, X. and Liu, X., 2000. *Experimental research on corrosion of reinforcement in concrete through cathode-to-anode area ratio.* ACI Materials Journal, 97(2) pp. 148-155.

Spiesz, P., Ballari, M.M. and Brouwers, H.J.H., 2012. *RCM: A new model accounting for the non-linear chloride binding isotherm and the non-equilibrium conditions between the free- and bound-chloride concentrations.* Construction and Building Materials, 27(1) pp.293-304.

Stanish, K. and Thomas, M.D.A., 2003. *The use of bulk diffusion tests to establish time-dependent concrete chloride diffusion coefficients.* Cement and Concrete Research, 33(1) pp.55-62.

Statoil, n.d. *Oseberg A*. [image online] Available at: <http://www.statoil.com/en/ouroperations/explorationprod/ncs/oseberg/pages/default.aspx> [Accessed 15/06/2012].

Stern, M. and Geary, A. L. , 1957. *Electrochemical polarisation: 1 A theoretical analysis of the shape of polarisation curves.* Journal of Electrochemical Society, 104(1) pp. 56-63.

Stewart, M.G., 2009. *Mechanical behaviour of pitting corrosion of flexural and shear reinforcement and its effects on structural reliability of corroding RC beams.* Structural Safety, 31(1) pp.19-30.

Subramaniam, K.V. and Bi., M., 2010. *Investigation of steel corrosion in cracked concrete: evaluation of macrocell and microcell rates using Tafel polarization response.* Corrosion Science, 52(8) pp.2725-2735.

Takewaka, K., Yamaguchi, T. and Maeda, S., 2003. *Simulation model for deterioration of concrete structures due to chloride attack.* Journal of Advanced Concrete Technology, 1(2) pp.139-146.

Tang, L. and Gulikers, J., 2007. *On the mathematics of time-dependent apparent chloride diffusion coefficient in concrete*. Cement and Conrete Research, 37(4) pp. 589-595.

Tang, L. and Sørensen, H.E., 2001. *Precision of the Nordic test methods for measuring the chloride diffusion/migration coefficients of concrete.* Materials and Structures, 34(8) pp.479-485.

Tang, L. and Utgenannt, P., 2008. *Chloride ingress and corrosion from the Swedish field exposures under the marine environment.* In: Nordic exposure sites – input to revision of EN 206-1, workshop proceedings, Hirtshals, Denmark, 12-14th November 2008.

Tegelaar, R.A. (1975). *Die Ölförderinsel ANDOC*. Concrete Information, issue 3, p.34.

TEP UK, n.d. *Decommissioning MCP01*. [image online] Available at: <http://www.uk.total.com/environment/SiteDecontamination.asp> [Accessed 15/6/2012].

Termkhajornkit, P., Nawa, T., Yamashiro, Y. and Saito, T., 2009. *Self-healing ability of fly ash-cement systems.* Cement and Concrete Composites, 31(3) pp.195-203.

Thomas, M.D.A. and Bamforth, P.B., 1999. *Modelling chloride diffusion in concrete – effect of fly ash and slag.* Cement and Concrete Research, 29(4) pp.487-495.

Thomas, M.D.A., Hooton, R.D., Scott, A. and Zibara, H., 2012. *The effect of supplementary cementitious materials on chloride binding in hardened cement paste.* Cement and Concrete Research, 42(1) pp.1-7.

Thomas, M.D.A. and Matthews, J.D., 2004. *Performance of pfa concrete in a marine environment – 10 year results.* Cement and Concrete Composites, 26(1) pp.5-20.

Tong, L. and Gjørv, O.E., 2001. *Chloride diffusivity based on migration testing.* Cement and Concrete Research, 31(7) pp.973-982.

Torres-Acosta, A.A., Navarro-Gutierrez, S. and Terán-Guillén, J., 2007. *Residual flexure capacity of corroded reinforced concrete beams.* Engingeering Structures, 29(6) pp.1145-1152.

Toro, L., Andrade, C., Fullea, J. and Martínez, I., 2011. *Steel corrosion in a chloride contaminated concrete pore solution with low oxygen availability.* In: Advances in modelling concrete service life, Eds. Andrade, C. and Gulikers, J., Proceedings of 4th International RILEM PhD Workshop, Madrid, Spain, November 19, 2010.

Total E&P Norge AS, 2003. *Frigg Field cessation plan. Stavanger,* Norway.

Total E&P Norge AS, 2011. *Frigg field cessation plan – close out report.* DM#946614. Stavanger, Norway.

Total E&P UK Limited, 2007. *MCP-01 decommissioning programme.* MCP01-00-A-00-00006, rev. 6. Aberdeen, Scotland.

Trethewey, K.R., 1988. *Corrosion: for students of science and engineering.* New York, US: Longman Scientific & Technical.

Val, D.V. and Trapper, P.A., 2008. *Probabilistic evaluation of initiation time of chloride-induced corrosion.* Reliability Engineering and System Safety, 93(3) pp. 364-372.

Vallini, D. and Aldred, J.M., 2003. *Durability assessment of concrete specimens in the tidal and splash zones in Fremantle Port. In:* Proceedings of the 16th Australasian Coastal and Ocean Engineering Conference and 9th Australasian Port and Harbour Conference, 9-12 September 2003, Auckland, NZ.

Vennesland, Ø., Climent, M.A. and Andrade, C., 2013. Recommendation of RILEM TC 178-TMC: Testing and modelling chloride penetration in concrete – methods for obtaining dust

samples by means of grinding concrete in order to determine the chloride concentration profile. Materials and Structures, 46 (3) pp. 337-344.

Vidal, T., Castel, A. and François, R., 2007. *Corrosion process and structural performance of a 17 year old reinforced concrete beam stored in chloride environments.* Cement and Concrete Research, 37(11) pp. 1551-1561.

VSL International 1992. *Floating concrete structures: examples from practice,* Second printing. Berne, Switzerland: VSL.

Wang, Y., Li, L. and Page, C.L., 2005. *Modelling of chloride ingress into concrete from a saline environment.* Building and Environment, 40(12) pp.1573-1582.

Warkus, J. and Raupach, M., 2008. *Numerical modelling of macrocells occurring during corrosion of steel in concrete.* Materials and Corrosion, 59(2) pp.122-130.

Warkus, J., Raupach, M. and Gulikers, J., 2006. *Numerical modelling of corrosion – theoretical backgrounds.* Materials and Corrosion, 57(8) pp.614-617.

Wenkenbach, I., 2011. *Tension stiffening in reinforced concrete members with large diameter reinforcement*. Durham University , undergraduate thesis. Available at Durham E-Theses Online: <http://etheses.dur.ac.uk/3250/> [Accessed 15/08/2012]

Win, P.P., Watanabe, M. and Machida, A., 2004. *Penetration profile of chloride ion in cracked reinforced concrete.* Cement and Concrete Research, 34(7) pp.1073-1079.

Yalciner, H., Eren, O. and Sensoy, S., 2012. *An experimental study on the bond strength between reinforcement bars and concrete as a function of concrete cover, strength and corrosion level.* Cement and Concrete Research, 42(5) pp.643-655.

Yamamoto, T., Yamaji, T., Mizuma, S. 2008. *Durability of carbon and stainless steel reinforced concrete members in a marine environment.* In: proceedings of the Eleventh International Conference on Durability of Building Materials and Components, Istanbul, Turkey, 11-14 May 2008.

Yuan, Q., Shi, C., He, F., De Schutter, G., Audenaert, K. and Zheng, K., 2008. *Effect of hydroxyl ions on chloride penetration depth measurement using the colorimetric method.* Cement and Conrete Research, 38(10) pp. 1177-1180.

Zhang, M., Chen, J., Lv, Y., Wang, D. and Ye, J., 2013. *Study on the expansion of concrete under attack of sulphate and sulphate-chloride ions.* Construction and Building Materials 39(1) pp.26-32.

Zhang, R., Castel, A. and François, R., 2009a. *Serviceability Limit State criteria based on steel-concrete bond loss for corroded reinforced concrete in chloride environment.* Materials and Structures, 42(10) pp. 1407-1421.

Zhang, R., Castel, A. and François, R., 2009b. *The corrosion pattern of reinforcement and its influence on serviceability of reinforced concrete members in chloride environment.* Cement and Concrete Research, 39(11) pp. 1077-1086.

Zuquan, J., Wei, S., Yunsheng, Z., Jinyang, J. and Jianzhong, L., 2007. *Interaction between sulphate and chloride solution attack of concretes with and without fly ash.* Cement and Concrete Research 37(8) pp.1223-1232.

University of Dundee Undergraduate and MSc Theses

Hope, T., 2013. *Validattion of the effect of fully submerged, low oxygen content, marine environments on corrosion process in reinforced concrete.*

Horne, T., 2012. *The effects of low oxygen diffusion, limestone aggregate and the ratio between anode and cathode size on the rate of reinforcement steel corrosion, with regards to the serviceability lifespan of fully submerged offshore gravity platforms.*

Khosravi, N., 2012. *Potential service life of decommissioned concrete platforms in the North Sea.*

Loh, L., 2013. *Stress distribution of submerged RC structures under the influence of corrosion.*

Mackenzie, E., 2013. *Effect of cracking on corrosion in relation to concrete degradation.*

McKinley, K., 2013. *The effect of statically loaded cracks on the corrosion of reinforced concrete in the offshore submerged environment*.

Robinson, M., 2012. *The effect of low oxygen and varying anode to cathode ratio on the corrosion process.*

Robinson, M., 2013. T*he effect of corrosion on small scale structural elements.*

Yun, B., 2012. *Improving understanding of low oxygen reinforcement corrosion and chloride diffusion on service life modelling of marine concrete.*